

Universiteit
Leiden
The Netherlands

The endothelial glycocalyx in diabetic nephropathy and beyond

Boels, M.G.S.

Citation

Boels, M. G. S. (2018, September 6). *The endothelial glycocalyx in diabetic nephropathy and beyond*. Retrieved from https://hdl.handle.net/1887/64937

Version:	Not Applicable (or Unknown)
License:	Licence agreement concerning inclusion of doctoral thesis in the Institutional Repository of the University of Leiden
Downloaded from:	https://hdl.handle.net/1887/64937

Note: To cite this publication please use the final published version (if applicable).

Cover Page



Universiteit Leiden

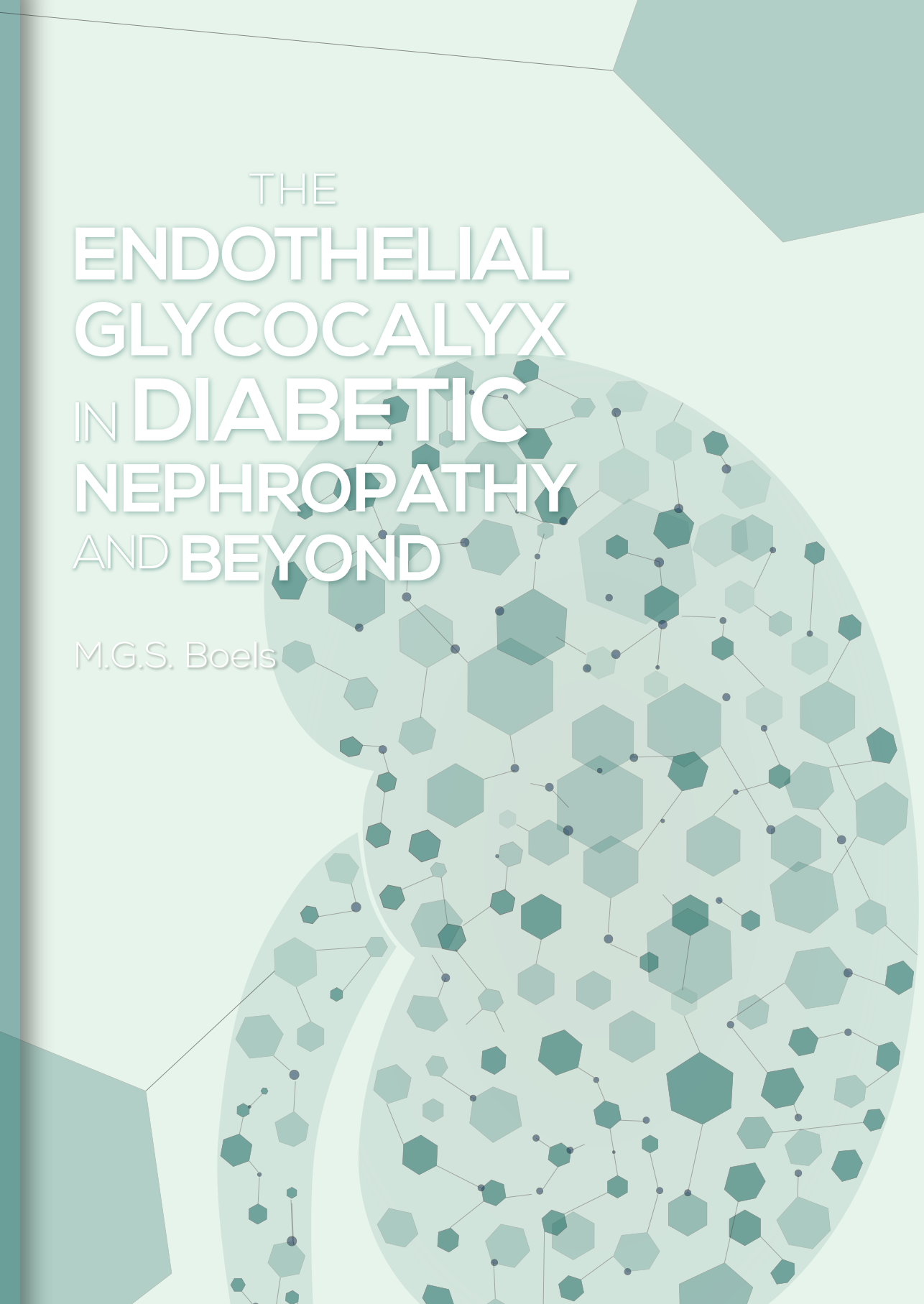


The handle http://hdl.handle.net/1887/64937 holds various files of this Leiden University dissertation.

Author: Boels, M.G.S.
Title: The endothelial glycocalyx in diabetic nephropathy and beyond
Issue Date: 2018-09-06

THE ENDOTHELIAL GLYCOCALYX IN DIABETIC NEPHROPATHY AND BEYOND

M.G.S. Boels



The endothelial glycocalyx in diabetic nephropathy and beyond

M.G.S. Boels

The endothelial glycocalyx in diabetic nephropathy and beyond

ISBN 978-94-930-1959-1
Cover Design Claudia Agostinho
Lay-out and Printing ProefschriftMaken // www.proefschriftmaken.nl

© M.G.S. Boels, 2018
All rights reserved. No part of this publication may be reproduced, stored in a retrieval system, or transmitted, in any form or by any means, electronically, mechanically, by photo-copying, recording or otherwise, without the prior written permission of the author.

The endothelial glycocalyx in diabetic nephropathy and beyond

Proefschrift

Ter verkrijging van de graad van Doctor aan de Universiteit Leiden,
op gezag van Rector Magnificus prof.mr. C.J.J.M. Stolker,
volgens besluit van het College voor Promoties
te verdedigen op donderdag 6 september 2018
klokke 15.00 uur

door

Martha Geesje Sientje Boels
geboren te Groningen
in 1987

Promotor
Prof. Dr. T.J. Rabelink

Co-promotor
Dr. B.M. van den Berg

Promotiecommissie

Prof. H Pijl	
Prof. Dr. P.H.A. Quax	
Prof. G. Molema	*Universitair Medisch Centrum Groningen*
Dr. J. van der Vlag	*Radboud Universitair Medisch Centrum, Nijmegen*
Prof. Dr. H. Haller	*Medizinische Hochschule, Hannover*

The studies presented in this thesis were carried out at the Department of Nephrology, Leiden University Medical Center, The Netherlands. The work was supported by the Dutch Kidney Foundation (Glycoren Consortium grant agreement number CP09.03) and by AbbVie (grant agreement number REN-11-0026).

Financial support by the Dutch Heart Foundation for the publication of this thesis is gratefully acknowledged.

Contents

Chapter 1	General Introduction & Outline of the thesis Adapted from: The endothelial glycocalyx as a potential modifier of the hemolytic uremic syndrome *European Journal of Internal Medicine 24:503–509, 2013*	7
Chapter 2	Atrasentan Reduces Albuminuria by Restoring the Glomerular Endothelial Glycocalyx Barrier in Diabetic Nephropathy *Diabetes 65(8):2429-2439, 2016*	27
Chapter 3	Systemic MCP-1 inhibition modifies renal macrophages and restores glomerular endothelial glycocalyx in diabetic nephropathy *American Journal of Pathology 187(11):2430-2440, 2017*	51
Chapter 4	Direct observation of enhanced nitric oxide in a murine model of diabetic nephropathy *PLoS One 12(1): e0170065, 2017*	73
Chapter 5	Remodeling of the endothelial glycocalyx with heparanase induces endothelial dysfunction *In preparation*	91
Chapter 6	Endothelial glycolytic activity regulates microvascular structure by modulating Angiopoietin 1 binding to endothelial glycocalyx hyaluronan *In submission*	109
Chapter 7	Summary & General Discussion	151
Chapter 8	Samenvatting in het Nederlands	163
	About the author	171
	List of Publications	173

Chapter 1

General Introduction & Outline of the thesis

Partly published in

European Journal of Internal Medicine 24:503–509, 2013

The endothelial glycocalyx as a potential modifier of the hemolytic uremic syndrome

Margien G.S. Boels, Dae Hyun Lee, Bernard M. van den Berg, Martijn J.C. Dane, Johan van der Vlag, Ton J. Rabelink

In 1979 the significance of the endothelial glycocalyx has been described for the first time (1). Though it was recognized earlier with electron microscopy, most methods of histological fixation and processing flushed away most substances of the endothelial glycocalyx (2). This loss resulted in under appreciation of its role in physiological processes. Another reason for insufficient appreciation is that during standard culture of endothelial cells, it is hard to replicate a robust glycocalyx due to the lack of hydrodynamics (3). Recently, interest in the function and role of the glycocalyx has increased, mainly through advances in preservation and visualization of the glycocalyx.

Function of the endothelial glycocalyx

Endothelial cells that line the luminal side of blood vessels, are covered with a dense bioactive gel-like layer, the endothelial glycocalyx, which is thus the first barrier of the vascular wall. The glycocalyx functions in a vasculoprotective way (4) by acting as a permeability barrier (5-7), a mechanosensor (4, 8-11), and by playing an important role in anti-inflammatory (12-15) and anti-thrombotic pathways (16, 17). The 500 to 2000 nm thick endothelial glycocalyx consists of proteoglycans and glycosaminoglycans produced by the endothelial cell. Together with adsorbed proteins, growth hormones, and cytokines from the surrounding plasma this results in a highly interactive matrix: the endothelial surface layer that excludes large molecules and erythrocytes (2, 18).

Structure of the endothelial glycocalyx

Proteoglycans and glycosaminoglycans form the basis of the endothelial glycocalyx. Proteoglycans, attached to- or protruding the plasma membrane, to transmit signals to the cell, consist of a core protein with covalently attached the long negatively charged unbranched polysaccharide glycosaminoglycans (18). Proteoglycans are also present in other extracellular matrices, such as the glomerular basement membrane in the kidney. There are many types of proteoglycans, including, but not limited to, syndecans, glypicans, perlecan, versican, thrombomodulin and some CD44 variants. In the endothelial surface glycocalyx, heparan sulfate represents the largest part of glycosaminoglycans (50-90%), while hyaluronan, chondroitin sulfate and dermatan sulfate are less abundantly present (18).

Heparan Sulfate

Heparan sulfate is made of repeats of disaccharides of uronic acid with N-acetyl-glucosamine (Figure 1). The high structural diversity depends on different modifications on the mature chains that are dictated by various enzymes, such as N-deacetylase / N-sulfotransferases (NDST), O-sulfotransferases, and 6-O-endosulfatases (19-21). This variation in heparan sulfate motifs also explains the heterogeneity of endothelial function in various vascular beds and has turned out to be the key to endothelial adaptation to circumstances such as hypoxia and inflammation

(22-26). For instance, inflammatory cytokines such as tumor necrosis factor α (TNF-α) increases specific inflammatory sulfated motifs of heparan sulfate, which allows for increased leukocyte adhesion (13, 27, 28). Systemic inflammatory stimuli such as the presence of LPS have been shown to induce endothelial heparanase production. Heparanase is the heparan sulfate degrading enzyme that is synthesized as a pre-proheparanase. Pre-proheparanase is targeted to the endoplasmic reticulum and processed into proheparanase enzymatic cleavage. The proheparanase is then transported to the Golgi apparatus and subsequently packaged into vesicles and secreted (29). Activated heparanase is 100-fold more active than proheparanase, though the latter is suggested to have some catalytic activity (30, 31). Heparanase cleaves/hydrolyzes the endothelial glycocalyx, specifically the heparan sulfate chains at the GlcA(b1→4)GlcNAc linkages into fragments of 10-20 sugar units (32). This degradation exposes endothelial adhesion and signaling molecules for leukocytes (33). The importance of modifications in heparan sulfates as a regulator of inflammation is illustrated by observations in mice which lacks the enzyme heparanase. Without the capacity to shed heparan sulfate from the endothelial surface, these mice can survive endotoxemia (33) and do not develop albuminuria upon the induction of diabetes (34).

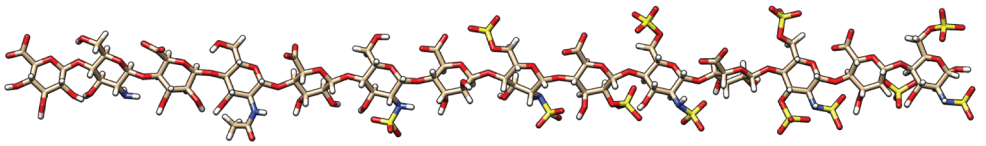


Figure 1. Structure model of heparan sulfate. 3D ribbon representation of the disaccharide repeat of glucuronic acid (GlcUA) and glucosamine. Glucosamine is represented as N-,6-O-sulfated glucosamine GlcN(NS,6S). In the structure the carbon backbone (brown), oxygen (red), hydrogen (white), sulfide (yellow) and nitrogen (blue) are depicted.

Hyaluronan

Hyaluronan is a nonsulfated glycosaminoglycan composed of repeating polymeric disaccharides D-glucuronic acid and N-acetyl-D-glucosamine linked by a glucuronidic bond (35). It is the only glycosaminoglycan that is not covalently attached to a core protein, but it can be bound to CD44 or its membrane bound assembly proteins (hyaluronic acid synthases [HAS] 1, 2 and 3). These synthases produce high molecular weight hyaluronan (36). Hyaluronidase and other sheddases cleave the high molecular weight chains of hyaluronan into smaller fragments (low molecular weight), that can induce endothelial stress as well as endothelial leakage (37). Also endothelial deletion of the hyaluronan synthase 2 gene, has been shown to result in albuminuria (38), whereas systemic treatment with high molecular weight hyaluronan reduced inflammation in diabetic mice (39).

Apart from chain length, the origin and (cellular) location of hyaluran determines its function. For example, hyluronan in the mesangial area has been shown to be an immunocytes attractant and induces fibrosis and inflammation, whereas this can be prevented by the prevention of hyaluronan accumulation with 4-methylumbelliferone (4-MU) (40). Also in other stromal cells,

such as vascular smooth muscle cells, hyaluronan accumulation is detrimental for cellular function (41), whereas in endothelial cells this relation is relatively unknown.

Endothelial glycocalyx in the glomerular filtration barrier

The heterogeneity of endothelial cells and their glycocalyx has been shown in various vascular beds (21, 27, 42-46). Endothelial cells within the functional filtration units of the kidney, the glomeruli, are defined by fenestrae to allow passage of high volumes of fluid. To prevent undesirable protein leakage, these fenestrae are filled with a dense glycocalyx that serves as the first barrier against albumin filtration (47). Similar glycosaminoglycans are also present in the other parts of the glomerular filtration barrier. For example, heparan sulfates are important components of the glomerular basement membrane (GBM) (48) and also the podocytes are covered with this carbohydrate rich layer (fig. 2) (47). The role of the podocyte glycocalyx is relatively unknown (49), whereas heparan sulfate expression is known to be reduced in glomerular nephritis (50) and diabetes (51) in the GBM. Nevertheless, animal models of reduced heparan sulfate expression in the GBM do not develop albuminuria (52).

The endothelial glycocalyx not only acts as a size barrier against albumin filtration (53), but also as a charge selective barrier. Negatively charged polysaccharides in de endothelial glycocalyx can repel negatively charged circulating proteins, such as albumin (54). Being the first layer in the glomerular filtration barrier, the glycocalyx is of vital importance to maintain normal filtration barrier function, however all layers of the glomerular filtration barrier are interrelated and therefore must be intact to prevent proteinuria, a marker for renal dysfunction (55, 56).

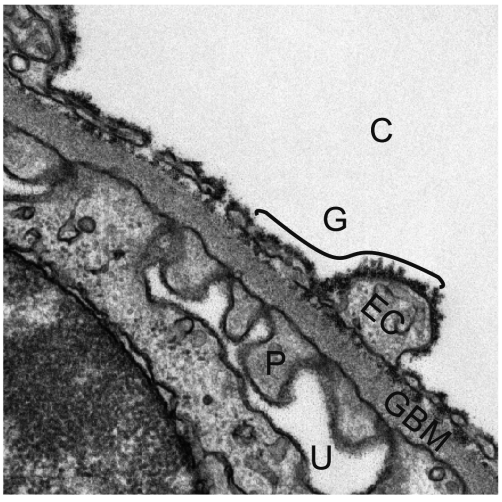


Figure 2. Transmission electron microscopic picture of the glomerular filtration barrier. The glomerular filtration barrier separates the blood circulation (C) from the urinary space (U) and is composed of fenestrated endothelial cells (EC) with its glycocalyx (G), the glomerular basement membrane (GBM) and podocytes (P). The glycocalyx is labeled with cationic ferritin

Glycocalyx dysfunction in renal diseases

Various disease conditions such as diabetes (57), atherosclerosis (6, 16, 58), infection (33), sepsis, and ischemia–reperfusion injury (15, 59-61) have been associated with loss or structural alterations of the glycocalyx (62). In renal diseases, glycocalyx involvement has been observed in atypical hemolytic uremic syndrome, acute kidney injury and diabetic nephropathy. In these three pathophysiological processes, glycocalyx modifications play a central role in the immune response and are potentially causal for these diseases.

Hemolytic uremic syndrome

The hemolytic uremic syndrome (HUS) is characterized by nonimmune hemolytic anemia, thrombocytopenia and renal impairment (63). The 10% of the HUS cases that are not induced through Shiga-like toxins (64), are due to alternative complement pathway dysregulation and are called atypical HUS. Atypical HUS is mostly accompanied with poor prognosis with progression to end-stage renal disease in more than half of the cases (65, 66). Of these, 50-60% is related to genetic mutations in complement genes, which are predisposing rather than directly causal for the disease: One or two pathological mutations under favorable conditions probably still allows for an adequate regulation of the complement system. Increasing evidence, suggests that a secondary trigger like inflammatory conditions, such as infection (67, 68), diabetes (69, 70), or pregnancy (71), may cause the onset of the disease under such circumstances (72-74). One explanation can be that host endothelial cells demand more protection via regulatory proteins under susceptible conditions (72, 75).

To date, solid evidence lacks to explain why HUS predominantly affects the kidney (63, 76). One possible factor in renal predisposition of the disease might be endothelial cell heterogeneity (42-46). Fenestration in the endothelium (63) and impaired signaling of vascular endothelial growth factor (VEGF) A by the surrounding podocytes to the glomerular endothelium (77) have been postulated to play a role as a modifier in renal manifestations of HUS. Moreover, the glomerular endothelium already has a lower baseline expression of membrane bound complement regulatory proteins such as CD55 and CD59 and is thereby more susceptible to a decrease in expression of complement regulatory proteins upon TNF-α stimulation (78).

One of the most important regulatory proteins of the alternative pathway of complement activation is complement factor H (CFH) (66, 79). This abundantly present 155 kDa glycoprotein blocks the formation of C3 convertase by competing with CFB to bind C3b, resulting in decreased activity of the alternative complement pathway. Loss-of-function mutations within CFH are considered the most common genetic alterations in atypical HUS (63). To date, more than 80 types of mutations have been found in CFH associated with atypical HUS (80). CFH consists of 20 short consensus repeat (SCR) domains and different SCR regions are responsible for the regulatory function of CFH including binding to C3b and heparan sulfate (81, 82). Notably, mutations in CFH are predominantly clustered within the C-terminus SCR 19-20 domains, in which the main binding site for heparan sulfate and endothelial cells is located (81). On the other hand, both the N-terminus SCR 1-4 and C-terminus SCR 19-20 domains are responsible

for binding and regulating C3b. It was shown that proper binding and detachment of CFH to heparan sulfate is required for the control of C3b (83). Heparan sulfate on the endothelial surface has been postulated to form the structural motif that CFH uses to recognize the host (Figure 3) (84-89). This is further supported by observations that the C-terminus of CFH is the location on the protein with the highest probability of mutations associated with atypical HUS (63, 79, 81). While the specific motif in heparan sulfate for binding CFH still needs to be identified, it also raises the question whether not only mutations in CFH could have functional consequences, but that alterations in heparan sulfate itself, or genetic polymorphisms of heparan sulfate synthesis, could result in altered binding of CFH and be a predisposition for atypical HUS.

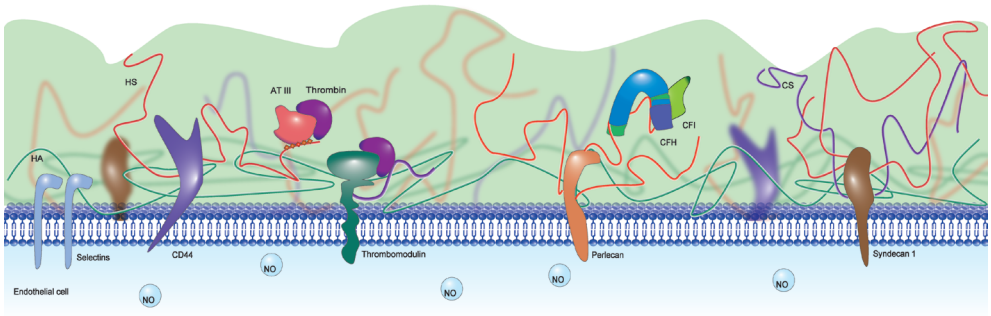


Figure 3. Interaction of the endothelial surface layer with anticoagulant and complement regulatory proteins. The endothelial surface glycocalyx consists of glycosaminoglycans (hyaluronan, HA; heparan sulfate, HS; chondroitin sulfate, CS), proteoglycans and glycoproteins. Possible interactions of complement factor H (CFH), thrombomodulin and ATIII with specific glycosaminoglycans are visualized. CFH has specific binding sites for HS to recognize the host cells. The chondroitin side chain of thrombomodulin influences its function in the coagulation cascade and ATIII activity is highly increased by HS binding. Endothelial nitric oxide (NO) is involved in cell quiescence, necessary for normal glycocalyx production.

Acute kidney injury

Acute kidney injury is common in critically ill patients (sepsis) and associated with a high mortality rate. It is characterized by sudden and sustained decline in kidney function with rapid decreased glomerular filtration rate (GFR) and the microvasculature plays a central role in acute kidney injury (90). In sepsis, shedding of glycocalyx in the vasculature that is induced by endothelial cell damage (91), can predict organ failure and mortality (92, 93). Soluble thrombomodulin, an endothelial transmembrane glycoprotein, is released upon endothelial cell disruption and increased with severity of sepsis (94). Syndecan-1 shows a similar pattern in sepsis (94), and can also be used to predict acute kidney injury after decompensated heart failure (95).

Apart from predicting the severity of disease, the pathophysiological process that is initiated by shedding of the glycocalyx is important for the observed symptoms. First, dysregulated systemic hemodynamics induces a hyper inflammatory cytokine storm (e.g. via Toll-like receptors (96)), thereby increasing leukocyte-endothelium interactions. This process further accelerates

glycocalyx shedding which facilitates access of leukocytes to transmigrate the endothelium into the injured kidney (61). In a mouse model, sepsis induces systemic heparanase levels, with distinct effects in lung and renal injury. In lung, glycocalyx injury was induced by TNFα dependent neutrophil influx (33). Heparanase inhibitors in this model could not affect systemic inflammation, whereas renal inflammatory genes could be attenuated, demonstrating that heparanase activation contributes to early septic renal glomerular dysfunction (97).

Acute kidney injury can be induced by sepsis, as well as ischemia, as is for example observed in transplantation with similar pathophysiological consequences. After kidney transplant, urinary heparanase was elevated and positively associated with proteinuria, while negatively associated with estimated glomerular filtration rate (eGFR) (22, 23). Similarly, heparanase-induced glycocalyx loss in other conditions that induce leukocyte extravasation or changes in vascular pressure (e.g. dialyses) should be considered in treatment and/or cure.

Diabetic nephropathy

Diabetes mellitus is one of the most important health problems in the Western world (98). It is characterized by sustained hyperglycemia that leads, if untreated, to secondary macro- and microvascular complications, and eventually multiple organ damage. Prolonged exposure to high levels of blood glucose in diabetes induces glycocalyx loss (99), as well as advanced glycation end products (AGEs) (100), reactive oxygen species (101) and immunocyte extravasation (102). In the kidney that may result in diabetic nephropathy. Current treatment options for diabetic nephropathy are mainly focused on the prevention of secondary symptoms, such as blockage of the renin-angiotensin-aldosteron system (RAAS; ACE inhibitors) to control blood pressure. The majority of these patients still progress to end-stage renal disease.

Diabetes-induced glycocalyx loss causes pathological activation of endothelial cells that results in altered heparan sulfate synthesis, thereby creating modified domains that allow chemokine and lectin binding (103, 104). In addition, elevated insulin and glucose levels induce elevated heparanase levels in the urine of diabetic patients (105). This suggests that urinary heparanase potentially could serve as a direct biomarker for diabetic renal disease, but also indicates that increased renal heparanase could be expected to modulate heparan sulfate structures in the glomeruli, thus contributes to diabetic nephropathy.

Inactive renal proheparanase is produced by podocytes, endothelial cells and platelets (106), which is increased in diabetes (51, 107). Monocytes and macrophages that infiltrate the glomeruli upon proinflammatory heparan sulfate domains promote cleavage of proheparanase into active heparanase which leads to further enzymatic degradation of the glycocalyx (106).

Cathepsin L, a lysosomal cysteine protease, is essential for the proteolytically activation of proheparanase into its active heparan sulfate degrading form (108). Activation of proheparanase generally occurs after uptake into the early endosome and lysosome through cathepsin L in epithelial cells, where heparanase subsequently serves intracellular regulatory processes (109). However, macrophages can also secrete cathepsin L, thus allowing the activation of proheparanase in the extracellular environment (110, 111). This process can be further accelerated

by diabetes-induced changes in the extracellular matrix (112) as well as by active heparanase itself that activates macrophages by inducing toll like receptor signalling (107). Additionally, cathepsin L deficient mice do not develop albuminuria upon streptozotocin-induced diabetes (113). This shows an important role for macrophage activation in diabetic nephropathy.

The endothelial glycocalyx is not only enzymatically cleaved by heparanase during diabetes, but also, through induction of the hyaluronan degrading enzyme hyaluronidase II, hyaluronan is shed (114, 115). The latter inducese low molecular weight hyaluronan, which induces endothelial stress and consequently endothelial leakage (36). Furthermore, high glucose concentrations and AGE-derivatives directly affect glycosaminoglycan production negatively (116). Reduced synthesis in combination with increased enzymatic cleavage of the endothelial glycocalyx increases macrophage influx, which by activating heparanase further reduces glycocalyx dimensions as well as induces self-stimulation. Targeting this vicious circle is therefore a promising strategy to restore the endothelial glycocalyx in diabetic nephropathy.

The glycocalyx as a therapeutic target

The obvious question is whether the glycocalyx could also be pharmacologically protected or replenished. Recent interest in the role of the endothelial glycocalyx in vasculoprotective properties resulted in the development of new drugs specifically targeting glycocalyx components. These drugs aim to directly increase the synthesis and restoration of glycocalyx components (117) or to inhibit its degradation (118, 119). For example, the pharmacological preparation sulodexide, consisting of low molecular weight heparin (80%) and dermatan sulfate (20%), has been advanced as a therapy to restore glycocalyx function. This compound was shown to have anti-inflammatory (120), pro-fibrinolytic and anti-thrombotic activity (121). Sulodexide also effectively inhibits the action of heparanase. In this way, sulodexide has been proposed to have a beneficial effect in membranoproliferative glomerulonephritis type 2 (122). Sulodexide was shown to have clinical activity in various cardiovascular diseases including myocardial infarction (123) and diabetic nephropathy (117, 124) in early phase studies. However, a phase III study on diabetic nephropathy could not corroborate these findings (125, 126). It has been suggested that this was related to the advanced stage of kidney injury with irreversible renal morphological changes, because glycocalyx mimetics can only be expected to be effective at the early onset of disease (127). Another explanation may be that the sulodexide used in the preclinical studies was of a different structural composition than the sulodexide preparations used during the first trials, due to different manufacture protocols and/or resources, since the raw heparin material is isolated form pig intestinal mucosa.

It has further been suggested that glycocalyx protection or restoration could be achieved through restoration of endothelial function (128). In this respect, it is of interest to note that the glycocalyx and its functional properties are strongly regulated by shear. Laminar shear stress on endothelial cells, sensed by the glycocalyx (11), ignites a pattern of S-nitrosylation in the endothelial cell through activation of endothelial nitric oxide synthase (eNOS), leading

to endothelial quiescence (129, 130). Therefore, drugs that increase eNOS signaling, such as endothelin A receptor blockers (chapter 2) (131, 132), could be of promising therapeutic value in the restoration of the glycocalyx under disease conditions. In addition, targeting inflammatory motifs that are involved in chemokine binding and leukocyte adhesion with monoclonal antibodies can be considered: The phage display-derived anti-heparan sulfate antibody NS4F5 that defines a specific stretch of highly sulfated disaccharides (GlcNS6S-IdoA2S)3, which is upregulated during endothelial activation, reduces cell proliferation and leukocyte adhesion (27).

Glycocalyx degradation increases endothelial-immunocyte interaction. Immunocytes are involved in further glycocalyx degradation via increased delivery or activation of glycocalyx degrading enzymes. Inhibiting aforementioned heparanase and hyaluronidase in various diseases, could potentially be a therapeutic approach to stabilize glycocalyx function and thus reduce immunocyte influx. The further exploration of the interaction of immunocytes with the endothelial glycocalyx may provide druggable targets that could potentially be analogous to how the discovery of the interaction of the pentasaccharide sequence of heparan sulfate with antithrombin III has changed the field of thrombosis.

Outline of this thesis

In this introduction, the basic principles of the endothelial glycocalyx are described. It's role in pathophysiology has been studied extensively, with an exponential increase of publications in the last years. In this thesis, the glycocalyx is studied in the pathological setting of diabetic nephropathy, which results in glycocalyx modifications that can be causal for disease progression. Also, the effect of remodeling the endothelial glycocalyx on downstream intracellular signaling is described.

As diabetes progresses, different organs are under stress and endothelial damage can be seen as a common denominator. In **chapter 2**, we focus on the role of restoration of endothelial function and tissue homeostasis in an antialbuminuric therapeutic approach with atrasentan, an endothelin A receptor blocker. This chapter provides a mechanistic explanation for the clinical observations of reduced albuminuria with atrasentan in patients with diabetic nephropathy, with a pivotal role for the endothelial glycocalyx.

Chapter 3 continues with a similar approach, i.e. a therapeutic approach is tested in a mouse model for diabetic nephropathy to find the mechanism of its antialbuminuric effect. This chapter focusses on the effect of systemic monocyte chemotactic protein-1 (MCP-1) inhibition on the inflammatory processes in diabetic nephropathy where macrophages play a crucial role. We exposed isolated renal macrophages *ex vivo* to an inflammatory stimulus, to address the role of macrophages in the treatment effects.

The structure and content of the endothelial glycocalyx is the result of its synthesis as well as enzymatic cleavage. Synthesis of the glycosaminoglycan chains can be affected by the senescent status of cells in disease. Nitric oxide is an important regulator of endothelial cell function.

Nitric oxide levels in diabetes, however, is subject of great debate, with arguments pro and contra therapeutic NO interference. In **chapter 4** we show that enhancing diabetes-induced renal NO levels further through inhibiting NOS uncoupling with sepiapterin will not restore glycocalyx presence nor rescue kidney function. This chapter affirms the important role for macrophages in glycocalyx degradation in diabetic nephropathy.

Once the endothelial glycocalyx is synthesized, it can be modified and/or removed extracellularly. This is a physiological process, however, glycocalyx loss is increased in oxidative stress and inflammation, both present in diabetes. Focusing on enzymatic degradation, heparanase sheds one of the major components of the glycocalyx, heparan sulfates. In chapter 2 and 3 we read that glomerular heparanase expression is increased in diabetic nephropathy. In **chapter 5**, we explore how heparanase precisely remodels the endothelial glycocalyx in endothelial cell culture as well as in the vasculature of zebrafish. We show that heparanase induces specific heparan sulfate sequences that are associated with inflammation.

In **chapter 6** we focus on another important component of the endothelial glycocalyx: hyaluronan. With an endothelial cell-specific conditional knockout mouse model, we modulate the endothelial glycocalyx, resulting in a plethora of organ damage. In this chapter, we explore the development of glomerular and cardiac dysfunction and narrow this down to a loss of angiopoietin-1 signaling.

The final chapter, **chapter 7**, provides a summary and discussion of this thesis including future perspectives.

References

1. Klitzman B, Duling BR. Microvascular hematocrit and red cell flow in resting and contracting striated muscle. The American journal of physiology. 1979;237(4):H481-90.
2. Weinbaum S, Tarbell JM, Damiano ER. The structure and function of the endothelial glycocalyx layer. Annual review of biomedical engineering. 2007;9:121-67.
3. Potter DR, Damiano ER. The hydrodynamically relevant endothelial cell glycocalyx observed in vivo is absent in vitro. Circulation research. 2008;102(7):770-6.
4. Gouverneur M, Berg B, Nieuwdorp M, Stroes E, Vink H. Vasculoprotective properties of the endothelial glycocalyx: effects of fluid shear stress. Journal of internal medicine. 2006;259(4):393-400.
5. Singh A, Satchell SC, Neal CR, McKenzie EA, Tooke JE, Mathieson PW. Glomerular endothelial glycocalyx constitutes a barrier to protein permeability. Journal of the American Society of Nephrology : JASN. 2007;18(11):2885-93.
6. van den Berg BM, Vink H, Spaan JA. The endothelial glycocalyx protects against myocardial edema. Circulation research. 2003;92(6):592-4.
7. van den Berg BM, Spaan JA, Vink H. Impaired glycocalyx barrier properties contribute to enhanced intimal low-density lipoprotein accumulation at the carotid artery bifurcation in mice. Pflugers Archiv : European journal of physiology. 2009;457(6):1199-206.
8. Florian JA, Kosky JR, Ainslie K, Pang Z, Dull RO, Tarbell JM. Heparan sulfate proteoglycan is a mechanosensor on endothelial cells. Circulation research. 2003;93(10):e136-42.
9. Weinbaum S, Zhang X, Han Y, Vink H, Cowin SC. Mechanotransduction and flow across the endothelial glycocalyx. Proceedings of the National Academy of Sciences of the United States of America. 2003;100(13):7988-95.
10. Pahakis MY, Kosky JR, Dull RO, Tarbell JM. The role of endothelial glycocalyx components in mechanotransduction of fluid shear stress. Biochemical and biophysical research communications. 2007;355(1):228-33.
11. Tarbell JM, Ebong EE. The endothelial glycocalyx: a mechano-sensor and -transducer. Science signaling. 2008;1(40):pt8.
12. Constantinescu AA, Vink H, Spaan JA. Endothelial cell glycocalyx modulates immobilization of leukocytes at the endothelial surface. Arteriosclerosis, thrombosis, and vascular biology. 2003;23(9):1541-7.
13. Rops AL, van den Hoven MJ, Baselmans MM, Lensen JF, Wijnhoven TJ, van den Heuvel LP, et al. Heparan sulfate domains on cultured activated glomerular endothelial cells mediate leukocyte trafficking. Kidney international. 2008;73(1):52-62.
14. Mulivor AW, Lipowsky HH. Role of glycocalyx in leukocyte-endothelial cell adhesion. American journal of physiology Heart and circulatory physiology. 2002;283(4):H1282-91.
15. Chappell D, Dorfler N, Jacob M, Rehm M, Welsch U, Conzen P, et al. Glycocalyx protection reduces leukocyte adhesion after ischemia/reperfusion. Shock. 2010;34(2):133-9.
16. Reitsma S, Oude Egbrink MG, Heijnen VV, Megens RT, Engels W, Vink H, et al. Endothelial glycocalyx thickness and platelet-vessel wall interactions during atherogenesis. Thrombosis and haemostasis. 2011;106(5):939-46.
17. Vink H, Constantinescu AA, Spaan JA. Oxidized lipoproteins degrade the endothelial surface layer : implications for platelet-endothelial cell adhesion. Circulation. 2000;101(13):1500-2.
18. Reitsma S, Slaaf DW, Vink H, van Zandvoort MA, oude Egbrink MG. The endothelial glycocalyx: composition, functions, and visualization. Pflugers Archiv : European journal of physiology. 2007;454(3):345-59.
19. Esko JD, Selleck SB. Order out of chaos: assembly of ligand binding sites in heparan sulfate. Annual review of biochemistry. 2002;71(1):435-71.
20. Uchimura K, Morimoto-Tomita M, Bistrup A, Li J, Lyon M, Gallagher J, et al. HSulf-2, an extracellular endoglucosamine-6-sulfatase, selectively mobilizes heparin-bound growth factors and chemokines: effects on VEGF, FGF-1, and SDF-1. BMC biochemistry. 2006;7(1):2.
21. Rops AL, van der Vlag J, Lensen JF, Wijnhoven TJ, van den Heuvel LP, van Kuppevelt TH, et al. Hepa-

ran sulfate proteoglycans in glomerular inflammation. Kidney international. 2004;65(3):768-85.

22. Esko JD, Lindahl U. Molecular diversity of heparan sulfate. The Journal of clinical investigation. 2001;108(2):169-73.
23. Lensen JF, Rops AL, Wijnhoven TJ, Hafmans T, Feitz WF, Oosterwijk E, et al. Localization and functional characterization of glycosaminoglycan domains in the normal human kidney as revealed by phage display-derived single chain antibodies. Journal of the American Society of Nephrology : JASN. 2005;16(5):1279-88.
24. Maccarana M, Sakura Y, Tawada A, Yoshida K, Lindahl U. Domain structure of heparan sulfates from bovine organs. The Journal of biological chemistry. 1996;271(30):17804-10.
25. Tekotte H, Engel M, Margolis RU, Margolis RK. Disaccharide composition of heparan sulfates: brain, nervous tissue storage organelles, kidney, and lung. Journal of neurochemistry. 1994;62(3):1126-30.
26. van den Born J, van den Heuvel LP, Bakker MA, Veerkamp JH, Assmann KJ, Berden JH. Monoclonal antibodies against the protein core and glycosaminoglycan side chain of glomerular basement membrane heparan sulfate proteoglycan: characterization and immunohistological application in human tissues. The journal of histochemistry and cytochemistry : official journal of the Histochemistry Society. 1994;42(1):89-102.
27. Smits NC, Kurup S, Rops AL, ten Dam GB, Massuger LF, Hafmans T, et al. The heparan sulfate motif (GlcNS6S-IdoA2S)3, common in heparin, has a strict topography and is involved in cell behavior and disease. The Journal of biological chemistry. 2010;285(52):41143-51.
28. Wang L, Fuster M, Sriramarao P, Esko JD. Endothelial heparan sulfate deficiency impairs L-selectin- and chemokine-mediated neutrophil trafficking during inflammatory responses. Nature immunology. 2005;6(9):902-10.
29. Gingis-Velitski S, Zetser A, Kaplan V, Ben-Zaken O, Cohen E, Levy-Adam F, et al. Heparanase uptake is mediated by cell membrane heparan sulfate proteoglycans. The Journal of biological chemistry. 2004;279(42):44084-92.
30. Vlodavsky I, Friedmann Y, Elkin M, Aingorn H, Atzmon R, Ishai-Michaeli R, et al. Mammalian heparanase: gene cloning, expression and function in tumor progression and metastasis. Nature medicine. 1999;5(7):793-802.
31. Wu L, Viola CM, Brzozowski AM, Davies GJ. Structural characterization of human heparanase reveals insights into substrate recognition. Nature structural & molecular biology. 2015;22(12):1016-22.
32. Wilson JC, Laloo AE, Singh S, Ferro V. 1H NMR spectroscopic studies establish that heparanase is a retaining glycosidase. Biochemical and biophysical research communications. 2014;443(1):185-8.
33. Schmidt EP, Yang Y, Janssen WJ, Gandjeva A, Perez MJ, Barthel L, et al. The pulmonary endothelial glycocalyx regulates neutrophil adhesion and lung injury during experimental sepsis. Nature medicine. 2012;18(8):1217.
34. Garsen M, Benner M, Dijkman HB, van Kuppevelt TH, Li JP, Rabelink TJ, et al. Heparanase Is Essential for the Development of Acute Experimental Glomerulonephritis. The American journal of pathology. 2016;186(4):805-15.
35. Laurent TC, Fraser JR. Hyaluronan. FASEB journal : official publication of the Federation of American Societies for Experimental Biology. 1992;6(7):2397-404.
36. Lennon FE, Singleton PA. Hyaluronan regulation of vascular integrity. Am J Cardiovasc Dis. 2011;1(3):200-13.
37. Becker BF, Jacob M, Leipert S, Salmon AH, Chappell D. Degradation of the endothelial glycocalyx in clinical settings: searching for the sheddases. British journal of clinical pharmacology. 2015; Sep;80(3):389-402.
38. Berg vd, BM; Boels, M.G.S.; Avramut, MC; Jansen, E; Meldner, S; Dane, MJC; Vlag, van der, J; Vink, H; Koster, AJ; Zonneveld, van, AJ; Groene, HJ; Koning, de, E; Rabelink, TJ Genetic Deletion of Endothelial Hyaluronan Synthase 2 Results in Glomerular Injury and Albuminuria (Abstract). Journal of the American Society of Nephrology : JASN. 2014;25: 29A:TH-OR119.
39. Campo GM, Avenoso A, Micali A, Nastasi G, Squadrito F, Altavilla D, et al. High-molecular weight hyaluronan reduced renal PKC activation in genetically diabetic mice. Biochimica et biophysica acta. 2010;1802(11):1118-30.
40. Colombaro V, Decleves AE, Jadot I, Voisin V, Giordano L, Habsch I, et al. Inhibition of hyaluronan

is protective against renal ischaemia-reperfusion injury. Nephrology, dialysis, transplantation : official publication of the European Dialysis and Transplant Association - European Renal Association. 2013;28(10):2484-93.

41. Kashima Y, Takahashi M, Shiba Y, Itano N, Izawa A, Koyama J, et al. Crucial role of hyaluronan in neointimal formation after vascular injury. PloS one. 2013;8(3):e58760.
42. Molema G, Aird WC. Vascular heterogeneity in the kidney. Seminars in nephrology. 2012;32(2):145-55.
43. Rosenberg RD, Aird WC. Vascular-bed--specific hemostasis and hypercoagulable states. The New England journal of medicine. 1999;340(20):1555-64.
44. Aird WC. Vascular bed-specific hemostasis: role of endothelium in sepsis pathogenesis. Critical care medicine. 2001;29(7 Suppl):S28-34; discussion S-5.
45. Gerritsen ME. Functional heterogeneity of vascular endothelial cells. Biochemical pharmacology. 1987;36(17):2701-11.
46. Stevens T, Rosenberg R, Aird W, Quertermous T, Johnson FL, Garcia JG, et al. NHLBI workshop report: endothelial cell phenotypes in heart, lung, and blood diseases. American journal of physiology Cell physiology. 2001;281(5):C1422-33.
47. Dane MJ, van den Berg BM, Avramut MC, Faas FG, van der Vlag J, Rops AL, et al. Glomerular endothelial surface layer acts as a barrier against albumin filtration. The American journal of pathology. 2013;182(5):1532-40.
48. Raats CJ, van den Born J, Bakker MA, Oppers-Walgreen B, Pisa BJ, Dijkman HB, et al. Expression of agrin, dystroglycan, and utrophin in normal renal tissue and in experimental glomerulopathies. The American journal of pathology. 2000;156(5):1749-65.
49. Doyonnas R, Kershaw DB, Duhme C, Merkens H, Chelliah S, Graf T, et al. Anuria, omphalocele, and perinatal lethality in mice lacking the CD34-related protein podocalyxin. The Journal of experimental medicine. 2001;194(1):13-27.
50. van den Born J, van den Heuvel LP, Bakker MA, Veerkamp JH, Assmann KJ, Weening JJ, et al. Distribution of GBM heparan sulfate proteoglycan core protein and side chains in human glomerular diseases. Kidney international. 1993;43(2):454-63.
51. van den Hoven MJ, Rops AL, Bakker MA, Aten J, Rutjes N, Roestenberg P, et al. Increased expression of heparanase in overt diabetic nephropathy. Kidney international. 2006;70(12):2100-8.
52. Goldberg S, Harvey SJ, Cunningham J, Tryggvason K, Miner JH. Glomerular filtration is normal in the absence of both agrin and perlecan-heparan sulfate from the glomerular basement membrane. Nephrology, dialysis, transplantation : official publication of the European Dialysis and Transplant Association - European Renal Association. 2009;24(7):2044-51.
53. Friden V, Oveland E, Tenstad O, Ebefors K, Nystrom J, Nilsson UA, et al. The glomerular endothelial cell coat is essential for glomerular filtration. Kidney international. 2011;79(12):1322-30.
54. Chang RL, Ueki IF, Troy JL, Deen WM, Robertson CR, Brenner BM. Permselectivity of the glomerular capillary wall to macromolecules. II. Experimental studies in rats using neutral dextran. Biophys J. 1975;15(9):887-906.
55. Haraldsson B, Nystrom J, Deen WM. Properties of the glomerular barrier and mechanisms of proteinuria. Physiological reviews. 2008;88(2):451-87.
56. Siddiqi FS, Advani A. Endothelial-podocyte crosstalk: the missing link between endothelial dysfunction and albuminuria in diabetes. Diabetes. 2013;62(11):3647-55.
57. Lemkes BA, Nieuwdorp M, Hoekstra JB, Holleman F. The glycocalyx and cardiovascular disease in diabetes: should we judge the endothelium by its cover? Diabetes technology & therapeutics. 2012;14 Suppl 1:S3-10.
58. Noble MI, Drake-Holland AJ, Vink H. Hypothesis: arterial glycocalyx dysfunction is the first step in the atherothrombotic process. QJM : monthly journal of the Association of Physicians. 2008;101(7):513-8.
59. Mulivor AW, Lipowsky HH. Inflammation- and ischemia-induced shedding of venular glycocalyx. American journal of physiology Heart and circulatory physiology. 2004;286(5):H1672-80.
60. Rubio-Gayosso I, Platts SH, Duling BR. Reactive oxygen species mediate modification of glycocalyx during ischemia-reperfusion injury. American

journal of physiology Heart and circulatory physiology. 2006;290(6):H2247-56.

61. Rehm M, Bruegger D, Christ F, Conzen P, Thiel M, Jacob M, et al. Shedding of the endothelial glycocalyx in patients undergoing major vascular surgery with global and regional ischemia. Circulation. 2007;116(17):1896-906.
62. van den Berg B, Vink H. Glycocalyx perturbation: cause or consequence of damage to the vasculature? American journal of physiology Heart and circulatory physiology. 2006;290(6):H2174-5.
63. Noris M, Remuzzi G. Atypical hemolytic-uremic syndrome. The New England journal of medicine. 2009;361(17):1676-87.
64. Besbas N, Karpman D, Landau D, Loirat C, Proesmans W, Remuzzi G, et al. A classification of hemolytic uremic syndrome and thrombotic thrombocytopenic purpura and related disorders. Kidney international. 2006;70(3):423-31.
65. Constantinescu AR, Bitzan M, Weiss LS, Christen E, Kaplan BS, Cnaan A, et al. Non-enteropathic hemolytic uremic syndrome: causes and short-term course. American journal of kidney diseases : the official journal of the National Kidney Foundation. 2004;43(6):976-82.
66. Westra D, Wetzels JF, Volokhina EB, van den Heuvel LP, van de Kar NC. A new era in the diagnosis and treatment of atypical haemolytic uraemic syndrome. The Netherlands journal of medicine. 2012;70(3):121-9.
67. Olie KH, Goodship TH, Verlaak R, Florquin S, Groothoff JW, Strain L, et al. Posttransplantation cytomegalovirus-induced recurrence of atypical hemolytic uremic syndrome associated with a factor H mutation: successful treatment with intensive plasma exchanges and ganciclovir. American journal of kidney diseases : the official journal of the National Kidney Foundation. 2005;45(1):e12-5.
68. Berner R, Krause MF, Gordjani N, Zipfel PF, Boehm N, Krueger M, et al. Hemolytic uremic syndrome due to an altered factor H triggered by neonatal pertussis. Pediatr Nephrol. 2002;17(3):190-2.
69. Acosta J, Hettinga J, Fluckiger R, Krumrei N, Goldfine A, Angarita L, et al. Molecular basis for a link between complement and the vascular complications of diabetes. P Natl Acad Sci USA. 2000;97(10):5450-5.
70. Cheng Y, Gao M. The effect of glycation of CD59 on complement-mediated cytolysis. Cellular & molecular immunology. 2005;2(4):313-7.
71. George JN, Vesely SK, Terrell DR. The Oklahoma Thrombotic Thrombocytopenic Purpura-Hemolytic Uremic Syndrome (TTP-HUS) Registry: a community perspective of patients with clinically diagnosed TTP-HUS. Seminars in hematology. 2004;41(1):60-7.
72. Jokiranta TS, Zipfel PF, Fremeaux-Bacchi V, Taylor CM, Goodship TJ, Noris M. Where next with atypical hemolytic uremic syndrome? Molecular immunology. 2007;44(16):3889-900.
73. Esparza-Gordillo J, Goicoechea de Jorge E, Buil A, Carreras Berges L, Lopez-Trascasa M, Sanchez-Corral P, et al. Predisposition to atypical hemolytic uremic syndrome involves the concurrence of different susceptibility alleles in the regulators of complement activation gene cluster in 1q32. Human molecular genetics. 2005;14(5):703-12.
74. Fremeaux-Bacchi V, Kemp EJ, Goodship JA, Dragon-Durey MA, Strain L, Loirat C, et al. The development of atypical haemolytic-uraemic syndrome is influenced by susceptibility factors in factor H and membrane cofactor protein: evidence from two independent cohorts. Journal of medical genetics. 2005;42(11):852-6.
75. Kerr H, Richards A. Complement-mediated injury and protection of endothelium: lessons from atypical haemolytic uraemic syndrome. Immunobiology. 2012;217(2):195-203.
76. Kavanagh D, Goodship T. Genetics and complement in atypical HUS. Pediatric nephrology. 2010;25(12):2431-42.
77. Eremina V, Jefferson JA, Kowalewska J, Hochster H, Haas M, Weisstuch J, et al. VEGF inhibition and renal thrombotic microangiopathy. The New England journal of medicine. 2008;358(11):1129-36.
78. Richards A. Glomerular endothelial microvascular heterogeneity and response to cytokines predispose to the development of atypical HUS. Mol Immunol. 2011;48(14):1732-.
79. Pangburn MK. Cutting edge: Localization of the host recognition functions of complement factor H at the carboxyl-terminal: Implications for hemolytic uremic syndrome. J Immunol. 2002;169(9):4702-6.

80. Zipfel PF, Heinen S, Jozsi M, Skerka C. Complement and diseases: defective alternative pathway control results in kidney and eye diseases. Molecular immunology. 2006;43(1-2):97-106.

81. Morgan HP, Schmidt CQ, Guariento M, Blaum BS, Gillespie D, Herbert AP, et al. Structural basis for engagement by complement factor H of C3b on a self surface. Nature structural & molecular biology. 2011;18(4):463-70.

82. Ripoche J, Day AJ, Willis AC, Belt KT, Campbell RD, Sim RB. Partial characterization of human complement factor H by protein and cDNA sequencing: homology with other complement and non-complement proteins. Bioscience reports. 1986;6(1):65-72.

83. Lehtinen MJ, Rops AL, Isenman DE, van der Vlag J, Jokiranta TS. Mutations of factor H impair regulation of surface-bound C3b by three mechanisms in atypical hemolytic uremic syndrome. The Journal of biological chemistry. 2009;284(23):15650-8.

84. Loeven MA, Rops AL, Lehtinen MJ, van Kuppevelt TH, Daha MR, Smith RJ, et al. Mutations in Complement Factor H Impair Alternative Pathway Regulation on Mouse Glomerular Endothelial Cells in Vitro. The Journal of biological chemistry. 2016;291(10):4974-81.

85. Richards A, Buddles MR, Donne RL, Kaplan BS, Kirk E, Venning MC, et al. Factor H mutations in hemolytic uremic syndrome cluster in exons 18-20, a domain important for host cell recognition. American journal of human genetics. 2001;68(2):485-90.

86. Kazatchkine MD, Fearon DT, Silbert JE, Austen KF. Surface-associated heparin inhibits zymosan-induced activation of the human alternative complement pathway by augmenting the regulatory action of the control proteins on particle-bound C3b. The Journal of experimental medicine. 1979;150(5):1202-15.

87. Schmidt CQ, Herbert AP, Kavanagh D, Gandy C, Fenton CJ, Blaum BS, et al. A new map of glycosaminoglycan and C3b binding sites on factor H. Journal of immunology. 2008;181(4):2610-9.

88. Meri S, Pangburn MK. Regulation of alternative pathway complement activation by glycosaminoglycans: specificity of the polyanion binding site on factor H. Biochemical and biophysical research communications. 1994;198(1):52-9.

89. Manuelian T, Hellwage J, Meri S, Caprioli J, Noris M, Heinen S, et al. Mutations in factor H reduce binding affinity to C3b and heparin and surface attachment to endothelial cells in hemolytic uremic syndrome. The Journal of clinical investigation. 2003;111(8):1181-90.

90. Ince C. The central role of renal microcirculatory dysfunction in the pathogenesis of acute kidney injury. Nephron Clin Pract. 2014;127(1-4):124-8.

91. Steppan J, Hofer S, Funke B, Brenner T, Henrich M, Martin E, et al. Sepsis and major abdominal surgery lead to flaking of the endothelial glycocalix. The Journal of surgical research. 2011;165(1):136-41.

92. Chelazzi C, Villa G, Mancinelli P, De Gaudio AR, Adembri C. Glycocalyx and sepsis-induced alterations in vascular permeability. Critical care. 2015;19(1):741.

93. Schmidt EP, Overdier KH, Sun X, Lin L, Liu X, Yang Y, et al. Urinary Glycosaminoglycans Predict Outcomes in Septic Shock and Acute Respiratory Distress Syndrome. Am J Respir Crit Care Med. 2016;194(4):439-49.

94. Johansen ME, Johansson PI, Ostrowski SR, Bestle MH, Hein L, Jensen AL, et al. Profound endothelial damage predicts impending organ failure and death in sepsis. Seminars in thrombosis and hemostasis. 2015;41(1):16-25.

95. Neves FM, Meneses GC, Sousa NE, Menezes RR, Parahyba MC, Martins AM, et al. Syndecan-1 in Acute Decompensated Heart Failure--Association With Renal Function and Mortality. Circ J. 2015;79(7):1511-9.

96. Gluba A, Banach M, Hannam S, Mikhailidis DP, Sakowicz A, Rysz J. The role of Toll-like receptors in renal diseases. Nature reviews Nephrology. 2010;6(4):224-35.

97. Lygizos MI, Yang Y, Altmann CJ, Okamura K, Hernando AA, Perez MJ, et al. Heparanase mediates renal dysfunction during early sepsis in mice. Physiological reports. 2013;1(6):e00153.

98. U.S. Renal Data System (2012) Annual Data Report: Atlas of Chronic Kidney Disease and End-Stage Renal Disease in the United States. National Institute of Diabetes and Digestive and Kidney Diseases, Bethesda, MD., 2012.

99. Zuurbier CJ, Demirci C, Koeman A, Vink H, Ince C. Short-term hyperglycemia increases endothelial glycocalyx permeability and acutely decreases

lineal density of capillaries with flowing red blood cells. J Appl Physiol (1985). 2005;99(4):1471-6.

100. Yan SF, Ramasamy R, Schmidt AM. Mechanisms of disease: advanced glycation end-products and their receptor in inflammation and diabetes complications. Nature clinical practice Endocrinology & metabolism. 2008;4(5):285-93.

101. Singh A, Ramnath RD, Foster RR, Wylie EC, Friden V, Dasgupta I, et al. Reactive oxygen species modulate the barrier function of the human glomerular endothelial glycocalyx. PloS one. 2013;8(2):e55852.

102. Henry CB, Duling BR. TNF-alpha increases entry of macromolecules into luminal endothelial cell glycocalyx. American journal of physiology Heart and circulatory physiology. 2000;279(6):H2815-23.

103. Axelsson J, Xu D, Kang BN, Nussbacher JK, Handel TM, Ley K, et al. Inactivation of heparan sulfate 2-O-sulfotransferase accentuates neutrophil infiltration during acute inflammation in mice. Blood. 2012;120(8):1742-51.

104. Xu D, Olson J, Cole JN, van Wijk XM, Brinkmann V, Zychlinsky A, et al. Heparan Sulfate Modulates Neutrophil and Endothelial Function in Antibacterial Innate Immunity. Infection and immunity. 2015;83(9):3648-56.

105. Shafat I, Ilan N, Zoabi S, Vlodavsky I, Nakhoul F. Heparanase levels are elevated in the urine and plasma of type 2 diabetes patients and associate with blood glucose levels. PloS one. 2011;6(2):e17312.

106. Rabelink TJ, de Zeeuw D. The glycocalyx--linking albuminuria with renal and cardiovascular disease. Nature reviews Nephrology. 2015;11(11):667-76.

107. Goldberg R, Rubinstein AM, Gil N, Hermano E, Li JP, van der Vlag J, et al. Role of heparanase-driven inflammatory cascade in pathogenesis of diabetic nephropathy. Diabetes. 2014;63(12):4302-13.

108. Abboud-Jarrous G, Atzmon R, Peretz T, Palermo C, Gadea BB, Joyce JA, et al. Cathepsin L is responsible for processing and activation of proheparanase through multiple cleavages of a linker segment. The Journal of biological chemistry. 2008;283(26):18167-76.

109. Wang F, Wang Y, Zhang D, Puthanveetil P, Johnson JD, Rodrigues B. Fatty acid-induced nuclear translocation of heparanase uncouples glucose metabolism in endothelial cells. Arteriosclerosis, thrombosis, and vascular biology. 2012;32(2):406-14.

110. Simeonovic CJ, Ziolkowski AF, Wu Z, Choong FJ, Freeman C, Parish CR. Heparanase and autoimmune diabetes. Frontiers in immunology. 2013;4:471.

111. Fiebiger E, Maehr R, Villadangos J, Weber E, Erickson A, Bikoff E, et al. Invariant chain controls the activity of extracellular cathepsin L. The Journal of experimental medicine. 2002;196(9):1263-9.

112. Bogdani M, Johnson PY, Potter-Perigo S, Nagy N, Day AJ, Bollyky PL, et al. Hyaluronan and Hyaluronan Binding Proteins Accumulate in both Human Type 1 Diabetic Islets and Lymphoid Tissues and Associate with Inflammatory Cells in Insulitis. Diabetes. 2014; Aug;63(8):2727-43.

113. Garsen M, Rops AL, Dijkman H, Willemsen B, van Kuppevelt TH, Russel FG, et al. Cathepsin L is crucial for the development of early experimental diabetic nephropathy. Kidney international. 2016; Nov;90(5):1012-1022.

114. Ikegami-Kawai M, Suzuki A, Karita I, Takahashi T. Increased hyaluronidase activity in the kidney of streptozotocin-induced diabetic rats. J Biochem. 2003;134(6):875-80.

115. Chajara A, Raoudi M, Delpech B, Leroy M, Basuyau JP, Levesque H. Circulating hyaluronan and hyaluronidase are increased in diabetic rats. Diabetologia. 2000;43(3):387-8.

116. Singh A, Friden V, Dasgupta I, Foster RR, Welsh GI, Tooke JE, et al. High glucose causes dysfunction of the human glomerular endothelial glycocalyx. American journal of physiology Renal physiology. 2011;300(1):F40-8.

117. Lauver DA, Lucchesi BR. Sulodexide: A renewed interest in this glycosaminoglycan. Cardiovasc Drug Rev. 2006;24(3-4):214-26.

118. Ferro V, Liu L, Johnstone KD, Wimmer N, Karoli T, Handley P, et al. Discovery of PG545: a highly potent and simultaneous inhibitor of angiogenesis, tumor growth, and metastasis. Journal of medicinal chemistry. 2012;55(8):3804-13.

119. Liang XJ, Yuan L, Hu J, Yu HH, Li T, Lin SF, et al. Phosphomannopentaose sulfate (PI-88) suppresses angiogenesis by downregulating heparanase and vascular endothelial growth factor in an

oxygen-induced retinal neovascularization animal model. Molecular vision. 2012;18:1649-57.

120. Karon J, Polubinska A, Antoniewicz AA, Suminska-Jasinska K, Breborowicz A. Anti-inflammatory effect of sulodexide during acute peritonitis in rats. Blood purification. 2007;25(5-6):510-4.
121. Ofosu FA. Pharmacological actions of sulodexide. Seminars in thrombosis and hemostasis. 1998;24(2):127-38.
122. Smith RJ, Alexander J, Barlow PN, Botto M, Cassavant TL, Cook HT, et al. New approaches to the treatment of dense deposit disease. Journal of the American Society of Nephrology : JASN. 2007;18(9):2447-56.
123. Lauver DA, Booth EA, White AJ, Poradosu E, Lucchesi BR. Sulodexide attenuates myocardial ischemia/reperfusion injury and the deposition of C-reactive protein in areas of infarction without affecting hemostasis. The Journal of pharmacology and experimental therapeutics. 2005;312(2):794-800.
124. Skrha J, Perusicova J, Pont'uch P, Oksa A. Glycosaminoglycan sulodexide decreases albuminuria in diabetic patients. Diabetes research and clinical practice. 1997;38(1):25-31.
125. Lambers Heerspink HJ, Fowler MJ, Volgi J, Reutens AT, Klein I, Herskovits TA, et al. Rationale for and study design of the sulodexide trials in Type 2 diabetic, hypertensive patients with microalbuminuria or overt nephropathy. Diabetic medicine : a journal of the British Diabetic Association. 2007;24(11):1290-5.
126. Packham DK, Wolfe R, Reutens AT, Berl T, Heerspink HL, Rohde R, et al. Sulodexide Fails to Demonstrate Renoprotection in Overt Type 2 Diabetic Nephropathy. Journal of the American Society of Nephrology. 2012;23(1):123-30.
127. Rossini M, Naito T, Yang H, Freeman M, Donnert E, Ma LJ, et al. Sulodexide ameliorates early but not late kidney disease in models of radiation nephropathy and diabetic nephropathy. Nephrology, dialysis, transplantation : official publication of the European Dialysis and Transplant Association - European Renal Association. 2010;25(6):1803-10.
128. Rabelink TJ, de Boer HC, van Zonneveld AJ. Endothelial activation and circulating markers of endothelial activation in kidney disease. Nature reviews Nephrology. 2010;6(7):404-14.
129. Chen XL, Varner SE, Rao AS, Grey JY, Thomas S, Cook CK, et al. Laminar flow induction of antioxidant response element-mediated genes in endothelial cells. A novel anti-inflammatory mechanism. The Journal of biological chemistry. 2003;278(2):703-11.
130. Mochizuki S, Vink H, Hiramatsu O, Kajita T, Shigeto F, Spaan JA, et al. Role of hyaluronic acid glycosaminoglycans in shear-induced endothelium-derived nitric oxide release. American journal of physiology Heart and circulatory physiology. 2003;285(2):H722-6.
131. Verhaar MC, Strachan FE, Newby DE, Cruden NL, Koomans HA, Rabelink TJ, et al. Endothelin-A receptor antagonist-mediated vasodilatation is attenuated by inhibition of nitric oxide synthesis and by endothelin-B receptor blockade. Circulation. 1998;97(8):752-6.
132. Boels MG, Avramut MC, Koudijs A, Dane MJ, Lee DH, van der Vlag J, et al. Atrasentan Reduces Albuminuria by Restoring the Glomerular Endothelial Glycocalyx Barrier in Diabetic Nephropathy. Diabetes. 2016;65(8):2429-39.

Chapter 2

Atrasentan reduces albuminuria by restoring the glomerular endothelial glycocalyx barrier in diabetic nephropathy

Diabetes 65(8):2429-2439, 2016

Margien G.S. Boels, M. Cristina Avramut, Angela Koudijs, Martijn J.C. Dane, Dae Hyun Lee, Johan van der Vlag, Abraham J. Koster, Anton Jan van Zonneveld, Ernst van Faassen, Hermann-Josef Gröne, Bernard M. van den Berg, Ton J. Rabelink

Abstract

The selective endothelin A receptor antagonist, atrasentan, has been shown to reduce albuminuria in type 2 diabetes mellitus. We previously showed that the structural integrity of a glomerular endothelial glycocalyx is required to prevent albuminuria. Therefore we tested in diabetic apolipoprotein E deficient mice, the potential of atrasentan to stabilize the endothelial glycocalyx in relation to its anti-albuminuric effects. Treatment with atrasentan (7.5mg/kg/day) for four weeks, reduced urinary albumin-creatinine ratios with 26.0±6.5% ($p<0.01$) in streptozotocin induced diabetic apoE KO mice on an atherogenic diet, without changes in gross glomerular morphology, systemic blood pressure and blood glucose levels. Endothelial cationic ferritin surface coverage, with large-scale digital transmission electron microscopy revealed that atrasentan treatment increases glycocalyx coverage from 40.7±3.2% in diabetic apoE KO mice to 81.0±12.5%, ($p<0.05$). This restoration is accompanied by increased renal nitric oxide levels, reduced expression of glomerular heparanase and a marked shift in the balance from M1 to M2 glomerular macrophages. *In vitro* experiments of endothelial cells exposed to laminar flow and co-cultured with pericytes, confirmed that atrasentan reduced endothelial heparanase expression and increased glycocalyx thickness in the presence of a diabetic milieu. Together these data point towards a role for restoration of endothelial function and tissue homeostasis in the anti-albuminuric effects of atrasentan, and provide a mechanistic explanation for the clinical observations on lowering of albuminuria with atrasentan in diabetic nephropathy.

Introduction

End-stage renal disease is inevitable in a majority of patients with diabetic nephropathy (1), despite optimal blood pressure treatment using drugs that interfere with the renin-angiotensin system (RAS). Therefore, there is a great need for additional strategies to slow the progression of chronic kidney disease in patients with diabetic nephropathy. One such strategy involves interaction with the endothelin (ET) system. Numerous studies involving experimental animal models have implicated ET in the pathogenesis of diabetic nephropathy (2). Moreover, clinical studies show promise for ET receptor antagonists in the treatment of diabetic nephropathy (3-6). This is particularly true for selective ET_A receptor blockers, as ET_A receptor signaling appears to be involved in key renal pathophysiological processes such as the inflammatory response of renal epithelium to albumin (7), while the associated concomitant ET_B receptor stimulation can restore endothelial dysfunction by inducing endothelial nitric oxide production activity (8-10). Because actual loss of renal function is a late indicator of disease, albuminuria has been put forward as a sensitive surrogate marker for ongoing renal injury in diabetic nephropathy. In this respect ET_A receptor blockers appear to have a striking anti-proteinuric effect, which cannot be fully explained by blood pressure lowering (11).

We and others previously demonstrated that maintenance of the structural integrity of a glomerular endothelial glycocalyx is crucial to prevent albuminuria (12, 13). The endothelial glycocalyx is a gel-like polyanionic carbohydrate layer that covers endothelial cells. The glomerular fenestrae appear to be densely filled with the carbohydrate polymer hyaluronan, and its enzymatic removal greatly enhances albumin passage across the glomerular filtration barrier (13). Increased activity of both heparanase and hyaluronidase reduces the dimensions of the glomerular endothelial glycocalyx and has long been recognized in diabetic nephropathy (14). Also increased circulating levels of hyaluronan have been measured in patients with diabetic nephropathy (15).

We therefore hypothesized that selective ET_A receptor blockade confers antialbuminuric and renoprotective effects by restoring the endothelial glycocalyx barrier against albumin filtration. To this end we examined the renoprotective effects of orally administrated atrasentan, a selective ET_A receptor blocker (16), in a diabetic nephropathy model, using apolipoprotein E knockout (apoE KO) mice. This model combines renal and vascular injury with both hyperglycemia and hyperlipidemia, thus mimicking features of diabetic nephropathy (17, 18); moreover, it has been shown that the model can be used for pharmacological intervention studies, including studies of ET blockers (17). In this study we show that atrasentan improves endothelial function and results in almost complete restoration of the endothelial glycocalyx, while it concomitantly reduces albuminuria. *In vitro* analysis shows that this effect of atrasentan can be mediated through the reduction of endothelial heparanase expression.

Research design and methods

Diabetic ApoE KO mouse model

Six-weeks-old male apoE KO mice (The Jackson Laboratory, Bar Harbor, ME) were rendered diabetic by intraperitoneal injections of streptozotocin (STZ) (Sigma-Aldrich, St Louis, MO, USA) in citrate buffer at a dose of 60 mg/kg for 5 consecutive days (19, 20). Control apoE KO mice received citrate buffer alone, were fed a diet of chow and used for baseline measurements. Only animals with average blood glucose concentrations >20 mmol/L 2 weeks after the induction of diabetes were included in the study. Twelve weeks after induction of diabetes, mice were further randomized into two groups: 1) nontreated mice and 2) mice treated with atrasentan (7.5 mg/kg/day via drinking water; AbbVie, North Chicago, IL) for 4 weeks. Concentrations of atrasentan in drinking water were adjusted weekly, based on the preceding intake to adjust for the short half-life of atrasentan in mice. All diabetic animals had free access to cholesterol enriched (0.15%) chow (Technilab-BMI, Someren, the Netherlands). Animal experiments were approved by the Ethical Committee on Animal Care and Experimentation at the Leiden University Medical Center (Leiden, the Netherlands). All work with animals was performed in compliance with the Dutch government's guidelines.

Blood glucose concentrations were measured using a glucose meter (Accu-Chek, Roche, Basel, Switzerland). When concentrations exceeded 25 mmol/L, mice were treated with 1-2 U insulin (Lantus, Aventis Pharmaceuticals, Bridgewater, NJ) for a maximum of three times per week. Systolic blood pressure was assessed using CODA noninvasive tail cuff system (Kent Scientific, Torrington, CT) in conscious mice at start, middle and end of treatment. Animals were habituated to the device before measurements.

Urine collection and analyses

Urine was collected (via the 24-hours test) at the start of the study period and after 2 and 4 weeks of treatment. Mice were acclimatized to metabolic cages, after which 24-hours urine was collected. Urine was centrifuged to remove debris and stored at -20°C. Albumin concentrations were quantified with Rocket immunoelectrophoresis, using the protocol described by Tran et al (21), with modifications. Urine creatinine concentrations were determined by the Jaffé method using 0.13% picric acid (Sigma-Aldrich), and were quantified using a creatinine standard set (Sigma-Aldrich). Excretion of 24-hour urinary kidney injury molecule-1 (KIM-1) was determined with an ELISA kit (R&D Systems, Minneapolis, MN). Optical densities for creatinine and KIM-1 were measured with an ELISA plate reader.

Determination of glomerular endothelial glycocalyx coverage

We indentified glomerular areas of the endothelial glycocalyx in two ways. First, for electron microscopic visualisztion of the glycocalyx, three mice per group were anesthetized (intraperitoneally) with a cocktail of midazolam (1 mg/mL, Roche), dexmedetomidine (50 µg/mL, Orion Corporation, Espoo, Finland), and fentanyl (10 µg/mL, Hameln Pharmaceuticals GmbH,

Hameln, Germany) in water. The abdominal aorta was exposed and cannulated adjacent to the left renal artery. The right renal artery was ligated at the renal stalk. The left kidney was perfused with 0.5% BSA and 5 U/mL heparin in 5 mL HEPES-buffered salt solution (HBSS) at 2 mL/minute to remove blood, followed by 2 mL of cationic ferritin (horse spleen, 2.5 mg/mL, Electron Microscopy Sciences, Fort Washington, PA) in HBSS alone at 2 mL/minute. This kidney was excised, and the capsule was removed and stored in a fixative (1.5% glutaraldehyde + 1% paraformaldehyde in 0.1 M sodium-cacodylate buffered solution [pH 7.4]) overnight at 4˚C. The kidney was subsequently sectioned in 180 µm thick sections, rinsed with 0.1 M sodium-cacodylate buffered solution, and post-fixed in 1% osmium tetroxide and 1.5% potassium ferrocyanide in ultrapure water. Samples were dehydrated, stained and embedded in Epon LX-112. Sections (100 nm) were mounted on copper slot grids and further stained with 7% uranyl acetate and Reynold's lead citrate. Transmission electron microscopy (TEM) data were collected at an acceleration voltage of 120 kV on a Tecnai G^2 Spirit BioTWIN microscope (FEI, Eindhoven, the Netherlands), equipped with an FEI Eagle charge-coupled device camera. To create an overview of the glomerulus, albeit with a high resolution, images with x18,500 magnification at the detector plane, corresponding to a 1.2 nm pixel size at the specimen level, were automatically combined with stitching software (22). The resulting large digital image provides an overview of the glomerulus, which one can zoom in to view high detail, allowing for quantitative analyses. The polyanionic glycocalyx on the surface of endothelial cells can be visualized in TEM through the binding of electron-dense cationic substances such as cationic ferritin to it (23). Within the stitches, individual capillary loops were captured and glycocalyx coverage was quantified in 6 - 11 capillary loops in three glomeruli per mouse (n = 3/group). The percentage of positive coverage of the endothelium with cationic ferritin was determined using an automatic grid overlay in the public domain (ImageJ version 1.46; National Institutes of Health, Bethesda, MD). For every glomerulus, a minimum of 80 crosshairs were at the intersection of the endothelium and scored for percentage positive.

Second, endothelial glycocalyx coverage was also determined using fluorescently labeled lectin, as described previously (13). In short, 100 µm sections of nonperfused kidneys of three mice per group were incubated with 10 mg/mL of fluorescently labelled *Lycopersicon esculentum* (LEA) to visualize the glycocalyx, in combination with 5 mg/mL monoclonal mouse antimouse CD31 antibody (Santa Cruz Biotechnology, Santa Cruz, CA) to identify the endothelial cell membrane. Next, slices were incubated with 10 mg/mL Alexa Fluor-568 conjugated goat antimouse IgG (Molecular Probes, Grand Island, NY) and Hoechst 33528 (Sigma-Aldrich, 1/1,000) for 1 hour. The amount of endothelial glycocalyx was quantified by calculating the distance from the peak of the CD31 signal to the half-width of the intraluminal lectin signal along a line of interest, using intensity profiles in ImageJ software.

Immunohistochemistry and morphometric analysis

Eight mice per treatment group were anesthetized by isoflurane inhalation and perfused via the left ventricle with HBSS containing 0.5% BSA and 5 U/mL heparin to remove blood. Kidneys

were excised, and cut in half after removing the capsules. One half was fixed in paraformaldehyde solution (4%) for 1 - 2 hours, then was embedded in paraffin for periodic acid Schiff and trichrome staining and podocyte and macrophage quantification. The other half was snap-frozen in 2-methylbutane (Sigma-Aldrich) for immunohistochemistry. Frozen kidney sections (4 µm thick) were fixed in acetone for 10 minutes at room temperature. Nonspecific antibody binding was prevented by incubation with normal goat serum (4%) in PBS for 30 minutes. Heparanase expression was detected after overnight incubation with primary antibody (polyclonal rabbit antiheparanase 1.5 µg/mL, InSight Biopharmaceuticals, Rehovot, Israel), followed by goat anti-rabbit IgG-Alexa 594 (1/1,000), for 1 hour, both in blocking buffer. Sections were counterstained with Hoechst (1/1,000) and embedded in Vectashield mounting medium (Vector Laboratories Inc., Burlingame, CA). Cathepsin-L polyclonal antibody (R&D Systems) was incubated overnight, followed by horseradish peroxidase-conjugated secondary antibody and 3,3'-diaminobezidine. Heparanase and cathepsin-L staining was quantified as the percentage of stained area divided by the glomerular area.

Podocytes were quantified after being identified with Wilms' tumor-1 antibody (0.5 µg/mL, Santa Cruz Biotechnology, CA). Macrophages were identified using a rat monoclonal antibody against mouse F4/80 (Abcam, Cambridge, MA) and a rabbit monoclonal anti-CD206 (Abcam). F4/80 recognizes a glycoprotein on the surface of most mouse macrophages (24), whereas CD206 is solely expressed by M2 macrophages (25).

Thickness of the glomerular basement membrane (GBM) was analyzed in the cationic ferritin stained glomeruli of three mice per group, using a similar grid overlay with 15 crosshairs at the intersection of the endothelium where thickness was measured. In every glomerulus eight capillary loops were analyzed for thickness of the GBM.

Nitric oxide determination

Endogenous renal nitric oxide (NO) bioavailability was measured in eight mice per treatment group using an *in vivo* trapping method with iron-diethyldithiocarbamate (Fe^{2+}-DETC) complexes. After anesthesia was induced (intraperitoneally, as previously described), mice were injected consecutively with iron-citrate (subcutaneously) and sodium diethyldithiocarbamate salt (intraperitoneally). When it comes in contact with free NO radicals, Fe^{2+}-DETC instantly precipitates, and detection of the resulting paramagnetic ferrous mononitrosyl-iron complex (MNIC) allows for highly specific and quantitative detection of basal (i.e., unstimulated) and elevated NO concentrations in various tissues (26-28). After 30 minutes of incubation, mice were killed and the organs excised. Freshly extracted renal tissue (350 mg) was submerged in strong HEPES buffer (150 µmol/L, pH 7.4) to a total volume of 450 µl, then snap-frozen in liquid nitrogen for electron paramagnetic resonance (EPR) spectroscopy.

EPR spectra were measured at 77 K with an X-band EMX-Plus spectrometer (Bruker Biospin, Rheinstetten, Germany). Spectrometer settings were microwave power 20 mW; time constant 82 ms, analog-to-digital conversion time 82 ms and detector gain 10^4. The magnetic field was modulated at a frequency of 100kHz and 5G amplitude. During experiments, the inside of the

EPR cavity (ER4119 HS-W1, cylindrical TE_{011} mode; Bruker) was continuously flushed with dry nitrogen to prevent condensation of ambient humidity on the cool Dewar flask.

The MNIC yields in the tissue sections were quantified by comparison with frozen reference samples of paramagnetic NO-Fe^{2+}-N-methyl-D-glucamine dithiocarbamate complexes (10 µmol/L in PBS), in which NO concentrations could be quantified. This procedure achieves an absolute accuracy of about 10%. The lower detection limit in our setup was 40 pmol MNIC.

Coculture of human umbilical vein endothelial cells and human brain pericytes under flow

Coculture experiments were performed using an Ibidi flow system (Ibidi GmbH, Marensried, Germany). Freshly isolated human umbilical vein endothelial cells (HUVECs) were cultured on 0.5% gelatin coated plastic flasks in endothelial basal medium (CC-3121, Lonza, Basel, Switzerland), supplemented with human epidermal growth factor, vascular endothelial growth factor, human fibroblast growth factor-B, R3-IGF-1, ascorbic acid, heparin, and 10% human serum (control medium). Cells were used at passage 3 or earlier. Human brain pericytes (HBPs) (ACBRI 499; Cell Systems, Kirkland, WA) were used in a 1:4 ratio with HUVECs. First HBP were seeded into perfusion chambers (ibiTreat 6 lanes µ-Slide VI 0.4 Luer) at a concentration of $3*10^5$ cells/mL. After cells were allowed to adhere for 2 hours, HUVECs were seeded on top of them at a concentration of $1.2*10^6$ cells/mL. After another 2 hours of adherence, chambers were connected to a computer-controlled air pressure pump which allowed for unidirectional perfusion of 15 mL medium over the cell layers, generating a constant shear stress of 10 dyne/cm^2. The chamber and the reservoirs containing the medium were kept in an incubator at 37°C and 5% CO_2. Control medium was refreshed after 1 day to remove nonadherent cells, after which five conditions were tested: 1) control medium, 2) medium with 10% serum from a patient with diabetes (diabetic human serum [DHS]), 3) DHS + 0.5 µmol/L atrasentan, 4) DHS + 0.8 µmol/L heparanase inhibitor (OGT2115, Tocris, Bristol, UK) and 5) DHS + 0.5 µmol/L atrasentan + 0.8 µmol/L heparanase inhibitor, n=5. For each individual experiment, DHS was obtained from the blood of patients with diabetes and chronic hyperglycemia (HbA1c > 8.2% [66 mmol/mol]). After 3 days, two lanes of cells were fixed with 4% paraformaldehyde in HBSS for 10 minutes, washed twice with HBSS and blocked with 3% normal goat serum in HBSS for 30 minutes. Cells were incubated with an antibody against N-acetylated and N-sulfated heparan sulfate domains (clone 10E4, 10 µg/ml, Amsbio) or control IgM, both diluted in HBSS and incubated overnight at 4°C. Cells were subsequently washed and incubated with appropriate secondary antibodies and Hoechst 33528 (1/1,000) for 1 hour, followed by tetramethylrhodamine-labeled wheat germ agglutinin (WGA) (1/100; Sigma-Aldrich) for 30 minutes. In the remaining lanes, cells were fixed with ice-cold methanol for 10 minutes to allow heparanase staining (HPA1, 1/20; InSight Biopharmaceuticals, Israel) or control IgG.

After being washed, cells were imaged using confocal microscopy and Leica Application Suite Advanced Fluorescence image software (Leica) to create image stacks. Luminal glycocalyx staining was analyzed using ImageJ software by first selecting the endothelial nuclear region.

The thickness of the glycocalyx was quantified by calculating the distance from the half-maximum signal of the nuclear staining at the luminal side, to the half-maximum signal at the luminal end of the staining in the z-direction. Luminal heparanase expression was quantified by selecting a similar endothelial nuclear region. The average intensity of every z-plane above the maximal intensity of the nucleus, until the background level, was quantified and expressed as fold change compared with the control medium.

RNA Isolation and Quantitative RT-PCR Analysis

Murine glomerular endothelial cells from kidneys of eight mice per treatment group were isolated according to Takemoto et al (29). After removing CD45-positive cells with CD45 MicroBeads (Miltenyi Biotech, Germany), endothelial cells were selected by CD31 MicroBeads, according to the manufacturer's protocol. Total RNA was isolated from these cells or HUVECs, using TRIzol (Invitrogen) and processed for real-time-quantitative PCR, using SYBR Green (Applied Biosystems). Human heparanase expression was identified with forward 5'-TCCTGC-GTACCTGAGGTTTG-3' and reverse 5'-CCATTCCAACCGTAACTTCTCCT-3' primers. Relative mRNA expression was determined by normalizing to GAPDH.

Statistical analysis

Data are presented as mean ± SD. Changes in albumin-to-creatinine ratios during treatment were analyzed using linear mixed model regression analysis. This takes into account that samples taken over time from the same animal are not independent (SPSS Statistics, version 20; IBM). Differences in all other experiments with continuous variables were determined using the *t* test in SPSS. $P<0.05$ was considered statistically significant.

Results

The diabetic apoE KO mouse model recapitulates features of human diabetic nephropathy

Glomerular changes in diabetic apoE KO mice were determined 14 weeks after diabetes was induced and eating a cholesterol-enriched diet (0.15%). While glomeruli of nondiabetic apoE KO mice appeared healthy, with thin capillary loops and normal distribution of mesangial matrix, glomeruli of diabetic mice showed typical features of diabetic nephropathy, with heterogeneous lesions, including increased mesangial matrix accumulation and dilated capillaries. Computer-aided quantification of periodic acid Schiff- and trichrome-stained glomeruli revealed significantly larger capillary size and increased mesangial expansion (Figure 1A-C, E-F).

Glomerular changes on an ultrastructural level were analyzed by exploiting large digital transmission electron microscopy (TEM) images of full glomerular cross sections. Diabetes leads to thickening of the glomerular basement membrane (268 ± 20 nm in diabetic mice vs. 216 ± 17 nm in healthy mice, $p<0.05$, $n = 3$), increased mesangial foam cell formation and increased

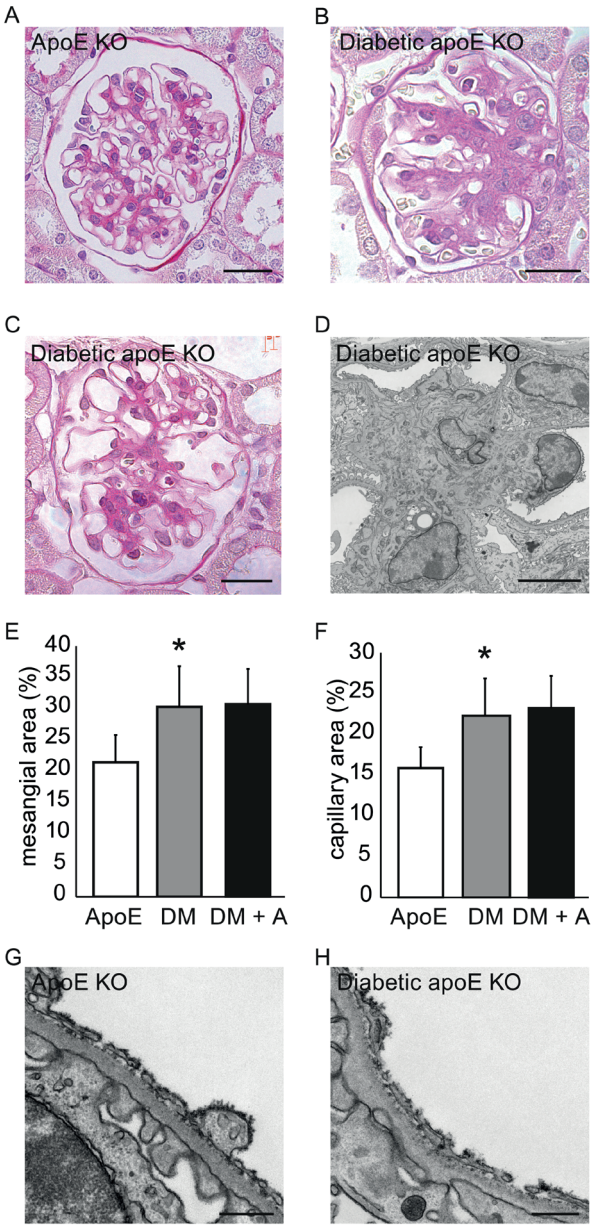


Figure 1. The diabetic apoE KO mouse model recapitulates the features of human diabetic nephropathy. A: The healthy glomerulus of a nondiabetic apoE KO mouse. Heterogeneous lesions in age- matched apoE KO mice 14 weeks after induction of diabetes with STZ show mesangial expansion (B), mesangiolysis (C and D), and, subsequently, glomerular hypertrophy, as quantified in E and F. D: TEM reveals a typical pathological process of mesangial foam cell formation and increased extracellular matrix deposition, resulting in decreased endothelial and mesangial cell interaction. TEM also shows differences in cationic ferritin coverage between nondiabetic (G) and diabetic (H) apoE KO mice. The occurrence of podocyte foot process effacement can be observed in H. Data are shown as mean ± SD (n = 8). *P < 0.05. Scale bars: 20 μm (A–C), 5 mm (D), 500 nm (G and H). ApoE, apoE KO mice; DM, diabetic apoE KO mice; DM + A, diabetic apoE KO mice + atrasentan.

extracellular matrix, which results in decreased interaction between endothelial and mesangial cells (Figure 1D). Endothelial fenestration was not affected by diabetes: 34.6 ± 9.0% of the endothelium in nondiabetic mice was fenestrated, compared with 40.3 ± 7.2% in diabetic apoE KO mice (n=3). Furthermore, an impaired glomerular filtration barrier was observed through focal podocyte foot process effacement and a decreased charge barrier, as shown by decreased cationic ferritin binding to the negatively charged glycocalyx (Figure 1G and H).

Tubulointerstitial lesions were observed next to areas of glomerular damage in diabetic apoE KO mice, including focal tubulointerstitial extracellular matrix deposition and dilation of proximal and distal tubules. However, diabetes did not increase urinary KIM-1 excretion (1.09 ± 0.54 vs. 1.45 ± 0.48 ng/24h; n = 8).

Atrasentan reduces albuminuria in diabetic apoE KO mice

We tested the effect of 4 weeks of treatment with atrasentan (7.5 mg/kg/day) on albuminuria. At the end of the intervention, body weight of treated mice was comparable to that of nontreated diabetic apoE KO mice (27.0 ± 2.4 g vs. 26.4 ± 2.6 g), which was lower than that of nondiabetic apoE KO mice (31.7 ± 2.8g, $p<0.05$). Nontreated diabetic apoE KO mice showed progressive albuminuria, which is in line with a parallel increase in urine production and albumin excretion (data not shown). Multiple comparisons demonstrate that treatment with atrasentan reduces progressive albuminuria by 26.0 ± 6.5% ($p<0.01$), compared with control treatment (Figure 2A). Renal morphology and capillary and mesangial areas were comparable to those in nontreated diabetic mice (23.3 ± 3.7% and 30.9 ± 6.0% respectively, Figure 1E and F and 2B and C). The number of podocytes stayed the same (data not shown), and at the current dose, treatment with atrasentan did not affect blood glucose concentrations (Figure 2D) or blood pressure (Figure 2E).

Atrasentan restores endothelial glycocalyx coverage

As a direct result of treatment of diabetic apoE KO mice with atrasentan, the negatively charged glomerular endothelial glycocalyx coverage was almost restored to control levels. This was visualized and quantified by glomerular endothelial cationic ferritin coverage (Figure 3A-C) and lectin binding (Figure 3D-F). Throughout the glomerular filtration barrier cationic ferritin was present at the luminal endothelial cell surface, within the fenestrae, and directly underneath the endothelium, penetrating slightly into but never passing through the GBM. The presence of cationic ferritin in capillaries was used as an endogenous control: to control for possible bias introduced by perfusion staining bias, only capillaries that showed cationic ferritin on the surface of the endothelium or below the endothelium in the GBM were used for analyses. Diabetes results in less endothelial coverage (40.7 ± 3.2%) compared with nondiabetic apoE KO mice (83.6 ± 5.6%) (Figure 3C). Treatment with atrasentan increases glomerular glycocalyx coverage back to the control (nondiabetic) state (81.0 ± 12.5%, $p<0.05$).

In addition, nonperfused renal sections were stained with *Lycopersicon esculentum* (LEA) a lectin that binds b-(1,4)-linked N-acetyl-glucosamine residues to visualize the glycocalyx.

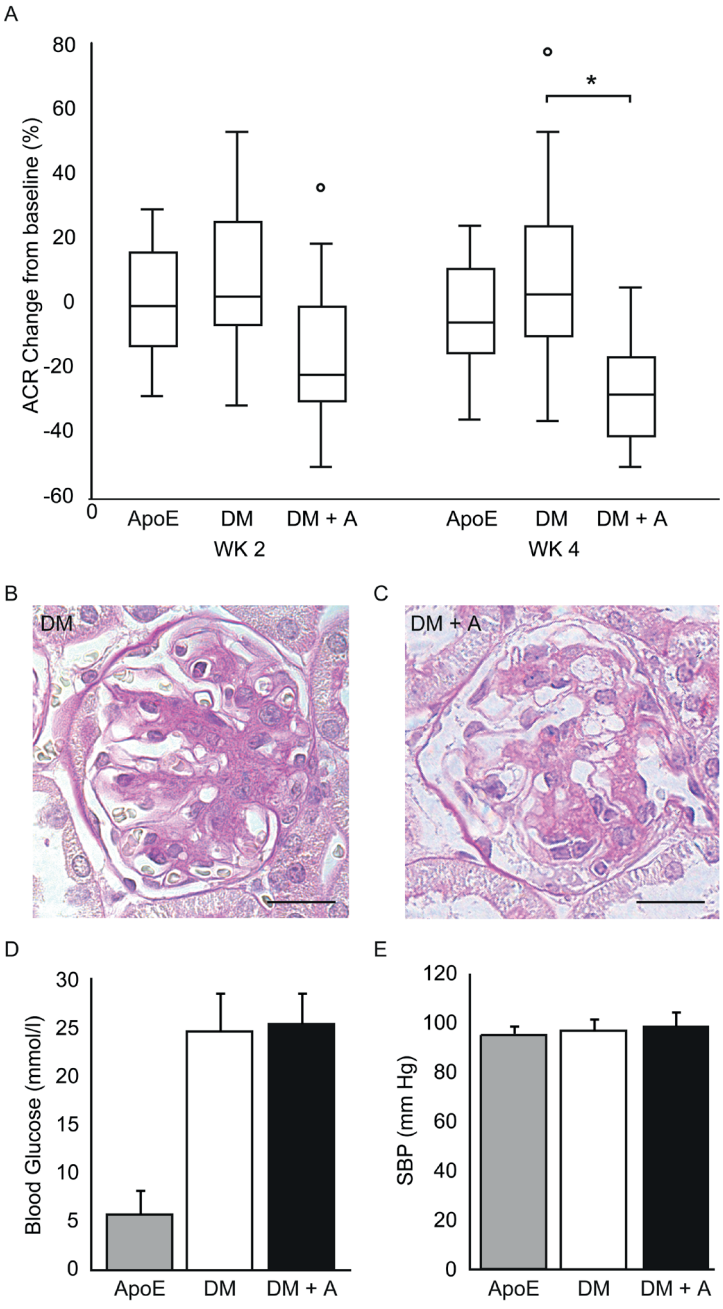


Figure 2. Atrasentan reduces albuminuria in diabetic apoE KO mice. A: Changes in urinary albumin-to-creatinine ratios (ACRs) from baseline to 4 weeks after treatment, indicated by percentage change from baseline. Data are shown as mean ± SD (n = 19–23). *P < 0.01. B and C: Glomerular morphology in diabetic apoE KO mice is not affected by treatment with atrasentan (DM + A) for 4 weeks compared with untreated diabetic apoE KO mice (DM). After treatment, no change in blood glucose concentrations (D) or systolic blood pressure (n = 8) (E) is observed. Scale bars: 20 µm. ApoE, apoE KO mice.

(13) Diabetes decreases intraluminal lectin thickness from 1.62 ± 0.30 µm to 0.67 ± 0.17 µm ($p<0.05$) (Figure 3F). Treatment with atrasentan restores intraluminal LEA thickness to 1.18 ± 0.25 µm ($p<0.05$) .

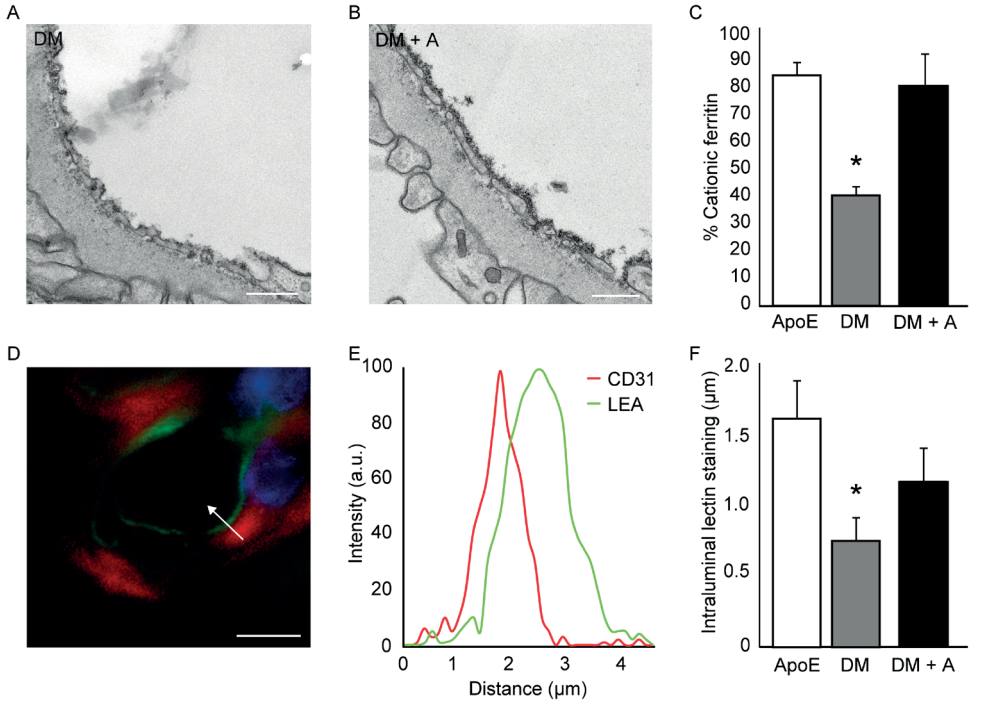


Figure 3. Atrasentan restores endothelial glycocalyx coverage. A and B: Representative TEM images of cationic ferritin bound to the negatively charged endothelial glycocalyx in glomeruli of diabetic (A) and atrasentan-treated diabetic (B) mice. C: Quantification of endothelial cationic ferritin coverage in capillary loops in three glomeruli of three mice, shown as the mean percentage of the total capillary length ± SD. D: Confocal fluorescent image of a glomerular capillary loop, stained for endothelial cells (CD31, red) and luminal glycocalyx (fluorescent-labeled LEA lectin, green). The arrow indicates the line of interest used in the intensity plot. E: Example of a fluorescence intensity plot depicting the area used for quantification of luminal glycocalyx thickness, which is determined by the distance of the CD31 peak to the half-maximum intensity of the LEA peak. F: Quantification of LEA thickness in capillary loops in three glomeruli of three mice. Data are shown as mean ± SD. Scale bars: 500 nm (A and B), 5 µm (D). *$P < 0.05$ compared with apoE KO mice (ApoE) and diabetic apoE KO mice + atrasentan (DM + A). a.u., arbitrary units; DM, diabetic apoE KO mice.

Atrasentan increases nitric oxide bioavailability

To confirm that activation of the ET_B receptor with ET-1 during the ET_A receptor blockade can induce the production of nitric oxide (NO) in the endothelium, endogenous renal NO bioavailability was measured using an *in vivo* NO-trapping method with Fe-DETC complexes (26). A typical electron paramagnetic resonance (EPR) spectrum from renal mouse tissue is shown in figure 4A. It represents a yield of ~140 pmol paramagnetic ferrous mononitrosyl-iron complex (MNIC) in 246 mg of renal tissue from a diabetic apoE KO mouse after treatment with atrasen-

tan. The renal NO yield in diabetic apoE KO mice increases from 0.29 ± 0.20 to 0.51 ± 0.15 pmol/mg (MNIC yield) (Figure 4B). When diabetic mice are treated with atrasentan for 4 weeks, NO concentrations increase considerably to 0.74 ± 0.21 pmol/mg ($p<0.05$).

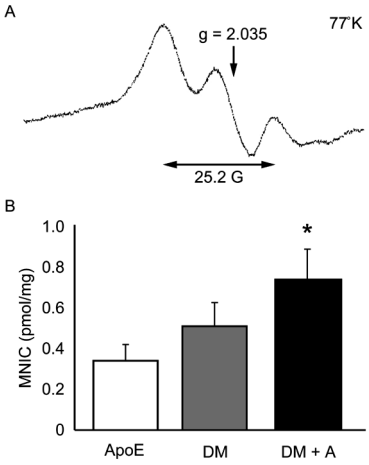


Figure 4. Atrasentan increases nitric oxide bioavailability. A: Example of the EPR spectrum of a frozen murine diabetic kidney sample after atrasentan treatment. The characteristic triplet structure of the MNIC (arrow) represents the formation of local NO. B: Quantification of renal NO formation, shown as mean MNIC ± SD (n = 8–9). *P < 0.05 compared with diabetic apoE KO mice (DM). ApoE, apoE KO mice; DM + A, diabetic apoE KO mice + atrasentan.

Atrasentan reduces heparanase expression and shifts macrophage phenotype

A mechanism of reduced glycocalyx coverage is through increased breakdown of heparan sulfates, one of its major components, by heparanase. Diabetic mice show increased glomerular heparanase protein expression compared with nondiabetic apoE KO mice (39.3 ± 10.8% vs. 13.1 ± 9.2%; $p<0.01$) (Figure 5A and C). Treatment of diabetic mice with atrasentan effectively reduces glomerular heparanase protein expression to 19.4 ± 5.1% ($p<0.01$). To explore the regulation of heparanase, mRNA expression in isolated glomerular endothelial cells was assessed. A strong transcriptional induction of heparanase expression was observed in the presence of diabetes (3.0 ± 1.2 fold; $p<0.05$), which was reduced after treatment with atrasentan (1.6 ± 0.5), albeit not significantly ($p=0.11$) (Supplementary Figure S1). Inflammatory cells such as macrophages have been shown to increase heparanase activity by activation of secreted pro-heparanase by cathepsin-L (30, 31). While the absolute number of macrophages remained equal between atrasentan treated and nontreated diabetic mice (F4/80-positive cells: 2.15 ± 0.37 vs. 2.53 ± 0.42 per glomerulus respectively), there was a shift from proinflammatory M1 macrophages toward regulatory noninflammatory CD206-positive M2 macrophages in atrasentan treated mice (62.2 ± 11.1% vs. 44.8 ± 6.1%, $p<0.01$), resulting in a distribution similar to that observed in nondiabetic apoE KO mice (64.8 ± 4.1%) (Figure 5A and B). Concomitant with this shift in the macrophages phenotype and increased heparanase expression, we also observed increased cathepsin-L protein expression in diabetic apoE KO mice (27.3 ± 11.3% vs. 10.5 ± 2.8%; $p<0.01$) and a reduction by atrasentan (10.1 ± 5.1%) (Figure 5A,D). Notably,

although cathepsin-L is more prominent in the tubular epithelium, glomerular F4/80 positive macrophages also colocalize with cathepsin-L expression (Supplementary Figure S2).

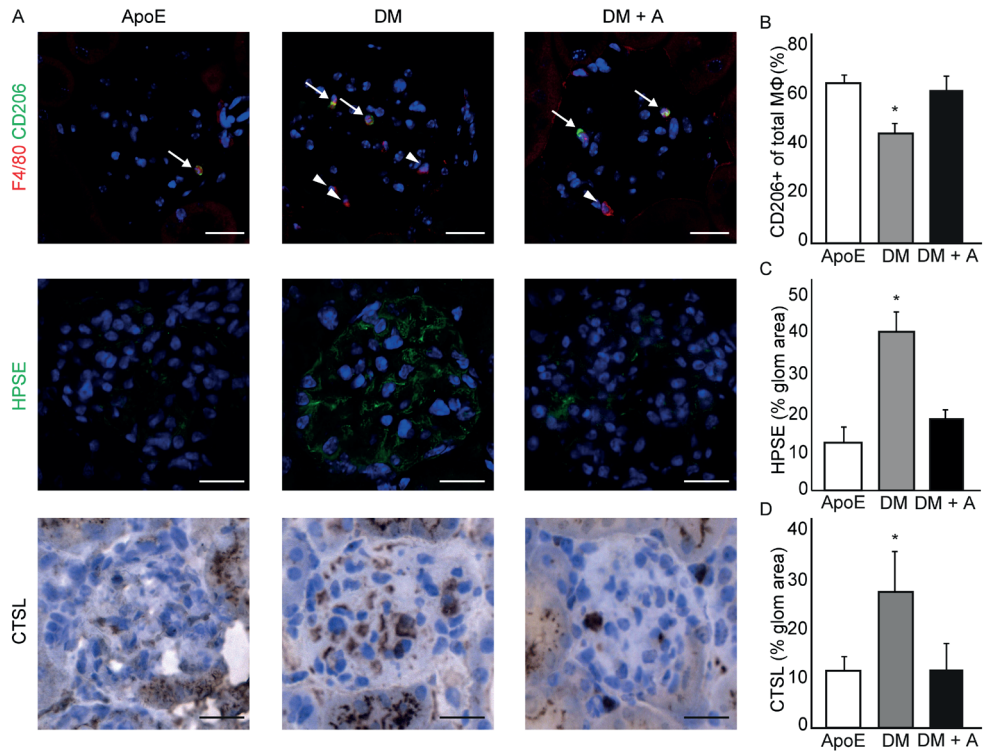


Figure 5. Atrasentan changes the glomerular M1-to-M2 macrophage ratio and reduces heparanase (HPSE) and cathepsin-L (CTSL) expression. A: Representative fluorescent images of glomerular F4/80 positive (arrowheads, top row) and F4/80-CD206 double-positive macrophages (arrows, top row), HPSE expression (middle row), and CTSL expression (bottom row) in apoE KO mice (ApoE), nontreated diabetic apoE KO mice (DM), and diabetic apoE KO mice treated with atrasentan (DM + A). Scale bar: 20 µm. Quantification of percent CD206-positive cells per total macrophage cell count (B), percent HPSE (C) and CTSL (D) positive area per glomerulus. Data are shown as mean ± SD (n = 8). *P < 0.01 compared with ApoE and DM + A. glom, glomerular.

Atrasentan restores glycocalyx thickness on endothelial cells in a diabetic milieu by reducing heparanase

To further study our hypothesis that atrasentan can reduce endothelial heparanase expression under conditions of endothelial activation in diabetes, and subsequently can increase glycocalyx thickness, we examined glycocalyx thickness on human umbilical vein endothelial cells (HUVECs) in the presence of diabetic and control human serum. HUVECs were cultured under flow (10 dyn/cm^2) for 4 days, on top of a layer of human brain pericytes (HBPs) to induce a quiescent endothelial phenotype and to resemble the *in vivo* cell-cell interactions that determine this endothelial phenotype. Under control conditions, these cells express a glycocalyx of 1.84 ± 0.36 µm

as shown with the lectin wheat germ agglutinin (WGA) (Figure 6). To mimic the conditions present in diabetes, we exposed the endothelial cells to the serum of patients with poorly controlled diabetes. Importantly, while diabetes obviously is characterized by hyperglycemia, plasma from patients with diabetes contains a wide range of factors that may cause endothelial activation, including advanced glycation end products, chemokines such as MCP-1, and vasoactive peptides such as angiotensin and endothelin (32). To mimic these circumstances, cells were incubated for 3 days with a medium supplemented with the serum of patient with poorly controlled diabetes; consequently, glycocalyx thickness decreased to 1.12 ± 0.26 µm ($p<0.05$). The addition of 0.5 µmol/L atrasentan to cells cultured in the presence of diabetic serum restored glycocalyx thickness to 1.48 ± 0.19 µm ($p<0.05$). The heparanase inhibitor OGT2115 also increased the glycocalyx thickness (1.38 ± 0.33 µm; $p<0.05$). Adding both compounds simultaneously, however, had no synergetic effect (1,38 ± 0,33 µm; $p<0.05$; data not shown). Staining with the antibody 10E4, against the N-acetylated and N-sulfated heparan sulfate domains, which was done to look more closely at the specific composition, showed results similar to the WGA staining (Figure 6A-B).

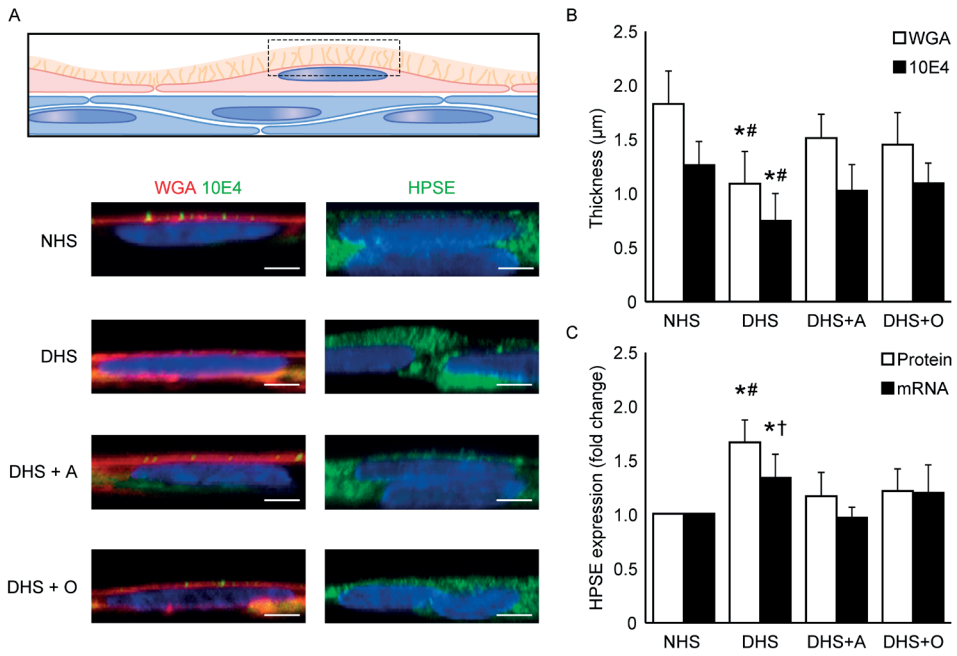


Figure 6. Atrasentan restores glycocalyx thickness on HUVECs. A: Schematic showing the area of interest for quantification (top, dotted line). Confocal fluorescent z-axis average-intensity projections of HUVECs cultured on top of HBPs under laminar flow for 4 days is shown on the bottom. On the left are intensities of WGA lectin (red) and specific anti–heparan sulfate staining (10E4; green). On the right is anti- heparanase (HPSE) staining. B: Glycocalyx thickness is quantified by estimating the distance from the half-maximum signal of the nuclear staining to the half maximum signal at the luminal end of WGA and 10E4 staining. C: Endothelial HPSE protein and mRNA expression are shown as relative to the control (normal human serum [NHS]). Protein expression is quantified as average intensity staining in the area of interest (A). Data are shown as mean ± SD (n = 4–5). *P < 0.05 compared with NHS. #P < 0.05 versus each treatment. †P < 0.05 versus atrasentan treatment. Scale bars: 10 µm. DHS + A = DHS + 5 µmol/L atrasentan; DHS + O = DHS + HPSE inhibitor (OGT2115).

To further test the involvement of heparanase in the modulation of the endothelial glycocalyx, we analyzed heparanase gene expression and heparanase protein presence at the luminal surface of the endothelial cells (Figure 6C). In agreement with the *in vivo* studies, incubation with diabetic serum for 3 days induced 1.63 ± 0.27 fold increased luminal protein expression, which was paralleled by 1.46 ± 0.28 fold increased mRNA expression compared with incubation in nondiabetic serum ($p<0.05$). Supplementation of these cells by 0.5 μmol/L atrasentan cultured in the presence of diabetic serum, normalized both luminal heparanase protein expression, as well as mRNA expression (to 1.19 ± 0.23 fold and 1.10 ± 0.11 fold, compared with control, respectively). The heparanase inhibitor decreased luminal expression of heparanase 1.25 ± 0.22 fold, $p<0.05$, but not gene expression (1.2 ± 0.46 fold) and there was no amplification of the effect of atrasentan.

Discussion

In this study selective ET_A receptor blockade in diabetic nephropathy is associated with almost complete restoration of glomerular endothelial glycocalyx dimensions toward control values and a reduction of albuminuria. Especially, the profound reduction of albuminuria occurs in the absence of any changes in systemic blood pressure and metabolic activators, such as high glucose concentrations. Both the *in vivo* data as well as the mechanistic studies *in vitro* show that atrasentan is capable of reducing heparanase expression in the presence of a diabetic milieu. This study provides a new mechanism of action for ongoing clinical studies with ET_A receptor blockers in diabetic nephropathy, where similar strong reductions in proteinuria were observed in the presence of only minor hemodynamic effects (11).

There has been controversy with respect to both the mechanism of albuminuria and the possible consequences of albuminuria in diabetic nephropathy. Most experimental data point to size selectivity of the glomerular filter. The glomerular glycocalyx, through its mesh of glycosaminoglycans and associated proteins, constitutes a size selective hydrogel that covers the surface and in particular the fenestrae (33). Disruption of this structure by enzymatic treatment, or more recently by endothelial deletion of the hyaluronan synthase 2 gene, has been shown to result in albuminuria (13, 34). Moreover, the high heparan sulfate content and the presence of sialylated proteins may give the endothelial surface a net negative charge, thus possibly further modulating the sieving of macromolecules. Since diabetes is associated with endothelial dysfunction and reduced systemic glycocalyx dimensions (12, 15), restoration of endothelial function and glycocalyx dimensions may thus prevent albuminuria. Such a therapy would be meaningful in the setting of diabetes, where chronic exposure of the glomerular and tubular endothelium to glycated albumin has been shown to induce epithelial inflammation and set the stage for tubulointerstitial disease (35).

To corroborate the beneficial effects of atrasentan on endothelial function, we used paramagnetic ferrous mononitrosyl-iron complex (MNIC) spin trap measurements; this model allows for quantitative measurements of the amount of nitric oxide molecules produced locally (27).

Atrasentan increased nitric oxide production at the renal tissue level (26), thus confirming endothelial ET_B receptor stimulation and restoration of endothelial function (36), despite the presence of diabetes.

To further address the mechanism behind the beneficial effects of atrasentan on heparanase reduction and its effect on endothelial glycocalyx dimensions, we also studied the effect of atrasentan on the endothelial glycocalyx *in vitro*. Because the glycocalyx composition is critically dependent upon shear, the cellular environment, and endothelial function, we used an experimental setup in which endothelial cells were exposed to laminar flow and cultured on top of pericytes, meant to mimic as closely as possible the *in vivo* situation. Endothelial cells show a remarkable heterogeneity throughout the vascular tree and may therefore differ in their response to injury (37, 38). Despite this heterogeneity, HUVECs are capable of expressing heparanase (39), and in this model, adding diabetic serum thereby mimicking the diabetic milieu increased endothelial heparanase expression. Heparanase is the main enzyme that can break down heparan sulfate side chains of glycosaminoglycans, and consequently glycocalyx thickness is reduced. In line with our observations in mice, atrasentan reduced heparanase expression through transcriptional regulation and restored the reduction of glycocalyx thickness in the presence of diabetic serum. Atrasentan was as effective as a heparanase inhibitor and the heparanase inhibitor did not amplify the effect of atrasentan, indicating that direct modulation of endothelial heparanase expression may be a mechanism by which atrasentan restores the glycocalyx.

Atrasentan has been studied previously in other diabetic animal models. In a streptozotocin induced diabetic rat model atrasentan reduced the onset of albuminuria, independent of changes in blood pressure (7, 40). Using the same model as in this study, avosentan, another ET_A selective blocker, was also shown to have strong antialbuminuric effects (17). Similar to our study, this was accompanied by anti-inflammatory effects, such as reduced influx of renal macrophages and additional decreased plasma concentrations of the inflammatory markers MCP-1 and soluble intracellular adhesion molecule-1. Such anti-inflammatory effects may have contributed further to the reduction in heparanase expression that was observed in the diabetic mice, since infiltrating monocytes have been shown to contribute to the activation of secreted proheparanase (41). This is supported by our observations that atrasentan reduced glomerular expression of cathepsin L, the enzyme that activates pro-heparanase; cathepsin-L expression colocalized with inflammatory glomerular macrophages.

Sixaxsentan, another ET_A receptor blocker, was shown to reduce podocyte loss in adriamycin-induced nephropathy (42). However, we did not observe a change in podocyte numbers in our model. Furthermore, we did not see changes in systemic blood pressure during atrasentan treatment. However, a reduction in glomerular capillary pressure cannot be ruled out as a possible mechanism to explain the beneficial effects on glomerular ultrastructure and glomerular endothelial glycocalyx function, particularly because micropuncture studies in rats have demonstrated the presence of increased glomerular capillary pressure in models of STZ-induced diabetes (43). Unfortunately, this technology cannot be applied to mice.

While our model studied only the short-term effects of atrasentan in already developed diabetic nephropathy, it would, of course, be relevant to know whether prolonged restoration of the glomerular glycocalyx also results in restoration of the cellular morphology or the prevention of (further) renal lesions. Both the effectiveness in preventing albuminuria as well as the fact that the glomerular glycocalyx functions as a molecular scaffold that modulates renal inflammation makes this question pertinent. Unfortunately, the long duration of the model, which was required to faithfully replicate changes seen in human diabetic nephropathy, precluded such follow-up studies in STZ-treated animals. This does not, however, detract from the fact that this study corroborates the rationale for the clinical use of ET_A selective receptor blockade in diabetic nephropathy; given the systemic nature of loss of the glycocalyx in diabetes, it also provides a mechanism of action that can be monitored noninvasively (44) in patients before and during treatment.

Acknowledgement

The authors thank E. Bouwman (Department of Inorganic Chemistry, Leiden University) for the use of the EPR facilities.

This study was supported by the Dutch Kidney Foundation (Glycoren Consortium grant no. CP09.03) and by AbbVie (grant no. REN-11-0026).

References

1. U.S. Renal Data System (2012) Annual Data Report: Atlas of Chronic Kidney Disease and End-Stage Renal Disease in the United States. National Institute of Diabetes and Digestive and Kidney Diseases, Bethesda, MD., 2012.
2. Hocher B, Thone-Reineke C, Rohmeiss P, Schmager F, Slowinski T, Burst V, et al. Endothelin-1 transgenic mice develop glomerulosclerosis, interstitial fibrosis, and renal cysts but not hypertension. The Journal of clinical investigation. 1997;99(6):1380-9.
3. Barton M. Therapeutic potential of endothelin receptor antagonists for chronic proteinuric renal disease in humans. Biochimica et biophysica acta. 2010;1802(12):1203-13.
4. Kohan DE, Pollock DM. Endothelin antagonists for diabetic and non-diabetic chronic kidney disease. British journal of clinical pharmacology. 2013;76(4):573-9.
5. Kohan DE, Pritchett Y, Molitch M, Wen S, Garimella T, Audhya P, et al. Addition of atrasentan to renin-angiotensin system blockade reduces albuminuria in diabetic nephropathy. Journal of the American Society of Nephrology : JASN. 2011;22(4):763-72.
6. Kohan DE, Barton M. Endothelin and endothelin antagonists in chronic kidney disease. Kidney international. 2014;86(5):896-904.
7. Sasser JM, Sullivan JC, Hobbs JL, Yamamoto T, Pollock DM, Carmines PK, et al. Endothelin A receptor blockade reduces diabetic renal injury via an anti-inflammatory mechanism. Journal of the American Society of Nephrology : JASN. 2007;18(1):143-54.
8. Edwards RM, Pullen M, Nambi P. Activation of endothelin ET_B receptors increases glomerular cGMP via an L-arginine-dependent pathway. The American journal of physiology. 1992;263(6 Pt 2):F1020-5.
9. Hirata Y, Emori T, Eguchi S, Kanno K, Imai T, Ohta K, et al. Endothelin receptor subtype B mediates synthesis of nitric oxide by cultured bovine endothelial cells. The Journal of clinical investigation. 1993;91(4):1367-73.
10. Nakano D, Pollock JS, Pollock DM. Renal medullary ET_B receptors produce diuresis and natriuresis via NOS1. American journal of physiology Renal physiology. 2008;294(5):F1205-11.
11. de Zeeuw D, Coll B, Andress D, Brennan JJ, Tang H, Houser M, et al. The endothelin antagonist atrasentan lowers residual albuminuria in patients with type 2 diabetic nephropathy. Journal of the American Society of Nephrology : JASN. 2014;25(5):1083-93.
12. Meuwese MC, Broekhuizen LN, Kuikhoven M, Heeneman S, Lutgens E, Gijbels MJJ, et al. Endothelial surface layer degradation by chronic hyaluronidase infusion induces proteinuria in apolipoprotein E-deficient mice. PloS one. 2010;5(12):e14262.
13. Dane MJ, van den Berg BM, Avramut MC, Faas FG, van der Vlag J, Rops AL, et al. Glomerular endothelial surface layer acts as a barrier against albumin filtration. The American journal of pathology. 2013;182(5):1532-40.
14. van den Hoven MJ, Rops AL, Bakker MA, Aten J, Rutjes N, Roestenberg P, et al. Increased expression of heparanase in overt diabetic nephropathy. Kidney international. 2006;70(12):2100-8.
15. Nieuwdorp M, Mooij HL, Kroon J, Atasever B, Spaan JA, Ince C, et al. Endothelial glycocalyx damage coincides with microalbuminuria in type 1 diabetes. Diabetes. 2006;55(4):1127-32.
16. Opgenorth TJ, Adler AL, Calzadilla SV, Chiou WJ, Dayton BD, Dixon DB, et al. Pharmacological characterization of A-127722: an orally active and highly potent ET_A-selective receptor antagonist. Journal of Pharmacology and Experimental Therapeutics. 1996;276(2):473-81.
17. Watson AM, Li J, Schumacher C, de Gasparo M, Feng B, Thomas MC, et al. The endothelin receptor antagonist avosentan ameliorates nephropathy and atherosclerosis in diabetic apolipoprotein E knockout mice. Diabetologia. 2010;53(1):192-203.
18. Lassila M, Jandeleit-Dahm K, Seah KK, Smith CM, Calkin AC, Allen TJ, et al. Imatinib attenuates diabetic nephropathy in apolipoprotein E-knockout mice. Journal of the American Society of Nephrology : JASN. 2005;16(2):363-73.
19. Meyrelles SS, Peotta VA, Pereira TM, Vasquez EC. Endothelial dysfunction in the apolipoprotein E-deficient mouse: insights into the influence

of diet, gender and aging. Lipids in health and disease. 2011;10:211.

20. Lassila M, Seah KK, Allen TJ, Thallas V, Thomas MC, Candido R, et al. Accelerated nephropathy in diabetic apolipoprotein e-knockout mouse: role of advanced glycation end products. Journal of the American Society of Nephrology. 2004;15(8):2125-38.
21. Tran TN, Eubanks SK, Schaffer KJ, Zhou CY, Linder MC. Secretion of ferritin by rat hepatoma cells and its regulation by inflammatory cytokines and iron. Blood. 1997;90(12):4979-86.
22. Faas FG, Avramut MC, van den Berg BM, Mommaas AM, Koster AJ, Ravelli RB. Virtual nanoscopy: generation of ultra-large high resolution electron microscopy maps. The Journal of cell biology. 2012;198(3):457-69.
23. Avasthi PS, Koshy V. The anionic matrix at the rat glomerular endothelial surface. The Anatomical record. 1988;220(3):258-66.
24. Austyn JM, Gordon S. F4/80, a monoclonal antibody directed specifically against the mouse macrophage. European journal of immunology. 1981;11(10):805-15.
25. Ezekowitz RA, Gordon S. Alterations of surface properties by macrophage activation: expression of receptors for Fc and mannose-terminal glycoproteins and differentiation antigens. Contemporary topics in immunobiology. 1984;13:33-56.
26. Vanin AF, Huisman A, Van Faassen EE. Iron dithiocarbamate as spin trap for nitric oxide detection: pitfalls and successes. Methods in enzymology. 2002;359:27-42.
27. van Faassen EE, Koeners MP, Joles JA, Vanin AF. Detection of basal NO production in rat tissues using iron–dithiocarbamate complexes. Nitric Oxide. 2008;18(4):279-86.
28. Berliner LJ, Fujii H. In vivo spin trapping of nitric oxide. Antioxidants & redox signaling. 2004;6(3):649-56.
29. Takemoto M, Asker N, Gerhardt H, Lundkvist A, Johansson BR, Saito Y, et al. A new method for large scale isolation of kidney glomeruli from mice. The American journal of pathology. 2002;161(3):799-805.
30. Garsen M, Rops AL, Rabelink TJ, Berden JH, van der Vlag J. The role of heparanase and the endothelial glycocalyx in the development of proteinuria. Nephrology, dialysis, transplantation : official publication of the European Dialysis and Transplant Association - European Renal Association. 2014;29(1):49-55.
31. Goldberg R, Rubinstein AM, Gil N, Hermano E, Li JP, van der Vlag J, et al. Role of heparanase-driven inflammatory cascade in pathogenesis of diabetic nephropathy. Diabetes. 2014;63(12):4302-13.
32. Eelen G, de Zeeuw P, Simons M, Carmeliet P. Endothelial cell metabolism in normal and diseased vasculature. Circulation research. 2015;116(7):1231-44.
33. Rostgaard J, Qvortrup K. Electron microscopic demonstrations of filamentous molecular sieve plugs in capillary fenestrae. Microvascular research. 1997;53(1):1-13.
34. Berg vd, BM; Boels, M.G.S.; Avramut, MC; Jansen, E; Meldner, S; Dane, MJC; Vlag, van der, J; Vink, H; Koster, AJ; Zonneveld, van, AJ; Groene, HJ; Koning, de, E; Rabelink, TJ Genetic Deletion of Endothelial Hyaluronan Synthase 2 Results in Glomerular Injury and Albuminuria (Abstract). Journal of the American Society of Nephrology : JASN. 2014;25: 29A:TH-OR119.
35. Nauta FL, Boertien WE, Bakker SJ, van Goor H, van Oeveren W, de Jong PE, et al. Glomerular and tubular damage markers are elevated in patients with diabetes. Diabetes care. 2011;34(4):975-81.
36. Tsukahara H, Ende H, Magazine HI, Bahou WF, Goligorsky MS. Molecular and functional characterization of the non-isopeptide-selective ETB receptor in endothelial cells. Receptor coupling to nitric oxide synthase. The Journal of biological chemistry. 1994;269(34):21778-85.
37. Yuan L, Chan GC, Beeler D, Janes L, Spokes KC, Dharaneeswaran H, et al. A role of stochastic phenotype switching in generating mosaic endothelial cell heterogeneity. Nature communications. 2016;7:10160.
38. Ligresti G, Nagao RJ, Xue J, Choi YJ, Xu J, Ren S, et al. A Novel Three-Dimensional Human Peritubular Microvascular System. Journal of the American Society of Nephrology : JASN. 2016 Aug;27(8):2370-81.
39. Godder K, Vlodavsky I, Eldor A, Weksler BB, Haimovitz-Freidman A, Fuks Z. Heparanase activity in cultured endothelial cells. Journal of cellular physiology. 1991;148(2):274-80.

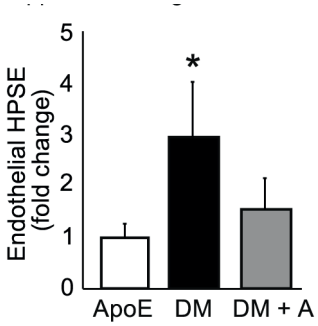
40. Saleh MA, Boesen EI, Pollock JS, Savin VJ, Pollock DM. Endothelin receptor A-specific stimulation of glomerular inflammation and injury in a streptozotocin-induced rat model of diabetes. Diabetologia. 2011;54(4):979-88.

41. Fiebiger E, Maehr R, Villadangos J, Weber E, Erickson A, Bikoff E, et al. Invariant chain controls the activity of extracellular cathepsin L. The Journal of experimental medicine. 2002;196(9):1263-9.

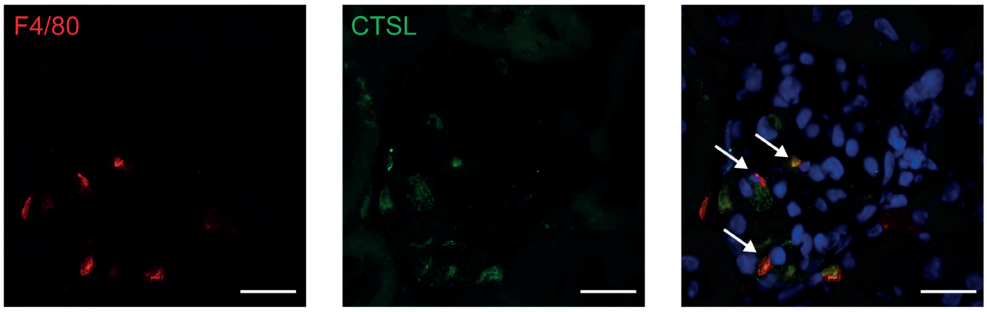
42. Buelli S, Rosano L, Gagliardini E, Corna D, Longaretti L, Pezzotta A, et al. beta-arrestin-1 drives endothelin-1-mediated podocyte activation and sustains renal injury. Journal of the American Society of Nephrology : JASN. 2014;25(3):523-33.

43. Qiu C, Samsell L, Baylis C. Actions of endogenous endothelin on glomerular hemodynamics in the rat. The American journal of physiology. 1995;269(2 Pt 2):R469-73.

44. Dane MJ, Khairoun M, Lee DH, van den Berg BM, Eskens BJ, Boels MG, et al. Association of kidney function with changes in the endothelial surface layer. Clinical journal of the American Society of Nephrology : CJASN. 2014;9(4):698-704.



Supplementary figure S1. Diabetes increases endothelial heparanase mRNA expression. Quantification of glomerular endothelial heparanase mRNA expression, relatively to non-diabetic apoE KO mice (ApoE). Murine heparanase was identified with forward 5'-GAGCGGAGCAAACTCCGAGTGTATC-3' and reverse 5'-GATCCAGAATTTGACCGTTC AGTTGG-3' primers. Data is shown as mean ± SD, n = 3-4, *P<0.05, compared with ApoE. DM = diabetic apoE KO mice, DM + A = diabetic apoE KO mice + atrasentan.



Supplementary figure S2. Glomerular macrophages co-localize with cathepsin-L. Representative fluorescent images of glomerular F4/80 positive macrophages (red) and cathepsin-L (green) in diabetic apoE KO mouse. Arrows indicate co-localization in merged image, scale bar: 20 µm.

Chapter 3

Systemic Monocyte chemotactic protein-1 inhibition modifies renal macrophages and restores glomerular endothelial glycocalyx and barrier function in diabetic nephropathy

American Journal of Pathology 187(11):2430-2440, 2017

Margien G.S. Boels, Angela Koudijs, M. Cristina Avramut, Wendy M.P.J. Sol, Gangqi Wang, Annemarie M. van Oeveren-Rietdijk, Anton Jan van Zonneveld, Hetty C. de Boer, Johan van der Vlag, Cees van Kooten, Dirk Eulberg, Bernard M. van den Berg, Daphne H.T. IJpelaar, Ton J. Rabelink

Abstract

Inhibition of monocyte chemotactic protein-1 (MCP-1) with the Spiegelmer® emapticap pegol (NOX-E36) shows long-lasting albuminuria reducing effects in diabetic nephropathy. MCP-1 regulates inflammatory cell recruitment and differentiation of macrophages. Because the endothelial glycocalyx is also reduced in diabetic nephropathy, we hypothesized that MCP-1 inhibition restores glomerular barrier function through influencing macrophage cathepsin L secretion, thus reducing activation of the glycocalyx degrading enzyme heparanase.

Four weeks treatment of diabetic *apoE* knockout mice with the mouse specific NOX-E36 attenuated albuminuria without any change in systemic hemodynamics, despite persistent loss of podocyte function. MCP-1 inhibition, however, increased glomerular endothelial glycocalyx coverage with preservation of heparan sulfate. Mechanistically, both glomerular cathepsin L and heparanase expression were reduced. MCP-1 inhibition resulted in reduced CCR2 expressing $Ly6C^{hi}$ monocytes in the peripheral blood, without affecting overall number of kidney macrophages at the tissue level. However, $CD206^{+}$/$Mac3^{+}$ cell-ratio as an index of presence of anti-inflammatory macrophages was increased in diabetic mice after treatment. Functional analysis of isolated renal macrophages showed increased release of IL-10, whereas tumor necrosis factor and cathepsin L release was reduced, further confirming polarization of tissue macrophages towards an anti-inflammatory phenotype during mouse specific NOX-E36 treatment.

We show that MCP-1 inhibition restores glomerular endothelial glycocalyx and barrier function and reduces tissue inflammation in the presence of ongoing diabetic injury, suggesting a therapeutic potential for this compound in diabetic nephropathy.

Introduction

Diabetic nephropathy is the major cause of end-stage renal disease. Although optimal blood pressure treatment using drugs that interfere with the renin-angiotensin system has been shown to slow progression of diabetic nephropathy, many patients still progress to end-stage renal disease(1). In recent years, new strategies to slow the progression of chronic kidney disease in patients with diabetic nephropathy focused on inhibition of inflammation(2). One such strategy constitutes inhibition of monocyte chemotactic protein-1 (MCP-1) to prevent binding to its cognate receptor CCR2. MCP-1 is considered to be involved in recruitment of monocytes and migration of monocytes and macrophages(3-6). In patients with diabetic nephropathy, the increased presence of MCP-1 in renal tissue and elevated levels in urine suggests that macrophages play a pathogenic role in the development of proteinuria, glomerular damage, and the progression of renal disease in humans(7). Indeed, Nguyen et al showed that macrophages are already present in glomeruli in early diabetic nephropathy, whereas the number of interstitial macrophages correlate with progression of renal insufficiency(8). Recently, we demonstrated similar findings in a large autopsy study showing that glomerular macrophages were already present in biopsies with mild diabetic nephropathy, suggesting a role for macrophages in proteinuria and early diabetes-induced damage(9).

In experimental models of streptozotocin-induced diabetic nephropathy, macrophage recruitment to the glomeruli could be prevented by genetic deletion of MCP-1(10). Similarly, pharmacologic blockade of MCP-1 prevented glomerular macrophage recruitment and attenuated albuminuria in uninephrectomized *db/db* mice(11, 12). In addition, observations on alleviation of acute rejection through MCP-1 blockade point towards the potential of the MCP-1/CCR2 pathway to modulate inflammation. Clinically, the MCP-1/CCR2 axis has been targeted by receptor-specific antibodies and small molecules. For example, blockade of CCR2 with the small molecule CCX140-B in patients with diabetic nephropathy reduced albuminuria(13). Recently, inhibition of MCP-1 with emapticap pegol (NOX-E36), a structured L-enantiomeric RNA (so-called Spiegelmer®), decreased albuminuria in patients with diabetic nephropathy(14). The mechanism of the reduction in albuminuria by MCP-1 inhibition, however, is still not understood.

The glomerular barrier for albumin filtration is an interplay between endothelial cells, podocytes and the glomerular basement membrane. Fenestrated glomerular endothelial cells are covered with the glycocalyx, a gel-like polyanionic carbohydrate layer with embedded proteins(15, 16). Increased activity of glycocalyx degrading enzymes, such as heparanase and hyaluronidase, has long been recognized in diabetic nephropathy(17). The activity of heparanase, which is secreted as an inactive precursor by endothelial cells and podocytes, is increased dramatically after subsequent activation by the enzyme cathepsin L(18). Cathepsin L can also be secreted into the extracellular space by infiltrated glomerular macrophages, making these cells candidates for renal heparanase activation and loss of glycocalyx. This mechanism of action of MCP-1 inhibition was evaluated in this study in diabetic *apoE* knockout (KO) mice

and further validated in fluorescence-activated cell sorting (FACS) isolated macrophages of the renal tissue of these mice.

Materials and methods

Animal studies

Six-weeks-old male *apoE* KO C57BL/6J mice (Jackson Laboratory, Bar Harbor, ME) were rendered diabetic as described before(15). In short, 60 mg/kg streptozotocin (Sigma-Aldrich, St Louis, MO, USA) in citrate buffer was injected i.p. for 5 consecutive days; control *apoE* KO mice received citrate buffer alone. Twelve weeks after induction of diabetes, mice were treated with s.c. injections of 20 mg/kg mouse-specific NOX-E36 (mNOX-E36) or inactive control Spiegelmer (revmNOX-E36) in 5% glucose three times a week for 4 weeks. This dose is based on previous studies with mNOX-E36 in C57BL/6J mice(19), n = 23 per group were followed until the end of treatment, n = 10 per group were followed up until 4 weeks after treatment (n = 11 for control). (rev)mNOX-E36 concentrations were determined 1-6 hours after injections in lithium heparin plasma. All diabetic animals had free access to cholesterol enriched (0.15%) chow (Technilab-BMI, Someren, The Netherlands), control *apoE* KO mice were fed with standard chow for baseline measurements (n = 13). Animal experiments were approved by the ethical committee on animal care and experimentation of the Leiden University Medical Center (The Netherlands). All animal work was performed in compliance with the Dutch government guidelines.

Blood glucose concentrations were measured using a glucose meter (Accu-Chek, Roche, Basel, Switzerland). To prevent ketoacidosis and mortality, diabetic mice were treated when blood glucose levels were >25 mmol/L, with 1 to 2 U of insulin (s.c.; Lantus, Aventis Pharmaceuticals, Bridgewater, NJ, USA), maximally three times per week.

Systolic blood pressure was assessed with the non-invasive tail cuff system in conscious mice at start and end of treatment, and at the end of the follow-up period, using the CODA system (Kent Scientific, Torrington, CT) according to manufacturer's instructions. n = 8 per treatment group (7 for nondiabetic *apoE* KO mice).

Urine collection and analyses

Twenty-four-hours urine was collected at study start and after the 4-week treatment period. In a subset of animals, urine was also collected 4 weeks after terminating of the treatment. Mice were acclimatized to metabolic cages, after which 24-hours urine was collected. Albumin levels were quantified with ELISA (Bethyl Laboratories, Montgomery, TX). Urinary creatinine levels were determined by the Jaffé method using 0.13% picric acid (Sigma-Aldrich), and quantified using a creatinine standard (Sigma-Aldrich) after ODs were measured with an ELISA plate reader. Urinary MCP-1 concentrations were quantified with ELISA (Anogen, Mississauga, Ontario, Canada) according to protocol provided by manufacturer.

Immunohistochemistry

Eight mice per treatment group were anaesthetized by isoflurane inhalation and perfused via the left ventricle with HEPES-buffered salt solution containing 0.5% BSA and 5 U/mL heparin to remove blood. Kidney capsules were removed and one half of the right kidney was fixed in paraformaldehyde solution (4%) for 1-2 hours, followed by paraffin embedding for periodic acid-Schiff (PAS) and trichrome staining and quantification of macrophages. The proportion of the glomerulus positive for PAS stain was determined according to Animal Models of Diabetic Complications Consortium protocols, using color deconvolution in ImageJ (public domain, version 1.49m; http://imagej.nih.gov/ij) to determine mesangial area.

The other half was snap-frozen in 2-methylbutane (Sigma-Aldrich) for immunofluorescence staining. Frozen kidney sections (4 µm thick) were fixed in acetone for 10 minutes at room temperature. Non-specific antibody binding was prevented by incubation with normal goat serum (4%) in phosphate buffered saline (PBS) for 30 minutes. Glomerular heparanase expression was detected after overnight incubation with primary antibody (Polyclonal rabbit anti-heparanase, InSight Biopharmaceuticals, Rehovot, Israel) in combination with mouse pan-endothelial cell marker (BD Biosciences, San Jose, CA, USA), followed by fluorescent-labeled secondary antibody for 1 hour, both in blocking buffer. Sections were counterstained with Hoechst (1/1000) and embedded in Vectashield mounting medium (Vector Laboratories Inc., Burlingame, CA). Cathepsin L polyclonal antibody (R&D Systems Europe Ltd, Abingdon, UK) was incubated overnight, followed by HRP-conjugated secondary antibody and DAB. Glomerular staining area was quantified on blinded sections, as percentage stained area / glomerular area using ImageJ.

Glycocalyx composition was further analyzed on paraffin embedded sections with antibodies against heparan sulfate (10E4, AMS-Biotechnology, Bioggio-Lugano, Switzerland; and JM403 provided by Dr. J van der Vlag, Nijmegen, The Netherlands) and chondroitin sulfate (CS56, AMS-Biotechnology).

Podocytes were quantified after being identified with Wilms tumor-1 antibody (0.5 mg/mL; Santa Cruz Biotechnology, Dellas, TX) in paraffin embedded sections. Podocyte damage was further investigated in frozen kidney sections by incubation with primary antibodies against mouse synaptopodin (Progen Biotechnik GmbH, Heidelberg, Germany) or nephrin (R&D Systems), followed by fluorescent-labeled secondary antibody for 1 hour. Staining intensity was quantified as percentage stained area / glomerular area in ImageJ.

Macrophages were identified using a rat monoclonal antibody against mouse F4/80 (Abcam, Cambridge, MA), recognizing most mouse macrophages(20); rabbit polyclonal antibody against mouse mannose receptor CD206 (Abcam), expressed specifically by regulatory macrophages(21) and rat monoclonal antibody against mouse CD107b (Mac3; M3/84, BD-Pharmingen; BD-Biosciences Europe, Vianen, The Netherlands). The number of macrophages present was quantified in a minimum of 25 glomeruli per mouse or in 10 non-overlapping high power fields (HPF) in case of tubulointerstitium (n = 5-8 per group for all immunohistochemical analyses, unless stated otherwise).

Determination of glomerular endothelial glycocalyx coverage

Glomerular endothelial glycocalyx coverage was determined with electron microscopy, as previously described(15). In short, the left kidney of three mice per group was perfused with 0.5% bovine serum albumin (BSA) and 5 U/mL heparin in 5 mL HEPES-buffered salt solution at 2 mL/minute to remove blood, followed by 2 mL of cationic ferritin (horse spleen, 2.5 mg/mL, Electron Microscopy Sciences, Fort Washington, PA) in HEPES-buffered salt solution alone at 2 mL/minute. Kidneys were fixated with 1.5% glutaraldehyde + 1% paraformaldehyde (both from Electron Microscopy Sciences, Hatfield, PA) in 0.1 mol/L sodium-cacodylate buffered solution (pH 7.4) overnight at 4˚C. The kidney was subsequently sectioned in 180 µm thick sections, rinsed twice with 0.1M sodium-cacodylate buffered solution and post-fixed in 1% osmium tetroxide and 1.5% potassium ferrocyanide on ice. Finally, samples were washed, dehydrated, embedded in epon and polymerized at 60˚C for 48 hours. Sections (100 nm thick) were further stained with 7% uranyl acetate and Reynold's lead citrate. Transmission electron microscopy (TEM) data were collected at an acceleration voltage of 120 kV on a Tecnai G2 Spirit BioTWIN microscope (FEI, Eindhoven, The Netherlands), equipped with an FEI 4k Eagle CCD camera. Extensive sets of images were automatically acquired with X18,500 magnification, and combined using stitching software(22). The resulting large digital image provides an overview of the glomerulus, in which one can zoom into high detail, allowing for quantitative analyses. The previously perfused cationic ferritin binds to the polyanionic glycocalyx, which thereby can be visualized. Within the stitches, individual capillary loops were captured and glycocalyx coverage was quantified in 8-9 capillary loops in 3 glomeruli per mouse (n = 3/group). The percentage of positive coverage of the endothelium with cationic ferritin was determined using an automatic grid overlay in the public domain NIH ImageJ version 1.46. For every glomerulus, a minimum of 80 crosshairs were at the intersection of endothelium and scored for percentage positive.

Ex vivo macrophage phenotype in kidney and peripheral blood

Three kidneys per treatment group were perfused with HEPES-buffered salt solution containing 0.5% BSA and 5 U/mL heparin to remove blood and stored in ice-cold phosphate-buffered saline. Kidneys were cut into small pieces and digested with 1.6 mg/mL collagenase type 1A (Sigma-Aldrich) and 60 U/mL DNAse I (Sigma-Aldrich) solution for 30 minutes at 37 °C. Tissues were minced through a 100-µm and subsequently a 40-µm cell strainer (BD Biosciences) to obtain a single cell suspension. Labeling and gating strategy is detailed in Supplementary Figure S1. For comparison of mean fluorescent intensities between the different samples (blood, spleen and kidney cells) a stain index was used, given as ($mean_{positive}$ - $mean_{background}$) / 2x ($S.D._{.background}$), in which the lymphocyte population is used as background (negative for CCR2)(23). A subset of cells was counted on an LSRII flow cytometer (BD Biosciences) and data was analyzed using FACSDiva software 6.1.2. (BD Biosciences). Peripheral blood, drawn from the tail vein, was analyzed accordingly.

The remaining renal cells were sorted on a FACS ARIA^{TM} III (BD Biosciences; Supplementary Figure S1). CD11b^{+}, B220^{-}, Lyc6G^{-}, F4/80^{+} macrophages were isolated and cultured in a

96-wells plate at a density of 10,000 cells/well in Iscove's Modified Dulbecco's Medium (IMDM) supplemented with 10% fetal calf serum, 100 U/mL penicillin and 100 mg/mL streptomycin. Cells were maintained at 37°C in humidified atmosphere of 5% CO_2. After 1 hour, cells were stimulated with 1 µg/mL LPS for 24 hours. Supernatant was analyzed for IL-6, IL-10 and TNFα (BD Biosciences) levels with ELISA, as well as for secreted cathepsin L activity (Abcam), according to the manufacturer's protocol.

Statistical analysis

Data are presented as mean ± SD. Changes in continuous variables during treatment were analyzed using two-way analysis of variance with post hoc Tukey's multiple-comparison analysis in GraphPad Prism version 6 (GraphPad Prism software, Inc., San Diego, CA). This takes into account that samples over time from the same animal are not independent. Differences in other experiments were determined using analysis of variance and post hoc analyses with Tukey's multiple comparison test. Comparison of expression between two different groups was evaluated using *t*-test. $P < 0.05$ was considered statistically significant.

Results

MCP-1 inhibition does not affect the diabetes characteristics in streptozotocin treated apoE KO mice

Blood glucose levels in *apoE* KO mice after streptozotocin treatment, and cholesterol (0.15%)-enriched diet, were elevated during the 12 weeks up to the start of mNOX-E36 treatment (9.9 ± 1.4 mmol/l to 24.5 ± 6.3 mmol/l, Figure 1A). Similar to previous mNOX-E36 studies(11, 19, 24), treatment with 20mg/kg mNOX-E36, or non-functional Spiegelmer as a control, for 4 weeks resulted in pharmacologically relevant plasma levels (data not shown). This 4-week mNOX-E36 intervention did not affect the blood glucose levels (27.4 ± 5.4 mmol/L versus 26.6 ± 6.5 mmol/L for control) and levels remained high during the four weeks of follow-up (mNOX-E36, 27.7 ± 6.5 mmol/L versus control, 27.9 ± 6.2 mmol/L). In contrast, in nondiabetic *apoE* KO mice receiving normal chow, blood glucose levels remained low during the entire experimental period (week 22: 10.7 ± 1.0 mmol/L and week 26: 8.1 ± 2.0 mmol/L).

At the end of the 4-week intervention (week 22 of age), the body weight of mNOX-E36-treated mice was comparable to control-treated mice (29.5 ± 1.7 g versus 29.3 ± 2.6 g, Figure 1B), both of which were lower than nondiabetic *apoE* KO mice (32.53 ± 1.4 g, $p < 0.05$). No change in body weight was observed at the end of the follow-up period (mNOX-E36 30.6 ± 1.8 g versus control 29.1 ± 1.8 g), which was still lower compared with nondiabetic *apoE* KO mice (32.8 ± 1.8 g, $p < 0.05$).

To assess whether our observations are independent of changes in blood pressure, we measured systolic blood pressure before and after treatment and at the end of the follow-up period. No changes in systolic blood pressure were observed between diabetic and nondiabetic

mice (99.5 ± 6.6 mmHg versus 99.8 ± 6.5 mmHg at week 18) and after the entire experimental period (mNOX-E36 97.1 ± 5.1 mmHg versus control 97.2 ± 9.7 mmHg at 22 weeks, and 100.4 ± 5.1 mmHg versus 100.0 ± 7.2 mmHg at 26 weeks of age, Figure 1C).

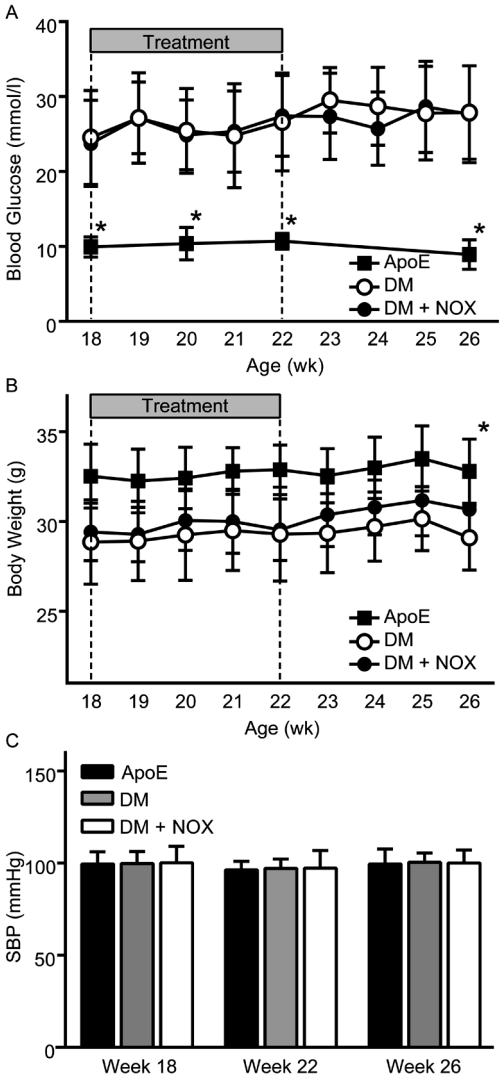


Figure 1. Monocyte chemotactic protein-1 inhibition does not change diabetic characteristics in *apoE* knockout (KO) mice. A) Blood glucose levels increase in diabetic *apoE* KO mice and do not change during and after treatment. B) Body weight slightly decreases on induction of diabetes, but does not change during and after treatment. C) Diabetes and (rev)mNOX-E36 treatment do not alter systolic blood pressure (SBP). Data are expressed as mean ± SD. N = 13 [A and B, *apoE* KO mice (ApoE)]; n = 23 [A and B, diabetic apoE KO mice treated with inactive revmNOX-E36 (DM) and diabetic apoE KO mice treated with mNOX-E36 (DM + NOX) at week 22]; n = 10 [A and B, DM at week 26]; n = 11 [A and B, DM + NOX at week 26]; n = 7 [C, apoE]; n = 8 [C, DM + (rev)mNOX-E36 at week 22]; n = 5 [C, DM + (rev)mNOX-E36 at week 26]. *P<0.05 versus DM ± mNOX-E36.

MCP-1 inhibition reduces albuminuria and restores the glomerular endothelial glycocalyx

Treatment of diabetic *apoE* KO mice for four weeks with mNOX-E36 reduced the albumin/creatinine ratio to 118.6 ± 11.9 µg/mg in comparison to treatment with control Spiegelmer (157.9 ± 19.4 µg/mg; $P < 0.05$, Figure 2A). Nondiabetic control mice had an albumin/creatinine ratio of 58.5 ± 13.2 µg/mg. Because MCP-1 inhibition in diabetic patients revealed a strong legacy effect with regard to reduced albuminuria(14), we also investigated albumin leakage after a 4-week follow-up period. Four weeks after cessation of mNOX-E36 treatment, mice still showed a trend towards lower albumin/creatinine ratio compared to control-treated diabetic mice (132.4 ± 17.8 versus 98.8 ± 15.2, $P = 0.180$). After mNOX-E36 treatment and the follow up period no changes were observed in mesangial area in comparison to control diabetic *apoE* KO mice (8.6 ± 4.6% versus 11.9 ± 4.4%, mNOX-E36 and control, respectively; Figure 2B). With respect to podocyte injury, no changes were found in the number of Wilms tumor-1-positive podocytes or expression of slit diaphragm proteins nephrin and synaptopodin on MCP-1 inhibition (Figure 2C and D). Furthermore, mNOX-E36 did not prevent interstitial tubular epithelial injury, as indicated by similar urinary kidney injury molecule-1 excretion levels (data not shown).

Urinary MCP-1 concentrations were lower than the detection limit of our assays (< 15.6 pg/ml) in nondiabetic *apoE* KO mice as well as diabetes *apoE* KO mice. This is in support of the concept that our observations can be best explained by local changes at the tissue level. However, increased MCP-1 concentrations were observed in the mice treated with mNOX-E36 after 4 weeks of treatment (40.2 ± 15.8 pg/ml), whereas these levels were diminished 4 weeks after termination of treatment (< 15.6 pg/ml). These findings are in line with previous observations by Darisipudi et al(12). They demonstrated that mNOX-E36 forms an inactive complex with its molecular target (MCP-1), which is cleared much slower than MCP-1, and is detectable in the ELISA. In this case, the MCP-1 levels therefore reflect the pharmacodynamics of the compound.

Next, we tested the effect of mNOX-E36 treatment on the glomerular endothelial glycocalyx coverage, being the first layer in the glomerular filtration barrier. This was visualized and quantified by cationic ferritin binding to the negatively charged glomerular endothelial glycocalyx (Figure 2E). Renal perfusion resulted in cationic ferritin binding to the luminal endothelial cell surface, but also directly underneath the endothelium. The latter served as an endogenous control: only capillaries that showed cationic ferritin on the surface of the endothelium and / or in the GBM were used for analysis. Diabetes resulted in less endothelial coverage at 22 weeks of age (57.3 ± 20.2%) compared with nondiabetic *apoE* KO mice (83.6 ± 8.4%, Figure 2F). Treatment with mNOX-E36 increased glomerular glycocalyx coverage to a percentage comparable to nondiabetic glomeruli (81.9 ± 17.1%, $P < 0.05$). Interestingly, although the endothelial glycocalyx has a high turnover, its recovery upon treatment remained visible 4 weeks after treatment pointing towards a legacy effect of the treatment. At week 26, cationic ferritin coverage in control-treated diabetic mice was reduced (37.0 ± 9.2%, $P < 0.05$), compared with nondiabetic *apoE* KO mice, whereas coverage in mNOX-E36 treated mice still remained higher compared with control-treated diabetic mice (74.7 ± 16.9%, $P < 0.05$).

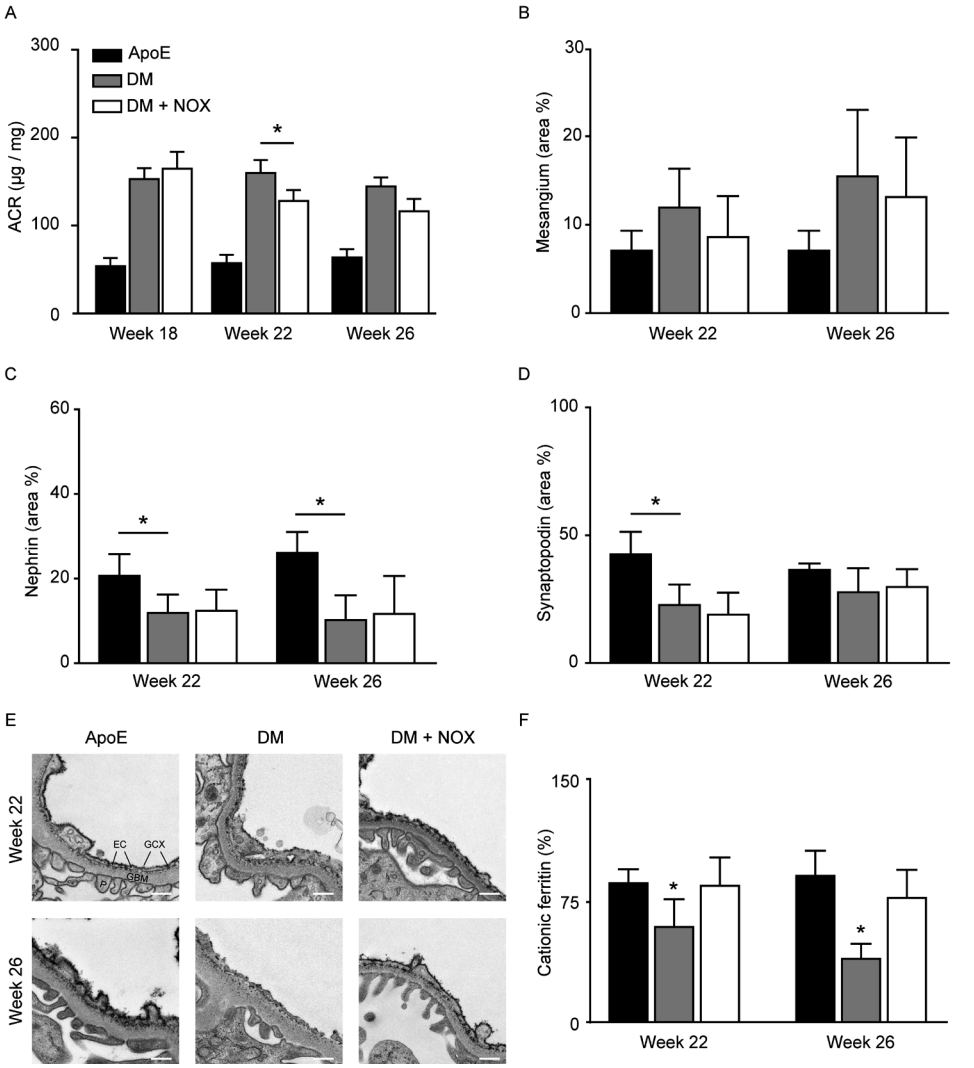


Figure 2. Monocyte chemotactic protein-1 inhibition reduces albuminuria in diabetic *apoE* knockout (KO) mice. A) Urinary albumin/creatinine ratios (ACRs) at baseline (week 18), 4 weeks of treatment (week 22) and after four weeks of follow-up (week 26). B) Mesangial area is not affected by treatment, as measured by percentage periodic acid-Schiff positive area per glomerulus. C and D) Nephrin (C) and Synaptopodin (D) are expressed as percentage glomerular area. Both are not affected by treatment. E) Representative transmission electron microscopic images of cationic ferritin bound to the negatively charged endothelial glycocalyx in glomeruli. F) Quantification of endothelial cationic ferritin coverage in capillary loops in 9 glomeruli of 3 mice, shown as percentage of total capillary length. Significance compared with *apoE* O mice (ApoE) and diabetic Apoe KO mice treated with inactive revmNOX-E36 (DM). Data are expressed as means ± SD (D and F). *P<0.05. n = 13 (A, ApoE); n = 23 (A, DM and diabetic Apoe KO mice treated with mNOX-E36 (DM+NOX) at week 22); n = 10 (A, DM at week 26); n = 11 (A, DM + NOX at week 26); n = 8 per group (B); n = 5 to 8 per treatment group (C and D). EC = endothelium; GBM = Glomerular basement membrane; GCX = cationic ferritin bound to endothelial glycocalyx; P = podocyte. Scale bars: 500 nm (E).

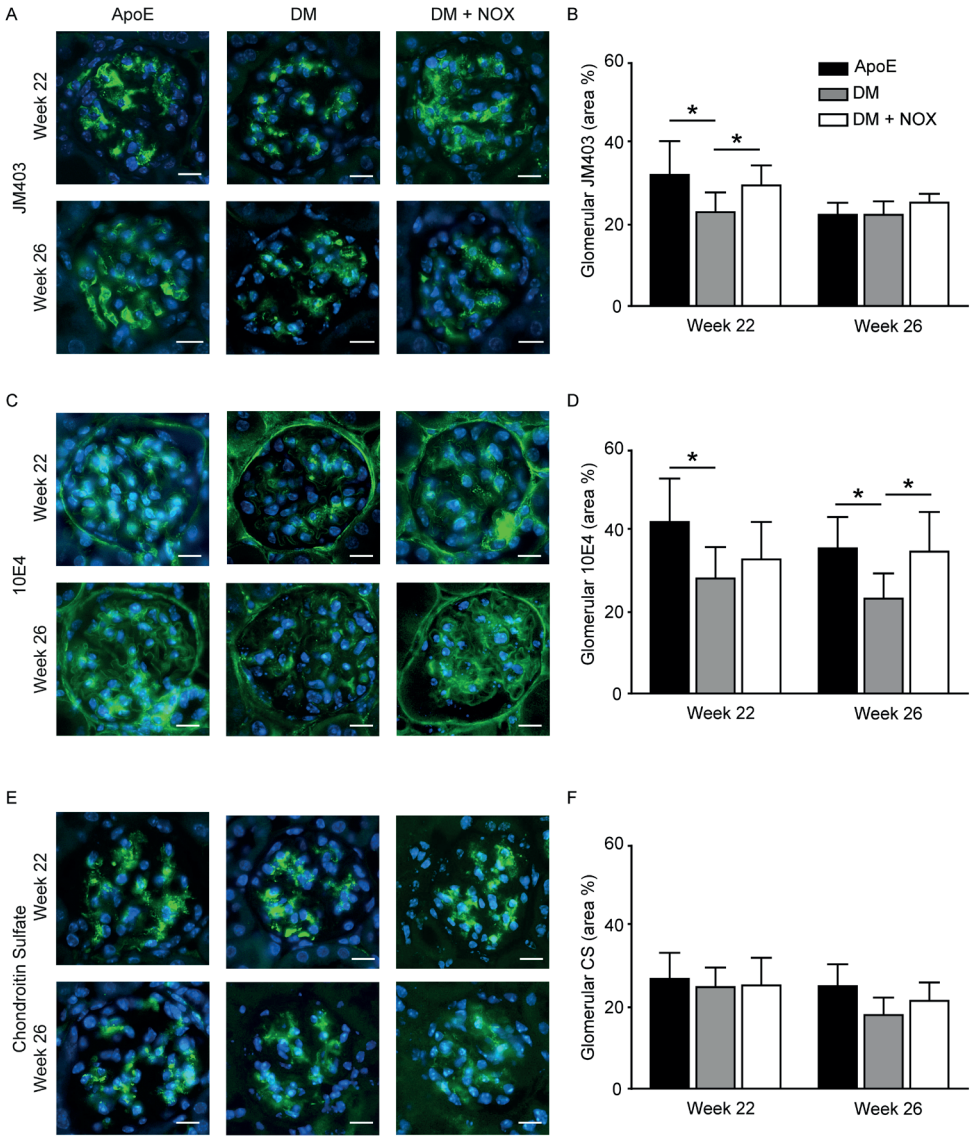


Figure 3. Monocyte chemotactic protein-1 inhibition changes glomerular heparan sulfate expression. A, C and E) Representative images of glomerular JM403 (A), 10E4 (C) and chondroitin sulfate (CS; E) expression in *apoE* knockout (KO) mice (ApoE), diabetic *apoE* KO mice treated with inactive revmNOX-E36 (DM), or active mNOX-E36 (DM + NOX). B, D and F) Quantification of glomerular expression, shown as percentage positivity. Data are expressed as mean ± SD. n = 5-8 per treatment group. *P<0.05. Scale bar: 20 µm (A, C and E).

The changes in glomerular endothelial glycocalyx coverage were further analyzed with respect to specific glycocalyx heparan and chondroitin sulfate composition. Heparan sulfate (HS) structures were analyzed using 10E4 and JM403 antibodies, recognizing so-called mixed HS domains, containing both N-acetylated and N-sulfated disaccharide units (10E4) or N-unsubstituted glucosamine residues (JM403). Diabetes reduced glomerular JM403 expression to 23.7 ± 7.6%, whereas in mNOX-E36 treated mice expression was higher (33.1 ± 8.0%, $P < 0.05$), comparable to nondiabetic mice (Figure 3A-B). 10E4 levels were reduced in diabetic mice, but in mNOX-E36 treated mice they were comparable to nondiabetic mice (Figure 3C-D). Four weeks after cessation of treatment there was still a legacy effect both with respect to both the diabetes effect on HS composition and the amelioration by mNOX-E36. Chondroitin sulfate expression was neither affected by diabetes nor by mNOX-E36 treatment at all points measured (Figure 3E-F).

MCP-1 inhibition reduces heparanase and cathepsin L expression

The glycocalyx consists of multiple glycoproteins and glycosaminoglycans, of which heparan sulfates are the most dominant. To analyze the mechanism of restored glycocalyx dimensions

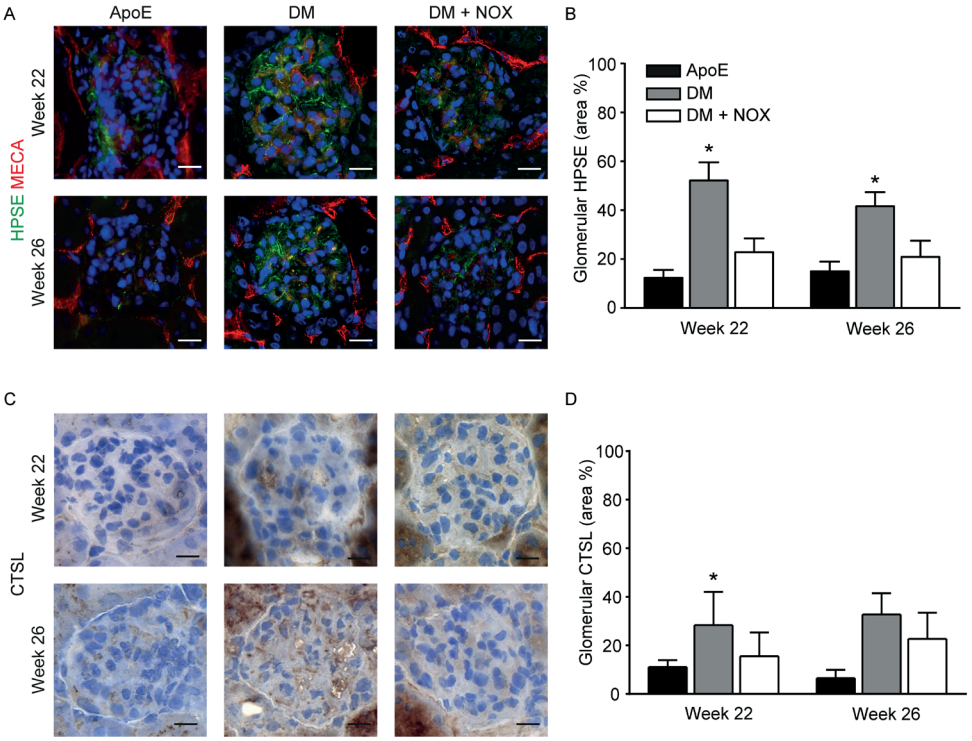


Figure 4. Monocyte chemotactic protein-1 inhibition reduces glomerular HPSE and Cathepsin-L expression. A and C) Representative images of glomerular heparanase (A) and cathepsin-L (CTSL; C) expression in *apoE* KO mice (ApoE), diabetic *apoE* KO mice treated with inactive revmNOX-E36 (DM), or active mNOX-E36 (DM + NOX). B and D) Quantification of glomerular expression shown as percentage positivity. Data are expressed as mean ± SD. n = 5-8 per treatment group. *P<0.05, compared with *apoE* and DM + mNOX-E36. Scale bar: 20 µm (A and C).

upon treatment, we looked at the expression of the heparan sulfate degrading enzyme heparanase. Diabetic mice show increased glomerular heparanase protein expression compared with nondiabetic *apoE* KO mice (48.9 ± 20.9% versus 12.7 ± 9.3%, $P < 0.05$; Figure 4A-B). Treatment of diabetic mice with mNOX-E36 effectively reduced glomerular heparanase protein expression to 25.4 ± 13.8% ($P < 0.05$). This effect remained present 4 weeks after treatment with mNOX-E36 has stopped (52.8 ± 17.7% versus 22.6 ± 18.2%, $P < 0.05$). Secreted latent proheparanase is activated by cathepsin L(18, 25). We previously showed by immunohistochemistry that the macrophage marker F4/80 co-localizes with cathepsin L(15). Together with the elevated heparanase expression, increased glomerular cathepsin L protein expression was observerd in diabetic *apoE* KO mice (27.6 ± 12.0% versus 11.1 ± 2.8% in nondiabetic control, $P < 0.05$) and after treatment with mNOX-E26, cathepsin L expression was significantly reduced (13.7 ± 9.5%, $P < 0.05$, Figure 4C-D). However, 4 weeks after cessation of treatment, cathepsin L expression in the mNOX-E36-treated group was not significantly different from control-treated diabetic mice (33.4 ± 9.5% versus 22.9 ± 11.9%, $P = 0.105$).

MCP-1 inhibition changes macrophage properties

Inflammatory cells, such as monocytes and macrophages, can secrete cathepsin L. Although the number of peripheral blood monocytes did not change on treatment with mNOX-E36 (FACS analysis, data not shown), a lower mean fluorescence intensity of CCR2 was observed (mNOX-E36 versus control treated, 181.5 ± 132.3 versus 437.5 ± 282.6) on the $Ly6C^{hi}$ subset of monocytes (Supplementary Figure S2A). These inflammatory-prone $Ly6C^{hi}$ monocytes, in particular, depend on MCP-1/CCR2 recruitment to inflamed tissues(26). In accordance, the reduced CCR2 expression on these cells correlated with increased chemokine C-X3-C motif receptor 1 expression (Pearson $r = 0.962$; $P = 0.038$; data not shown)(27).

Immunohistochemistry revealed that the number of $F4/80^+$ macrophages in the tubulointerstitial and glomerular compartment was increased in diabetic mice compared with controls, but no change in absolute number of macrophages was observed upon MCP-1 inhibition based on immunofluorescence (Figure 5A-B). Further analysis of $CD206^+/Mac3^+$ cells showed that in mNOX-E36-treated mice the ratio $CD206^+/Mac3^+$ over $Mac3^+$ increased, revealing more regulatory macrophages within the glomeruli (week 22: 46.8 ± 12.4% versus 31.2 ± 5.2%; week 26: 56.7 ± 11.4% versus 28.1 ± 10.1%; $P < 0.05$; Figure 5C).

FACS analysis to quantify $F4/80^+$ macrophages in whole kidney confirmed this lack in change of absolute macrophage number (control versus mNOX-E36-treated mice, 4.6 ± 2.5% versus 3.8 ± 1.6% at week 22 and 6.1 ± 1.6% versus 5.0 ± 1.6% at week 26; Figure 5D), as well as unchanged CCR2 expression of monocytes ($Ly6C^{low/med/hi}$; Supplementary Figure S2). The functional phenotype of renal macrophages was further analyzed in detail. Isolated renal $CD11b^+$, $B220^-$, $Lyc6G^-$, $F4/80^+$ macrophages from diabetic mice treated with mNOX-E-36 or control Spiegelmer (Figure 5C; isolation protocol in Supplementary Figure S1) were stimulated with LPS to determine their cytokine profile. Macrophages from mNOX-E36-treated diabetic mice responded with increased production and release of IL-10 (from 18.8 ± 4.6 pg/mL to 34.3 ±

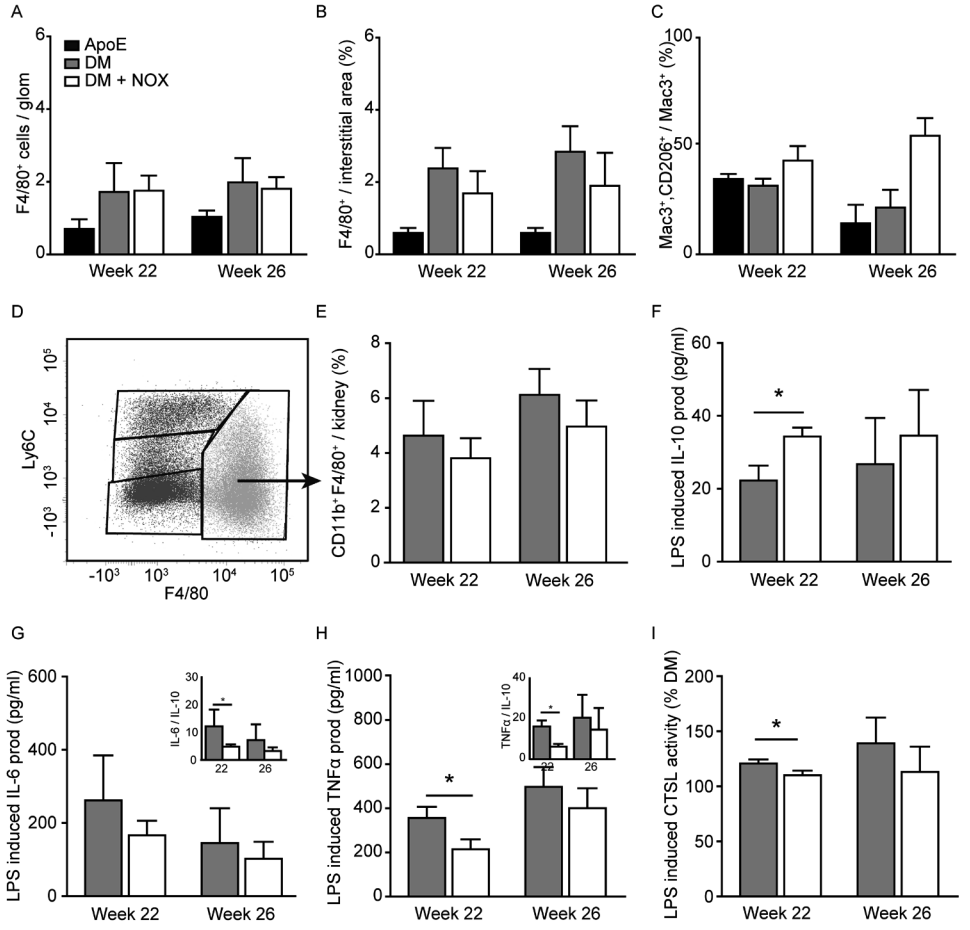


Figure 5. Monocyte chemotactic protein-1 inhibition changes glomerular macrophages towards a regulatory phenotype. A and B) The number of glomerular (A) and tubulointerstitial (B) F4/80$^+$ macrophages increases in diabetes, but does not differ between treatment groups. Macrophages were isolated from the kidney by fluorescence-activated cell sorting (FACS), based on CD11b$^+$F4/80$^+$ positivity. C) The ratio of MAC3 and CD206 double-positive macrophages compared to MAC3-positive cells is affected by mNOX-E36. D) Representative FACS plot; orange dots are selected macrophages for isolation. E) Quantification of renal macrophages. F-H) IL-10, IL-6 and tumor necrosis factor (TNF)-α secretion by renal macrophages after *ex vivo* lipopolysaccharide (LPS) treatment for 24 hours; Inserted figures in F and G show IL6/IL10 and TNFα/IL10 ratios, respectively. I) Cathepsin L (CTSL) activity in the supernatant of isolated macrophages was measured and expressed relatively to unstimulated macrophages.

Data are expressed as means ± SD (). n = 3 mice per group (). *P < 0.05. ApoE = *apoE* KO mice, DM = (macrophages isolated from) diabetic *apoE* KO mice treated with inactive revmNOX-E36, DM + NOX = (macrophages isolated from) diabetic *apoE* KO mice treated with mNOX-E36; KO = knockout.

2.5 pg/mL), which was higher compared to macrophages of control-treated mice (22.3 ± 4.1 pg/mL, P <0.05, Figure 5F). The production of IL-6, determined as an intermediate cytokine with both pro- and anti-inflammatory effects(28), did not differ significantly between these groups (Figure 5G). However, release of the pro-inflammatory cytokine TNFα, was significantly

decreased upon treatment with mNOX-E36 (214.4 ± 45.2 pg/mL versus 356.1 ± 50.8 pg/mL, control and mNOX-E36, respectively; P<0.05; Figure 5H). Accordingly, the reduction in individual IL-6/IL-10 (insert Figure 5G) and TNFα/IL-10 ratios (insert Figure 5H) confirmed the overall anti-inflammatory cytokine expression of renal macrophages after treatment with mNOX-E36. Moreover, LPS induced a 20.7 ± 3.7% increase in active cathepsin L release, which was reduced by mNOX-E36 to 10.1 ± 4.2% (Figure 5I).

In addition, mNOX-E36 exerted a similar effect on cathepsin L secretion by murine RAW264.7 macrophages after MCP-1 and lipopolysaccharide stimulation (Supplementary Figure S3). Thus, mNOX-E36 can directly reduce the capacity of macrophages to secrete cathepsin L.

Discussion

In the present study, we show that MCP-1 inhibition in diabetic nephropathy effectively reduces albuminuria in association with restoration of glomerular endothelial glycocalyx dimensions. This effect was observed in the absence of hemodynamic changes and in the presence of podocyte injury, underscoring the importance of the glomerular endothelial glycocalyx for its barrier function. MCP-1 inhibition was also accompanied by a reduction in glomerular cathepsin L and heparanase expression *in vivo*, as well as a shift towards anti-inflammatory resident renal macrophages, as we could show functionally after *ex vivo* stimulation. One aspect of this polarization of macrophage function by MCP-1 inhibition is a decreased ability to secrete cathepsin L.

In a diabetic milieu, the glycocalyx is degraded in a heparanase-dependent manner(17, 29). In our model this was reflected by selective changes in heparan sulfate structures as well as reduction of N-unsubstituted glucosamine domains, while chondroitin sulfates did not change. In glomeruli, heparanase is produced as inactive proheparanase by podocytes, endothelial cells and platelets(30). Activation of proheparanase generally occurs after uptake into the early endosome and lysosome through cathepsin L(31). Cathepsin L proteolytically activates proheparanase into its active heparan sulfate degrading form(25), after which heparanase serves intracellular regulatory processes(32). However, macrophages also secrete cathepsin L during lysosomal delivery, thus allowing the activation of proheparanase in the extracellular environment(33, 34). This process can be further accelerated by diabetes-induced changes in the extracellular matrix(35), as well as by active heparanase itself that activates macrophages by inducing toll like receptor signaling(29).

Monocytes high in CCR2 expression (Ly6C^{hi} subset) exhibit pro-inflammatory properties(27). mNOX-E36 reduces CCR2 expression in peripheral circulating monocytes in our study, as was observed in the clinical study(14), suggesting less inflammatory potential and less sensitivity towards MCP-1 gradients in tissue(4). Nevertheless, tissue levels in the spleen and kidney of these CCR2 expressing monocytes were not reduced. Yet, we found that mNOX-E36 markedly changed the functional behavior of resident kidney macrophages: Although there was no difference in total number of renal macrophages, their differentiation and function had

changed after MCP-1 inhibition. mNOX-E36 induced an anti-inflammatory phenotype of the renal macrophages. For example, the capacity to produce TNF-α was reduced, which is relevant as TNF-α induces heparanase gene expression in mouse glomerular endothelial cells and podocytes(36). Moreover, there was a reduction in the release of cathepsin L, the enzyme that has been shown to be essential in the development of diabetic nephropathy(18). TNF-α induced secretion of cathepsin L from macrophages(37), contributes to the vicious circle of self-stimulation of macrophages.

Podocytes also have been shown to express the CCR2 receptor(38). This suggests that MCP-1 could possibly have influenced glomerular filtration barrier function via podocytes as well. In our current study, however, MCP-1 inhibition neither restored diabetes-induced decrease of slit diaphragm proteins nephrin and synaptopodin nor affected the number of podocytes. In podocytes, cathepsin L is involved in breakdown of Synaptopodin(18, 39), but apparently, this process was not ameliorated by MCP-1 inhibition. These data suggest that mNOX-E36 did not reduce albuminuria by improving podocyte function.

Interestingly, there appears to be a treatment legacy effect on some parameters in this study, at 4 weeks after cessation of treatment. More specific, heparanase expression was still reduced and the glycocalyx as well as heparan sulfate composition still preserved. This further corroborates that the effects of MCP-1 inhibition are independent of hemodynamic changes and are related to (ultra)structural glomerular restoration. These findings on treatment legacy were also noted in the clinical study where emapticap pegol induced beneficial effects on albumin/creatinine ratio and HbA1c, without hemodynamic changes, were maintained on termination of treatment(14). The presence of MCP-1-mNOX-E36 complexes in the urine up to 4 weeks after treatment further suggests a prolonged pharmacodynamic effect of this compound. Together, MCP-1 blockade has additional potential in the treatment of diabetic nephropathy where therapeutic options are currently still limited. This notion is supported by observations in human diabetic nephropathy, where increased renal and urinary MCP-1 levels have been found(40), and provides a mechanism of action for recent observations in human diabetic nephropathy where blockade of MCP-1 reduced albuminuria(14).

In conclusion, we found persistent restoration of the glomerular endothelial glycocalyx in diabetic nephropathy with MCP-1 inhibition. Our data suggest that interference with macrophage function attenuates the degradation of the glycocalyx by heparanase, resulting in less albuminuria.

Acknowledgements

We thank Prof A.J. Koster (Molecular Cell Biology, LUMC) for the use of the electron microscope facilities. We thank NOXXON Pharma AG (Berlin, Germany) for providing mNOX-E36 and for analysis of mNOX-E36 plasma levels.

This study was financially supported by the Dutch Kidney Foundation: Kolff Grant 14OKG06 (DI) and Glycoren consortium (CP09.03; TR)

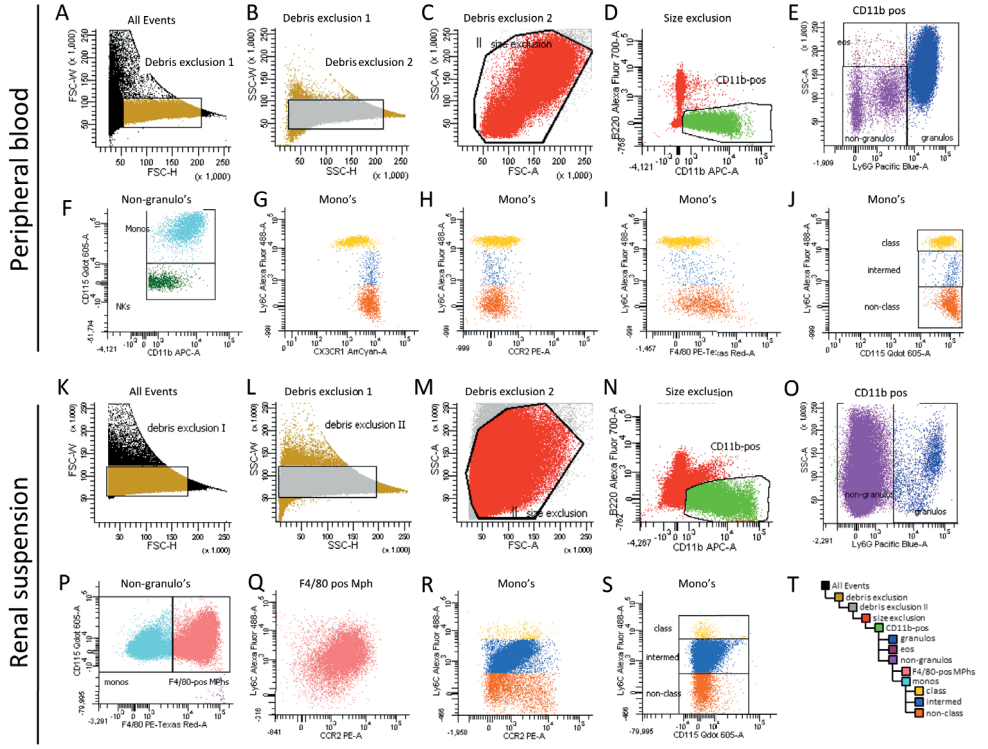
References

1. U.S. Renal Data System (2012) Annual Data Report: Atlas of Chronic Kidney Disease and End-Stage Renal Disease in the United States. National Institute of Diabetes and Digestive and Kidney Diseases, Bethesda, MD., 2012.
2. Heerspink HJ, De Zeeuw D. Novel anti-inflammatory drugs for the treatment of diabetic kidney disease. Diabetologia. 2016;59(8):1621-3.
3. Van Coillie E, Van Damme J, Opdenakker G. The MCP/eotaxin subfamily of CC chemokines. Cytokine & growth factor reviews. 1999;10(1):61-86.
4. Haller H, Bertram A, Nadrowitz F, Menne J. Monocyte chemoattractant protein-1 and the kidney. Current opinion in nephrology and hypertension. 2016;25(1):42-9.
5. Biswas SK, Sodhi A, Paul S. Regulation of nitric oxide production by murine peritoneal macrophages treated in vitro with chemokine monocyte chemoattractant protein 1. Nitric Oxide. 2001;5(6):566-79.
6. Biswas SK, Sodhi A. In vitro activation of murine peritoneal macrophages by monocyte chemoattractant protein-1: upregulation of CD11b, production of proinflammatory cytokines, and the signal transduction pathway. J Interferon Cytokine Res. 2002;22(5):527-38.
7. Tashiro K, Koyanagi I, Saitoh A, Shimizu A, Shike T, Ishiguro C, et al. Urinary levels of monocyte chemoattractant protein-1 (MCP-1) and interleukin-8 (IL-8), and renal injuries in patients with type 2 diabetic nephropathy. J Clin Lab Anal. 2002;16(1):1-4.
8. Nguyen D, Ping F, Mu W, Hill P, Atkins RC, Chadban SJ. Macrophage accumulation in human progressive diabetic nephropathy. Nephrology. 2006;11(3):226-31.
9. Klessens CQ, Zandbergen M, Wolterbeek R, Bruijn JA, Rabelink TJ, Bajema IM, et al. Macrophages in diabetic nephropathy in patients with type 2 diabetes. Nephrology, dialysis, transplantation : official publication of the European Dialysis and Transplant Association - European Renal Association. 2017 Aug 1;32(8):1322-1329.
10. Chow FY, Nikolic-Paterson DJ, Ozols E, Atkins RC, Rollin BJ, Tesch GH. Monocyte chemoattractant protein-1 promotes the development of diabetic renal injury in streptozotocin-treated mice. Kidney international. 2006;69(1):73-80.
11. Ninichuk V, Clauss S, Kulkarni O, Schmid H, Segerer S, Radomska E, et al. Late onset of Ccl2 blockade with the Spiegelmer mNOX-E36-3'PEG prevents glomerulosclerosis and improves glomerular filtration rate in db/db mice. The American journal of pathology. 2008;172(3):628-37.
12. Darisipudi MN, Kulkarni OP, Sayyed SG, Ryu M, Migliorini A, Sagrinati C, et al. Dual blockade of the homeostatic chemokine CXCL12 and the proinflammatory chemokine CCL2 has additive protective effects on diabetic kidney disease. The American journal of pathology. 2011;179(1):116-24.
13. de Zeeuw D, Bekker P, Henkel E, Hasslacher C, Gouni-Berthold I, Mehling H, et al. The effect of CCR2 inhibitor CCX140-B on residual albuminuria in patients with type 2 diabetes and nephropathy: a randomised trial. Lancet Diabetes Endocrinol. 2015;3(9):687-96.
14. Menne J, Eulberg D, Beyer D, Baumann M, Saudek F, Valkusz Z, et al. C-C motif-ligand 2 inhibition with emapticap pegol (NOX-E36) in type 2 diabetic patients with albuminuria. Nephrology, dialysis, transplantation : official publication of the European Dialysis and Transplant Association - European Renal Association. 2017 Feb 1;32(2):307-315.
15. Boels MG, Avramut MC, Koudijs A, Dane MJ, Lee DH, van der Vlag J, et al. Atrasentan Reduces Albuminuria by Restoring the Glomerular Endothelial Glycocalyx Barrier in Diabetic Nephropathy. Diabetes. 2016;65(8):2429-39.
16. Nieuwdorp M, Mooij HL, Kroon J, Atasever B, Spaan JA, Ince C, et al. Endothelial glycocalyx damage coincides with microalbuminuria in type 1 diabetes. Diabetes. 2006;55(4):1127-32.
17. van den Hoven MJ, Rops AL, Bakker MA, Aten J, Rutjes N, Roestenberg P, et al. Increased expression of heparanase in overt diabetic nephropathy. Kidney international. 2006;70(12):2100-8.
18. Garsen M, Rops AL, Dijkman H, Willemsen B, van Kuppevelt TH, Russel FG, et al. Cathepsin L is crucial for the development of early experimental diabetic nephropathy. Kidney international. 2016 Nov;90(5):1012-1022.

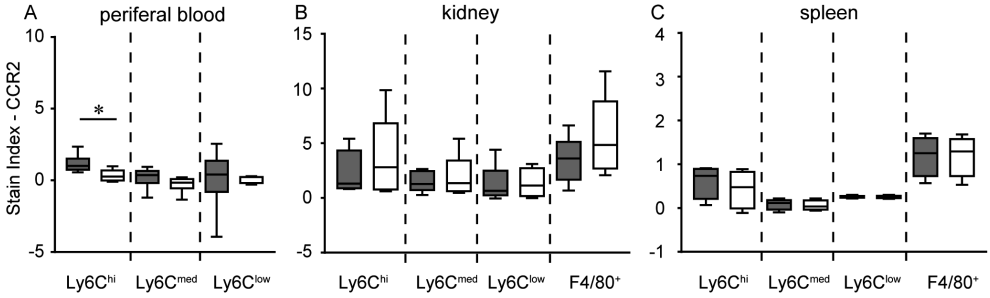
19. Kalnins A, Thomas MN, Andrassy M, Muller S, Wagner A, Pratschke S, et al. Spiegelmer Inhibition of MCP-1/CCR2--Potential as an Adjunct Immunosuppressive Therapy in Transplantation. Scandinavian journal of immunology. 2015;82(2):102-9.
20. Austyn JM, Gordon S. F4/80, a monoclonal antibody directed specifically against the mouse macrophage. European journal of immunology. 1981;11(10):805-15.
21. Ezekowitz RA, Gordon S. Alterations of surface properties by macrophage activation: expression of receptors for Fc and mannose-terminal glycoproteins and differentiation antigens. Contemporary topics in immunobiology. 1984;13:33-56.
22. Faas FG, Avramut MC, van den Berg BM, Mommaas AM, Koster AJ, Ravelli RB. Virtual nanoscopy: generation of ultra-large high resolution electron microscopy maps. The Journal of cell biology. 2012;198(3):457-69.
23. Maecker HT, Frey T, Nomura LE, Trotter J. Selecting fluorochrome conjugates for maximum sensitivity. Cytometry Part A : the journal of the International Society for Analytical Cytology. 2004;62(2):169-73.
24. Ehling J, Bartneck M, Wei X, Gremse F, Fech V, Mockel D, et al. CCL2-dependent infiltrating macrophages promote angiogenesis in progressive liver fibrosis. Gut. 2014;63(12):1960-71.
25. Abboud-Jarrous G, Atzmon R, Peretz T, Palermo C, Gadea BB, Joyce JA, et al. Cathepsin L is responsible for processing and activation of proheparanase through multiple cleavages of a linker segment. The Journal of biological chemistry. 2008;283(26):18167-76.
26. Shi C, Pamer EG. Monocyte recruitment during infection and inflammation. Nature reviews Immunology. 2011;11(11):762-74.
27. Geissmann F, Jung S, Littman DR. Blood monocytes consist of two principal subsets with distinct migratory properties. Immunity. 2003;19(1):71-82.
28. Stenvinkel P, Ketteler M, Johnson RJ, Lindholm B, Pecoits-Filho R, Riella M, et al. IL-10, IL-6, and TNF-alpha: central factors in the altered cytokine network of uremia--the good, the bad, and the ugly. Kidney international. 2005;67(4):1216-33.
29. Goldberg R, Rubinstein AM, Gil N, Hermano E, Li JP, van der Vlag J, et al. Role of heparanase-driven inflammatory cascade in pathogenesis of diabetic nephropathy. Diabetes. 2014;63(12):4302-13.
30. Rabelink TJ, de Zeeuw D. The glycocalyx--linking albuminuria with renal and cardiovascular disease. Nature reviews Nephrology. 2015;11(11):667-76.
31. Zetser A, Levy-Adam F, Kaplan V, Gingis-Velitski S, Bashenko Y, Schubert S, et al. Processing and activation of latent heparanase occurs in lysosomes. J Cell Sci. 2004;117(Pt 11):2249-58.
32. Wang F, Wang Y, Zhang D, Puthanveetil P, Johnson JD, Rodrigues B. Fatty acid-induced nuclear translocation of heparanase uncouples glucose metabolism in endothelial cells. Arteriosclerosis, thrombosis, and vascular biology. 2012;32(2):406-14.
33. Simeonovic CJ, Ziolkowski AF, Wu Z, Choong FJ, Freeman C, Parish CR. Heparanase and autoimmune diabetes. Frontiers in immunology. 2013;4:471.
34. Rabelink TJ, van den Berg BM, Garsen M, Wang G, Elkin M, van der Vlag J. Heparanase: roles in cell survival, extracellular matrix remodelling and the development of kidney disease. Nature reviews Nephrology. 2017;13(4):201-12.
35. Bogdani M, Johnson PY, Potter-Perigo S, Nagy N, Day AJ, Bollyky PL, et al. Hyaluronan and Hyaluronan Binding Proteins Accumulate in both Human Type 1 Diabetic Islets and Lymphoid Tissues and Associate with Inflammatory Cells in Insulitis. Diabetes. 2014 Aug;63(8):2727-43.
36. Garsen M, Benner M, Dijkman HB, van Kuppevelt TH, Li JP, Rabelink TJ, et al. Heparanase Is Essential for the Development of Acute Experimental Glomerulonephritis. The American journal of pathology. 2016;186(4):805-15.
37. Shi GP, Dolganov GM. Comprehensive transcriptome of proteases and protease inhibitors in vascular cells. Stroke. 2006;37(2):537-41.
38. Tarabra E, Giunti S, Barutta F, Salvidio G, Burt D, Deferrari G, et al. Effect of the monocyte chemoattractant protein-1/CC chemokine receptor 2 system on nephrin expression in streptozotocin-treated mice and human cultured podocytes. Diabetes. 2009;58(9):2109-18.

39. Faul C, Donnelly M, Merscher-Gomez S, Chang YH, Franz S, Delfgaauw J, et al. The actin cytoskeleton of kidney podocytes is a direct target of the antiproteinuric effect of cyclosporine A. Nature medicine. 2008;14(9):931-8.

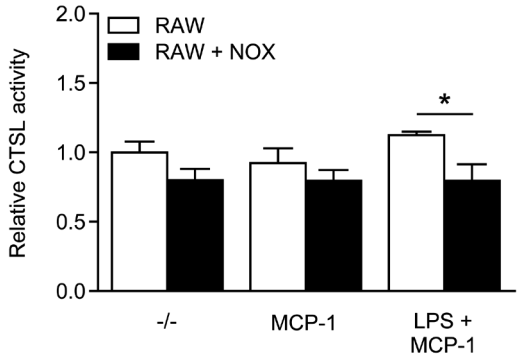
40. Wada T, Furuichi K, Sakai N, Iwata Y, Yoshimoto K, Shimizu M, et al. Up-regulation of monocyte chemoattractant protein-1 in tubulointerstitial lesions of human diabetic nephropathy. Kidney international. 2000;58(4):1492-9.



Supplementary Figure S1. Gating strategies for flow cytometry analysis in peripheral blood and renal suspension. A-C) For peripheral blood, a gate is drawn on all cells in forward/side scatter (FSC/SSC) plots to exclude debris. C and D) Of the cells gated in plot C, the expression of CD11b (x axis) and B220 (y axis) is shown in plot D, on which gates are placed on the $CD11^+$ cells. E) $CD11^+$ cells are selected in plot, showing expression of Ly6G (x axis) and SSC (y axis), in which the $Ly6G^-/SSC^{low}$ cells represent the nongranulocytic cells (Nongranulos). F) These cells are selected in plot, showing their expression of CD11b (x axis) and CD115 (y axis). G-I: The CD115-positive (pos) monocytes (Monos) are selected in plot to determine CX3CR1, CCR2, and F4/80 expression in classic (class), proinflammatory (Ly6Chi), intermediate (intermed; Ly6Cmed), and nonclassic (non-class), anti-inflammatory, and repair-associated (Ly6Clow) monocytes. J) An overview of all CD115-positive cells. K-M: For macrophage isolation from renal suspension, a gate is drawn on all cells in FSC/SSC plots to exclude debris. M and N) Of the cells gated in plot M, the expression of CD11b (x axis) and B220 (y axis) is shown in plot N, on which gates are placed on the $CD11^+$ cells. O) The $CD11^+$ cells are selected in plot O, showing expression of Ly6G (x axis) and SSC (y axis), in which the $Ly6G^-$ cells represent the nongranulocytic cells. P) These cells are selected in plot P, showing their expression of CD11b (x axis) and CD115 (y axis). P and Q) $F4/80^+$ cells (pink) are selected for isolation. R and S) The $F4/80^+$ monocytes are selected in plot R to determine CCR2 expression and classic (Ly6Chi), intermediate (Ly6Cmed), and nonclassic (Ly6Clow) monocytes. S) An overview of all cells. T) The color legends.



Supplementary Figure S2. Fluorescence-activated cell sorting analyses of cellular subpopulations. Mean fluorescence intensity (MFI) for CCR2 was measured in peripheral blood (A), renal cells (B), and spleen (C). MFI is expressed as stain index for CCR expression in classic, proinflammatory (Ly6Chi), intermediate (Ly6Cmed), and non-classic, anti-inflammatory, and repair-associated (Ly6Clow) monocytes. *P < 0.05.



Supplementary Figure S3. mNOX-E36 reduces cathepsin L (CTSL) secretion in RAW264.7 macrophages. The murine RAW264.7 macrophage cell line was obtained from ATCC (Manassas, VA) and cultured as recommended in Dulbecco's modified Eagle's medium supplemented with 10% fetal calf serum, 100 U/mL penicillin, and 100 mg/mL streptomycin. The RAW264.7 cell line was used to determine the capacity of mNOX-E36 to directly affect macrophage cathepsin L production. To prime macrophages, RAW264.7 cells were made quiescent by incubation in medium containing 0.5% fetal bovine serum for 24 hours. Similarly to the ex vivo experiments, macrophages were stimulated with 100 ng/mL monocyte chemotactic protein-1 (MCP-1; R&D Systems, Minneapolis, MN) with or without 1 mg/mL lipopolysaccharide (LPS) for 24 hours in serum-free medium. A subset of cells was treated with 20 mg/mL (rev)mNOX-E36 (starting 30 minutes 1412 before stimulation), after which cathepsin L activity was determined in cell lysate. Data are expressed as means ± SD (expressed relatively to unstimulated macrophages). *P < 0.05. RAW, unstimulated RAW264.7 macrophages; RAW + NOX, RAW264.7 macrophages treated with mNOX-E36.

Chapter 4

Direct observation of enhanced nitric oxide in a murine model of diabetic nephropathy

PLoS One, 12(1): e0170065, 2017

Margien G.S. Boels, Ernst E.H. van Faassen, M. Cristina Avramut,
Johan van der Vlag, Bernard M. van den Berg, Ton J. Rabelink

Abstract

Uncoupling of nitric oxide synthase (NOS) secondary to redox signaling is a central mechanism in endothelial and macrophage activation. To date studies on the production of nitric oxide (NO) during the development of diabetic complications show paradoxical results. We previously showed that recoupling eNOS by increasing the eNOS cofactor tetrahydrobiopterin (BH_4) could restore endothelial function and prevent kidney injury in experimental kidney transplantation. Here, we employed a diabetic mouse model to investigate the effects of diabetes on renal tissue NO bioavailability. For this, we used *in vivo* NO trapping, followed by electron paramagnetic resonance spectroscopy. In addition, we investigated whether coupling of NOS by supplying the cofactor BH_4 could restore glomerular endothelial barrier function. Our data show that overall NO availability at the tissue level is not reduced sixteen weeks after the induction of diabetes in apoE knockout mice, despite the presence of factors that cause endothelial dysfunction, and the presence of the endogenous NOS inhibitor ADMA. Targeting uncoupled NOS with the BH_4 precursor sepiapterin further increases NO availability, but did not modify renal glomerular injury. Notably, glomerular heparanase activity as a driver for loss of glomerular barrier function was not reduced, pointing towards NOS-independent mechanisms. This was confirmed by unaltered increased glomerular presence of cathepsin L, the protease that activates heparanase.

Introduction

Endothelial dysfunction is assumed to contribute to kidney disease progression in diabetes (1) with endothelial nitric oxide (NO) production as a key feature of healthy endothelium. Uncoupling of NOS secondary to redox signaling is a central mechanism in endothelial activation. We previously showed that recoupling eNOS by increasing the NOS cofactor tetrahydrobiopterin (BH_4) could restore endothelial function and prevent kidney injury in experimental kidney transplantation (2, 3). BH_4 was also shown to modulate the iNOS isoform in macrophages, counterbalancing the redox effector pathway in these cells (4), where macrophage activation has also been implicated in progression of diabetic nephropathy (5, 6).

Conflicting results about the role of NO in diabetic nephropathy have, however, been publish *in vitro* as well as *in vivo*. Enhanced NO generation have been reported in studies of cultured hyperglycemic endothelial cells, advanced diabetes and diabetic nephropathy (7-9), whereas NO availability has also been reported to be diminished in the setting of human (10-12) and rodent (13-15) diabetic nephropathy. Also a time dependent effect has been reported: NO generation during the early stages of nephropathy was increased while it decreased in later stages (16, 17).

While eNOS knockout mice have proved to be invaluable for studies assessing the consequences of reduced NO availability in diabetic nephropathy (18), the absence of NO make these mice unsuited for our studies. Therefore, we treated apolipoprotein E knockout mice (apoE KO) with streptozotocin to induce stable and reproducible diabetic nephropathy (19, 20). We used *in vivo* NO spin-trapping with iron-dithiocarbamate complexes, a highly-sensitive quantitative technique that enables one to detect localized concentrations of trapped NO *in vivo* (21-24). Also, we assessed glomerular endothelial function, by determining glycocalyx integrity and barrier function.

Surprisingly, we observed enhanced renal NO bioavailability in the setting of diabetic nephropathy. We also found that sepiapterin, a BH_4 precursor, while further augmenting local NO levels, did not modify renal glomerular injury. This suggests that diabetes-induced endothelial dysfunction is not directly associated with renal NO deficiency. Notably, glomerular heparanase activity as a driver for loss of glomerular barrier function was not reduced, pointing towards NOS-independent mechanisms.

Materials and Methods

Diabetic ApoE KO mouse model

All animal experiments were approved by the ethical committee on animal care and experimentation of the Leiden University Medical Centre. All animal work was performed in compliance with the Dutch governmental guidelines. For our experiments, we used three groups of six weeks old male ApoE KO mice (Jackson Laboratory, Bar Harbor, ME). Diabetes was induced in two groups by intraperitoneal injections with streptozotocin (STZ, 60 mg/kg; Sigma-Aldrich, St. Louis, MO) in citrate buffer (0.1 mol/L, pH= 4.5) for five consecutive days, according to the DiaComp protocol (Fig 1). The non-diabetic control group was injected with citrate buffer alone. All mice were housed under normal day-night cycle with free access to drinking water and chow. Non-diabetic apoE KO mice received standard chow, whereas diabetic apoE KO mice

received cholesterol-enriched chow (0.15 wt%) (Technilab-BMI, Someren, The Netherlands). Twelve weeks after the induction of diabetes, these mice were divided in two groups: one group was treated with sepiapterin (10 mg/kg daily) in drinking water for four consecutive weeks, to increase NO levels. The other group received normal drinking water. Data obtained from non-diabetic apoE KO mice as well as control diabetic apoE KO mice are previously published (19).

Blood glucose concentrations were measured with an Accu-check glucose meter (Roche, Basel, Switzerland). When glucose concentrations exceeded 25 mmol/L, mice were treated with 1-2 units insulin (Lantus, Aventis Pharmaceuticals, Bridgewater, NJ, US) up to three times per week. Sixteen weeks after STZ injections, at 22 weeks of age, mice were sacrificed to perform NO-trapping in kidney, liver and heart.

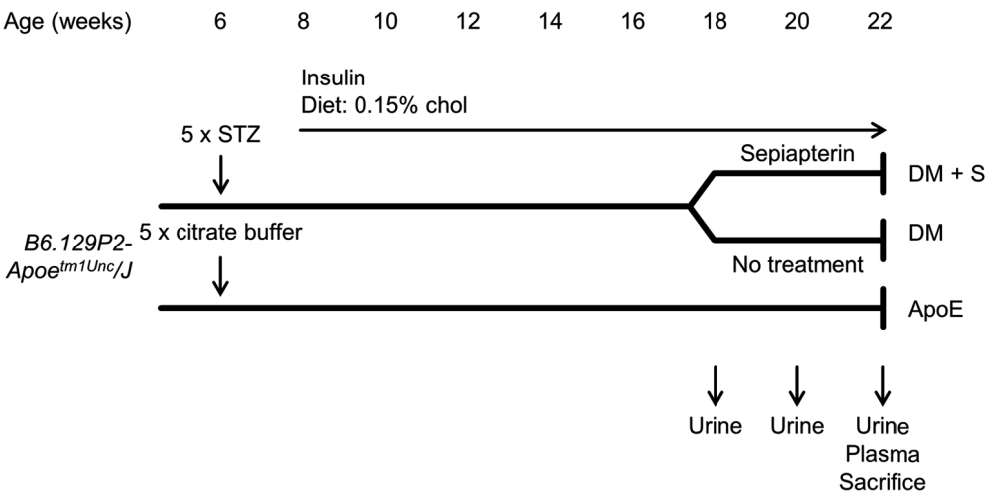


Figure 1. Experimental set-up for assessment of NO bioavailability (A) male ApoE KO mice (*B6.129P2-Apoe^{tm1Unc}/J*) were injected with citrate buffer ± STZ. Diabetic mice received cholesterol enriched diet and insulin from week 8 onwards. At 18 week of age, diabetic mice were treated with sepiapterin or received normal drinking water for 4 weeks. Urine was collected upon commencing with the experimental procedure and after 2 and 4 weeks of treatment. At 22 weeks, plasma was collected and the mice were sacrificed.

Urine Collection and Analyses

A 24-hour urine sample was collected at 12, 14 and 16 weeks after STZ injections. Urinary albumin and creatinine concentrations were determined as previously described (19). In brief, albumin concentrations were quantified with Rocket immunoelectrophoresis (25) and creatinine concentrations were quantified by the Jaffé method using 0.13% picric acid and a creatinine standard set (Sigma-Aldrich).

Immunohistochemistry

Following sacrificing by CO_2 asphyxiation, one half of a kidney was used for histological assessment of classical markers of glomerular damage and morphometric changes to confirm

diabetic nephropathy. For this, capillary and mesangial matrix area were quantified in Periodic acid-Schiff (PAS) or Trichrome-stained paraffin embedded 4 µm sections, respectively. We used a semiautomatic image analyzing system (Leica Q600 Qwin; Leica Microsystems, Cambridge, UK) to determine the fraction of glomerular surface area by the point-counting method.

Glomerular heparanase expression was quantified after overnight incubation with primary antibody (Polyclonal rabbit anti-heparanase 1.5 µg/mL, InSight Biopharmaceuticals, Rehovot, Israel), followed by goat anti-rabbit IgG-Alexa 594 (1/1000), for 1 hour, both in blocking buffer. Sections were counterstained with Hoechst (1/1000) and embedded in Vectashield mounting medium (Vector Laboratories Inc., Burlingame, CA). Cathepsin L polyclonal antibody (R&D Systems) was incubated overnight, followed by horseradish peroxidase–conjugated secondary antibody and 3,3'-diaminobenzidine and counterstained with hematoxylin. Staining area was quantified as the percentage of stained area divided by the glomerular area.

Determination of Nitric Oxide

In all three groups, endogenous NO bioavailability was measured by *in vivo* spin trapping with iron-diethyldithiocarbamates (Fe^{2+}-DETC) complexes as previously described (19). After 30 minutes of spin-trapping, mice were sacrificed using CO_2 asphyxiation. Subsequently, ~350 mg sections of kidney, liver and heart tissues were submerged in HEPES buffer (450 µl, 150 mmol/L, pH 7.4) and snap frozen with liquid nitrogen. The yield of paramagnetic ferrous mononitrosyl-iron complexes (MNIC) was determined with electron paramagnetic resonance (EPR) spectroscopy. For this, frozen tissue samples were measured at 77 K with an X-band EMX-Plus spectrometer (Bruker BioSpin, Rheinstetten, Germany) equipped with a Bruker liquid finger Dewar flask filled with liquid nitrogen. Spectrometer settings were microwave power, 20 mW; time constant, 82 ms; analog-to-digital conversion time, 82 ms; and detector gain, 10^4. The magnetic field was modulated with 5-G amplitude at a frequency of 100 kHz. With these settings, a single field sweep provided adequate sensitivity. During the experiments, the inside of the EPR cavity (ER 4119 HS-W1, cylindrical TE_{011} mode; Bruker) was continuously flushed with dry nitrogen to prevent condensation of ambient humidity on the cool Dewar flask.

Determination of plasma ADMA concentrations

Asymmetric N^G, N^G-dimethyl-L-arginine (ADMA) is an endogenous inhibitor of nitric oxide synthases. Therefore, we measured plasma ADMA concentrations with a commercially available enzyme-linked immunosorbent assay kit (DLD Diagnostika GmbH, Hamburg, Germany) according to the manufacturer's protocol.

Determination of glomerular endothelial glycocalyx coverage

For electron microscopic visualization of the glycocalyx, three mice per group were anesthetized (intraperitoneal). Left kidneys were perfused with 0.5% bovine serum albumin (BSA) and 5 U/mL heparin in 5 mL Hepes-buffered salt solution (HBSS), followed by 2 mL of cationic ferritin (horse spleen, 2.5 mg/mL, Electron Microscopy Sciences, Fort Washington, PA) in HBSS

alone at 2 mL/minute, as described before (19). Kidneys were excised, the capsules removed and stored in fixative (1.5% glutaraldehyde + 1% paraformaldehyde in 0.1 mol/L sodium-cacodylate buffered solution, pH 7.4) overnight at 4˚C and further prepared for transmission electron microscopy (TEM). Data was collected into large virtual slides (stitches) that provide an overview of the glomeruli, allowing for high-detail assessment and quantitative analysis of glomerular (patho)physiology (26). Images (2Kx2K) were acquired at an acceleration voltage of 120 kV, on FEI Tecnai T12 microscopes (FEI, Eindhoven, the Netherlands), equipped with FEI Eagle 4Kx4K CCD cameras. The polyanionic glycocalyx on the surface of endothelial cells can be visualized using TEM by binding of electron-dense cationic substances, such as cationic ferritin (27). Within the stitches, individual capillary loops were captured and glycocalyx coverage was quantified in 6-11 capillary loops in 9 glomeruli. The percentage of cationic ferritin positive endothelial surface coverage was determined using an automatic grid overlay in the public domain NIH ImageJ version 1.46. For every capillary, a minimum of 80 crosshairs was at the intersection of the endothelium. This resulted in a percentage glycocalyx positive area.

Statistical analysis

Data are presented as mean ± SD, unless stated otherwise. Changes in ACR during treatment were analyzed using a linear-mixed model regression analysis, since samples were collected over time and were therefore animal dependent (SPSS Statistics, version 20, IBM). Differences in other experiments with continuous variables were determined using one-way ANOVA and post hoc analysis with Tukey's multiple comparison test. $P<0.05$ was considered statistically significant.

Results

Diabetes increases renal NO levels

NO levels were determined as MNIC yields in various tissues (Fig 2), showing considerable variation between the tissue types. In particular, the liver was found to produce higher quantities of NO compared to renal and cardiac tissue. The findings in non-diabetic apoE KO mice are in qualitative concordance with previous findings in other rodent models such as rats (28) and C57Bl/6 mice (the latter revealing 0.34 ± 0.1 pmol MNIC / mg in kidney; 2.1 ± 1.0 in liver and 0.52 ± 0.1 pmol MNIC / mg heart). Upon STZ-induced diabetes, apoE KO mice revealed increased renal NO (0.51 ± 0.16 in diabetic apoE KO mice vs. 0.29 ± 0.12 pmol MNIC / mg tissue in non-diabetic apoE KO, $P<0.01$ (19)). Of note, the effect of diabetes on NO bioavailability in cardiac tissue was considerably smaller ($P<0.02$), whereas STZ induced a reduction in NO bioavailability in hepatic tissue ($P<0.01$). Clearly, STZ-induced diabetes affects NO homeostasis in a tissue-dependent fashion, although prolonged treatment of diabetic mice with sepiapterin, a tetrahydrobiopterin (BH_4) precursor, was found to induce a 2- to 3-fold increase of bioavailable NO in kidney, heart and liver tissue (Fig 2).

To see how these different observations at the tissue level reflect those observed in plasma, we also determined the formation of asymmetric dimethyl arginine (ADMA), a known endogenous inhibitor of eNOS. These studies uncovered a small increase in plasma ADMA concentrations upon STZ-induced diabetes (0.48 ± 0.13 µmol/L vs. 0.61 ±0.11 µmol/L, P<0.05; Fig 2E). Treatment with sepiapterin for four weeks did not affect plasma ADMA concentrations.

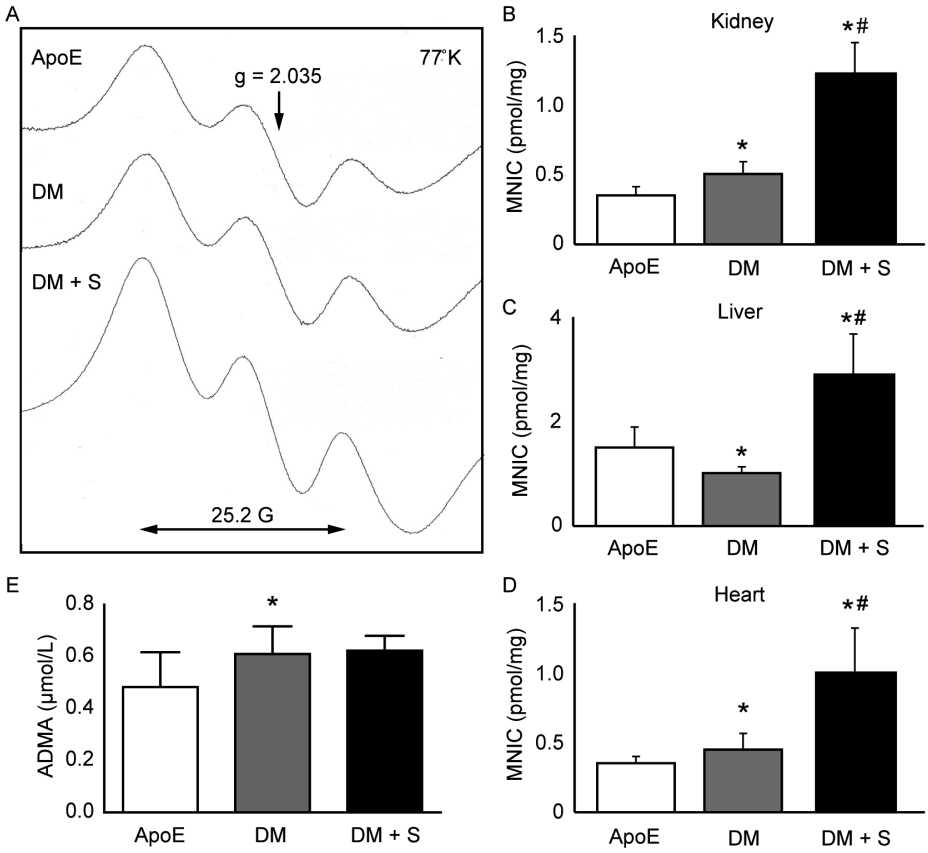


Figure 2. Tissue-dependent variation in NO free radical induction. (A) EPR spectrum of frozen kidney samples. The characteristic triplet structure of the mononitrosyl-iron complex (MNIC, double-headed arrow) centers around g=2.035 and represents the formation of local nitric oxide in 334-370 mg tissue. (B-D) Quantification of nitric oxide formation in kidney, liver and heart tissue, shown as mean pmol MNIC / mg wet tissue ± SD, n = 7-9. E) Plasma ADMA concentrations, shows as mean ± SD, n = 8. *P<0.05, compared with ApoE; #P<0.05 compared with DM. ApoE = ApoE KO mice, DM = diabetic apoE KO mice, DM + S = diabetic apoE KO mice + sepiapterin.

Increased NO levels do not improve diabetic nephropathy in diabetic apoE KO mice

Fourteen weeks after inducing diabetes, we observed common characteristics of diabetic nephropathy, including mesangial expansion, mesangiolysis, and, glomerular hypertrophy, as

we described elsewhere (19). An ensuing treatment with sepiapterin for four weeks did not prevent the development of diabetic renal lesions as quantified in PAS- and Trichrome-stained glomeruli (Fig 3A-C). Importantly, for these studies we verified that sepiapterin did not affect blood glucose concentrations at the selected dose (Fig 3D).

To assess the effect of sepiapterin on kidney function, we collected 24-hours urine samples prior to treatment with sepiapterin, as well as at 2 and 4 weeks after treatment. Diabetic apoE

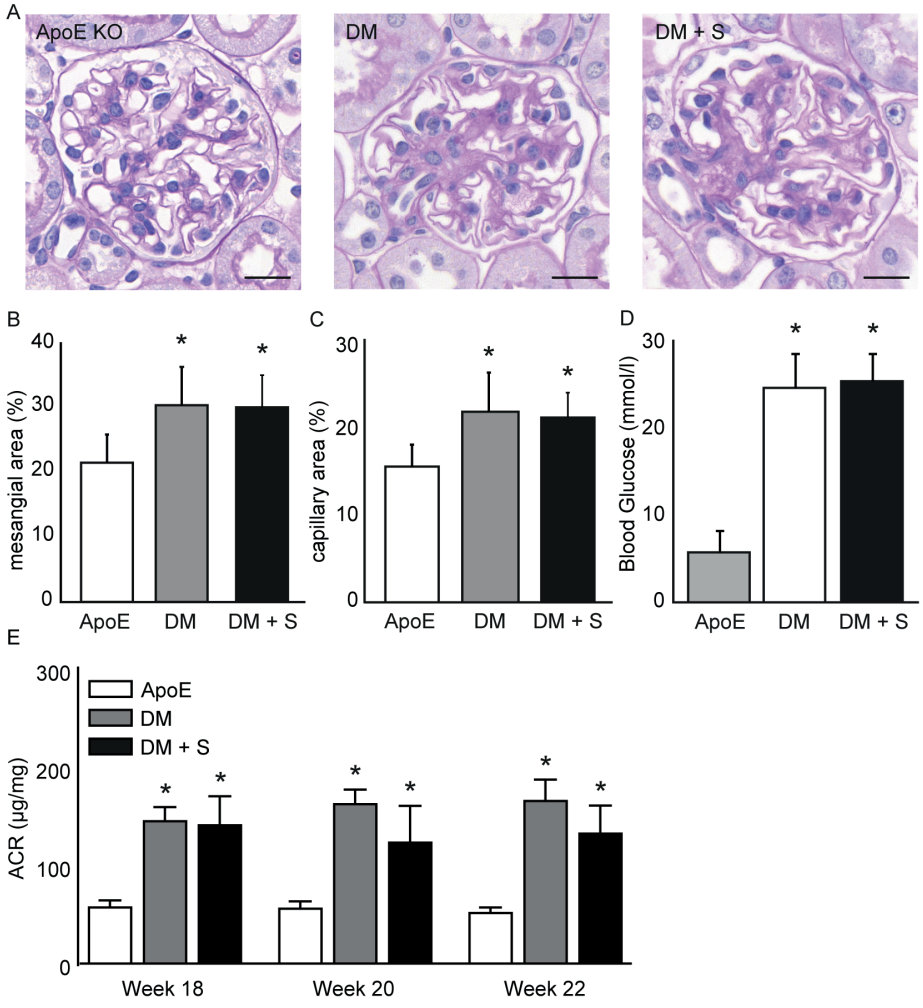


Figure 3. Sepiapterin does not reduce albuminuria in diabetic apoE KO mice. (A) PAS-stained glomeruli of apoE KO mice (apoE), diabetic apoE KO mice (DM) and diabetic apoE KO mice treated with sepiapterin (DM + S), showing heterogeneous diabetic lesions 14 weeks after induction of diabetes with STZ (20). Scale bars: 20 µm. Sepiapterin did not affect mesangial area (B,C), nor blood glucose concentrations (D). Data are shown as mean ± SD, *P<0.05 compared with apoE, n = 8. (E) Albumin-creatinine ratios (ACR) at baseline, 2- and 4 weeks after treatment, as indicated by mean ± SEM, *P<0.05 compared with apoE, n = 14-23.

KO mice were characterized by progressive albuminuria (Fig 3E (19)), which is in keeping with a parallel increase in urine production and urinary albumin excretion (19). Multiple comparisons reveal that a 4-week sepiapterin treatment regimen is insufficient to reduce albuminuria as compared to non-treated mice (-11.8 ± 7.1%, p=0.46).

To visualize the consequences of sepiapterin treatment on the endothelial glycocalyx, we quantified the binding of cationic ferritin to the negatively-charged glycocalyx. As shown in Fig 4, diabetic mice displayed decreased endothelial coverage (40.7 ± 7.5%), as compared to non-diabetic apoE KO mice (83.6 ± 8.3%, P<0.05; Fig 4A,B (19)). Interestingly, treatment with sepiapterin seems to lead to a partial restoration of the glycocalyx, based on the observation that some glomeruli in non-diabetic mice display cationic ferritin coverage, whereas other glomeruli do not. This phenomenon resulted in high variability in glycocalyx-coverage data (61.6 ± 25.8%, P<0.1).

In diabetes, various factors can lead to disruption of the glycocalyx (29). Heparanase-mediated degradation of heparan sulphate represents one of the most widely recognized causes of glycocalyx perturbation. In particular locally active heparanase plays a critical role in the development of diabetic nephropathy in mice (30). We previously confirmed enhanced glomerular heparanase protein expression in diabetic apoE mice, compared to non-diabetic apoE KO mice (39.3 ± 10.8% vs. 13.1 ± 9.2%, P<0.01; Fig 4A,C). A notable observation is that sepiapterin treatment did not lead to a reduction in the expression levels of this enzyme (36.1 ± 7.4.8%),

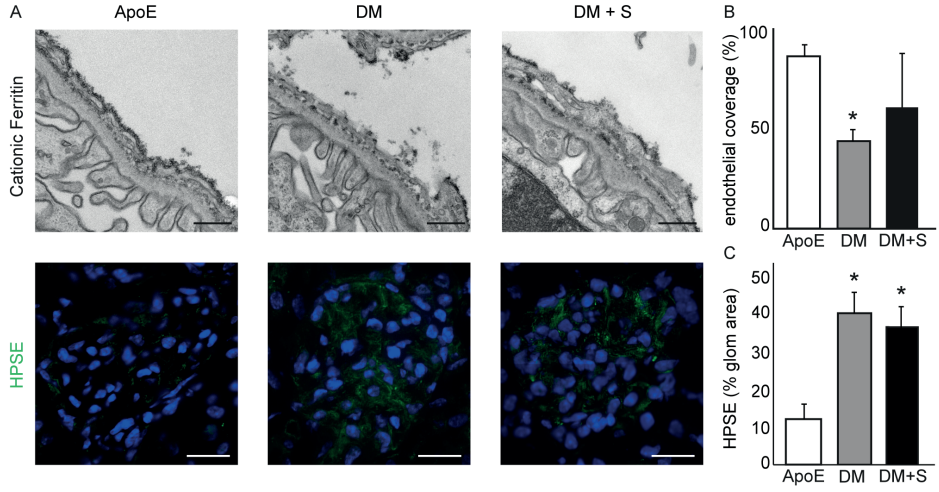


Figure 4. Increased NO levels affect endothelial glycocalyx non-uniformly. (A) Representative microscopic images of cationic ferritin (TEM; top), heparanase (HPSE, immunofluorescence; middle) and cathepsin L (CTSL; bottom) in glomeruli of apoE KO mice (apoE), diabetic apoE KO mice (DM) and diabetic apoE KO mice treated with sepiapterin (DM + S). (B) Quantification of endothelial cationic ferritin coverage in 6-8 capillary loops in 9 glomeruli of 3 mice, shown as mean percentage of total capillary length ± SD, (C) Quantification of glomerular heparanase expression, shown as mean area percentage ± SD. (D) Quantification of glomerular cathepsin L expression, shown as mean area percentage ± SD. *P<0.05 compared with ApoE, n=6-8. Scale bars: 500 nm in TEM images; 20 µm in fluorescent and light microscopic images.

nor in the heparanase activator cathepsin L (30.2 ± 12.5 % vs. 27.3 ± 11.3 for non-treated diabetic mice). This suggests that heparanase is continuously activated by immunocyte-derived cathepsin L despite treatment with sepiapterin, which could potentially explain that restoration of glycocalyx coverage by sepiapterin in diabetic nephropathy was only partial.

Despite the observed partial restoration of the luminal glycocalyx and possible regulatory effect of eNOS on heparanase (31), increasing NO bioavailability with sepiapterin was not capable to restore endothelial function.

Discussion

Endothelial dysfunction plays a critical role in the pathogenesis of diabetes. Diabetes is associated with loss of glomerular barrier function. Activation of extracellular heparanase by inflammatory cells or injured epithelial cells was shown to be of critical importance to cause loss of the glomerular endothelial glycocalyx and proteinuria (30, 32). Nitric oxide (NO) through intracellular s-nitrosylation is a key modifier of cellular function and to ensure cellular quiescence and tissue homeostasis. The three NO synthases (eNOS, iNOS and nNOS) are however complex oxidoreductases with the potential to produce NO as well as reactive oxygen species (33). Specifically, for the production of NO they require the cofactor tetrahydrobiopterin (BH_4). Diabetes has been shown to result in loss of BH_4 availability and uncoupling of NOS (7, 34).

The present study shows that improving the NO producing capacity at the tissue level in the kidney does not result in reduction of glomerular heparanase activity or improvement of glomerular barrier function. Our observations add several new insights about 1] NO measurements, 2] NO sources in different diabetes models, and 3] the glomerular endothelial glycocalyx:

1] When measuring NO availability at the tissue level using state-of-the-art spin trapping technique (EPR) that allows for quantitative NO measurements, diabetes perse is not associated with overall reduction in NO. In fact, NO availability was increased in the kidney and heart upon diabetes, while liver NO was decreased, despite elevated levels of the endogenous NOS inhibitor asymmetric dimethylarginine (ADMA). Reports on NO availability in diabetes have varied from decreased to increased, pointing to the variation in models and the often indirect measurements of NO activity. Given the complex nature of *in vivo* NO radical detection, surrogate markers for free NO levels have oftentimes been utilized as a readout, including plasma NOx levels, nitrate, nitrosothiols or nitrosylated heme. In this context, we note that previous reports of enhanced NO production in diabetes (8) were based on the quantification of downstream metabolites of NO, such as NOx or nitrate. Furthermore, previous reports on decreased renal NO production in rat 7 - 10 days after induction of diabetes are based on decreased urinary nitrite/nitrate excretion (35, 36) or decreased plasma nitrite/nitrate levels at 8 weeks after induction of diabetes (15). Importantly, these NO metabolites serve as poor indicators of the actual NO free radical levels. This is largely in part due to the fact that enhanced synthesis of NO augments NOx generation, whereas a concomitant increase in oxidative stress or reactive oxygen species (ROS) has been established to trigger a rapid depletion of local NO levels. As

such, the detection of MNIC, the formation of which is specific for NO free radicals in biological tissues, represents a more suitable experimental and diagnostic approach for detecting local NO levels (21, 22, 37).

2] Renal NO production in diabetes will be dependent upon different sources including endothelium, macrophages (38) and the tubular system (39). Chronic uncoupling or inhibition of eNOS has been shown to accelerate kidney disease (40, 41). Conditions commonly observed in patients with kidney disease, such as hyperglycemia, are characterized by an increase in the generation of advanced glycation end products (AGEs) (42). AGEs actively promote NO insufficiency by scavenging NO free radicals (13) via pro-inflammatory AGE-specific receptors (43-45), or modification of plasma proteins such as albumin (46). We recently described that the streptozotocin induced diabetic apoE mouse model, which faithfully recapitulates the renal changes in diabetes, is characterized by macrophage activation, which may explain the increased NO availability. McNeill et al showed in a series of elegant studies that macrophage function is modulated by NOS coupling and BH_4 availability (4), as was previously also shown by us for endothelial function (3). The current data show that it is possible to increase NO production further in diabetes by coupling through BH_4 availability, indicating that uncoupling of NOS enzymes was present in the model. In contrast to the current study, sepiapterin showed renal protective effect in diabetic db/db mice (47) and ZSF_1 rats, which can possibly be explained by the fact that these models are primarily characterized by insulin resistance. Insulin signaling is coupled to NOS activation and impaired insulin signaling may thus have altered the coupling state of NOS in these models. In our model, mice received small amounts of insulin to keep blood glucose concentrations within reasonable range. Given that insulin stimulates NO release by endothelial cells (48, 49), this could serve as an explanation for the fact that we did not observe overall NO deficiency in our diabetic apoE KO mice.

3] Endothelial cells are covered with a dense layer of proteoglycans and glycosaminoglycans, the endothelial glycocalyx. It is the first barrier of the vascular wall and is vasculoprotective (50) by acting as a permeability barrier (51-53), a mechanosensor (50, 54-57), and by regulating inflammation (58-61). Loss of endothelial glycocalyx occurs, amongst others, during oxidative stress and inflammation, both present in diabetes. This is related to the induction of glycocalyx degrading enzymes, such as hyaluronidase, heparanase and chondroitinase (62, 63). Of these, heparanase activity has been suggested to be affected by NO bioavailability (31). Heparanase-induced glycocalyx degradation leads to albuminuria (1) and increased glomerular heparanase expression was shown to be associated with the development of diabetic nephropathy in humans and mice (30, 64).

Immunocytes have been implicated in activation of extracellular heparanase and degradation of heparan sulfate in the glycocalyx (1). Whereas multiple cells can secrete heparanase upon activation, including endothelium, podocytes and immunocytes (30), its activation requires the cleavage of a linker protein by the protease cathepsin L (30, 65). While sepiapterin successfully increased the modulating potential of NO in this model of diabetic nephropathy, immunocytes

were not affected, hence glomerular heparanase and cathepsin L were not reduced and glycocalyx properties not restored.

Conclusion

In conclusion, our data show that overall NO availability at the tissue level is not reduced in diabetes, despite the presence of factors causing endothelial dysfunction, and the presence of increased levels of the endogenous NOS inhibitor ADMA. Targeting uncoupled NOS with the BH_4 precursor sepiapterin increases NO availability, but does not modify renal glomerular endothelial barrier function.

Acknowledgements

We thank Prof E. Bouwman (Inorganic Chemistry, Leiden University) for the use of the electron paramagnetic resonance facilities.

We thank Prof A.J. Koster (Molecular Cell Biology, Leiden University Medical Center) for the use of electron microscope facilities.

We thank Dr. E.P. van der Veer (Department of Internal Medicine, Leiden University Medical Center) for help in the preparation of this manuscript.

References

1. Rabelink TJ, de Zeeuw D. The glycocalyx--linking albuminuria with renal and cardiovascular disease. Nature reviews Nephrology. 2015;11(11):667-76.
2. Vos IH, Rabelink TJ, Dorland B, Loos R, Van Middelaar B, Grone HJ, et al. L-arginine supplementation improves function and reduces inflammation in renal allografts. Journal of the American Society of Nephrology : JASN. 2001;12(2):361-7.
3. Huisman A, Vos I, van Faassen EE, Joles JA, Grone HJ, Martasek P, et al. Anti-inflammatory effects of tetrahydrobiopterin on early rejection in renal allografts: modulation of inducible nitric oxide synthase. FASEB journal : official publication of the Federation of American Societies for Experimental Biology. 2002;16(9):1135-7.
4. McNeill E, Crabtree MJ, Sahgal N, Patel J, Chuaiphichai S, Iqbal AJ, et al. Regulation of iNOS function and cellular redox state by macrophage Gch1 reveals specific requirements for tetrahydrobiopterin in NRF2 activation. Free radical biology & medicine. 2015;79:206-16.
5. Nguyen D, Ping F, Mu W, Hill P, Atkins RC, Chadban SJ. Macrophage accumulation in human progressive diabetic nephropathy. Nephrology. 2006;11(3):226-31.
6. Klessens CQ, Zandbergen M, Wolterbeek R, Bruijn JA, Rabelink TJ, Bajema IM, et al. Macrophages in diabetic nephropathy in patients with type 2 diabetes. Nephrology, dialysis, transplantation : official publication of the European Dialysis and Transplant Association - European Renal Association. 2017 Aug 1;32(8):1322-1329.
7. Cai S, Khoo J, Channon KM. Augmented BH4 by gene transfer restores nitric oxide synthase function in hyperglycemic human endothelial cells. Cardiovascular research. 2005;65(4):823-31.
8. Adela R, Nethi SK, Bagul PK, Barui AK, Mattapally S, Kuncha M, et al. Hyperglycaemia enhances nitric oxide production in diabetes: a study from South Indian patients. PloS one. 2015;10(4):e0125270.
9. Hohenstein B, Hugo CP, Hausknecht B, Boehmer KP, Riess RH, Schmieder RE. Analysis of NO-synthase expression and clinical risk factors in human diabetic nephropathy. Nephrology, dialysis, transplantation : official publication of the European Dialysis and Transplant Association - European Renal Association. 2008;23(4):1346-54.
10. Tessari P, Cecchet D, Cosma A, Vettore M, Coracina A, Millioni R, et al. Nitric oxide synthesis is reduced in subjects with type 2 diabetes and nephropathy. Diabetes. 2010;59(9):2152-9.
11. Tessari P, Cecchet D, Artusi C, Vettore M, Millioni R, Plebani M, et al. Roles of insulin, age, and asymmetric dimethylarginine on nitric oxide synthesis in vivo. Diabetes. 2013;62(8):2699-708.
12. Shiekh GA, Ayub T, Khan SN, Dar R, Andrabi KI. Reduced nitrate level in individuals with hypertension and diabetes. J Cardiovasc Dis Res. 2011;2(3):172-6.
13. Bucala R, Tracey KJ, Cerami A. Advanced glycosylation products quench nitric oxide and mediate defective endothelium-dependent vasodilatation in experimental diabetes. The Journal of clinical investigation. 1991;87(2):432-8.
14. Prabhakar S, Starnes J, Shi S, Lonis B, Tran R. Diabetic nephropathy is associated with oxidative stress and decreased renal nitric oxide production. Journal of the American Society of Nephrology : JASN. 2007;18(11):2945-52.
15. Arya A, Yadav HN, Sharma PL. Involvement of vascular endothelial nitric oxide synthase in development of experimental diabetic nephropathy in rats. Molecular and cellular biochemistry. 2011;354(1-2):57-66.
16. Komers R, Anderson S. Paradoxes of nitric oxide in the diabetic kidney. American journal of physiology Renal physiology. 2003;284(6):F1121-37.
17. Dellamea BS, Leitao CB, Friedman R, Canani LH. Nitric oxide system and diabetic nephropathy. Diabetol Metab Syndr. 2014;6(1):17.
18. Kanetsuna Y, Takahashi K, Nagata M, Gannon MA, Breyer MD, Harris RC, et al. Deficiency of endothelial nitric-oxide synthase confers susceptibility to diabetic nephropathy in nephropathy-resistant inbred mice. The American journal of pathology. 2007;170(5):1473-84.
19. Boels MG, Avramut MC, Koudijs A, Dane MJ, Lee DH, van der Vlag J, et al. Atrasentan Reduces Albuminuria by Restoring the Glomerular Endothelial Glycocalyx Barrier in Diabetic Nephropathy. Diabetes. 2016;65(8):2429-39.
20. Lassila M, Seah KK, Allen TJ, Thallas V, Thomas MC, Candido R, et al. Accelerated nephropathy in diabetic apolipoprotein e-knockout mouse:

role of advanced glycation end products. Journal of the American Society of Nephrology. 2004;15(8):2125-38.

21. Vanin AF, Huisman A, Van Faassen EE. Iron dithiocarbamate as spin trap for nitric oxide detection: pitfalls and successes. Methods in enzymology. 2002;359:27-42.
22. Vanin A, van Faassen, E Mononitrosyl-iron complexes with dithiocarbamate ligands: Physicochemical properties. In: Vanin EvFaA, editor. Radicals for life: The various forms of nitric oxide: Elsevier; 2007. p. 383-406.
23. van Faassen EE, Koeners MP, Joles JA, Vanin AF. Detection of basal NO production in rat tissues using iron–dithiocarbamate complexes. Nitric Oxide. 2008;18(4):279-86.
24. Ohnishi ST. Measurement of NO using electron paramagnetic resonance. Methods in molecular biology. 1998;100:129-54.
25. Tran TN, Eubanks SK, Schaffer KJ, Zhou CY, Linder MC. Secretion of ferritin by rat hepatoma cells and its regulation by inflammatory cytokines and iron. Blood. 1997;90(12):4979-86.
26. Faas FG, Avramut MC, van den Berg BM, Mommaas AM, Koster AJ, Ravelli RB. Virtual nanoscopy: generation of ultra-large high resolution electron microscopy maps. The Journal of cell biology. 2012;198(3):457-69.
27. Avasthi PS, Koshy V. The anionic matrix at the rat glomerular endothelial surface. The Anatomical record. 1988;220(3):258-66.
28. Koeners MP, van Faassen EE, Wesseling S, de Sain-van der Velden M, Koomans HA, Braam B, et al. Maternal supplementation with citrulline increases renal nitric oxide in young spontaneously hypertensive rats and has long-term antihypertensive effects. Hypertension. 2007;50(6):1077-84.
29. Schott U, Solomon C, Fries D, Bentzer P. The endothelial glycocalyx and its disruption, protection and regeneration: a narrative review. Scand J Trauma Resusc Emerg Med. 2016;24(1):48.
30. Gil N, Goldberg R, Neuman T, Garsen M, Zcharia E, Rubinstein AM, et al. Heparanase is essential for the development of diabetic nephropathy in mice. Diabetes. 2012;61(1):208-16.
31. Garsen M, Rops AL, Li J, van Beneden K, van den Branden C, Berden JH, et al. Endothelial Nitric Oxide Synthase Prevents Heparanase Induction and the Development of Proteinuria. PloS one. 2016;11(8):e0160894.
32. Goldberg R, Rubinstein AM, Gil N, Hermano E, Li JP, van der Vlag J, et al. Role of heparanase-driven inflammatory cascade in pathogenesis of diabetic nephropathy. Diabetes. 2014;63(12):4302-13.
33. Rabelink TJ, Luscher TF. Endothelial nitric oxide synthase: host defense enzyme of the endothelium? Arteriosclerosis, thrombosis, and vascular biology. 2006;26(2):267-71.
34. Lucotti P, Setola E, Monti LD, Galluccio E, Costa S, Sandoli EP, et al. Beneficial effects of a long-term oral L-arginine treatment added to a hypocaloric diet and exercise training program in obese, insulin-resistant type 2 diabetic patients. Am J Physiol Endocrinol Metab. 2006;291(5):E906-12.
35. Pflueger AC, Larson TS, Hagl S, Knox FG. Role of nitric oxide in intrarenal hemodynamics in experimental diabetes mellitus in rats. The American journal of physiology. 1999;277(3 Pt 2):R725-33.
36. Keynan S, Hirshberg B, Levin-Iaina N, Wexler ID, Dahan R, Reinhartz E, et al. Renal nitric oxide production during the early phase of experimental diabetes mellitus. Kidney international. 2000;58(2):740-7.
37. Vanin AF, Poltorakov AP, Mikoyan VD, Kubrina LN, van Faassen E. Why iron-dithiocarbamates ensure detection of nitric oxide in cells and tissues. Nitric Oxide. 2006;15(4):295-311.
38. Kashem A, Endoh M, Yano N, Yamauchi F, Nomoto Y, Sakai H. Expression of inducible-NOS in human glomerulonephritis: the possible source is infiltrating monocytes/macrophages. Kidney international. 1996;50(2):392-9.
39. Mohaupt MG, Elzie JL, Ahn KY, Clapp WL, Wilcox CS, Kone BC. Differential expression and induction of mRNAs encoding two inducible nitric oxide synthases in rat kidney. Kidney international. 1994;46(3):653-65.
40. Jover B, Mimran A. Nitric oxide inhibition and renal alterations. Journal of cardiovascular pharmacology. 2001;38 Suppl 2:S65-70.
41. Nakagawa T. Uncoupling of the VEGF-endothelial nitric oxide axis in diabetic nephropathy: an explanation for the paradoxical effects of VEGF in renal disease. American journal of physiology Renal physiology. 2007;292(6):F1665-72.

42. Noordzij MJ, Lefrandt JD, Smit AJ. Advanced glycation end products in renal failure: an overview. J Ren Care. 2008;34(4):207-12.

43. Yan SF, Ramasamy R, Schmidt AM. Mechanisms of disease: advanced glycation end-products and their receptor in inflammation and diabetes complications. Nature clinical practice Endocrinology & metabolism. 2008;4(5):285-93.

44. Vlassara H, Uribarri J, Ferrucci L, Cai W, Torreggiani M, Post JB, et al. Identifying advanced glycation end products as a major source of oxidants in aging: implications for the management and/or prevention of reduced renal function in elderly persons. Seminars in nephrology. 2009;29(6):594-603.

45. Vlassara H, Striker GE. AGE restriction in diabetes mellitus: a paradigm shift. Nat Rev Endocrinol. 2011;7(9):526-39.

46. Xu B, Ji Y, Yao K, Cao YX, Ferro A. Inhibition of human endothelial cell nitric oxide synthesis by advanced glycation end-products but not glucose: relevance to diabetes. Clinical science. 2005;109(5):439-46.

47. Cheng H, Wang H, Fan X, Paueksakon P, Harris RC. Improvement of endothelial nitric oxide synthase activity retards the progression of diabetic nephropathy in db/db mice. Kidney international. 2012;82(11):1176-83.

48. Zeng G, Nystrom FH, Ravichandran LV, Cong LN, Kirby M, Mostowski H, et al. Roles for insulin receptor, PI3-kinase, and Akt in insulin-signaling pathways related to production of nitric oxide in human vascular endothelial cells. Circulation. 2000;101(13):1539-45.

49. Dimmeler S, Fleming I, Fisslthaler B, Hermann C, Busse R, Zeiher AM. Activation of nitric oxide synthase in endothelial cells by Akt-dependent phosphorylation. Nature. 1999;399(6736):601-5.

50. Gouverneur M, Berg B, Nieuwdorp M, Stroes E, Vink H. Vasculoprotective properties of the endothelial glycocalyx: effects of fluid shear stress. Journal of internal medicine. 2006;259(4):393-400.

51. Singh A, Satchell SC, Neal CR, McKenzie EA, Tooke JE, Mathieson PW. Glomerular endothelial glycocalyx constitutes a barrier to protein permeability. Journal of the American Society of Nephrology : JASN. 2007;18(11):2885-93.

52. van den Berg BM, Vink H, Spaan JA. The endothelial glycocalyx protects against myocardial edema. Circulation research. 2003;92(6):592-4.

53. van den Berg BM, Spaan JA, Vink H. Impaired glycocalyx barrier properties contribute to enhanced intimal low-density lipoprotein accumulation at the carotid artery bifurcation in mice. Pflugers Archiv : European journal of physiology. 2009;457(6):1199-206.

54. Florian JA, Kosky JR, Ainslie K, Pang Z, Dull RO, Tarbell JM. Heparan sulfate proteoglycan is a mechanosensor on endothelial cells. Circulation research. 2003;93(10):e136-42.

55. Weinbaum S, Zhang X, Han Y, Vink H, Cowin SC. Mechanotransduction and flow across the endothelial glycocalyx. Proceedings of the National Academy of Sciences of the United States of America. 2003;100(13):7988-95.

56. Pahakis MY, Kosky JR, Dull RO, Tarbell JM. The role of endothelial glycocalyx components in mechanotransduction of fluid shear stress. Biochemical and biophysical research communications. 2007;355(1):228-33.

57. Tarbell JM, Ebong EE. The endothelial glycocalyx: a mechano-sensor and -transducer. Science signaling. 2008;1(40):pt8.

58. Constantinescu AA, Vink H, Spaan JA. Endothelial cell glycocalyx modulates immobilization of leukocytes at the endothelial surface. Arteriosclerosis, thrombosis, and vascular biology. 2003;23(9):1541-7.

59. Rops AL, van den Hoven MJ, Baselmans MM, Lensen JF, Wijnhoven TJ, van den Heuvel LP, et al. Heparan sulfate domains on cultured activated glomerular endothelial cells mediate leukocyte trafficking. Kidney international. 2008;73(1):52-62.

60. Mulivor AW, Lipowsky HH. Role of glycocalyx in leukocyte-endothelial cell adhesion. American journal of physiology Heart and circulatory physiology. 2002;283(4):H1282-91.

61. Chappell D, Dorfler N, Jacob M, Rehm M, Welsch U, Conzen P, et al. Glycocalyx protection reduces leukocyte adhesion after ischemia/reperfusion. Shock. 2010;34(2):133-9.

62. Nieuwdorp M, Holleman F, de Groot E, Vink H, Gort J, Kontush A, et al. Perturbation of hyaluronan metabolism predisposes patients with type 1

diabetes mellitus to atherosclerosis. Diabetologia. 2007;50(6):1288-93.

63. Shafat I, Ilan N, Zoabi S, Vlodavsky I, Nakhoul F. Heparanase levels are elevated in the urine and plasma of type 2 diabetes patients and associate with blood glucose levels. PloS one. 2011;6(2):e17312.
64. van den Hoven MJ, Rops AL, Bakker MA, Aten J, Rutjes N, Roestenberg P, et al. Increased expression of heparanase in overt diabetic nephropathy. Kidney international. 2006;70(12):2100-8.
65. Garsen M, Rops AL, Dijkman H, Willemsen B, van Kuppevelt TH, Russel FG, et al. Cathepsin L is crucial for the development of early experimental diabetic nephropathy. Kidney international. 2016 Nov;90(5):1012-1022.

Chapter 5

Endothelial glycocalyx remodeling by heparanase induces endothelial dysfunction

Margien G.S. Boels, Gangqi Wang, Wendy M.P.J. Sol, Annemarie M.A. de Graaf, Toine van Kuppevelt, Johan van der Vlag, Hermann Haller, Bernard M. van den Berg, Ton J. Rabelink

Abstract

Heparan sulfate chains are important constituents of the endothelial glycocalyx where they regulate the activity of numerous bioactive molecules such as cytokines and growth factors at the cell surface. Heparanase is an endo-b-glucuronidase that hydrolyzes glucuronic acid–*N*-acetylglucosamine linkages in heparan sulfate chains. Its synthesis and release is induced upon inflammation and during metabolic stress, and can be activated in the extracellular space by L cathepsin. We postulate that extracellular heparanase activity serves to adapt the endothelial surface to inflammation. While prolonged laminar shear stress is shown in our study to be associated with robust heparan sulfate synthesis and a quiescent phenotype in a microfluidic culture system, increasing luminal heparanase activity is not only accompanied by a reduction in endothelial surface glycocalyx, but also by increased expression of inflammatory heparan sulfate epitopes. In addition, endothelial gene expression of inflammatory cytokines is increased as well. To extend these observations to the *in vivo* situation, active heparanase was perfused in zebrafish larvae, where a similar change in inflammatory heparan sulfate domains was observed in the vasculature. We conclude that activation of heparanase at the endothelial surface, serves remodeling of the endothelial glycocalyx to support inflammatory processes.

Introduction

Heparanase is the only known mammalian endoglycosidase capable of enzymatic degradation of heparan sulfates (HS). Heparanase is involved in intracellular processes such as gene transcription and autophagy (1). However, in situations such as diabetes (2) and other inflammatory diseases (3), heparanase can be released to and activated in the extracellular matrix were it can degrade HS. HS is an important constituent of the endothelial glycocalyx, a delicate layer of interconnected carbohydrates, which is critical for endothelial function. Bound to proteins such as syndecans, glypican and versican, HS forms proteoglycans (4). In the Golgi apparatus, were HS is produced and attached to a core protein, extensive modification of HS occurs. The sulfation pattern of HS is responsible for highly specific binding of proteins at the endothelial surface (5,6). For example, the binding of various growth factors, such as fibroblast growth factor 2 (FGF-2) or vascular endothelial growth factor (VEGF), and cytokines critically depends on binding to a specifically HS moieties (7-9). In addition, HS within the extracellular matrix can via these modifications generate chemokine gradients over the endothelium to guide cells towards the underlying tissue (10). Since HS are made up of up to 150 modifiable disaccharide units there is a high variety in binding sites for different proteins (5,7,11). Consequently, HS are involved in a variety of processes such as cell attachment, migration, differentiation, blood coagulation, lipid metabolism, and inflammation (4,12-14). Because the production of HS is continuously ongoing and availability of enzymes and substrates can vary, the sulfation pattern can be rapidly modified and adjusted to changing environments (15,16). Next to the intracellular enzymes that are responsible for HS make-up, extracellular HS can be degraded by heparanase, an endo-beta-glucuronidase that cleaves/hydrolyzes HS chains at GlcA(b1→4) GlcNAc linkages into fragments of 10-20 sugar units (17).

In the current study we postulate that degradation of HS in the endothelial glycocalyx by heparanase facilitates glycocalyx turnover, and adaptation to inflammation and metabolic stress. To this end, we used a panel of glycoprobes against specific domains within the HS structures of the endothelial glycocalyx, in the absence and presence of active heparanase. Where the 10E4 antibody recognizes so-called mixed HS domains, containing both N-acetylated and N-sulfated disaccharide units, JM403 recognizes more N-unsubstituted glucosamine residues (18). Furthermore, single chain antibodies were used to map smaller HS domains, with more specific binding properties. For example, the N-, and 6-O-sulfated domains that are recognized by AO4B08 play a role in growth factor binding (19), such as VEGF and FGF, and are highly expressed in certain tumor cells (20). Using such variety of glycoprobes and single chain antibodies, we show that heparanase not only reduces total surface glycocalyx coverage but also changes the composition of HS binding domains to support inflammatory mediators.

Materials and Methods

Shear stress experiments

HUVEC were isolated from umbilical cords by perfusion and subsequent 20 minutes incubation of trypsin at 37°C. Freshly isolated HUVECs were cultured on 0.5% gelatin coated plastic flasks in EGM2 medium (Lonza, Basel, Switzerland) supplemented with antibiotics/antimycotics (Life technology, Gibco) and were used for experiments at passage 1-3. HUVECs were seeded into closed perfusion chambers (ibiTreat µ-Slide VI 0.4 Luer and µ-Slide I 0.4 Luer, Ibidi GmbH, Marensried, Germany) at a concentration of $1.5*10^6$ cells per mL. After cells were allowed to adhere for 3 hours, the chamber was connected to a computer-controlled air pressure pump and a fluidic unit with a two-way switching valve (Ibidi). The pump setup allowed pumping of 16 mL cell culture medium from two reservoirs in a unidirectional way through the flow channel over the monolayer of endothelial cells at a constant shear stress of 10 dyne/cm^2. Medium was refreshed after 1 day, to remove non-adhered cells, and continued with 4 days of culture. A subset of cells was exposed to active recombinant heparanase (100 ng/mL, R&D Systems Europe Ltd, Abingdon, UK) for the last 24 hours. The chamber and the reservoirs containing the medium were kept in an incubator at 37°C and 5% CO_2. For static control experiments, cells were cultured in perfusion chambers, not attached to an air pressure pump.

Cell culture and confocal immunofluorescence microscopy

After static culture (24 hours) or exposure to flow (1, 4 or 7 days) in a µ-Slide VI 0.4 Luer flow chamber (6 lanes), HUVECs were fixed in freshly made 4% paraformaldehyde for 10 minutes, washed twice with HBSS (life technologies) and blocked for 30 minutes with 3% normal goat serum (NGS) in HBSS. Cells were incubated overnight at 4°C with one of the primary antibodies (at 10 µg/mL): 10E4 (Amsbio), JM403 (kind gift of Dr. van der Vlag, Radboud University Medical Centre, Nijmegen, The Netherlands), the single chain antibodies EW4G2, AO4B08 and HS4C3 (kind gift of Dr. van Kuppevelt, Radboud University Medical Centre Nijmegen, The Netherlands), CS56 against chondroitin sulfate (Abcam, Cambridge, MA), VE-cadherin (BD biosciences, San Jose, CA), phalloidin-rhodamine (Sigma-Aldrich), or the appropriate control IgM or IgG isotype antibodies diluted in HBSS. After washing three times with HBSS, cells were incubated with a secondary antibody for 1 hour (anti-mouse IgM-Alexa488; anti-mouse IgG-Alexa488 or anti-VSV-DyLight488) and Hoechst 33528 (1/1,000, Sigma-Aldrich, St. Louis, MO), followed by tetramethylrhodamine-labeled wheat germ agglutinin (WGA) (1/100; Sigma-Aldrich) for 30 min. Cells were again washed for three times with HBSS and imaged using a confocal microscopy at 63x objective.

CLSM image analysis and quantification

Confocal 12-bit gray-scale axial image stacks (xyz dimensions, 0.08×0.08×0.13 µm) that covered 6724 μm^2 of surface area per image and a height of 5 to 10 µm above the EC nuclear plane were recorded using Leica Application Suite Advanced Fluorescence image software

(Leica) to create image stacks. The image stacks were analyzed with the public domain National Institutes of Health IMAGE program (available at http://rsb.info.nih.gov/nih-image). For luminal endothelial glycocalyx thickness quantification, first nuclear and peri-nuclear area was selected, to exclude the cell area in which the cell thickness was too thin to differentiate between luminal and abluminal staining. Thickness of the lectin (WGA and LEA) stained layer was estimated within this area of interest, between the half-maximum nuclear (Hoechst) signal and the luminal half-maximum of lectin fluorescence. Total luminal signal distribution and heterogeneity of specific HS sequences were calculated in the same 3-dimensional area of interest in every z-plane within this area (area%). A visualization of this method is shown in supplementary figure S1.

RNA Isolation and RT-qPCR

After static culture (24 hours) or exposure to flow (24 hours or 7 days) in a µ-Slide I 0.4 Luer flow chamber (1 lane), total RNA was isolated from HUVECs cultured in a µ-Slide I 0.4 using Trizol reagent (Life Technologies) and isolation kit (Qiagen). Reverse transcription was performed after a 5-minute 65°C incubation of 500 ng total RNA with deoxyribonucleotide triphosphates (Life Technologies) and oligo(dT) (Life Technologies): cDNA was synthesized using M-MLV First-Strand Synthesis (Life Technologies), and validation was carried out using SYBR Green Master Mix (Life technologies). Levels of expression were determined by normalizing to GAPDH levels.

Zebrafish larvae

Transgenic Tg(l-fabp:DBP-eGFP) zebrafish larvae were grown and mated at 28.5ºC (21). Embryos were kept and handled in standard E3 solution (5mM NaCl, 0.17 mM KCl, 0.33 mM CaCl2, 0.33 mM MgSO4, 10^{-5}% methylene blue) buffered with 2 mM HEPES (Sigma-Aldrich, St. Louis, MO). All zebrafish larvae studies were conducted in accordance with the National Institutes of Health (NIH) Guide for the Care and Use of Laboratory Animals. Using the Nanoject II injection device (Drummond Scientific, Broomall, PA), 5 nL heparanase (0.15 mg/mL, Amsbio) or control solution (PBS) was injected into zebrafish larvae 72 hours post fertilization (hpf). After 24 hours (4 days post fertilization (dpf)), glomerular function was measured, as described previously (21). These zebrafish larvae express a GFP-tagged vitamin D binding protein with a molecular weight of 78 kDa under the control of the l-fabp (liver-type fatty acid binding protein promotor), therefore diminished fluorescence in the vasculature indicates accelerated protein leakage though the pronephros. Zebrafish larvae were anesthetized with a 1:20 to 1:100 dilution of 4 mg/ml Tricaine (MESAB: ethyl-3-aminobenzoate, methanesulfonate acid salt, 1% Na2HPO4, pH 7.0) (Sigma-Aldrich). Pupils of the zebrafish larvae were imaged using a Zeiss inverted microscope (Axiovert 200) connected to an AxioCam MRm charge-coupled device camera. Images were taken with fixed exposure times and gain using the Axio Vision release 4.5 SP1 software package to quantify maximum fluorescence intensity. Subsequently, zebrafish larvae were sampled and fixed in 4% PFA for 24 hours. After fixation, the zebrafish

larvae were incubated for 24 hours with 30% sucrose, embedded in Tissue-Tek O.C.T. (Sakura Finetek, Alphen aan den Rijn, The Netherlands) and cryopreserved a -80°C. Sections of 10 µm were permeabilized with 0.3% Triton-X100 and stained as described above for HUVECs and were image with Leica DMI6000 and confocal microscopy for blinded quantification of staining intensity (percentage of stained area divided by the total area in ImageJ).

Statistical analyses

Data are presented as mean ± SEM obtained from four to six independent experiments (n = 4-6), unless indicated otherwise. All *in vitro* and *in vivo* results were analyzed using GraphPad software version 5.0 (GraphPad Prism Software Inc, San Diego, CA) with either a *t* test or analysis of variance (using a Bonferonni post-hoc test). Differences in P-values < 0.05 were considered statistically significant.

Results

Prolonged laminar shear stress induces quiescent endothelial phenotype

To confirm earlier reports on the effect of shear stress to endothelial cells (22-24) we analyzed cell morphology and expression of shear responsive genes and proteins. After 4 - 7 days of a laminar shear stress of 10 dyne/cm^2 HUVECs aligned into the direction of flow with increased expression of VE-cadherin at the cell borders and typical short F-actin shear fibers, in comparison to static cultures (Figure 1A). In addition, shear stress sensitive genes Krüppel-like Factor 2 (KLF2) and endothelial nitric oxide synthase (eNOS) were upregulated. In contrast, gene expression of the inflammatory markers E-selectin and IL-8 were decreased (Figure 1B). In line with previous data (25), IL-8 gene expression was highly increased after 24 hours of exposure to shear stress, which confirms an acute inflammatory response upon exposure to shear stress. However, IL-8 expression returned to base-line levels after 4 days of flow. In addition, superoxide dismutase-1 (SOD1) gene expression, which in the presence of catalase keeps intracellular oxidant levels low (26), is upregulated after 4 days of flow. In short, shear stress initially provokes an inflammatory cascade in endothelial cells, whereas prolonged shear stress induces a quiescent phenotype.

Prolonged laminar shear stress increases glycocalyx thickness

We tested the time necessary for endothelial cells to express a sufficient luminal glycocalyx. For this, we stained the glycocalyx after indicated time periods with the *N*-acetylneuraminic acid and *N*-acetyl-β-D-glucosamine binding lectin from *Triticum vulgaris* ((WGA), Figure 1C). Four days of exposure to 10 dyne/cm^2 shear stress induces a maximum total intensity of luminal WGA staining and was significantly ($p < 0.05$) increased in thickness in comparison to static and 1 day of flow (Figure 1D). Thickness remained equally high up to 7 days of flow. To determine whether the composition of HS within the endothelial glycocalyx could be affected by changes

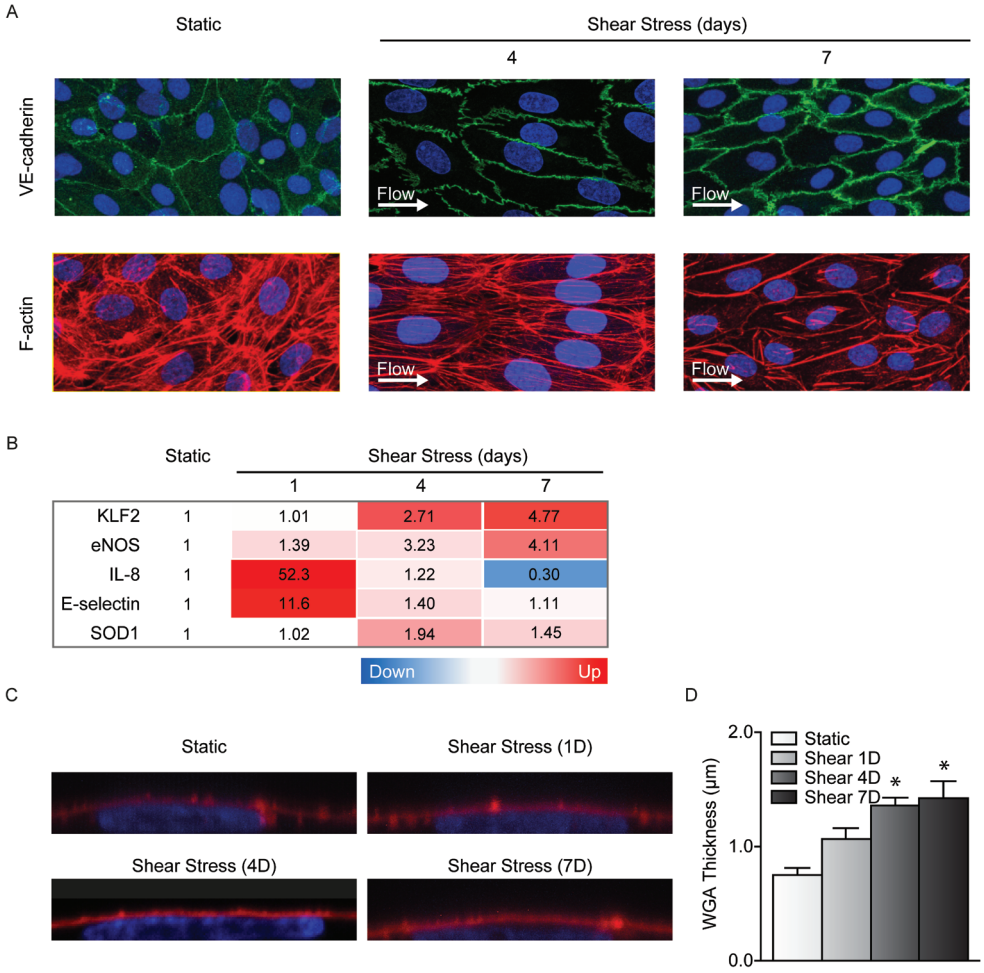


Figure 1. Prolonged shear stress induces quiescent endothelium. A) Cell morphology changes upon prolonged shear stress culture. HUVEC are stained with antibodies against VE-cadherin (upper) and the F-actin binding phalloidin-rhodamine (lower) to visualize endothelial phenotypic changes. Static cultured HUVEC (left) were compared to HUVEC cultured for 4 days (middle) and 7 days (right) at a shear stress of 10 dyne/cm^2. B) Relative expression of selected genes for endothelial function that show response to shear stress of 1, 4 or 7 days (fold change compared to static culture): Krüppel-like Factor 2 (KLF2), endothelial nitric oxide synthase (eNOS), Interleukine-8 (IL-8), E-selectin and Superoxide dismutase-1 (SOD1). C) Representative examples of wheat germ agglutinin (WGA) staining on top of the endothelial cells after 24 hours of static culture or exposure to shear stress for 1, 4 or 7 days (D). D) Quantification of luminal WGA staining relative to static culture (quantification method described in figure S1), expressed as mean ± SD of 4-5 independent experiments; *$p < 0.05$ compared to static and shear for 1 day.

in gene expression upon shear stress, gene expression levels of key enzymes involved in HS polymerizing and sulfation pattern modification were studied. Four days of flow exposure increases the HS polymerase enzymes exostosin 1 and 2 (EXT1 and EXT2), as well as the first enzyme in HS modification, N-deacetylase/Nsulfotransferase-1 (NDST1; Supplementary Figure S2A). Whereas, the intracellular HS chain modifying HS sulfotransferases (HS2ST1, HS3ST1 and

HS6ST1) were variably changed upon shear stress stimulation. In addition, the extracellular modifying enzymes 6-O-endosulfatase 1 and 2 (SULF1, SULF2) and heparanase (HPSE1) were all increased upon four days of shear stress.

Extracellular heparanase modifies the endothelial glycocalyx

To test the effect of extracellular heparanase on the endothelial glycocalyx we incubated endothelial cells with active heparanase during the last 24 hours of the 4-day shear stress experiments. Heparanase decreased total WGA luminal coverage ($p < 0.05$, data not shown). We further tested possible compositional changes using various antibodies against specific domains on the HS chain. For this purpose, we tested the two IgM-type antibodies 10E4 and JM403, and the three single chain antibodies EW4G2, AO4B08 and HS4C3 (27,28), with the specific domains recognized shown in Figure 2A. Quantification of luminal antibody staining was performed in the same area as described above (Supplementary Figure S1). After 4 days of flow exposure, luminal expression of 10E4 was most abundant (12.8 ± 6.5%), followed by JM403 (8.5 ± 3.7%), (Figure 2B and C). The expression levels of the single chain antibodies after 4 days of shear stress was highest for EW4G2 (2.5 ± 1.5%) while AO4B08 (0.2 ± 0.3%) and HS4C3 (0.6 ± 1.1%) expression levels were very low. Incubation with heparanase dramatically decreased both the presence of 10E4 and JM403 binding sites on the luminal surface (3.4 ± 2.7 and 4.4 ± 2.6%, respectively; $P<0.05$ compared to shear stress alone) Exposure to heparanase only resulted in a significant increase of AO4B08 (1.2 ± 0.7%; $p < 0.05$), while both EW4G2 and HS4C3 revealed only a small, non-significant, elevation.

We included an IgM-type antibody against chondroitin sulfate (CS56) to examine whether a reduction in HS induces compensatory chondroitin sulfate biosynthesis (29). While the expression level of chondroitin sulfate was very low in standard 4-day shear stress culture (1.5 ± 0.3%), heparanase treatment induces chondroitin sulfate to 4.3 ± 1.5% ($p < 0.05$).

Extracellular heparanase stimulates the expression of inflammatory genes in endothelial cells

Although heparanase was given extracellularly, glycocalyx degradation or direct enzyme uptake might influence the endothelial cell itself. Therefore, we also studied cell morphology and expression of shear responsive genes and proteins after 24 hours heparanase treatment of cells exposed to 4 days of 10 dyne/cm^2 shear stress. While no changes in expression of genes involved in HS biosynthesis and modification were observed (Supplementary Figure S2A), the presence of extracellular heparanase resulted in increased unstable focal adhesion junctions as visualized by VE-cadherin staining, less organized actin filaments, without evident changes in cell orientation in response to flow in comparison to 4 days flow exposure (Supplementary Figure S2B and C). Heparanase treatment resulted also in a reduced KLF2 and eNOS gene expression, while IL8 and E-selectin gene expression were increased (Figure 2D).

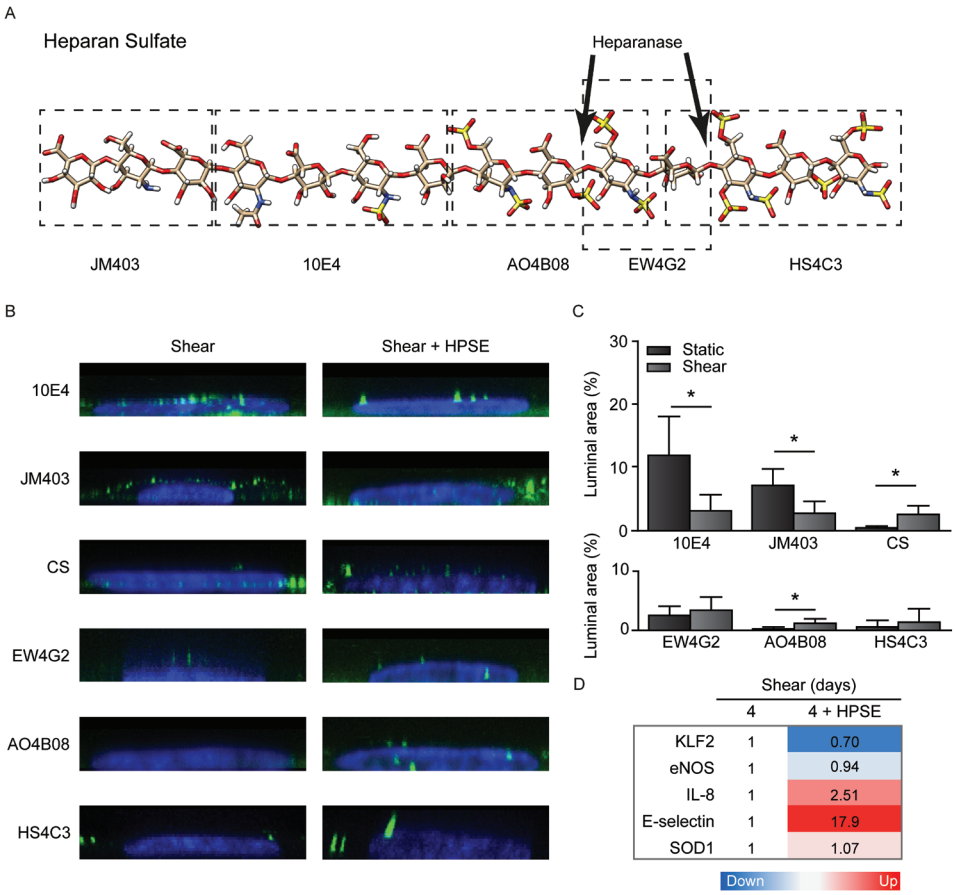


Figure 2. Heparanase changes endothelial glycocalyx in HUVEC cultured under flow. A) Structure model of heparan sulfate showing the tetrasaccharide repeat of glucuronic acid (GlcA) and N-, 6-O-sulfated glucosamine GlcN(NS,6S) in which, as a first step in cleavage, heparanase will cut the following tri-saccharide from the non-reducing end. In the structure the carbon backbone (brown), oxygen (red), hydrogen (white), sulfide (yellow) and nitrogen (blue) are depicted. The binding domains of used antibodies are shown (JM403, 10E4, AO4B08, EW4G2 and HS4C3). B) Representative examples of heparan sulfate specific domains (10E4, JM403, EW4G2, AO4B08 and HS4C3) and Chondroitin Sulfate (CS) staining in HUVEC exposed to shear stress for 4 days ± heparanase. C) Luminal staining area of B is quantified in the same area of interest as in figure S1 and expressed as area percentage ± SD; *p < 0.05 E) Expression of selected genes for endothelial glycocalyx stabilization after 4 days of shear stress ± heparanase: Krüppel-like Factor 2 (KLF2), endothelial nitric oxide synthase (eNOS), Interleukine-8 (IL-8), E-selectin and Superoxide dismutase-1 (SOD1). Genes are expressed as fold change compared to 4 days of culture and expressed as mean of 4-5 independent experiments; *p < 0.05.

Systemic heparanase changes vascular heparan sulfate composition in zebrafish

To test the effect of extracellular heparanase in the circulation *in vivo*, we injected heparanase in the cardinal vein of zebrafish larvae 3 days post fertilization (dpf). At 4 dpf, 24 hours after systemic heparanase injection, we quantified binding of the various anti-HS antibodies to all

vessels within the cross-sectional area of the pronephros, as shown in Figure 3A and B. Systemic heparanase treatment decreased the binding sites for both 10E4 (13.7 ± 5.8% vs. wild type 20.5 ± 6.2%) and JM403 (27.4 ± 8.0% vs. wildtype: 37.8 ±16.1%; $p < 0.05$; Figure 3B).

In line with the observations in HUVECS, AO4B08 expression was significantly increased upon extracellular heparanase presence (25.6 ± 9.2% vs. control 10.0 ± 8.4%; $p < 0.01$). In addition, the other antibody EW4G2 recognizing the N-, and 6-O-sulfated domains of HS was increased also significantly (10.9 ± 6.6% vs. wild type 1.6 ± 1.6%; $p < 0.01$). Throughout the vasculature analyzed, the typical 3-O-sulfated domains recognized by HS4C3 hardly was expressed in the zebrafish larvae, and not affected by systemic heparanase perfusion (0.8 ± 0.8% vs. wildtype:

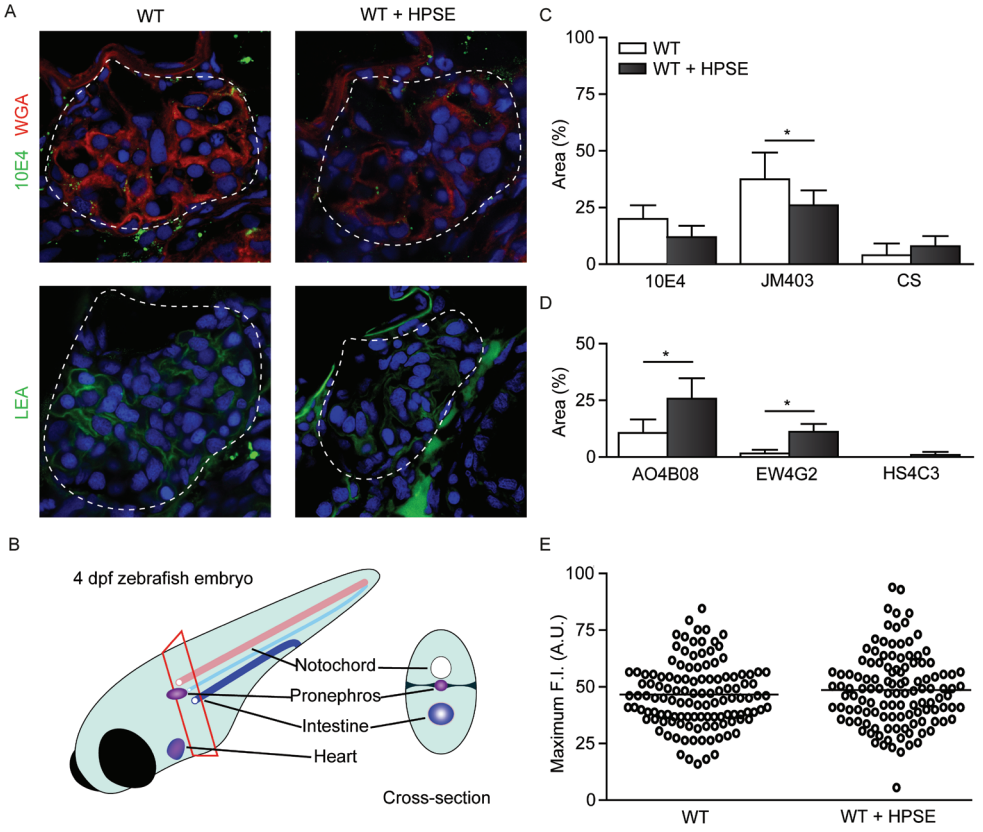


Figure 3. Systemic heparanase changes glycosaminoglycan composition in zebrafish larvae. A) Representative pictures of wheat germ agglutinin (WGA; top), and Lycopersicon esculentum (LEA; bottom) staining in the pronephros (encircled dashed) of zebrafish larvae with or without exposure to systemic heparanase (HPSE). B) schematic representation of zebrafish embryo, 4 days post fertilization (4 dpf; left) with cross-sectional area where quantification in C & D took place (right). C) Staining area of specific heparan sulfate epitopes are expressed as vascular area percentage ± SD; *$p < 0.05$. WT = wild type; WT + HPSE = WT perfused with heparanase for 24 hours; CS = Chondroitin Sulfate. D) Intravascular fluorescence loss is measured over the retinal blood vessel plexus in Tg(l-fabp:DBP-eGFP) fish after control (WT) and heparanase (WT + HPSE) injection at 4 days post fertilization to analyze vascular leakage in zebrafish larvae. Maximum Fluorescence levels (F.I.) of individual zebrafish larvae are displayed.

0.9 ± 1.4%, Figure 3D). Similar as was found in HUVECS, we observed a compensatory increase in chondroitin sulfate from 4.1 ± 2.7% to 9.2 ± 4.1%, Figure 3C).

To analyze the possible consequences of systemic glycocalyx alterations, we measured vascular leakage, as analyzed in the eye of the zebrafish larvae (21). Treatment with heparanase for 24 hours did not change fluorescence (Figure 3E), thus although systemic heparanase modified HS structure, it did not induce overt vascular leakage in these zebrafish larvae.

Discussion

Introducing extracellular active heparanase within the milieu of endothelial cells cultured under prolonged shear stress not only reduces total surface glycocalyx coverage but also changes the composition of HS binding domains to support inflammatory mediators.

Endothelial HS binds chemokines to create a gradient that supports initial leukocyte tethering and directs their migration across the endothelium (14). HS on the glycocalyx surface of inflammatory cells and endothelial cells enables direct physical interaction between the endothelial and inflammatory cells and enables the engagement of cell surface receptors with their ligands such as adhesion molecules (30). The HS constituent of the cell surface layer is very dynamically regulated. For example, rapid changes in sulfation patterns can occur in response to inflammatory stimuli through the upregulation of modifying enzymes such as *NDST-1* in a matter of hours (31). We have demonstrated that such HS modifications are key to the ability of inflammatory cells to invade the glomerulus during glomerulonephritis (27). To enable such rapid remodeling, an equally dynamic method for the degradation of HS components on the cell surface layer is required. HS carrying proteoglycans (HSPGs) and (pro)heparanase are continuously internalized (32). Once processed into its activated form in the endosome, heparanase can be taken up by the Golgi system again where it might remodel HS synthesis (33,34). This recycling of HSPGs and heparanase is hypothesized to contribute to the dynamic regulation of HS on the cell surface and cellular adaptation to processes such as inflammation. Our current studies further corroborate this hypothesis both *in vitro* as well as *in vivo*.

We also show that selective loss of HS structures via heparanase is compensated in part by increased chondroitin sulfate biosynthesis, as has also been described previously (29) This may have allowed preservation of barrier function. Indeed, in zebrafish larvae, the infusion of heparanase did not induce overt vascular leakage. This is most likely related to the fact that we chose our heparanase dosage to mimic concentrations that can be observed during inflammation, where the glycocalyx barrier structure is reduced (as illustrated by the reduction in lectin staining, Figure 3A) but not completely lost.

The relevance of these observations pertains to conditions where heparanase is secreted and subsequently activated in the extracellular space. These conditions include cancer invasion, neoangiogenesis, diabetic nephropathy and glomerulonephritis (35-42). Interestingly, the upregulation of endothelial HS domains by heparanase as was identified by the single chain antibodies AO4B08 and EW4G2 is very similar to what has been previously observed by us in

conditions with endothelial activation such as in glomerulonephritis (27). The potential relevance of heparanase in these conditions, and as a potential therapeutic avenue, is underscored by the fact that genetic deletion of heparanase can prevent the development of glomerulonephritis and diabetic nephropathy (2).

Acknowledgements

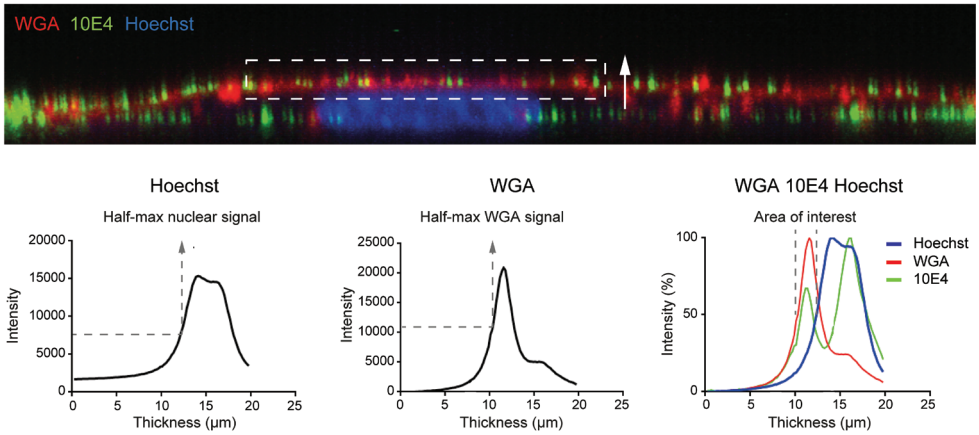
The Dutch Kidney Foundation financially supported this study: Glycoren consortium (CP09.03).

We thank L. Staggs, P. Schroder and Dr. S. Rieger (Mount Desert Island Biological Laboratory, Salisbury Cove, ME) for the use of the zebrafish facilities.

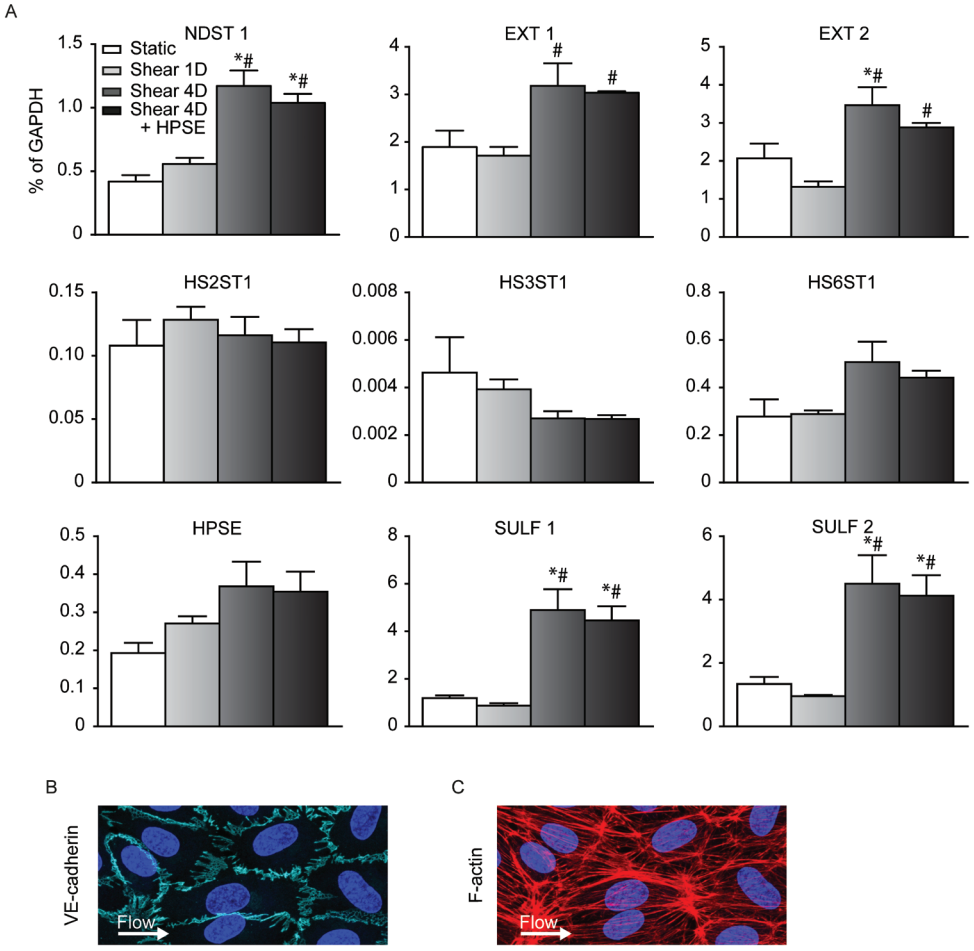
References

1. Rabelink TJ, van den Berg BM, Garsen M, Wang G, Elkin M, et al. (2017) Heparanase: roles in cell survival, extracellular matrix remodelling and the development of kidney disease. Nat Rev Nephrol 13: 201-212.
2. Gil N, Goldberg R, Neuman T, Garsen M, Zcharia E, et al. (2012) Heparanase is essential for the development of diabetic nephropathy in mice. Diabetes 61: 208-216.
3. Lever R, Rose MJ, McKenzie EA, Page CP (2014) Heparanase induces inflammatory cell recruitment in vivo by promoting adhesion to vascular endothelium. Am J Physiol Cell Physiol 306: C1184-1190.
4. Reitsma S, Slaaf DW, Vink H, van Zandvoort MA, oude Egbrink MG (2007) The endothelial glycocalyx: composition, functions, and visualization. Pflugers Arch 454: 345-359.
5. Esko JD, Selleck SB (2002) Order out of chaos: assembly of ligand binding sites in heparan sulfate. Annu Rev Biochem 71: 435-471.
6. Rops AL, Jacobs CW, Linssen PC, Boezeman JB, Lensen JF, et al. (2007) Heparan sulfate on activated glomerular endothelial cells and exogenous heparinoids influence the rolling and adhesion of leucocytes. Nephrol Dial Transplant 22: 1070-1077.
7. Esko JD, Lindahl U (2001) Molecular diversity of heparan sulfate. J Clin Invest 108: 169-173.
8. Quarto N, Amalric F (1994) Heparan sulfate proteoglycans as transducers of FGF-2 signalling. J Cell Sci 107 (Pt 11): 3201-3212.
9. Yayon A, Klagsbrun M, Esko JD, Leder P, Ornitz DM (1991) Cell surface, heparin-like molecules are required for binding of basic fibroblast growth factor to its high affinity receptor. Cell 64: 841-848.
10. Massena S, Christoffersson G, Hjertstrom E, Zcharia E, Vlodavsky I, et al. (2010) A chemotactic gradient sequestered on endothelial heparan sulfate induces directional intraluminal crawling of neutrophils. Blood 116: 1924-1931.
11. Lindahl U, Kusche-Gullberg M, Kjellen L (1998) Regulated diversity of heparan sulfate. J Biol Chem 273: 24979-24982.
12. Broekhuizen LN, Mooij HL, Kastelein JJ, Stroes ES, Vink H, et al. (2009) Endothelial glycocalyx as potential diagnostic and therapeutic target in cardiovascular disease. Curr Opin Lipidol 20: 57-62.
13. Lee DH, Dane MJ, van den Berg BM, Boels MG, van Teeffelen JW, et al. (2014) Deeper penetration of erythrocytes into the endothelial glycocalyx is associated with impaired microvascular perfusion. PLoS One 9: e96477.
14. Esko JD, Selleck SB (2002) Order out of chaos: assembly of ligand binding sites in heparan sulfate. Annu Rev Biochem 71: 435-471.
15. Kolset SO, Reinholt FP, Jenssen T (2012) Diabetic nephropathy and extracellular matrix. J Histochem Cytochem 60: 976-986.
16. Uchimura K, Lemjabbar-Alaoui H, van Kuppevelt TH, Rosen SD (2010) Use of a phage display antibody to measure the enzymatic activity of the Sulfs. Methods Enzymol 480: 51-64.
17. Wilson JC, Laloo AE, Singh S, Ferro V (2014) 1H NMR spectroscopic studies establish that heparanase is a retaining glycosidase. Biochem Biophys Res Commun 443: 185-188.
18. van den Born J, Salmivirta K, Henttinen T, Ostman N, Ishimaru T, et al. (2005) Novel heparan sulfate structures revealed by monoclonal antibodies. J Biol Chem 280: 20516-20523.
19. Kreuger J, Spillmann D, Li JP, Lindahl U (2006) Interactions between heparan sulfate and proteins: the concept of specificity. J Cell Biol 174: 323-327.
20. Ferreras C, Rushton G, Cole CL, Babur M, Telfer BA, et al. (2012) Endothelial heparan sulfate 6-O-sulfation levels regulate angiogenic responses of endothelial cells to fibroblast growth factor 2 and vascular endothelial growth factor. J Biol Chem 287: 36132-36146.
21. Kirsch T, Kaufeld J, Korstanje R, Hentschel DM, Staggs L, et al. (2013) Knockdown of the hypertension-associated gene NOSTRIN alters glomerular barrier function in zebrafish (Danio rerio). Hypertension 62: 726-730.
22. Dekker RJ, van Soest S, Fontijn RD, Salamanca S, de Groot PG, et al. (2002) Prolonged fluid shear stress induces a distinct set of endothelial cell genes, most specifically lung Kruppel-like factor (KLF2). Blood 100: 1689-1698.

23. Boon RA, Leyen TA, Fontijn RD, Fledderus JO, Baggen JM, et al. (2010) KLF2-induced actin shear fibers control both alignment to flow and JNK signaling in vascular endothelium. Blood 115: 2533-2542.
24. Dane MJC (2015) Structure and function of the endothelial glycocalyx in the microcirculation. (dissertation). Chapter 3, Prolonged shear stress modifies the composition of the endothelial glycocalyx; p. 50-67. Leiden: Leiden University Medical Center. 50-67 p.
25. Boon RA, Horrevoets AJ (2009) Key transcriptional regulators of the vasoprotective effects of shear stress. Hamostaseologie 29: 39-40, 41-33.
26. Grobe AC, Wells SM, Benavidez E, Oishi P, Azakie A, et al. (2006) Increased oxidative stress in lambs with increased pulmonary blood flow and pulmonary hypertension: role of NADPH oxidase and endothelial NO synthase. Am J Physiol Lung Cell Mol Physiol 290: L1069-1077.
27. Rops ALWM, Loeven MA, van Gemst JJ, Eversen I, Van Wijk XM, et al. (2014) Modulation of heparan sulfate in the glomerular endothelial glycocalyx decreases leukocyte influx during experimental glomerulonephritis. Kidney Int 86: 932-942.
28. Rops AL, van den Hoven MJ, Baselmans MM, Lensen JF, Wijnhoven TJ, et al. (2008) Heparan sulfate domains on cultured activated glomerular endothelial cells mediate leukocyte trafficking. Kidney Int 73: 52-62.
29. Le Jan S, Hayashi M, Kasza Z, Eriksson I, Bishop JR, et al. (2012) Functional overlap between chondroitin and heparan sulfate proteoglycans during VEGF-induced sprouting angiogenesis. Arterioscler Thromb Vasc Biol 32: 1255-1263.
30. Parish CR (2006) The role of heparan sulphate in inflammation. Nat Rev Immunol 6: 633-643.
31. Carter NM, Ali S, Kirby JA (2003) Endothelial inflammation: the role of differential expression of N-deacetylase/N-sulphotransferase enzymes in alteration of the immunological properties of heparan sulphate. J Cell Sci 116: 3591-3600.
32. Yanagishita M, Hascall VC (1992) Cell surface heparan sulfate proteoglycans. J Biol Chem 267: 9451-9454.
33. Roucourt B, Meeussen S, Bao J, Zimmermann P, David G (2015) Heparanase activates the syndecan-syntenin-ALIX exosome pathway. Cell Res 25: 412-428.
34. Nadanaka S, Purunomo E, Takeda N, Tamura J, Kitagawa H (2014) Heparan sulfate containing unsubstituted glucosamine residues: biosynthesis and heparanase-inhibitory activity. J Biol Chem 289: 15231-15243.
35. Escobar Galvis ML, Jia J, Zhang X, Jastrebova N, Spillmann D, et al. (2007) Transgenic or tumor-induced expression of heparanase upregulates sulfation of heparan sulfate. Nat Chem Biol 3: 773-778.
36. van den Born J, van den Heuvel LP, Bakker MA, Veerkamp JH, Assmann KJ, et al. (1993) Distribution of GBM heparan sulfate proteoglycan core protein and side chains in human glomerular diseases. Kidney Int 43: 454-463.
37. van den Hoven MJ, Rops AL, Vlodavsky I, Levidiotis V, Berden JH, et al. (2007) Heparanase in glomerular diseases. Kidney Int 72: 543-548.
38. Katz A, Van-Dijk DJ, Aingorn H, Erman A, Davies M, et al. (2002) Involvement of human heparanase in the pathogenesis of diabetic nephropathy. Isr Med Assoc J 4: 996-1002.
39. Maxhimer JB, Somenek M, Rao G, Pesce CE, Baldwin D, Jr., et al. (2005) Heparanase-1 gene expression and regulation by high glucose in renal epithelial cells: a potential role in the pathogenesis of proteinuria in diabetic patients. Diabetes 54: 2172-2178.
40. Shafat I, Zcharia E, Nisman B, Nadir Y, Nakhoul F, et al. (2006) An ELISA method for the detection and quantification of human heparanase. Biochem Biophys Res Commun 341: 958-963.
41. van den Hoven MJ, Rops AL, Bakker MA, Aten J, Rutjes N, et al. (2006) Increased expression of heparanase in overt diabetic nephropathy. Kidney Int 70: 2100-2108.
42. Wijnhoven TJ, van den Hoven MJ, Ding H, van Kuppevelt TH, van der Vlag J, et al. (2008) Heparanase induces a differential loss of heparan sulphate domains in overt diabetic nephropathy. Diabetologia 51: 372-382.



Supplementary Figure S1 Methods to quantify the luminal endothelial glycocalyx staining. A) Confocal fluorescent z-axis average-intensity projections of HUVEC cultured under laminar flow for 4 days and stained with wheat germ agglutinin (WGA), 10E4 and Hoechst. White box shows the area of interest which should be quantified. B) Example of quantification method. Glycocalyx thickness is quantified by estimating the distance from the half-maximum signal of the nuclear staining (left) to the half-maximum signal at the luminal end of WGA (middle) and 10E4 staining (right). Luminal staining area is quantified in the same area of interest in ImageJ.



Supplementary Figure S2 Effects of prolonged shear stress on gene expression enzymes involved in HS production and modification. A) Gene expressions as percentage of GAPDH expression after static and 1 or 4 days (D) of flow and 4 days of flow + heparanase (HPSE). Genes coding for enzymes involved in HS chain prolongation (EXT1, EXT2) and sulfation pattern modification (NDST1, HS2ST1, HS3ST1, HS6ST1, SULF1, SULF2) and breakdown (HPSE). Extracellular heparanase induces unstable focal adhesion junctions as visualized by VE-cadherin staining (B) and less organized actin filaments (C), without evident changes in cell orientation in response to flow in comparison to 4 days flow exposure without heparanase. *P<0.05 compared to static culture, #P<0.05 compared to 1day shear stress.

Chapter 6

Endothelial glycolytic activity regulates microvascular structure by modulating Angiopoietin 1 binding to endothelial glycocalyx hyaluronan

In submission

Bernard M. van den Berg, Ganggi Wang*, Margien G.S. Boels*, Anna Rita Cantelmo, Sarantos Kostidis, M. Cristina Avramut, Erik Jansen, Eelco J.P. de Koning, Wendy M.P.J. Sol, Franck Lebrin, Johan van der Vlag, Anton Jan van Zonneveld, Hermann-Josef Gröne, Hans Vink, Peter Carmeliet and Ton J. Rabelink

*Both authors contributed equally to this work

Abstract

The luminal surface of endothelial cells is covered by a glycocalyx layer, a poorly studied structure in vascular biology, whose loss promotes vascular destabilization in cancer and diabetes. How glycocalyx formation is regulated is largely unknown. Here, we show that endothelial deletion of hyaluronan synthase 2 (*has2*), synthesizing the glycocalyx component hyaluronan, causes glomerulopathy, retinopathy and cardiomyopathy due to microvascular destabilization. Mechanistically, endothelial *has2* inhibition impairs glycocalyx binding of angiopoietin-1, a key vessel stabilization regulator. Metabolically, the glycolytic activator PFKFB3 lowers the production of substrates for hyaluronan synthesis (UDP-GlcA, UDP-GlcNAc) from the glycolytic metabolite glucose-6-phosphate, by reprioritization glucose metabolism into glycolysis. In line, PFKFB3 is increased in endothelial cells in diabetes and cancer; tumor vessels express reduced endothelial surface hyaluronan; and endothelial PFKFB3 haplodeficiency increases tumor endothelial surface hyaluronan and angiopoietin1, and improves endothelial cell stabilization. Restoring the endothelial glycocalyx by reducing glycolysis could be targeted for vessel normalization.

Introduction

All cells in the body are covered with a glycocalyx layer (GL), a carbohydrate-gel composed of the glycosaminoglycans heparan sulfate (HS), hyaluronan (HA), chondroitin sulfate and associated proteins (1). The GL is especially critical for the homeostasis of the vasculature. Indeed, the GL controls vessel perfusion, ensures vessel patency (through its anti-thrombotic properties), regulates vascular barrier permeability, impairs cancer cell adhesion and extravasation, and prevents vascular inflammation (through precluding leukocyte adhesion to endothelial cells (ECs)) (2-4). Damage of the endothelial GL is associated with vascular destabilization in cancer, diabetes and other life-threatening diseases such as sepsis (5-7). Despite its importance, the GL is one of the most understudied structures in vascular biology and understanding of its regulation and role in vascular homeostasis is still very limited (8).

Recent studies highlighted the importance of EC metabolism in angiogenesis in health and disease, and illustrated that targeting EC metabolic targets inhibits pathological angiogenesis in inflammatory and malignant diseases in preclinical mouse models (9-11). We recently reported that lowering EC glycolysis induced tumor vessel normalization, thereby reducing metastasis and improving chemotherapy (9). Whether EC metabolism regulates the production of the GL has never been explored.

In tumors, vessels are structurally and functionally abnormal, characterized by EC destabilization (12), while in diabetes, ECs are dysfunctional with vascular barrier defects and enhanced leukocyte adhesion (13). Tumor vessel destabilization impairs tumor perfusion, promotes cancer cell intravasation and dissemination, and compromises the delivery and efficacy of chemo-, radio- and immunotherapy (14). Strategies promoting tumor vessel normalization reduce metastasis, while promoting anti-cancer therapy responses are increased (9,15). Whether strategies targeting EC metabolism can promote the formation of the endothelial GL is unknown.

The GL also importantly regulates binding of growth factors and other biologically important molecules to the EC surface (16,17). In contrast to heparan sulfates, HA lacks the specific chemical modifications (i.e., sulfation, acetylation, and epimerization), implicated in protein and growth factor binding (18). Remarkably, glycocalyx research has been mostly centered around the heparan sulfate (HS) component (2). The ubiquitous distribution of HA *in vivo*, the biological activity of HA fragments when using degradative enzymes (19), and the inability to specifically inhibit HA synthesis *in vivo* have hampered the study of the potential role of HA in endothelial glycocalyx function to date.

HA is a linear polysaccharide that is composed of repeating units of glucuronic acid (GlcA) and N-acetyl-glucosamine (GlcNAc) linked together through glycosidic bonds that can be repeated several thousand times, thus requiring very large amounts of substrates. Starting both from the glycolytic intermediate glucose-6-phosphate, the glucuronic acid biosynthesis pathway produces GlcA, while the hexosamine biosynthesis pathway produces GlcNAc (20). In contrast to the synthesis of other glycosaminoglycans, which takes place in the Golgi system, HA is produced at the plasma membrane using the cytoplasmic substrate pool. Therefore, cytosolic uridine diphospho-glucuronic acid (UDP-GlcA) and UDP-GlcNAc availability is critical

for this energy consuming process, rendering the metabolic state of the cell an important factor for production of HA (21-25). This may be even more relevant in ECs where an inherent high rate of glycolysis may shift glucose-6-phosphate away from the metabolic pathways that produce the HA substrates UDP-GlcA and UDP-GlcNAc. (11,26). However, whether glycolysis regulates the formation of the GL in ECs remains unknown.

Cell surface HA in mammals is predominantly synthesized by hyaluronan synthase 2 (HAS2). Mice that are null for *Has2* die early in gestation due to major defects in cardiovascular development, suggesting that HA may function as molecular platform for vascular signalling (27). A key regulator of endothelial quiescence and maintenance of the endothelial barrier function is angiopoietin 1 (Ang1), a secreted ligand of the endothelial Tie-2 kinase (28,29). Adult tissues, such as brain, heart and especially fenestrated glomerular and retinal endothelium constitutively show Ang1 signalling (30,31). Ang1 requires extracellular matrix (ECM) binding to signal to its receptor (32). Heparan sulfates are not a binding candidate for Ang1 (33). However, since Ang1 is sequestered into chemically crosslinked HA hydrogels (34), HA in the glycocalyx may act as a mediator in confining Ang1 to the cell surface and induce endothelial stabilization. However, it is unknown if Ang1 binds to HA, and if this binding relies on EC metabolism (glycolysis).

In this study, we explored whether: (i) endothelial deletion of the HA-synthesizing enzyme *has2* compromises endothelial GL formation and causes organ disease; (ii) the EC stabilization-promoting signal Ang1 binds to the endothelial GL, and impaired Ang1 binding to a compromised GL contributes to vascular destabilization; and (iii) manipulation of endothelial glycolysis can regulate GL formation. Our findings may have therapeutic relevance to induce vessel normalization and EC stabilization by promoting GL formation through inhibition of EC glycolysis.

Methods

Reagents

All materials are from Sigma-Aldrich (St. Louis, MO, USA) or stated otherwise.

Mice

Endothelial specific conditional homozygous has2 knockout (has2-cKO) mice were generated by breeding B6.*cdh5*-Cre-ER^{T2} with B6.has2$^{flox/flox}$ (19)·(35-38). For reporter analysis, *cdh5*-Cre-ER^{T2}.has2$^{fl/fl}$ and *cdh5*-Cre-ER^{T2} (ctrl) mice were crossed to Rosa-TdTomato$^{fl/fl}$ reporter mice, in which Cre-mediated excision resulted in Tomato expression, as illustrated in Figure S1a. Animal experiments were approved by the Animal Care Committee of the Royal Netherlands Academy of Arts and Sciences (permit no. HI 11.2504) or by the ethical committee on animal care and experimentation of the Leiden University Medical Center (permit no. 14-033). All animal work was performed in compliance with the Dutch government guidelines. Presence of introduced genes from ear pinched DNA samples is performed on all animals during breeding and for

confirmation of has2 gene mutation (exon 2 deletion) after tamoxifen on has2-cKO mice at the end of the experiment using PCR and primers (Figure S1b & Table S2). Only has2-cKO mice with a confirmed mutation within their has2 gene were examined further. Eight-week-old male has2-cKO and control mice (*n = 5-6*/time-point) received intra-peritoneal 2mg/0.2mL tamoxifen for 5 consecutive days. Two days before tamoxifen treatment and at indicated time intervals (2-, 4-, 8- and 12 weeks after induction), 24hrs-urine samples were collected together with body weight and blood pressure measurements. One week before the endpoints at 8- and 12 weeks, echocardiography was performed. Additional animals, 4wks after tamoxifen, were used for renal cationic ferritin perfusion (*n = 3/group*), renal tissue slice collection (*n = 3/group*) and at 6wks after tamoxifen for collection of retinas (n = 3-5/group).

C57BL/6 (WT, 7-9 weeks old) and *Pfkfb3*$^{+/\Delta}$ mice (9), used for the metastatic mouse model, were from the KU Leuven Animal Facility. Animal procedures were approved by the Institutional Animal Care and Research Advisory Committee (KU Leuven) (permit ECD207/2014) and were performed in accordance with the institutional and national guidelines and regulations. B16-F10 mouse melanoma cells were injected intravenously via the portal vein to obtain liver tumors (9,39). After anesthesia (100 mg/kg ketamine and 10 mg/kg xylazine), median laparotomy was performed, the hilum of the liver was exposed and 150,000 melanoma cells were injected in a volume of 100µL PBS into the portal vein using a 32 G needle. After the injection, a cotton swab was placed on the lesion until the bleeding stopped. In case of persistent bleeding, a cellulose fleece was placed on the injection site. After injection, the intestine was replaced and the abdominal wall was closed in a two-layer technique. The animals were sacrificed 12 days' post-injection and liver tissue containing metastases were placed in 4% paraformaldehyde solution for further processing. Normal liver tissue was examined as control of the metastases. All animals had free access to standard chow and tap water.

Urine collection and analysis

Mice (Has2-ckO and control) were weighted before and after residing in the metabolic cage (Tecniplast S.p.a, Buguggiate, Italy) and water- and food intake, urine and fecal excretion were collected. After acclimatization, 24hrs-urine was collected (maximal 4 times per mouse). Urine was centrifuged and subsequently stored at -20°C. Albumin levels were quantified using Rocket immunoelectrophoresis (40) and creatinine levels were determined by the Jaffé method using 0.13% picric acid, and quantified using a creatinine standard set. Optical densities were measured with an Ascent Multiscan (Thermo electron corp., Vantaa, Finland).

Blood urea determination

Plasma urea levels were determined using a Cobas Reflotron (Roche Diagnostics ltd., Rotkreuz, Switzerland).

Non-invasive tail-cuff blood pressure measurement

Blood pressure (BP) was measured in conscious animals using the tail-cuff method (CODA-2; Kent Scientific, Torrington, CT). Briefly, each session consisted of five acclimatization cycles, followed by 15 BP measurement cycles. The average from the automatic approved sessions (>50% valid) was used for mean BP, and heart rate in each individual mouse.

Echocardiographic assessment

Transthoracic echocardiography was performed on temperature controlled and lightly, isoflurane, anesthetized mice using a Vevo 2100 high-resolution system (Visual Sonics, Toronto, Canada) equipped with an 18-38-MHz MS400 scan head. Two-dimensional guided M-mode tracings were recorded in both parasternal long and short axis views at the level of the papillary muscles (41). Diastolic left ventricular posterior wall thickness, ventricular parameters including diastolic interventricular septal thickness and systolic left ventricular internal diameters were measured (data not shown) and left ventricle wall mass, ejection fraction and stroke volume were calculated with the established standard equation. For measuring systolic flow parameters pulse wave (PW) Doppler was used in the aortic arch for obtaining peak flow velocity and peak aortic velocity gradient (42). All measurements were made from more than three beats and averaged.

Tissue preparation and histology

Mice were anaesthetized by isoflurane and after abdominal exposure the right kidney was ligated and fixed immediately by injecting 2% paraformaldehyde (PFA) in PBS under its capsule. Next, the beating heart was excised and directly placed in 4% PFA, followed by excision of both kidneys, liver, spleen and lungs. Kidney capsules were removed, one half of the right kidney was fixed overnight at 4°C in 2% PFA in PBS for detection of endogenous albumin (43), data not shown, or detailed glomerular morphometric analysis, as described elsewhere (44). The other half was snap-frozen in liquid nitrogen for immunofluorescence staining. Both halves of the left kidney were placed in 2% PFA in PBS overnight at 4°C, followed by paraffin embedding for periodic acid-Schiff (PAS) and Goldner's elastica trichrome staining and computer aided glomerular quantification using customized software at Dr. Gröne's Laboratory (Heidelberg, Germany) or immunofluorescence staining. After fixation, heart tissue was processed for paraffin embedding and 4µm tangential sections of the entire heart were stained with Goldner's elastica trichrome, or incubated with fluorescent linked *Griffonia simplicifolia I* isolectin B4 (isolectin BS-I-FITC) for determination of capillary density. Renal and heart tissue slides were recorded using a 3D Histech Pannoramic MIDI Scanner (Sysmex, Etten-Leur, the Netherlands) and a 40x objective (Plan Apochromat, NA 0.95; Carl Zeiss). Quantification was performed using the public domain NIH ImageJ software (FIJI version 1.49m; http://rsb.info.nih.gov/ij); for renal morphology 20-25 sub-cortical glomeruli per kidney slice (*n = 5-6*/time-point), cardiomyocyte area determination of approximately 40-50 individual cells per cardiac segment (*n = 5*/

time-point), and number capillaries and cardiomyocytes (to calculate capillary to myocyte ratio) of 3 separate fields per cardiac segment (*n = 5*/time-point) were measured.

Immunohistochemistry

Deparaffinized left-kidney and heart sections (4 µm thick) were washed in PBS and antigen retrieval was performed in a Tris-EDTA (pH 9.0) buffer in an autoclave. Slides were incubated with 3% H_2O_2 for 15 minutes at rT and after washing with 0.01% Triton-X100 in PBS, blocked in Serum-Free Protein Block buffer (Dako) for 1hr at rT. Primary Goat Anti-Ang1 (AF923, R&D Systems) or Rabbit Anti-VCAM-1 (ab134047, Abcam), was incubated overnight (at 4°C), followed by Rabbit Anti-Goat-IgG-HRP (Dako), Rabbit Envision (DAKO, kidney anti-VCAM-1 samples) or Donkey Anti-Goat-IgG-AF488 (Mol Probes, heart samples) for 1 hour, both in blocking buffer. Kidney tissue samples were developed with DAB solution (1:100, Dako) for about 5-10 minutes and counterstained for 1-2 sec with Hematoxylin. Heart tissue samples were additionally stained with BS-1-TRITC and Hoechst.

Deparaffinized liver sections (4 µm thick), were washed in PBS and antigen retrieval was performed in a Tris-EDTA (pH 9.0) buffer in an autoclave. Slides were incubated with 3% H_2O_2 for 15 minutes at rT and after washing with 0.01% Triton-X100 in PBS, blocked in Serum-Free Protein Block buffer (X0909, Dako) for 1hr at rT. Primary Goat anti-Ang1 (AF923, R&D Systems) and BS-1-TRITC (endothelial labeling) were incubated overnight at 4°C, followed by Rabbit anti-Goat-IgG-HRP (Dako) for 30 minutes at rT. Samples were rinsed with PBS containing 0.1% Tween-20, and incubated for 10 minutes with tyramide-FITC (self-made) diluted in TSA dilution buffer (TSA Plus Cyanine 3 System, NEL744001KT, Perkin Elmer) and embedded with ProLong® Gold Antifade Reagent containing DAPI (8961, Cell Signaling Technology, Danvers, MA, USA). For Tie2 receptor labeling samples were, after blocking with Serum-Free Protein Block buffer, incubated with 3% normal goat serum (NGS), 1% BSA and 0.3% Triton X-100 and incubated with Goat anti-Pospho-Tie2 (Y1102/Y1100; AF3909, R&D Systems) and Mouse anti-Tie2 (ab24859, Abcam), overnight at 4°C followed by Rabbit Anti-Goat-IgG-HRP (Dako) for 30 minutes at rT. Samples were rinsed with PBS containing 0.1% Tween-20, and incubated for 10 minutes with TSA-Cy3 (Perkin Elmer) diluted in TSA dilution buffer (TSA Plus Cyanine 3 System, NEL744001KT, Perkin Elmer). Next, samples were rinsed with PBS-0.1% Tween-20, incubated with secondary Goat anti-Mouse-IgG1-AF488 (Mol Probes) for 1hr at rT and embedded with ProLong® Gold Antifade Reagent containing DAPI (Cell Signaling Technology).

Tissue slides were recorded using a 3D Histech Pannoramic MIDI Scanner and a 40x objective lens (Plan Apochromat, NA 0.95). Staining area is quantified using ImageJ software and displayed as percentage stained area / glomerular area, in heart as percentage Ang1 positive capillaries (*n = 4-5*/timepoint), in liver samples as Ang1 staining / µm vessel length, or as percentage p-Tie2 / Tie2 ratio (*n = 4 WT or 5 Pfkfb3*$^{+/\Delta EC}$).

In addition, frozen kidney sections (2µm thick) were fixed in 2% PFA/0.3% Triton X-100 in PBS for 10 minutes, washed in PBS, and blocked for 30 minutes at room temperature in 2% fetal calf serum (Bodinco, Alkmaar, The Netherlands), 2% bovine serum albumin (BSA), and 0.2%

fish gelatin (Amersham Biosciences, Buckinghamshire, UK) in PBS. Sections were incubated for 45 minutes with 1 to 10 mg/mL primary antibodies against mouse synaptopodin (Progen Biotechnik GmbH, Heidelberg, Germany), nephrin (R&D Systems Europe Ltd, Abingdon, UK), or desmin (Tebu-Bio, Heerhugowaard, The Netherlands). Subsequently, sections were rinsed and incubated for 45 minutes with 5 mg/mL Alexa 488- or 594-conjugated secondary antibodies (Life Technologies Europe BV, Bleiswijk, The Netherlands). Finally, sections were rinsed with PBS, post-fixed with 1% PFA in PBS, and embedded in VectaShield mounting medium H-1000 (Brunschwig Chemie, Amsterdam, The Netherlands). The staining intensities of antibodies were scored in 50 glomeruli (*n = 4-5*/time-point) on a 0 to 10 scale (0, no staining; 10, 100% staining intensity).

Isolation of retinal tissue

Six weeks after tamoxifen treatment of eyes of has2-cKO and control mice were excised and fixed in 4% paraformaldehyde in PBS at 20°C for 10 min. Retinas were dissected and post-fixed in 4% paraformaldehyde in PBS at 4°C overnight and embedded in Vectashield mounting medium (Vector Laboratories Inc., Burlingame, CA) for whole-mount examination of TdT-Tomato positive retinal vessels. Tissues were examined using a LEICA TCS SP8 X WLL (Leica, Rijswijk, The Netherlands) and a 20x objective (HC PL APO 20x/0.70 DRY, Leica). Sequential 16-bit confocal images (xyz dimensions, 0.758×0.758×1.0µm) were recorded using LAS-X Image software (Leica) and analyzed with ImageJ.

Detection of endothelial surface hyaluronan

Left kidneys from anesthetized mice (*n = 3/group*) were collected, capsule removed, and fixed overnight in freshly made 4% paraformaldehyde in PBS at 4°C. Next, 150 µm thick slices were obtained using a Leica VT1000S vibratome and collected in HBSS solution containing 10 mM hepes, 3% BSA (A7030) and 2% FCS (HBSS++). Tissue slices were incubated with 1:5 Ncan-eGFP (45) dilution, or 10 µg/mL LEA-FITC, overnight and 10 µg/mL Hoechst 33528 at 4°C on a flatbed rocker. As a control to Ncan-eGFP specific hyaluronan staining, separate slices were incubated with 50 Units/mL of hyaluronidase (hyal; Hyaluronidase IV-S, Sigma) and a 1/100 protease inhibitor cocktail (Protease & phosphatase inhibitors; Pierce, Life Technologies Europe BV) for 2hrs at 37°C prior to incubation with Ncan-eGFP.

Sections of liver containing B16-F10 tumors, fixed overnight in freshly made 4% paraformaldehyde at 4°C were cut into 200 µm thick slices (Vibratome, Leica) and collected in HBSS++. Tissue slices were incubated with 100 µg/mL Ncan-dsRed, or 10 µg/mL LEA-FITC, and 0.8 µg/mL Rat Anti-Mouse CD31 (BD-Biosciences, Breda, the Netherlands) overnight at 4°C on a flatbed rocker. After washing three times with HBSS++, slices were incubated with 8 µg/mL Goat Anti-Rat-IgG (AF488 or AF568, Molecular Probes, Life Technologies Europe BV) and 10 µg/mL Hoechst 33528 for at least 4hrs at 4°C on a flatbed rocker.

As a control to Ncan-dsRed specific hyaluronan staining, separate slices were incubated with 50 units/mL of hyaluronidase (Hyaluronidase IV-S, Sigma) and a 1/100 protease inhibitor cock-

tail (Protease & phosphatase inhibitors; Pierce, Life Technologies Europe BV) for 2hrs at 37°C. Slices were washed twice with HBSS++ and proceeded with Ncan-dsRed staining as above.

Tissue slice imaging

Slices were glued to the bottom of a Petri dish with Permabond 910 (Electron Microscopy Sciences), submerged in HBSS and examined using a Zeiss 710-NLO CLSM microscope (CarlZeiss, Göttingen, Germany) with a 20x water dipping objective (W-Plan Apochromat, NA 1.0 DIC M27 70mm; Carl Zeiss). Sequential 16-bit confocal images (xy dimensions, 0.05×0.05 µm) were recorded using ZEN-2009 Image software (Carl Zeiss) and analyzed with ImageJ, as described earlier(43). For each glomerular image, the amount and location of intensity profiles were quantified by estimating the distance from the luminal half-width of the endothelial TdTomato signal to the half-width of the intraluminal Ncan-eGFP (ctrl, *n = 7*; ctrl + hyal *n = 5*; has2cKO, *n = 12*; has2-cKO + hyal, *n= 10*) or LEA-FITC (ctrl, *n = 5*; has2cKO, *n = 9*) fluorescence along the lines (5 per image) of interest as shown in Figure 2A,B. Total luminal endothelial fluorescence was calculated from fluorescence within this section.

In a similar fashion the liver-tissue slices were examined. For each image, the amount and location of intensity profiles were quantified by estimating the distance from CD31 peak signal to the half-width of the intraluminal Ncan-dsRed (liver, n = 4; metastasis, n = 6), or LEA-FITC (liver, n = 3; metastasis, n = 6) fluorescence along the lines of interest (5 per image, line width 5 pixels). Total luminal endothelial fluorescence was calculated from fluorescence within this section. Per slice at least 3 images of blood vessels were analyzed.

Detection of glomerular endothelial surface layer with cationic ferritin

Four weeks after tamoxifen induction of control and has2-cKO mice (n = 3/group), or 22-week old diabetes and control apoE-KO mice (n = 3/group) were anesthetized, the abdominal aorta was exposed and cannulated adjacent to the left renal artery. The right renal artery was ligated at the renal stalk after which the left kidney was perfused with 5 mL Hanks-buffered salt solution (HBSS, Gibco) containing 0.5% BSA (Sigma, A7030, essentially globulin free) and 5U/mL heparin at 2mL/minute to remove blood, followed by 2mL of cationic ferritin (horse spleen, 2.5 mg/ml, Electron Microscopy Sciences, Fort Washington, PA) in HBSS at 2 mL/minute. The left kidney was excised, its capsule removed, and stored in fixative (1.5% glutaraldehyde and 1% paraformaldehyde (both from Electron Microscopy Sciences, Hatfield, PA) in 0.1M sodium-cacodylate buffered solution, pH 7.4) overnight at 4˚C. The tissue was subsequently sectioned in 180 µm thick slices with a Leica VT1000S vibratome, rinsed 2x with 0.1M sodium cacodylate-buffered solution, and post-fixated for 1hr with 1% osmium tetroxide (Electron Microscopy Sciences) and 1.5% potassium ferrocyanide in demineralized water. Samples were further washed, dehydrated in ethanol, infiltrated with a mixture of epon LX-112 and propylene oxide (1:1) for 1 hr, followed by pure epon for 2hrs, embedded in epon mounted in BEEM capsules (Agar Scientific, Essex, United Kingdom) and polymerized for 48hrs at 60°C. 100nm Thick sections were cut using a diamond knife (Diatome, Biel, Switzerland), collected

on single slot copper grids covered with formvar film and carbon layer, and then stained with 7% uranyl acetate in demineralized water for 20 minutes, followed by Reynold's lead citrate for 10 minutes. Data was collected at an acceleration voltage of 120kV on a Tecnai G2 Spirit BioTWIN transmission electron microscope (TEM), equipped with an FEI 4k Eagle CCD camera, in a similar fashion as described above. Virtual slides were acquired with 18,500x magnification at the detector plane, corresponding to a 1.2-nm pixel size at the specimen level. Each recorded glomerulus from representative virtual slides of ctrl ($n = 5$) and has2-cKO ($n = 7$) mice were divided into 4 quadrants from which 2 capillary loops per quadrant were selected for high resolution imaging. Quantification was performed using an automatic grid overlay (ImageJ). Cross-hairs at the intersection of endothelium (>80) were counted and the percentage of coverage with cationic ferritin was determined.

Ultrastructural Large-Scale Virtual Slides

For analysis of detailed morphologic changes in glomeruli of mice at 4-, 8- and 12 weeks after tamoxifen induction virtual slides were recorded using the Tecnai G2 Spirit BioTWIN transmission electron microscope (FEI, Eindhoven, The Netherlands), equipped with an FEI 4k Eagle CCD camera, at an acceleration voltage of 120 kV. To create an overview of the glomerulus, a large amount of 6800x magnification images, corresponding to a 3.2nm pixel size at the specimen level, collected automatically using stitching software (46). Quantification of morphologic changes was performed for ctrl and has2-cKO mice ($n = 3$ each) at 12 weeks after tamoxifen induction in 8 capillary loops per glomerulus, using an automatic grid overlay (in ImageJ). Cross-hairs were introduced in each image and at the intersection with the endothelium (>15) the endothelial cell thickness, basement membrane thickness and podocyte foot process width were measured, essentially as shown previously (44). Percentage fenestrations were calculated from counting fenestrated or non-fenestrated sites at the cross-hairs intersection.

In silico Angiopoietin 1 / hyaluronan prediction model

Angiopoietin 1 (GenBank: AAM92271.1) and Angiopoietin 2 (GenBank: AAI43903.1) amino acid sequences were analyzed using online *PredictProtein* software (www.predictprotein.org/home) and the predicted glycosaminoglycan binding domain within the secondary structure was evaluated against fibrinogen (GenBank: CAA50740.1) and a functional region map was drawn (Figure 1B). 3D structures of Ang1 (target; PDB code 4JYO) and HA (2BVK) from the protein databank (www.rcsb.org/pdb/home) were downloaded and the HA code was transformed to a mol2 format using UCSF *Chimera* software (www.cgl.ucsf.edu/chimera/) for use as ligand in the online *Swissdock* software (www.swissdock.ch/docking), to obtain 3D docking models of the Ang1-HA binding domain, as predicted above. Using the UCSF *Chimera* software, the predicted model with lowest binding energy is shown (Figure 1C).

Angiopoietin 1 / hyaluronan ELISA

Addition of 50 µL of Coating buffer (0.2 M sodium carbonate/bicarbonate pH 9.4) / well (Nunc-Covalink, Thermo-Fisher Scientific) was followed by 40 ng/ml hyaluronan standard (HA Quantikine ELISA kit, DHYALO, R&D Systems) or RD5-18 buffer (DHYALO, R&D Systems) to each well and incubated at room temperature for 2hrs on a horizontal orbital microplate shaker. Wells are washed 5x in between consecutive steps with wash buffer (DHYALO, R&D Systems). Next, recombinant human Ang1 protein (923-AN, R&D Systems) was added and incubated at room temperature for 2hrs on shaker, washed and blocked with Protein Block Serum-Free buffer (X0909, Dako) for 1hr at rT on shaker. Wells are aspirated and 100 µL of 0.2 µg/mL Goat Anti-Human angiopoietin-1 antibody (AF923, R&D Systems) was added, incubated for 1hr at rT on shaker, and washed. Secondary Rabbit Anti-Goat IgG HRP antibody (P0160, Dako) was added and incubated for 1hr at rT on shaker, washed and followed by 100 µL Substrate Solution (color reagent A and color reagent B; DHYALO, R&D Systems) for 30 minutes at rT. Reaction was stopped with Stop Solution (DHYALO, R&D Systems) and absorbance was read at 450 nm within 30 minutes with wavelength correction to 540 nm or 570 nm. Values are given as Δ Absorbance [A450(40 ng/mL HA)- A450(RD5-18 buffer)], of 3-6 separate experiments.

Cell isolation and culture

Primary human glomerular-derived microvascular endothelial cells (hgMVECs) were purchased from Cell Systems (ACBRI-128, Kirkland, WA) and cultured in serum-free endothelial cell medium (EC-SFM, Gibco, Thermo-Fisher Scientific, Waltham, MA) supplemented with 1% bovine platelet poor plasma-derived serum (Biomedical Technologies Inc., Stoughton, MA), 50 µg/mL VEGF-165 (R&D Systems) and 100 µg/mL hFGF (Miltenyi Biotech) (EC-SFM full medium) at 37°C and 5% CO_2.

Human umbilical vein endothelial cells (HUVECs) were freshly isolated, by perfusion and subsequent incubation (20 minutes) of trypsin at 37°C, from different donors as described (47) (with approval of the Medical Ethical Commission of the Leiden University Medical Center, and informed consent from all subjects) and used between passage 1 and 3. Freshly isolated HUVECs were cultured on 0.5% gelatin–coated plastic flasks in endothelial basal medium medium (CC-3121; Lonza, Basel, Switzerland), supplemented with human epidermal growth factor, vascular endothelial growth factor, human fibroblast growth factor-B, R3-IGF-I, ascorbic acid, heparin, and 10% human serum (Lonza, Basel, Switzerland) supplemented with antibiotics/antimycotics (Life technology, Gibco).

Lentiviral transductions

The hyaluronan synthase 2-short-hairpin RNA lentivirus (pLV-CMV-IE.HAS2shRNA) was created through transfecting Hek293 cells (60-80% confluence) with a mixture of combined plasmid DNA of Has2shRNA (Sigma-Aldrich, Mission shRNA library #9868), H1/VSVG and H23/pspax2 with polyethylenimine (PEI, 0.05 mg/mL final concentration) in DMEM (Gibco) to obtain the self-inactivating (SIN) lentiviral construct from supernatant, in principle as described (48). Pri-

mary hgMVECs were cultured to 40-60% confluency in T75 flasks (Greiner bio-one, Alphen a/d Rijn, The Netherlands) in EC-SFM full medium and transduced with pLV-CMV-IE.HAS2shRNA or control (pLV-CMV-IE) in combination with 8 µg/mL polybrene and incubated overnight at 37°C and 5% CO_2. After medium refreshment, the cells were incubated in EC-SFM full medium at 37°C and 5% CO_2, for another 4-6hrs before collecting the cells for experimental assays. For transduction of HUVECs or hgMVECs with the lentiviral expression vectors for $PFKFB3^{OE}$ or shPFKFB3, cells were cultured to 40-60% confluency in T75 flasks in EGM2 medium and transduced with the respective lentivirus (control pLV-CMV-IE) in combination with 8 µg/mL polybrene and incubated overnight at 37°C and 5% CO_2. After medium refreshment, the cells were incubated in EC-SFM full medium at 37°C and 5% CO_2, for another 16hrs before collecting the cells for experimental assays

Creation of Neurocan-dsRed construct

The N-terminus rat neurocan construct of the hyaluronan specific neurocan-eGFP (Ncan-eGFP, gift from J. Kappler) construct (45), linked to the BM 40 signal peptide with APLGRGSHHHHH-HGGLA and a GSSGA linker at the C-terminus, was excised and fused into a pDsRedMonoN1 (ClonTech, Mountain View, CA, USA) plasmid. The modified neurocan-dsRed (Ncan-dsRed) construct was incorporated into a self-inactivating (SIN) lentiviral vector (pLV-CMV-IE.Ncan-dsRed) and transduced into Hek293 cells for production. Ncan-eGFP and Ncan-dsRed were isolated from supernatant and purified on a Ni-NTA resin column using the incorporated 6xHistidine tag within the protein.

In vitro flow experiments

Flow experiments were performed using an ibidi flow system (Ibidi, Martinsried, Germany) and cells were cultured for 4 days at a constant laminar shear stress of 5 dyne/cm^2 in EC-SFM full medium in the presence of 100 ng/mL recombinant ANG1 (R&D Systems). Control hgMVEC (pLV-CMV-IE) or pLV-CMV-IE.HAS2shRNA silenced cells were seeded into closed perfusion chambers (ibiTreat, 0.4 µ-Slide VI Luer) at a concentration of 1.0 x 10^6 cells per mL. Hereafter, the chamber is connected to a computer-controlled air pressure pump and a fluidic unit with a two-ways switching valve which allows pumping of 16 mL cell culture medium from two reservoirs in a unidirectional way through the flow channel over the endothelial cell monolayer. Medium was refreshed after 1 day, non-adhered cells removed, and cultured under laminar flow for another three days at 37°C and 5% CO_2. Next, cells were fixed with 4% PFA and 0.2% Triton-X100 in HBSS for 10 minutes at rT, washed in HBSS containing 1% BSA (A7030), and blocked for 30 minutes at room temperature in 5% BSA in HBSS. Primary monoclonal Mouse Anti-Human VE cadherin (CD144, 55-7H1 BD Biosciences), monoclonal Mouse Anti-Human active β-catenin (anti-ABC, 8E7, Merck Millipore), Goat Anti-Human angiopoietin 1 (R&D Systems), or Ncan-dsRed were incubated overnight (at 4°C), followed by an appropriate secondary antibody and phalloidin-TRITC (VEcadherin, β-catenin samples) for 1 hour, all in blocking buffer. Cells were counterstained with 10µg/mL Hoechst 33528, embedded in Vectashield mounting

medium (Vector Laboratories Inc., Burlingame, CA). Cells were examined using a LEICA TCS SP8 X WLL (Leica, Rijswijk, The Netherlands) with a 40x objective (HC PL APO CS2 40x/1.30 oil, Leica) or LEICA TCS SP5 with a 100x objective (HCX PL APO CS 100x/1.40 oil, Leica). Sequential 16-bit confocal images (xyz dimensions, 0.142×0.142×0.3µm, 0.142×0.142×1µm or 0.116x0.116×1µm) were recorded using LAS-X Image software (Leica) and analyzed with ImageJ, as described earlier (43). Angiopoietin 1 binding was quantified as total fluorescence intensity per cell surface area. Surface hyaluronan expression (Ncan-dsRed) was quantified on 5 cells per field of view (5 views) in essence as described earlier (49). From a side-view, resliced from a line (10pixels wide) over the nucleus 3 additional lines were drawn at the nuclear position and the mean fluorescence was calculated between the distance from half-maximum signal of the nuclear staining to half-maximum signal at the luminal end. Membrane localization of β-catenin was quantified as percentage cell-perimeter coverage. Difference between stable adherence junctions (AJ) and focal adherence junctions (FAJ) upon junction remodeling (50) was quantified as ratio FAJ length over total junction length (51). From each independent experiment (*n = 5*) 25 cells are analyzed.

HUVECs were cultured for 4 days at a constant laminar shear stress of 10 dyne/cm^2 in EGM2 (Lonza) using an ibidi flow system (Ibidi, Martinsried, Germany) in the presence of 10µM 3PO (Calbiochem-Merck, Amsterdam, the Netherlands) or appropriate amount of DMSO for the last 3 days (or cultured statically for 3 days in the presence of 10µM 3PO or appropriate amount of DMSO). Medium was refreshed after 1 day, non-adhered cells removed, and cultured under laminar flow for another three days at 37°C and 5% CO_2. Next, cells were fixed with 4% PFA in HBSS for 10 minutes at rT, washed in HBSS containing 1% BSA, and blocked for 30 minutes at room temperature in 5% BSA in HBSS. Ncan-dsRed was incubated overnight (at 4°C), followed by 10µg/mL Hoechst 33528, embedded in Vectashield mounting medium (Vector Laboratories Inc., Burlingame, CA). Cells were examined using a LEICA TCS SP5 with a 100x objective (HCX PL APO CS 100x/1.40 oil, Leica). Sequential 16-bit confocal images (xyz dimensions, 0.142×0.142×0.3µm, 0.142×0.142×1µm or 0.116x0.116×1µm) were recorded using LAS-X Image software (Leica) and analyzed with ImageJ. From each independent experiment (*n = 4*) 25 cells are analyzed.

Western blot analysis

As described above, hgMVECs cultured 3 days at 5 dyne/cm^2 in EC-SFM full medium in the presence of 100 ng/mL recombinant Ang1 were washed with PBS and lysed in 50mM TRIS HCL buffer (pH 7.5) containing 150mM NaCl, 1% SDS, 0.5% deoxycholate and 0.5% triton X-100. Protein samples were diluted 5x in SDS sample buffer (pH 6.8; 10% SDS, 25% 2-mercaptoethanol, 50% glycerol, 0.01% bromophenol blue, 0.3125 M Tris-HCl, 0.5M DTT), incubated at 95°C for 10 minutes and subjected to SDS-PAGE and western blotting. Proteins, transferred to PVDF membrane (1704156, Bio-Rad Laboratories BV, Veenendaal, The Netherlands) were detected with antibodies against HAS2 (MABC712, Merck Millipore), Phospho-Tie2 (Y992; AF2720-SP, R&D Systems), Pospho-Tie2 (Y1102/Y1100; AF3909, R&D Systems), Tie2 (33,

557039, BD Biosciences), phospho-Akt (S473; P31749, Cell Signaling Technologies, Danvers, MA), Akt (C67E7; 4691, Cell Signaling) and GAPDH (NB300-221SS, Novus Biologicals) after blocking the membrane with 5% fat-free milk in PBS and 0.1% Tween-20. Followed by incubation with a secondary HRP-conjugated antibody and Pierce ECL Western Blotting substrate (32106, Thermo Scientific). Band intensity was analyzed using ImageJ software.

Metabolic assays

For intracellular NMR profiling, as published in detail(52), HUVECs were cultured in EGM2 medium, transduced with *Pfkfb3*^{OE}*, shPfkfb3* or respective mock controls and cultured for another 16hrs are transferred to 10cm dishes and kept further for another 3 days in culture until cell numbers reached about 5million per dish. Sample preparation was started by removing culture medium followed by quick rinsing with warm PBS (~5 mL, 37 ˚C) to remove residual culture medium. Both the removal of medium and washing with PBS occurred in less than 5s to avoid turnover of labile intracellular metabolites. Subsequently, cells were quenched with ~10 ml liquid nitrogen (LN_2) and plates were placed on dry-ice while the whole process was repeated for all samples. Prior to removal of the culture medium, an aliquot of 0.3 mL was collected and immediately mixed with 0.6 mL cold methanol (-80˚C, 100% LC-grade) and stored a -80 ˚C. This treatment ensures to remove by precipitation the proteins present in the medium.

Extraction of intracellular metabolites was performed in a cold room (4˚C) using 1.5 mL of methanol/chloroform/water, 8.1:0.9:1 (v/v/v) solution per plate. The extraction solution was kept cold on dry-ice throughout the whole procedure. The cells were scraped from the plates and transferred to 2mL micro-centrifuge tubes together with the extraction solvents and centrifuged at 16,000 × g for 15 min at 4 ˚C. The supernatants were collected, dried with nitrogen airflow and stored at -80˚C. The dried material was reconstituted with 0.25 mL of 150 mM K_2PO_4 buffer solution (pH = 7.4) in deuterated water (D2O; Cortecnet, France). The buffer solution included also 2 mM NaN_3 to prevent bacteria contamination of the samples during storage and analysis and 0.02 mM of TSP-*d4* (3-trimethylsilyl-propionate-d4 salt; Cambridge Isotope Laboratories Inc., UK) as a concentration and NMR chemical shift internal standard. Each extract-buffer mixture was vortexed for 10 s and 165 µL were transferred to 3 mm NMR tubes (Bruker Biospin Ltd., Germany) using a 215 Gilson robotic liquid handler. 30 µL from each sample leftovers were pooled and stored at -80˚C as aliquots of 180 µL. These pooled samples were used for 2D NMR spectroscopy and assignment of metabolites. NMR data were recorded using a Bruker 14.1 T AVANCE II spectrometer for 1H 600 MHz, equipped with a cryoprobe (TCI) and a SampleJet system (Bruker Biospin ltd.). The latter is equipped with cooling positions to accommodate 5 × 96-tube racks so that all samples are kept at a stable temperature of 4 ˚C while in que for analysis. The same automation routine was followed for all samples and included the placement for 5 min in the probe to adopt a stable temperature at 27 °C, tuning, matching, lock to the frequency of deuterium, shimming and 90˚ pulse calibration followed by the acquisition of a 1D ^{1}H NOESY and a 2D J-resolved (Jres) experiments. The 1D NOESY (doi:10.1002/cmr.a.20223) experiment (noesygppr1d experiment in Topspin 3.0 library;

Bruker Biospin Ltd.) uses the first increment of the 2D NOESY pulse sequence and it was used for metabolites quantification. 512 scans were recorded for each sample with 65536 points over a 20 ppm (12335 Hz) spectral width. Residual water signal was suppressed by a 50 Hz continuous wave soft pulse during the relaxation delay of 4 s and the mixing time of 10 ms. The collected data was 2-fold zero-filled, Fourier transformed, phased and referenced to the internal standard (TSP) chemical shift at 0.0 ppm. 2D Jres (http://dx.doi.org/10.1063/1.431994) were collected for the assignment of metabolites. The spectral width was set to 16.66 ppm (12288 Hz) for the direct dimension and 78 Hz for the indirect one and 4 scans were acquired over 40 increments. The free induction decays (FIDs) were automatically processed with Fourier transformation and calibrated using the TSP-*d4* signal at 0.0 ppm in the F2 dimension and at 0.0 Hz in the F1 dimension. A set of 2D NMR spectra were recorded for the pooled samples to be used for assignment of resonances. The set of 2D experiments included ^{1}H-^{1}H correlation spectroscopy (COSY), total correlation spectroscopy (TOCSY) and ^{1}H-^{13}C heteronuclear single quantum correlation (HSQC) using the standard parameters implemented in Topspin 3.0 (Bruker Biospin Ltd.). Identification of metabolites was performed by search of the total 1D and 2D Jres data using the Biorefcode database (Bruker Biospin Ltd.) and ChenomX NMR suite 8.1 (Chenonx Inc. Canada). The ID of the annotated resonances were further verified by the collected 2D NMR data. In cases of ambiguous annotation, spiking experiments of reference samples were performed to confirm the metabolites ID. Spiked compounds included UDP-glucose, UDP-glucuronic acid, UDP-N-acetyl-glucosamine. Quantification of the identified metabolites was performed with the ChenomX NMR suite 8.1 software. Concentrations were extracted using the known TSP-*d4* concentration (0.017 mM) and corrected to sample protein concentration. The exact concentration of the internal standard used for quantification was calculated by the ERETIC2 method implemented in Topspin 3.0 (Bruker Biospin Ltd.).

To measure endothelial glycolytic flux, HUVECs were seeded overnight at $6x10^4$ cells per well on fibronectin (Sigma) coated Seahorse XF96 polystyrene tissue culture plates (Seahorse Bioscience). The plate was incubated in unbuffered DMEM assay medium (Sigma) for 1 hour in a non-CO_2 incubator at 37°C before measuring in an XFe 96 extracellular flux analyzer (Seahorse Bioscience). Both OCR (oxygen consumption rate, data not shown) and extracellular acidification rate (ECAR) were measured over 4 min periods with a mixing of 2 min in each cycle, with five cycles in total. Inhibitors and activators were used at the following concentrations: Glucose (10mM), Oligomycin (3µM), 2-DG (100mM), FCCP (1µM), Antimycin A (1.5µM) and Rotenone (3µM). Cellular protein content was determined with a BCA-protein kit from Pierce (Thermo-Fischer Scientific) and the data is represented as ECAR normalized to protein. Each measurement was averaged from triplicate wells.

Statistical analysis

Results are presented as mean ± s.d. or mean ± s.e.m., n defines the number of biological replicates. Differences between groups were assessed by non-paired 2-tailed Student's t test, paired 2-tailed Student's t test or, when not normally distributed, by two-tailed F-test. Difference in

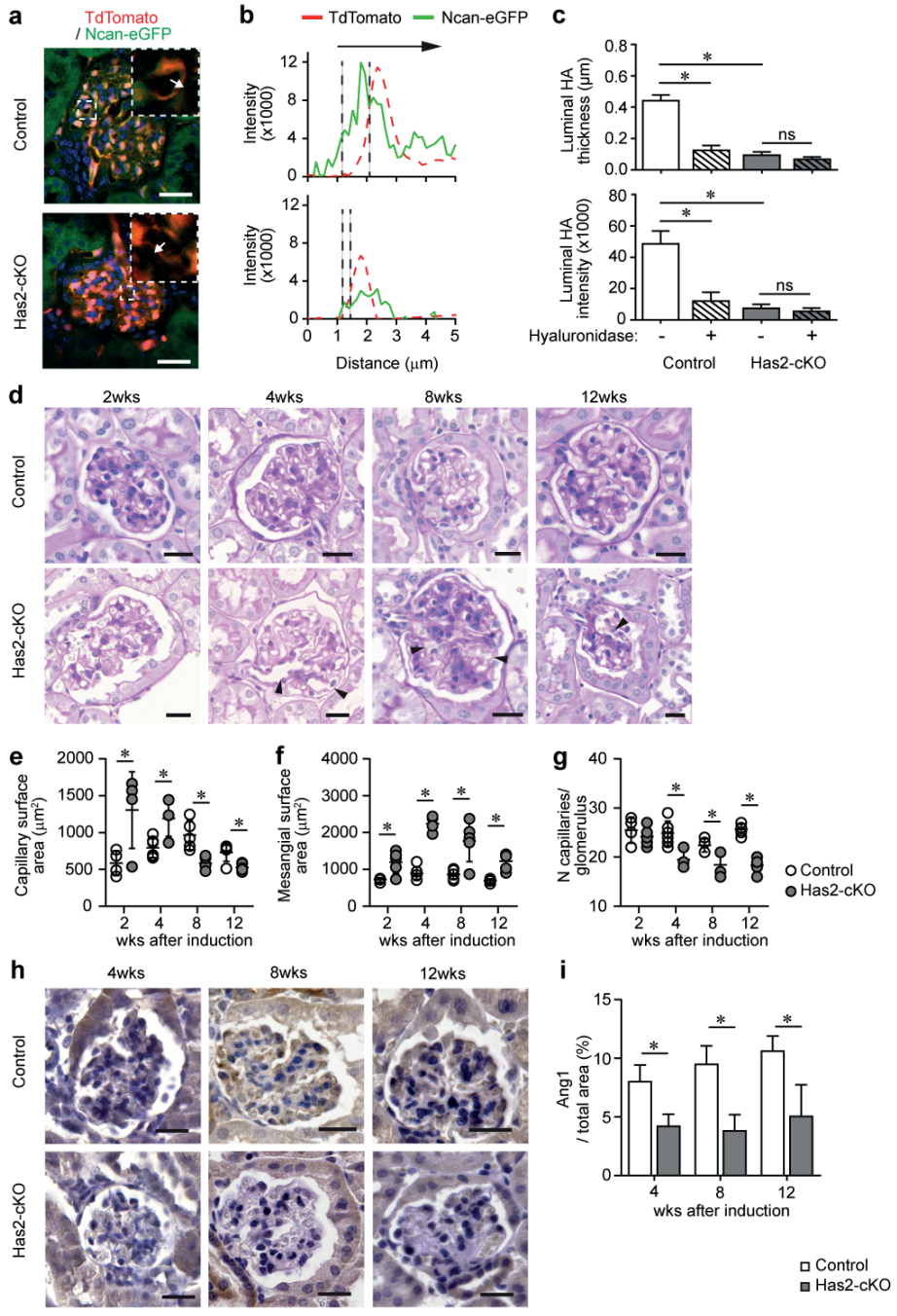

a
TdTomato
/ Ncan-eGFP
Control
Has2-cKO
b
TdTomato
Ncan-eGFP
Intensity (x1000)
Distance (μm)
c
Luminal HA thickness (μm)
Luminal HA intensity (x1000)
ns
Hyaluronidase:
Control
Has2-cKO
d
2wks
4wks
8wks
12wks
e
Capillary surface area (μm²)
wks after induction
f
Mesangial surface area (μm²)
g
N capillaries/ glomerulus
Control
Has2-cKO
h
i
Ang1 / total area (%)

Figure 1. Loss of endothelial hyaluronan results in progressive glomerulopathy and reduced Ang1 expression. To eliminate endothelial surface HA expression in adult mice, the *has2* gene was selectively deleted in mice carrying both floxed has2 alleles and the endothelial specific VE-cadherin tamoxifen-inducible Cre-recombinase (has2-cKO). **(a)** Representative cross-sectional confocal images of glomerular tissue sections, 4 weeks after tamoxifen induction. Sections were stained with the HA binding probe Ncan-eGFP (green), while successfully recombined endothelial cells are labelled with TdTomato (red). Has2-cKO mice show loss of the endothelial HA layer. Insets show examples of measurement lines. **(b)** Fluorescence intensity plots demonstrate intraluminal (green, left) and subendothelial (green, right) localization of HA in relation to the endothelial cell membrane position (red, dotted lines). **(c)** Intraluminal HA thickness and intensity was significantly lower when compared to control mice and was found to be comparable to levels after hyaluronidase treatment (*n = 3/group*). **(d)** Representative images of periodic acid Schiff's (PAS) stained glomeruli of control (upper panels) and has2-cKO (lower panels) mice at 2-, 4-, 8- and 12 weeks after tamoxifen induction. Arrowheads indicate diffuse widening of capillary loops through mesangiolysis (ballooning). Increased glomerular capillary surface area from week 2 onwards **(e),** while at this early stage, glomerular hypertrophy was the most prominent change in has2-cKO glomeruli, accompanied by induction of matrix expansion **(f)**, and developed in capillary rarefaction from week 4 onwards **(g)**. 2- (*n = 4-, 5/group*), 4- (*n = 6-, 4/group*), 8- (*n = 5/group*) and 12wks (*n = 5/group*). **(h)** Representative images of glomerular angiopoietin-1 (Ang1) presence at 4-, 8- and 12 weeks after tamoxifen induction in control (upper panels) and has2-cKO (lower panels) mice. **(i)** Quantification of glomerular Ang1 (*n = 5/group*). Scale bars 30µm (a), 20µm (d,h). Values are given as mean ± SEM (c,i) or mean ± s.d. (e-g). Differences between control (white) and has2-cKO (grey) mice were assessed by non-paired 2-tailed Student's *t* test (c,i) or, when not normally distributed, by two-tailed F-test (e-g); *P < 0.05.

Ang 1/HA binding between groups was assessed by ANOVA. In case, staining intensities were scored on a 0 to 10 scale, differences between groups were determined by 1-tailed Mann-Whitney U-test. P values < 0.05 were considered statistically significant.

Results

Loss of endothelial glycocalyx hyaluronan synthesis *in vivo* leads to glomerulopathy, retinopathy and cardiomyopathy

To determine the effects of reduced HA expression by ECs *in vivo*, we inactivated the HA synthesizing enzyme hyaluronan synthase 2 (*has2*) gene selectively in endothelial cells (ECs) in adult mice carrying both floxed *has2* alleles, and the endothelial specific *cdh5* tamoxifen-inducible Cre-recombinase with a TdTomato reporter to control for recombination efficacy (Supplementary Fig. 1a,b). Four weeks after tamoxifen, luminal HA was ~80% reduced from the endothelial surface in glomeruli of *has2*-cKO mice, while the specific HA binding probe Ncan-eGFP still showed the presence of intraluminal HA within the glomerular capillaries of control mice (Fig. 1a-c, Supplementary Fig. 1c,d; hyaluronidase control). Cationic ferritin coverage, that marks glycocalyx coverage, was reduced to 38 ± 15% in *has2*-cKO mice as compared to 79 ± 10% in control mice (Supplementary Fig. 1e,f). This indicates substantial loss of the glycocalyx structure, even though lectin binding of LEA-FITC still demonstrated preservation of other glycocalyx constituents on the endothelial surface (Supplementary Fig. 1g,h). Loss of glycocalyx was predominant on the endothelial surface but could also be noticed in the subendothelial space (Fig. 1b and Supplementary Fig. 1f).

Analysis of kidneys from *has2*-cKO mice revealed that endothelial loss of HA resulted in vascular destabilization, characterized by capillary ballooning, mesangiolysis and loss of endothelial fenestrations (Fig. 1d-g, Supplementary Fig. 2a-d and Supplementary Table 1). Over the observation period of 12 weeks, this led to capillary rarefaction and severe glomerular injury that included secondary podocyte effacement, loss of nephrin and synaptopodin expression (markers of podocyte health), and parietal epithelial cells that attached to denuded basement membrane where podocytes had disappeared, thus initiating focal segmental glomerulosclerotic lesions (Supplementary Fig. 2d-f and Supplementary Table 1). Albuminuria occurred secondary to changes in glomerular capillary structure (Fig. 1e and Supplementary Fig. 1i). These focal segmental glomerulosclerotic lesions highly resemble the kidney lesions observed in human patients (53,54). A causal role for glycocalyx production and the prominent importance of the glycocalyx layer to maintain vascular stability and homeostasis and prevent severe disease have not been documented previously.

We next studied the microvasculature in other organs, first focusing on the adult retina, a vascular bed where Ang1/Tie2 signaling has been shown to regulate blood vessel stabilization and functions (30,31). Typical vaso-regression was found within the deep retinal capillary plexus, resulting in reduced vascular density and branching (Supplementary Fig. 3a,b). We further tested whether endothelial deletion of HA affected the cardiac microvasculature. With loss of endothelial HA, capillary rarefaction developed in the left ventricle wall (Fig. 2a,b). Even though overall myocardial function (ejection fraction) and blood pressure were not altered during the experimental period (Supplementary Fig. 3c,d), myocardial contractility, as measured by aortic peak flow, was reduced (Fig. 2c,d). Likely as a result to compensate for the impaired contractility, there was an increase in ventricular mass (Fig. 2e) and the left ventricle myocyte cross-sectional area from 4 weeks on in *has2*-cKO mice (Supplementary Fig. 3e), though without visible myocardial interstitial fibrosis (Supplementary Fig. 3f). The phenomenon of capillary regression in the myocardium has been linked to future development of ischemic cardiomyopathy (55).

Angiopoietin 1 binds to endothelial HA and stabilizes the endothelial layer

Since (i) Ang1 promotes vascular stabilization (28,29), (ii) Ang1 is sequestered to chemically crosslinked HA hydrogels (34), and (iii) Ang1 requires extracellular matrix (ECM) binding to signal to its receptor (32), we explored whether HA in the glycocalyx may act as a mediator in confining Ang1 to the cell surface and induce endothelial stabilization. To investigate whether a direct link exists between HA and Ang1, we first looked at the secondary structure prediction of the fibrinogen-like domain of Ang1 (Fig. 3a,b). Prediction evaluation revealed potential binding motifs for HA through a lectin-like fold termed the Link module that has been previously shown to mediate the binding of fibrinogen to HA (56). This binding motif was different in angiopoietin 2 (Fig. 3b). In a 3D docking model, HA was predicted to bind to this domain with a free binding energy ΔG of -12.49 kcal/mol, a value similar to that of the binding of HA to its

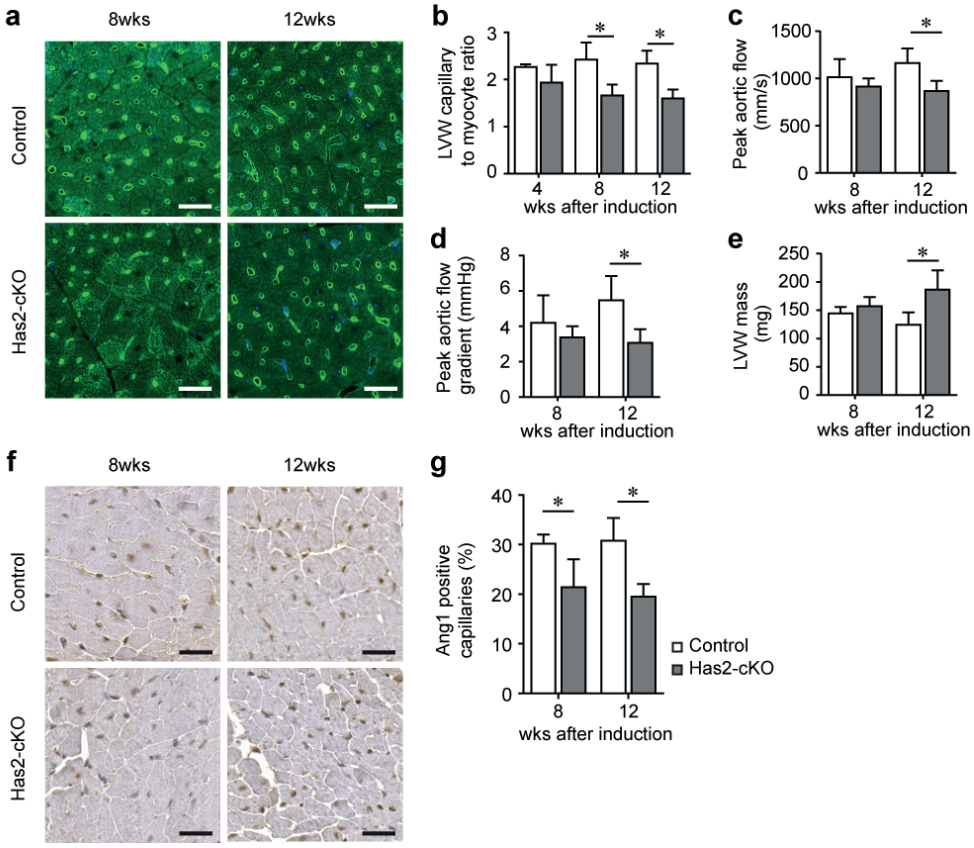


Figure 2. Loss of endothelial hyaluronan induces capillary loss in heart. (a) Representative images depicting capillary rarefaction developed in response to loss of endothelial hyaluronan expression in the myocardium as exemplified by *Griffonia simplicifolia* (isolectin BS-1) lectin left ventricle wall (LVW) staining for determination of capillary density. **(b)** Quantification of LVW capillary to myocyte ratio density at 4- (*n = 6-, 3/group*), 8- (*n = 5/group*) and 12wks (*n = 5/group*) after tamoxifen induction (*n = 5-6/group*). Further M- mode Doppler echocardiography, and ascending aortic pulse wave-Doppler flow measurements demonstrate reduced myocardial contractility as measured by a significant lower **(c)** peak aortic flow and **(d)** peak aortic flow gradient 12 weeks after tamoxifen induction, accompanied by an increased **(e)** left ventricular mass, accompanied gradient (n = 5-6/group). **(f)** representative myocardial angiopoietin-1 (Ang1) presence at 8- and 12 weeks after tamoxifen induction in control (upper panels) and has2-cKO (lower panels) mice. **(g)** In concordance with observations in the glomerular tufts, was significantly reduced.

Scale bars, 20μm (a and f). All values are given in mean ± s.e.m. and differences between control (white) and has2-cKO (grey) mice were assessed by non-paired 2-tailed Student's *t* test; *P < 0.05.

primary cell surface receptor CD44 (Fig. 3b,c and Supplementary Fig. 4a) (57). In agreement, we confirmed Ang1 binding to HA in an ELISA assay (Fig. 3d).

To further corroborate the requirement of endothelial HA as a binding molecule for Ang1 for vascular stabilization, we cultured glomerular ECs exposed to laminar flow, in the presence of Ang1, and silenced HAS2 with a lentiviral shRNA construct, which resulted in a ~64% reduction of HAS2 protein and over 95% reduction of surface HA (Fig. 4a,b and Supplementary

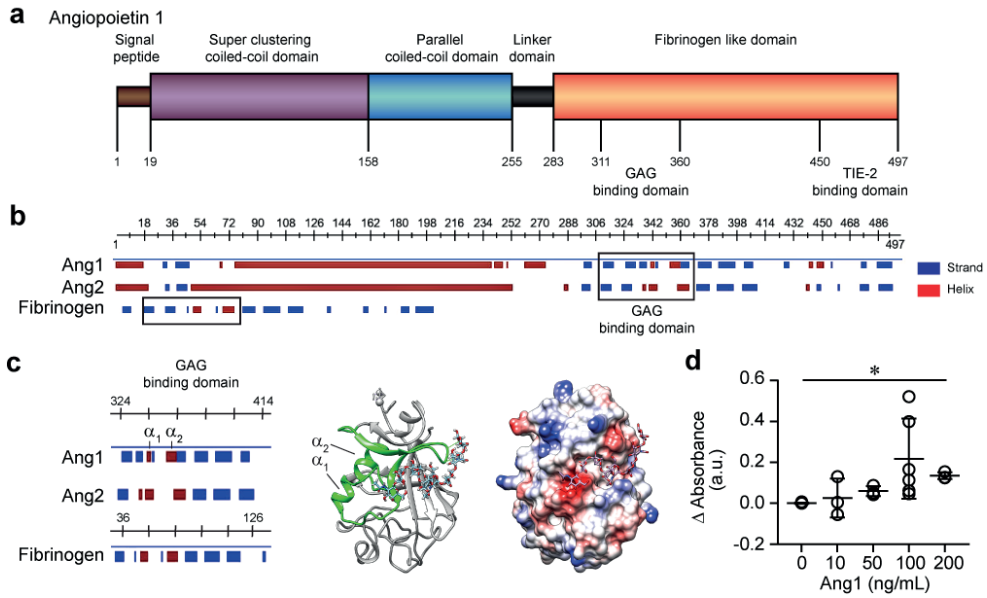


Figure 3. Hyaluronan binds angiopoietin 1. (a) Structural characteristics of angiopoietin 1 (Ang1) reveal, besides the super clustering coiled-coil domain (purple) and parallel coiled-coil domain (blue), allowing Ang1 to form clusters, a possible glycosaminoglycan (GAG) binding domain within the n-terminal fibrinogen like domain (orange) neighboring the Tie2 binding site. **(b)** In contrast to the predicted GAG binding domain (right box) of angiopoietin 2 (Ang2), the Ang1 GAG binding domain resembles the hyaluronan binding domain of fibrinogen (left box). **(c)** Like the predicted hyaluronan binding Link module superfamily, the Ang1 GAG binding domain contains two α-helices separated by an anti-parallel β strand (Left panel). The 3D ribbon configuration of the fibrinogen-like domain of Ang1 shows the position of the two α-helices in relation to the proposed HA binding domain (middle panel), while the electrostatic surface projection of the 3D crystallographic structure reveals the position of negative- (red), neutral- (white) and positive (blue) charged sites within the HA binding domain (right panel). **(d)** Direct binding of recombinant human Ang1 to hyaluronan is shown as the difference between absorbance of Ang1 bound to surface coated HA and absorbance of Ang1 binding to the surface in presence of buffer alone (Δ Absorbance) of 6 separate experiments. Difference in Ang1 binding was assessed using ANOVA; *P < 0.05.

Fig. 4b). At the endothelial surface, a significantly reduced presence of Ang1 was observed (Fig. 4c,d, left panels), especially at cell-cell contacts (Fig. 4d, left upper panel; arrow). This was associated with reduced membrane localization of active β-catenin (Fig. 4d, middle panels and 4e), which is required for the linkage between adherence junctions and the actin cytoskeleton. In agreement, more unstable focal adhesion junctions were observed (Fig. 4d, right panels and 4f). Finally, loss of Ang1 binding resulted in reduced activation of its receptor Tie2 and downstream Akt signaling molecules (Fig. 4g-i, Supplementary Fig. 4c,d). We also confirmed *in vivo* that endothelial loss of *has2* resulted in a ~50% reduction in Ang1 binding to the glomerular endothelium in association with glomerular injury and capillary rarefaction (Fig. 1h,i). Loss of myocardial capillaries was also accompanied by reduced Ang1 expression (Fig. 2f,g).

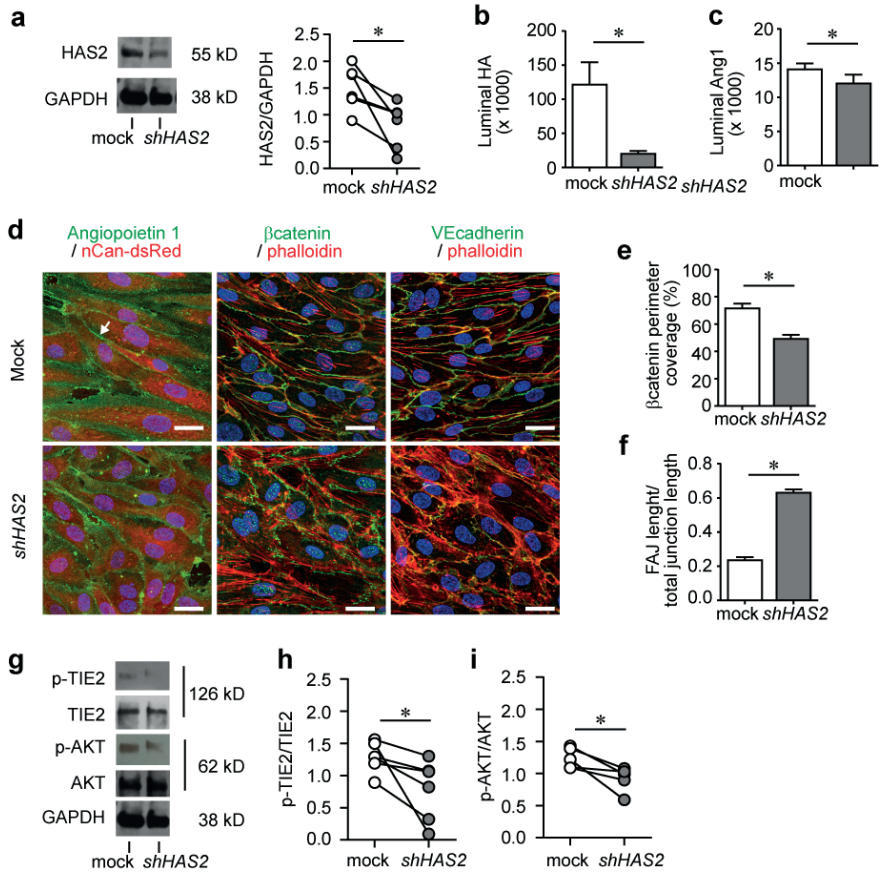


Figure 4. Hyaluronan angiopoietin 1 clustering stabilizes the endothelial layer. (a) Primary human glomerular-derived microvascular endothelial cells (hgMVEC), transduced with an empty- (mock) or a HAS2-shRNA containing lenti-viral construct (HAS2 shRNA), exposed to a laminar shear stress of 5 dyne/cm^2 for 3 days in the presence of 100ng/mL recombinant human Ang1 reveals that silencing of HAS2 results in **(b)** reduced HA expression and **(c)** Ang1 binding (*n = 5/group*). **(d)** Representative cross-sectional confocal images (left panels) stained for HA (red) and Ang1 (green) revealed that especially at cell - cell contact areas (arrow) Ang1 presence is reduced, which is accompanied with reduced (middle panels) membrane bound active β-catenin (anti-ABC, green) and increased (right panels) unstable focal adhesion junctions (FAJ) as visualized by VE-cadherin (CD144, green) staining. Both in combination with fluorescent-labeled phallotoxin (phalloidin-TRITC, red) to visualize intracellular F-actin and Hoechst 33258 (blue) nuclear stain. Quantification of **(e)** membrane bound β-catenin and **(f)** adherence junction remodeling as the ratio of unstable focal adherence junction (FAJ) length over total adherence junction (AJ) length in mock treated cells and after silencing of HAS2 expression (*n = 5/group*). **(g)** Representative immunoblotting and quantification of **(h)** p-Tie2(Y992) over Tie2 expression and the downstream signaling **(i)** Akt activation. Scale bars 20μm (a). Values are given as mean ± s.e.m. (b,c,e,f) or individual data points (a,h,i). Differences between control (white) and HAS2-shRNA (grey) treated cells were assessed by paired 2-tailed Student's *t*-test; *P < 0.05.

Endothelial HA synthesis is dependent on glycolytic PFKFB3 activity

Endothelial expression of Krüppel-Like Factor 2 (KLF2) and its inhibitory effect on the glycolytic activator phosphofructokinase-2/fructose-2,6-bisphosphatase-3 (PFKFB3), have been shown to be important regulators of endothelial quiescence and vessel stabilization (58). Further, HA

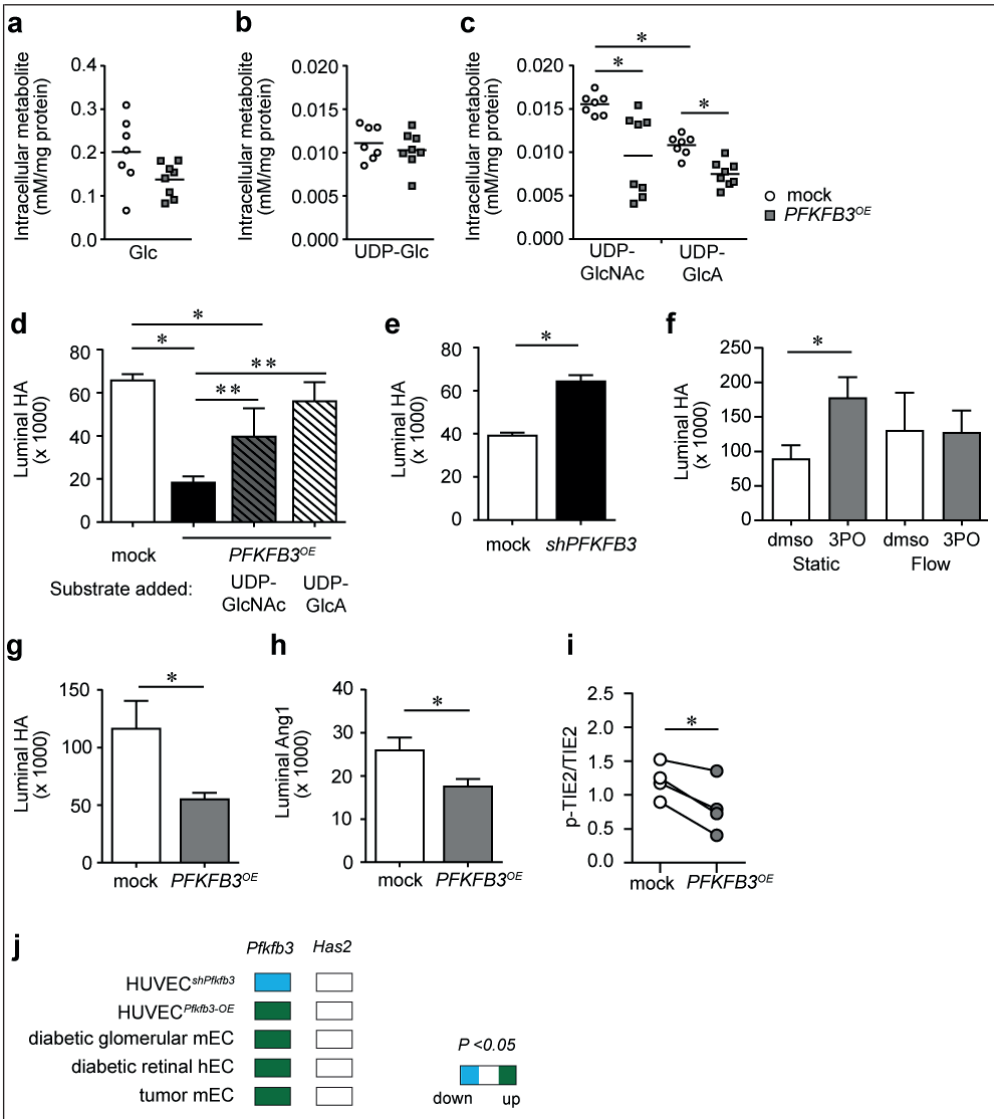

a
b
c
Intracellular metabolite (mM/mg protein)
Glc
UDP-Glc
UDP-GlcNAc
UDP-GlcA
mock
PFKFB3OE
d
e
f
Luminal HA (x 1000)
mock
PFKFB3OE
Substrate added:
UDP-GlcNAc
UDP-GlcA
shPFKFB3
dmso
3PO
Static
Flow
g
h
i
Luminal Ang1 (x 1000)
p-TIE2/TIE2
j
Pfkfb3
Has2
HUVECshPfkfb3
HUVECPfkfb3-OE
diabetic glomerular mEC
diabetic retinal hEC
tumor mEC
P <0.05
down
up

Figure 5. Elevated endothelial glycolysis results in reduced hyaluronan biosynthesis. Without changes in intracellular **(a)** glucose (Glc) and **(b)** the glucose metabolite UDP-Glc, overexpressing the glycolytic activator PFKFB3 (PFKFB3^{OE}) in HUVEC results in reduced availability of **(c)** both HA synthesis substrates UDP-GlcNAc and UDP-GlcA ($n = 8$). **(d)** Luminal hyaluronan (HA) presence on PFKFB3^{OE}-HUVECS and after addition of exogenous substrates UDP-GlcNAc or UDP-GlcA ($n = 4$), or **(e)** after silencing the glycolytic activator with a sh-PFKFB3 lentiviral construct ($n = 4$). **(f)** Luminal HA on cells treated with the pharmacological PFKFB3 inhibitor 3PO, cultured statically or exposed to a laminar shear stress dyne/cm^2 for 3 days ($n = 4$). Primary human glomerular-derived microvascular endothelial cells (hgMVEC), transduced with an empty- (mock) or a PFKFB3^{OE} lenti-viral construct, exposed to a laminar shear stress of 5 dyne/cm^2 for 3 days in the presence of 100ng/mL recombinant human Ang1 reveals a reduced luminal **(g)** hyaluronan and **(h)** angiopoietin1 (Ang1) presence that was accompanied with reduced Tie2 activation as shown **(i)** by quantification of p-Tie2(Y1102) over Tie2 expression. **(j)** Comparison of PFKFB3 and HAS2 gene expression in HUVECS silenced for PFKFB3 or PFKFB3 overexpression, diabetic murine glomerular EC and diabetic human retinal EC, and mouse liver tumor EC, compared to mock control, non-diabetic- and non-tumor endothelial cells. Differences are shown as significant ($P < 0.05$) reduction (blue) or increase (green), while white is given for non-significant changes. Values are given as mean ± s.d. (a-h) or individual data points (i). Differences between control (white) and PFKFB3^{OE} (grey) treated cells were assessed by paired 2-tailed Student's *t*-test; *P < 0.05.

synthesis requires the substrates UDP-GlcA and UDP-GlcNAc, produced from the glycolytic intermediate glucose-6-phosphate. Hence, we hypothesized that a high glycolysis flux in ECs can shift glucose-6-phosphate away from the metabolic pathways that produce UDP-GlcA and UDP-GlcNAc. Because of these reasons, we tested whether changes in endothelial metabolism affected HA biosynthesis.

First, static cultured ECs that overexpress the glycolytic activator PFKFB3 (PFKFB3^{OE}) show elevated *PFKFB3* mRNA expression, without however affecting HAS2 protein levels (Supplementary Fig. 5a-c). Conversely, silencing PFKFB3 (shPFKFB3) significantly reduced *PFKFB3* mRNA levels, also without changing total HAS2 protein levels (Supplementary Fig. 5d-f). Inducing the glycolytic pathway through PFKFB3^{OE} elevated the levels of the glycolytic end-product lactate (Supplementary Fig. 5g,h) and reduced levels of extracellular glucose, indicating enhanced glucose consumption (Supplementary Fig. 5i). Measuring the extracellular acidification rate (ECAR), as an indicator of lactate production, showed increased glucose-induced glycolysis and maximal glycolytic capacity (defined as ECAR induced by the mitochondrial respiration blocker oligomycin to force the cells to rely more on glycolysis) upon overexpression of PFKFB3 in ECs (Supplementary Fig. 5j,k).

Activation of glycolysis slightly reduced intracellular glucose (Glc), without changing the levels of the intermediate UDP-Glc, while both HA synthesis substrates UDP-GlcNAc and UDP-GlcA were reduced significantly (Fig. 5a-c). Furthermore, these high glycolytic ECs expressed less HA at their luminal side, which could be rescued by supplementing the HA substrates UDP-GlcNAc and UDP-GlcA (Fig. 5d). Reduction of the glycolytic rate in ECs in turn increased HA expression (Fig. 5e), which could also be achieved upon addition of the pharmacologic PFKFB3 inhibitor 3PO (Fig. 5f).

Notably, however, the increase in HA expression upon 3PO treatment was only observed in ECs in a static culture, and was no longer detected when ECs were exposed to laminar shear stress (10 dyne/cm^2) for a prolonged time (Fig. 5f). This is likely due to the finding that prolonged

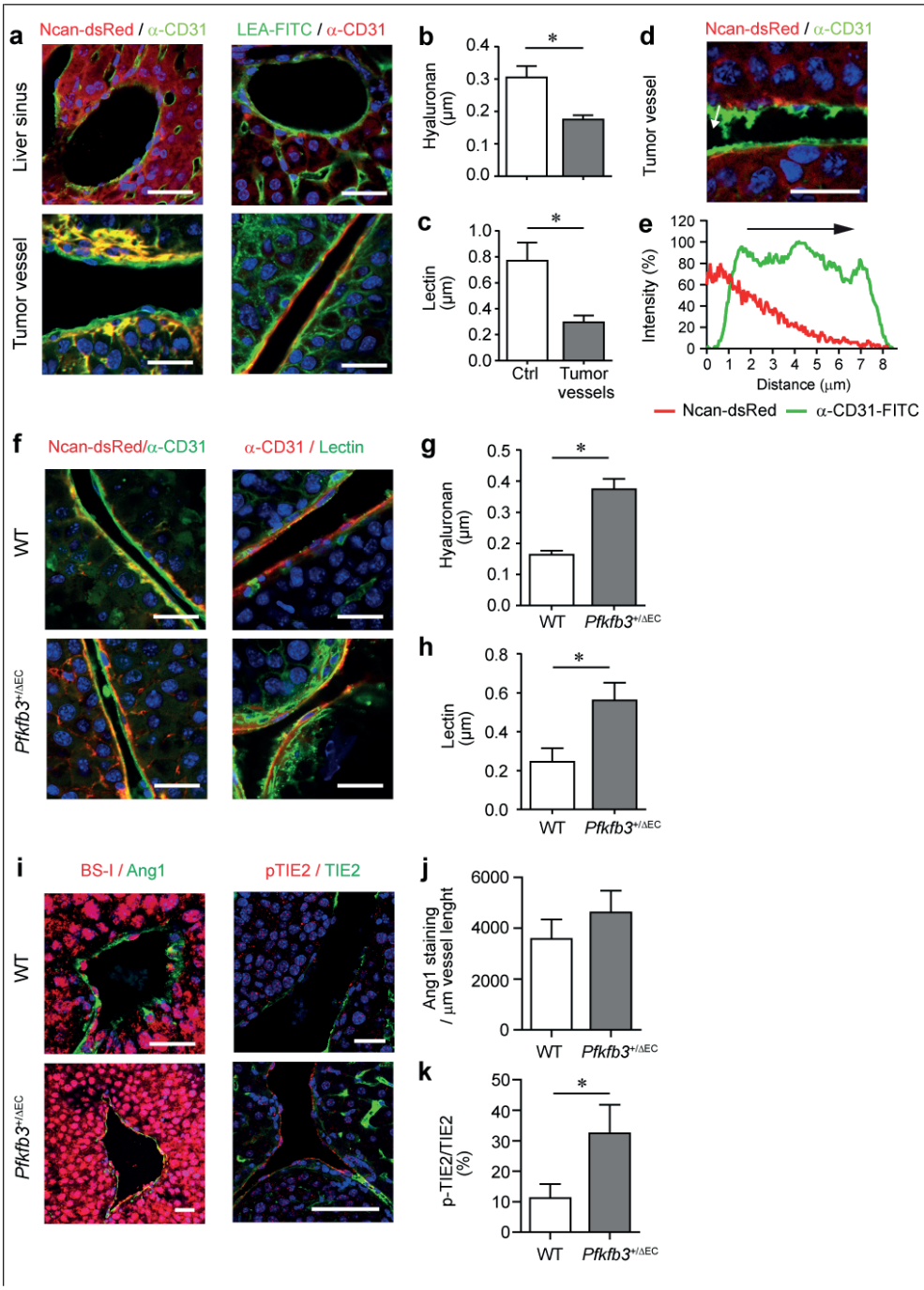

a
Ncan-dsRed / α-CD31
LEA-FITC / α-CD31
Liver sinus
Tumor vessel
b
Hyaluronan (μm)
0.4
0.3
0.2
0.1
0.0
*
c
Lectin (μm)
1.0
0.8
0.6
0.4
0.2
0.0
*
Ctrl
Tumor vessels
d
Ncan-dsRed / α-CD31
Tumor vessel
e
Intensity (%)
120
100
80
60
40
20
0
0 1 2 3 4 5 6 7 8
Distance (μm)
Ncan-dsRed
α-CD31-FITC
f
Ncan-dsRed/α-CD31
α-CD31 / Lectin
WT
Pfkfb3+/ΔEC
g
Hyaluronan (μm)
0.5
0.4
0.3
0.2
0.1
0.0
*
WT
Pfkfb3+/ΔEC
h
Lectin (μm)
0.8
0.6
0.4
0.2
0.0
*
WT
Pfkfb3+/ΔEC
i
BS-I / Ang1
pTIE2 / TIE2
WT
Pfkfb3+/ΔEC
j
Ang1 staining / μm vessel lenght
6000
4000
2000
0
WT
Pfkfb3+/ΔEC
k
p-TIE2/TIE2 (%)
50
40
30
20
10
0
*
WT
Pfkfb3+/ΔEC

Figure 6. Endothelial glycolytic activation reduces endothelial HA coverage in vivo and is associated with vessel destabilization and reduced Tie2 activation. (a) Representative confocal images of liver tissue (upper panel) adjacent to metastatic tissue of B16-F10 melanoma cancer cells (lower panel) stained for the luminal glycocalyx with the hyaluronan binding probe Ncan-dsRed (red) or the lectin *Lycopersicon esculentum* (LEA-FITC, green) and antibodies against CD31 for endothelial localization. Quantification of endothelial **(b)** luminal HA or **(c)** lectin expression in liver tissue (ctrl) and liver B16-F10 melanoma metastatic capillaries (*n = 3-6/group*). **(d)** Detailed confocal image of a tumor vessel stained for hyaluronan (Ncan-dsRed, red), endothelial cells (CD31, green) and annotated with an arrow of which the luminal distribution of hyaluronan is shown throughout the intraluminal tip of the angiogenic endothelial cell as displayed in **(e)** the fluorescence intensity line plot of endothelial (CD31, green) and hyaluronan (Ncan-dsRed, red) distribution. **(f)** Representative confocal images of B16-F10 melanoma metastatic capillaries in WT (upper panels) or in *Pfkfb3*$^{+/\Delta EC}$ (lower panel) mice in which endothelial glycolysis rate is genetically reduced. Tissues are stained for the luminal glycocalyx with the hyaluronan binding probe Ncan-dsRed (red) or the lectin *Lycopersicon esculentum* (LEA-FITC, green) and antibodies against CD31 for endothelial localization. Quantification of endothelial **(g)** luminal HA or **(h)** lectin expression in tumor vessels of WT and *Pfkfb3*$^{+/\Delta EC}$ mice (*n = 3-6/group*). **(i)** Representative confocal images of B16-F10 melanoma metastatic capillaries in WT or in *Pfkfb3*$^{+/\Delta EC}$ mice stained for the endothelial angiopoietin 1 (Ang1, green) and the *Griffonia simplicifolia* (isolectin BS-1, red) lectin for endothelial localization (left panels), or for endothelial bound p-Tie2(Y1102, red) and Tie2 (green) presence. **(j)** Quantification of endothelial luminal Ang1 expression in tumor vessels of WT and *Pfkfb3*$^{+/\Delta EC}$ mice (*n = 4-5/group*) or **(k)** ratio of endothelial p-Tie2 over Tie2 staining. Scale bars 30µm (a, d, f and i). Values are given as mean ± s.d. and differences between non-tumor liver sinus (white) and tumor vessels (grey) or WT (white) and *Pfkfb3*$^{+/\Delta EC}$ (grey) mice were assessed by paired 2-tailed Student's *t*-test; *P < 0.05.

shear elevates the expression of KLF2 while lowering the levels of PFKFB3 (58), a finding that we confirmed in our experimental conditions (data not shown). We therefore overexpressed PFKFB3 (PFKFB3^{OE}) in primary microvascular endothelial cells (hgMVECs) cultured under flow to elevate PFKFB3 levels again. PFKFB3^{OE} in these cells, cultured in the presence of Ang1, not only decreased luminal HA expression, but also reduced the luminal presence of Ang1 (Fig. 5g,h). As a result, activation of its receptor Tie-2 was reduced (Fig. 5i and Supplementary Fig. 5l).

Disease conditions associated with elevated PFKFB3 expression in ECs and glycocalyx loss

To evaluate whether disease conditions, known to be characterized by endothelial glycocalyx compromise / loss, were also associated with elevated PFKFB3 expression in ECs, we analyzed published transcriptomic data. Tumor ECs are known to have a damaged glycocalyx layer (3,59) (see also below). In accordance with the above findings, tumor ECs have elevated PFKFKB3 expression levels (Fig. 5j) (9). The glycocalyx layer is also reduced in diabetes (4,5,8,49). Of note, interrogating two independent gene expression profiling datasets of diabetic mouse primary glomerular ECs (60) and diabetic human retinal ECs (61) also revealed elevated PFKFB3 levels. HAS2 gene expression in tumor and diabetic ECs was however not changed. To verify this approach, we analyzed the expression of PFKFB3 and HAS2 in HUVECs upon silencing or overexpression of PFKFB3 (39). This analysis revealed that silencing or overexpression of PFKFB3 in these ECs caused a significant (*P<0.05*) reduction or increased expression, respectively, of PFKFB3, without however altering HAS2 gene expression.

Endothelial glycolytic activation reduces endothelial HA coverage *in vivo* and is associated with vessel destabilization

In vivo, glycolysis is increased in tumor ECs, whereby glycolytic intermediates are diverted into the pentose phosphate pathway (PPP) and serine biosynthesis pathway (SBP) to promote nucleotide synthesis (9). Since this could directly influence the synthesis of HA substrates, we evaluated endothelial surface HA presence in melanoma liver metastatic capillaries and compared these levels to quiescent liver sinusoid endothelial surface coverage. In metastatic capillaries, luminal HA was ~50% reduced from the endothelial surface (Fig. 6a, left panels and 6b). This substantial loss of the glycocalyx structure was further corroborated through reduced lectin binding of LEA-FITC on the endothelial surface (Fig. 6a, right panels and 6c). Detailed observations of a tumor vessel stained for HA clearly revealed such loss of HA expression along the line from basement up to the intraluminal tip of an angiogenic endothelial cell (Fig. 6d,e).

We then also explored whether inhibition of endothelial glycolysis might be useful to promote glycocalyx formation and vascular stabilization / homeostasis. We therefore analyzed HA expression in tumor ECs in *Pfkfb3*$^{+/\Delta EC}$ mice, a mouse model in which one allele of the PFKFB3 gene is inactivated in ECs in a tamoxifen-inducible manner (9). Tumor ECs in these mice exhibit signs of tumor vessel normalization, characterized by EC stabilization (9). In comparison to WT mice, luminal HA expression was nearly doubled in tumor ECs from *Pfkfb3*$^{+/\Delta EC}$ mice (Fig. 6f, left panels and 6g) and was accompanied by increased lectin staining (Fig. 6f, right panels and 6h). These data further corroborate the reliance of endothelial HA synthesis and vessel stabilization on endothelial glycolysis. Staining tumor vessels for endothelial bound Ang1 revealed no difference between WT and *Pfkfb3*$^{+/\Delta EC}$ mice (likely because this assay is not sufficiently sensitive to detect such changes) (Fig. 6i, left panels and 6i). However, analyzing activation of the Tie2 receptor clearly showed induced phosphorylation in *Pfkfb3*$^{+/\Delta EC}$ mice (Fig. 6i, right panels and 6k).

Discussion

The key findings of our study are: 1] high endothelial glycolysis activity impairs the formation of a glycocalyx layer by reducing the availability of UDP-GlcA and UDP-GlcNAc, cytosolic substrates for HA synthesis and glycocalyx function; 2] loss of endothelial HA synthesis results in loss of endothelial glycocalyx function, and specifically the ability of Ang1 to stabilize the endothelium and microvasculature, leading to the development of severe glomerulopathy, cardiomyopathy and retinopathy; and 3] ECs that are characterized by glycolytic activation and destabilization, such as occurs in ECs that are not exposed to shear or ECs in diabetes and tumors, also exhibit impaired endothelial HA synthesis, while inhibition of endothelial glycolysis can restore HA synthesis and Ang1 signaling, thereby stabilizing the vessel wall.

HA is a nonsulfated glycosaminoglycan composed of repeating polymeric disaccharides D-glucuronic acid and N-acetyl-D-glucosamine linked by a glucuronic bond (62). HA is synthesized by membrane bound synthases (HAS1, 2 and 3) as a macromolecule with a molecular weight

between 10^5 and 10^7 Dalton, thus requiring large amounts of available substrate in the cytosol. Following its synthesis, HA interacts with specific surface proteins (hyaladherins) such as CD44, or is assembled into the pericellular extracellular matrix (63,64). The repeating nature of the polysaccharide and hence its protein binding sites have been suggested to confer structural periodicity to the endothelial surface layer (65).

The current study documents for the first time that loss of HA synthesis reduces the glycocalyx on the endothelial surface, and *in vivo* causes microvascular destabilization. This was most prominent in the kidney and the retina, where microvascular changes resulted in organ damage, resembling those observed in diabetes, a condition that is also characterized by loss of glycocalyx function (2,49). While the endothelial glycocalyx has long been recognized as a molecular scaffold that is critical for growth factor binding, generation of chemokine gradients and surface-receptor organization (66), glycocalyx research has been mostly focused on the heparan sulfate (HS) component, where the negatively charged sulfate groups and IdoA residues in the HS chain are critical for presentation and concentration of protein ligands (2). The ubiquitous distribution of HA *in vivo*, the biological activity of HA fragments when using degradative enzymes (19) and the inability to specifically inhibit HA synthesis *in vivo* have hampered the study of the potential role of HA in endothelial glycocalyx function thus far. We here demonstrate using a conditional endothelial specific deletion mouse model that the HA component has a more important role than perhaps previously expected, and show that HA, like HS, hosts a specific binding site for Ang1. Loss of HA synthesis is thus associated with loss of endothelial Ang1 signalling and vascular destabilization, explaining the glomerular, retinal and cardiac microvascular injury in the mice with a conditional endothelial deletion of the HA producing enzyme *has2*.

This raises the question as to which circumstances lead to impaired HA synthesis *in vivo*. While the sugar nucleotide building blocks for HS synthesis are concentrated in the Golgi system, where subsequent elongation and modification of the HS chains on core proteoglycans involves a range of different enzymes (2), the synthesis of HA directly depends upon cytosolic availability of its sugar nucleotide substrates (67). Hyaluronan is produced by three isoforms of hyaluronan synthase (HAS1, 2, and 3), these enzymes act on the inner face of the plasma membrane and simultaneously translocate the growing polysaccharide through plasma membrane into extracellular space. Of these enzymes, HAS2 is the predominant enzyme in HA synthesis during development (68). HAS2 is expressed by most, if not all, cells and is essential for life. While HAS1 and HAS3 null mice are developmentally normal, the HAS2 null mouse dies at an early embryonic stage when the heart is formed (69). Since these alterations in HA synthesis also are expected to affect heart development in humans, DNA screening of children with a ventricular septal defect identified a single patient with a c.A1496T (p.Glu499Val) mutation that resulted in transiently reduced HAS2 expression, suggesting that partial HAS2 deficiency could be a cause of congenital heart defects (70).

The cytosolic domains of membrane-bound HAS2 adds UDP-GlcA and UDP-GlcNAc alternately onto the reducing end of the HA chain at the expense of removing the anchoring UDP.

The cellular content of UDP-GlcNAc is the highest among the different nucleotide sugars, as also shown in the current study. However, the HAS K_m for UDP-GlcNAc is also relatively high, necessitating high abundance of this substrate for efficient hyaluronan synthesis (71). These enzyme kinetics link HA synthesis directly to metabolic glucose regulation (72). ECs have a predominance of glycolysis for sugar metabolism, which probably allows the adaptation of the vasculature to hypoxia (10). Indeed, EC proliferation and neo-angiogenesis are characterized by further endothelial activation of glycolysis through enhanced expression of the activator PFKFB3 (9). This is of relevance e.g. for tumour angiogenesis, where PFKB3 activity is increased and results in glycolytic activation and vessel destabilisation (9). Here, we extend these observations, by showing that PFKFB3 activation lowers cytosolic UDP-GlcNAc and UDP-GlcA pools and thereby impairs HA synthesis, thus interfering with Ang-1-Tie2 signalling. Our findings that endothelial haplodeficiency of PFKFB3 increases HA synthesis and glycocalyx formation in tumour ECs, in association with enhanced Ang1/Tie2 signalling and tumour vessel normaliza-

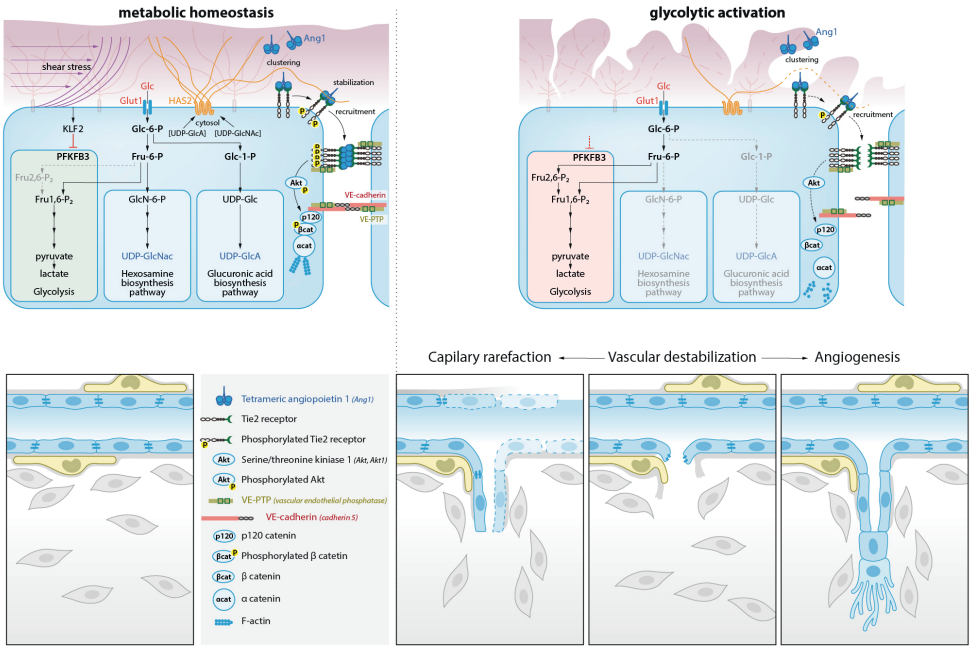


Figure 7. Model of hyaluronan – angiopoietin1 interaction in endothelial stability. Left upper panel shows normal endothelial metabolic homeostasis, where secondary to shear stress and KLF2 induction the glycolytic activator PFKFB3 is relatively suppressed. This allows for generation of UDP-GlcNAc and UDP-GlcA, the substrates for hyaluronan synthase 2 (HAS2) to produce hyaluronan. Hyaluronan on the endothelial surface acts as a molecular scaffold to bind and stabilize angiopoietin 1, a key protein for endothelial quiescence. The upper right panel shows endothelial cells such as can be found in diabetes, in tumors and in the absence of shear stress, where PFKFB3 activates glycolysis and reprioritizes glucose metabolism, reducing substrate availability for glycocalyx hyaluronan synthesis. This results in impaired Angiopoietin-1/Tie2 signaling and consequently endothelial destabilization. Loss of endothelial cell-cell contact can result in rarefaction or angiogenesis (in a tumor environment)

tion, provides genetic proof of evidence that inhibition of endothelial glycolysis by pharmacological PFKFB3 blockade may be of therapeutic benefit to promote EC stabilization and vessel homeostasis / normalization.

These observations provide a rationale to explore endothelial glucose metabolism and consequently HA synthesis as a target for microvascular stabilisation. This is probably not only of relevance for tumour angiogenesis, but may reflect a more general principle that can also be observed in other situations with endothelial cell activation such as diabetes or absence of normal shear (as occurs in atherosclerosis). Together, the present study expands the current concepts of endothelial metabolic homeostasis and vascular stability placing the high glycolytic flux of quiescent endothelial cells in key of regulating glycocalyx biosynthesis, in particular the presence of hyaluronan. Consequently, we conclude that HA plays a pivotal role in stabilisation of the Ang1 / Tie2 interaction on its surface and induction of downstream signalling. Loss of endothelial glycocalyx hyaluronan therefore, which leads to cell-cell contact destabilization can result in either endothelial rarefaction or angiogenesis (in a tumor environment) (Fig. 7).

Acknowledgements

We thank Dr. Yamaguchi (Sanford-Burnham Medical Research Institute, La Jolla, CA) for providing B6.has2$^{flox/flox}$ mice, Dr. Iruela-Arispe (Molecular Biology Institute, UCLA, Los Angeles, CA), Dr. Adams (Max Planck Institute for Molecular Biomedicine, University of Münster, Münster, Germany) for providing VE-cadherin(PAC)-CreERT2 mice, and Dr. Kappler (Institut für Biochemie und Molekularbiologie, Universität Bonn, Germany) for providing the neurocan-eGFP construct. We thank Dr. Koster (Department of Molecular Cell Biology, Leiden University Medical Center, Leiden, the Netherlands) for facilitating TEM, Dr. Robin and Dr. van Rooij (both Hubrecht Institute / KNAW and University Medical Center Utrecht, Utrecht, the Netherlands) for facilitating echocardiography equipment, Sacha Meldner (Department of Cellular and Molecular Pathology, Germany Cancer Research Institute, Heidelberg, Germany), Jasper van Gemst (Department of Nephrology, Nijmegen Centre for Molecular Life Sciences, Radboud University Nijmegen Medical Centre, Nijmegen, the Netherlands), and Angela Koudijs (The Einthoven laboratory for Vascular Medicine, Department of Internal Medicine, Division of Nephrology, Leiden University Medical Center, Leiden, the Netherlands) for technical assistance.

Financial Support by the Dutch Kidney Foundation (grants C08.2265 & GLYCOREN consortium C09.03) and the China Scholarship Council grant to Gangqi Wang (CSC no. 201406170050) are gratefully acknowledged.

References

1. Dane MJ, van den Berg BM, Lee DH, Boels MG, Tiemeier GL, et al. (2015) A microscopic view on the renal endothelial glycocalyx. Am J Physiol Renal Physiol: ajprenal 2015 May 1;308(9):F956-66.
2. Rabelink AJ, van den Berg BM, Garsen M, Wang G, Elkin M, et al. (2017) Heparanase: roles in cell survival, extracellular matrix remodelling and the development of kidney disease. Nat Rev Nephrol. 2017 Apr;13(4):201-212
3. Rai S, Nejadhamzeeigilani Z, Gutowski NJ, Whatmore JL (2015) Loss of the endothelial glycocalyx is associated with increased E-selectin mediated adhesion of lung tumour cells to the brain microvascular endothelium. J Exp Clin Cancer Res 34: 105.
4. Rabelink TJ, de Zeeuw D (2015) The glycocalyx--linking albuminuria with renal and cardiovascular disease. Nat Rev Nephrol 11: 667-676.
5. Tarbell JM, Cancel LM (2016) The glycocalyx and its significance in human medicine. J Intern Med. 2016 Jul;280(1):97-113.
6. Han S, Lee SJ, Kim KE, Lee HS, Oh N, et al. (2016) Amelioration of sepsis by TIE2 activation-induced vascular protection. Sci Transl Med 8: 335ra355.
7. Becker BF, Jacob M, Leipert S, Salmon AH, Chappell D (2015) Degradation of the endothelial glycocalyx in clinical settings: searching for the sheddases. Br J Clin Pharmacol 80: 389-402.
8. Rabelink TJ, van den Berg BM, Garsen M, Wang G, Elkin M, et al. (2017) Heparanase: roles in cell survival, extracellular matrix remodelling and the development of kidney disease. Nat Rev Nephrol 13: 201-212.
9. Cantelmo AR, Conradi LC, Brajic A, Goveia J, Kalucka J, et al. (2016) Inhibition of the Glycolytic Activator PFKFB3 in Endothelium Induces Tumor Vessel Normalization, Impairs Metastasis, and Improves Chemotherapy. Cancer Cell 30: 968-985.
10. Eelen G, de Zeeuw P, Simons M, Carmeliet P (2015) Endothelial cell metabolism in normal and diseased vasculature. Circ Res 116: 1231-1244.
11. Verdegem D, Moens S, Stapor P, Carmeliet P (2014) Endothelial cell metabolism: parallels and divergences with cancer cell metabolism. Cancer Metab 2: 19.
12. Carmeliet P, Jain RK (2011) Molecular mechanisms and clinical applications of angiogenesis. Nature 473: 298-307.
13. Cerutti C, Ridley AJ (2017) Endothelial cell-cell adhesion and signaling. Exp Cell Res. 2017 Sep 1;358(1):31-38.
14. Jain RK (2014) Antiangiogenesis strategies revisited: from starving tumors to alleviating hypoxia. Cancer Cell 26: 605-622.
15. Carmeliet P, Jain RK (2011) Principles and mechanisms of vessel normalization for cancer and other angiogenic diseases. Nat Rev Drug Discov 10: 417-427.
16. Sarrazin S, Lamanna WC, Esko JD (2011) Heparan sulfate proteoglycans. Cold Spring Harb Perspect Biol. 2011 Jul 1;3(7).
17. Bishop JR, Schuksz M, Esko JD (2007) Heparan sulphate proteoglycans fine-tune mammalian physiology. Nature 446: 1030-1037.
18. Vigetti D, Karousou E, Viola M, Deleonibus S, De Luca G, et al. (2014) Hyaluronan: biosynthesis and signaling. Biochim Biophys Acta 1840: 2452-2459.
19. Matsumoto K, Li Y, Jakuba C, Sugiyama Y, Sayo T, et al. (2009) Conditional inactivation of Has2 reveals a crucial role for hyaluronan in skeletal growth, patterning, chondrocyte maturation and joint formation in the developing limb. Development 136: 2825-2835.
20. Tammi RH, Passi AG, Rilla K, Karousou E, Vigetti D, et al. (2011) Transcriptional and post-translational regulation of hyaluronan synthesis. FEBS J 278: 1419-1428.
21. Vigetti D, Viola M, Karousou E, De Luca G, Passi A (2014) Metabolic control of hyaluronan synthases. Matrix Biol 35: 8-13.
22. Vigetti D, Ori M, Viola M, Genasetti A, Karousou E, et al. (2006) Molecular cloning and characterization of UDP-glucose dehydrogenase from the amphibian Xenopus laevis and its involvement in hyaluronan synthesis. J Biol Chem 281: 8254-8263.
23. Baggenstoss BA, Harris EN, Washburn JL, Medina AP, Nguyen L, et al. (2016) Hyaluronan synthase control of synthesis rate and hyaluronan product size are independent functions differentially affected by mutations in a conserved tandem B-X7-B motif. Glycobiology. 2017 Jan;27(2):154-164
24. Viola M, Karousou E, D'Angelo ML, Caon I, De Luca G, et al. (2015) Regulated Hyaluronan Synthesis by Vascular Cells. Int J Cell Biol 2015: 208303.

25. Slawson C, Copeland RJ, Hart GW (2010) O-GlcNAc signaling: a metabolic link between diabetes and cancer? Trends Biochem Sci 35: 547-555.

26. De Bock K, Georgiadou M, Carmeliet P (2013) Role of endothelial cell metabolism in vessel sprouting. Cell Metab 18: 634-647.

27. Moretto P, Karousou E, Viola M, Caon I, D'Angelo ML, et al. (2015) Regulation of Hyaluronan Synthesis in Vascular Diseases and Diabetes. J Diabetes Res 2015: 167283.

28. Augustin HG, Koh GY, Thurston G, Alitalo K (2009) Control of vascular morphogenesis and homeostasis through the angiopoietin-Tie system. Nat Rev Mol Cell Biol 10: 165-177.

29. Thurston G, Rudge JS, Ioffe E, Zhou H, Ross L, et al. (2000) Angiopoietin-1 protects the adult vasculature against plasma leakage. Nat Med 6: 460-463.

30. Campochiaro PA, Peters KG (2016) Targeting Tie2 for Treatment of Diabetic Retinopathy and Diabetic Macular Edema. Curr Diab Rep 16: 126.

31. Wong AL, Haroon ZA, Werner S, Dewhirst MW, Greenberg CS, et al. (1997) Tie2 expression and phosphorylation in angiogenic and quiescent adult tissues. Circ Res 81: 567-574.

32. Xu Y, Yu Q (2001) Angiopoietin-1, unlike angiopoietin-2, is incorporated into the extracellular matrix via its linker peptide region. J Biol Chem 276: 34990-34998.

33. Xu Y, Liu YJ, Yu Q (2004) Angiopoietin-3 is tethered on the cell surface via heparan sulfate proteoglycans. J Biol Chem 279: 41179-41188.

34. Riley CM, Fuegy PW, Firpo MA, Shu XZ, Prestwich GD, et al. (2006) Stimulation of in vivo angiogenesis using dual growth factor-loaded crosslinked glycosaminoglycan hydrogels. Biomaterials 27: 5935-5943.

35. Benedito R, Roca C, Sorensen I, Adams S, Gossler A, et al. (2009) The notch ligands Dll4 and Jagged1 have opposing effects on angiogenesis. Cell 137: 1124-1135.

36. Madisen L, Zwingman TA, Sunkin SM, Oh SW, Zariwala HA, et al. (2010) A robust and high-throughput Cre reporting and characterization system for the whole mouse brain. Nat Neurosci 13: 133-140.

37. Monvoisin A, Alva JA, Hofmann JJ, Zovein AC, Lane TF, et al. (2006) VE-cadherin-CreERT2 transgenic mouse: a model for inducible recombination in the endothelium. Dev Dyn 235: 3413-3422.

38. Wang Y, Nakayama M, Pitulescu ME, Schmidt TS, Bochenek ML, et al. (2010) Ephrin-B2 controls VEGF-induced angiogenesis and lymphangiogenesis. Nature 465: 483-486.

39. De Bock K, Georgiadou M, Schoors S, Kuchnio A, Wong BW, et al. (2013) Role of PFKFB3-driven glycolysis in vessel sprouting. Cell 154: 651-663.

40. Tran TN, Eubanks SK, Schaffer KJ, Zhou CY, Linder MC (1997) Secretion of ferritin by rat hepatoma cells and its regulation by inflammatory cytokines and iron. Blood 90: 4979-4986.

41. Ram R, Mickelsen DM, Theodoropoulos C, Blaxall BC (2011) New approaches in small animal echocardiography: imaging the sounds of silence. Am J Physiol Heart Circ Physiol 301: H1765-1780.

42. Nusayr E, Doetschman T (2013) Cardiac development and physiology are modulated by FGF2 in an isoform- and sex-specific manner. Physiol Rep 1.

43. Dane MJ, van den Berg BM, Avramut MC, Faas FG, van der Vlag J, et al. (2013) Glomerular endothelial surface layer acts as a barrier against albumin filtration. Am J Pathol 182: 1532-1540.

44. Friden V, Oveland E, Tenstad O, Ebefors K, Nystrom J, et al. (2011) The glomerular endothelial cell coat is essential for glomerular filtration. Kidney Int 79: 1322-1330.

45. Zhang H, Baader SL, Sixt M, Kappler J, Rauch U (2004) Neurocan-GFP fusion protein: a new approach to detect hyaluronan on tissue sections and living cells. J Histochem Cytochem 52: 915-922.

46. Faas FG, Avramut MC, van den Berg BM, Mommaas AM, Koster AJ, et al. (2012) Virtual nanoscopy: generation of ultra-large high resolution electron microscopy maps. J Cell Biol 198: 457-469.

47. Jaffe EA, Nachman RL, Becker CG, Minick CR (1973) Culture of human endothelial cells derived from umbilical veins. Identification by morphologic and immunologic criteria. J Clin Invest 52: 2745-2756.

48. van der Veer EP, de Bruin RG, Kraaijeveld AO, de Vries MR, Bot I, et al. (2013) Quaking, an RNA-binding protein, is a critical regulator of vascular smooth muscle cell phenotype. Circ Res 113: 1065-1075.

49. Boels MG, Avramut MC, Koudijs A, Dane MJ, Lee DH, et al. (2016) Atrasentan Reduces Albuminuria by Restoring the Glomerular Endothelial Glycoca-

lyx Barrier in Diabetic Nephropathy. Diabetes 65: 2429-2439.

50. Huveneers S, Oldenburg J, Spanjaard E, van der Krogt G, Grigoriev I, et al. (2012) Vinculin associates with endothelial VE-cadherin junctions to control force-dependent remodeling. J Cell Biol 196: 641-652.
51. Timmerman I, Heemskerk N, Kroon J, Schaefer A, van Rijssel J, et al. (2015) A local VE-cadherin and Trio-based signaling complex stabilizes endothelial junctions through Rac1. J Cell Sci 128: 3041-3054.
52. Kostidis S, Addie RD, Morreau H, Mayboroda OA, Giera M (2017) Quantitative NMR analysis of intra- and extracellular metabolism of mammalian cells: A tutorial. Anal Chim Acta 980: 1-24.
53. Nawroth PP, Isermann B (2010) Mechanisms of diabetic nephropathy--old buddies and newcomers part 2. Exp Clin Endocrinol Diabetes 118: 667-672.
54. Nawroth PP, Isermann B (2010) Mechanisms of diabetic nephropathy--old buddies and newcomers part 1. Exp Clin Endocrinol Diabetes 118: 571-576.
55. Crea F, Camici PG, Bairey Merz CN (2014) Coronary microvascular dysfunction: an update. Eur Heart J 35: 1101-1111.
56. Kohda D, Morton CJ, Parkar AA, Hatanaka H, Inagaki FM, et al. (1996) Solution structure of the link module: a hyaluronan-binding domain involved in extracellular matrix stability and cell migration. Cell 86: 767-775.
57. Favreau AJ, Faller CE, Guvench O (2013) CD44 receptor unfolding enhances binding by freeing basic amino acids to contact carbohydrate ligand. Biophys J 105: 1217-1226.
58. Doddaballapur A, Michalik KM, Manavski Y, Lucas T, Houtkooper RH, et al. (2015) Laminar shear stress inhibits endothelial cell metabolism via KLF2-mediated repression of PFKFB3. Arterioscler Thromb Vasc Biol 35: 137-145.
59. Mitchell MJ, King MR (2014) Physical biology in cancer. 3. The role of cell glycocalyx in vascular transport of circulating tumor cells. Am J Physiol Cell Physiol 306: C89-97.
60. Brunskill EW, Potter SS (2010) Gene expression programs of mouse endothelial cells in kidney development and disease. PLoS One 5: e12034.
61. Lam JD, Oh DJ, Wong LL, Amarnani D, Park-Windhol C, et al. (2017) Identification of RUNX1 as a Mediator of Aberrant Retinal Angiogenesis. Diabetes. 2017 Jul;66(7):1950-1956.
62. Laurent TC, Fraser JR (1992) Hyaluronan. FASEB J 6: 2397-2404.
63. Lennon FE, Singleton PA (2011) Hyaluronan regulation of vascular integrity. Am J Cardiovasc Dis 1: 200-213.
64. Mambetsariev N, Mirzapoiazova T, Mambetsariev B, Sammani S, Lennon FE, et al. (2010) Hyaluronic Acid binding protein 2 is a novel regulator of vascular integrity. Arterioscler Thromb Vasc Biol 30: 483-490.
65. Day AJ, Sheehan JK (2001) Hyaluronan: polysaccharide chaos to protein organisation. Curr Opin Struct Biol 11: 617-622.
66. Esko JD, Selleck SB (2002) Order out of chaos: assembly of ligand binding sites in heparan sulfate. Annu Rev Biochem 71: 435-471.
67. Rilla K, Oikari S, Jokela TA, Hyttinen JM, Karna R, et al. (2013) Hyaluronan synthase 1 (HAS1) requires higher cellular UDP-GlcNAc concentration than HAS2 and HAS3. J Biol Chem.
68. Triggs-Raine B, Natowicz MR (2015) Biology of hyaluronan: Insights from genetic disorders of hyaluronan metabolism. World J Biol Chem 6: 110-120.
69. Camenisch TD, Spicer AP, Brehm-Gibson T, Biesterfeldt J, Augustine ML, et al. (2000) Disruption of hyaluronan synthase-2 abrogates normal cardiac morphogenesis and hyaluronan-mediated transformation of epithelium to mesenchyme. J Clin Invest 106: 349-360.
70. Zhu X, Deng X, Huang G, Wang J, Yang J, et al. (2014) A novel mutation of Hyaluronan synthase 2 gene in Chinese children with ventricular septal defect. PLoS One 9: e87437.
71. Itano N, Sawai T, Yoshida M, Lenas P, Yamada Y, et al. (1999) Three isoforms of mammalian hyaluronan synthases have distinct enzymatic properties. J Biol Chem 274: 25085-25092.
72. Wang A, Hascall VC (2009) Hyperglycemia, intracellular hyaluronan synthesis, cyclin D3 and autophagy. Autophagy 5: 864-865.

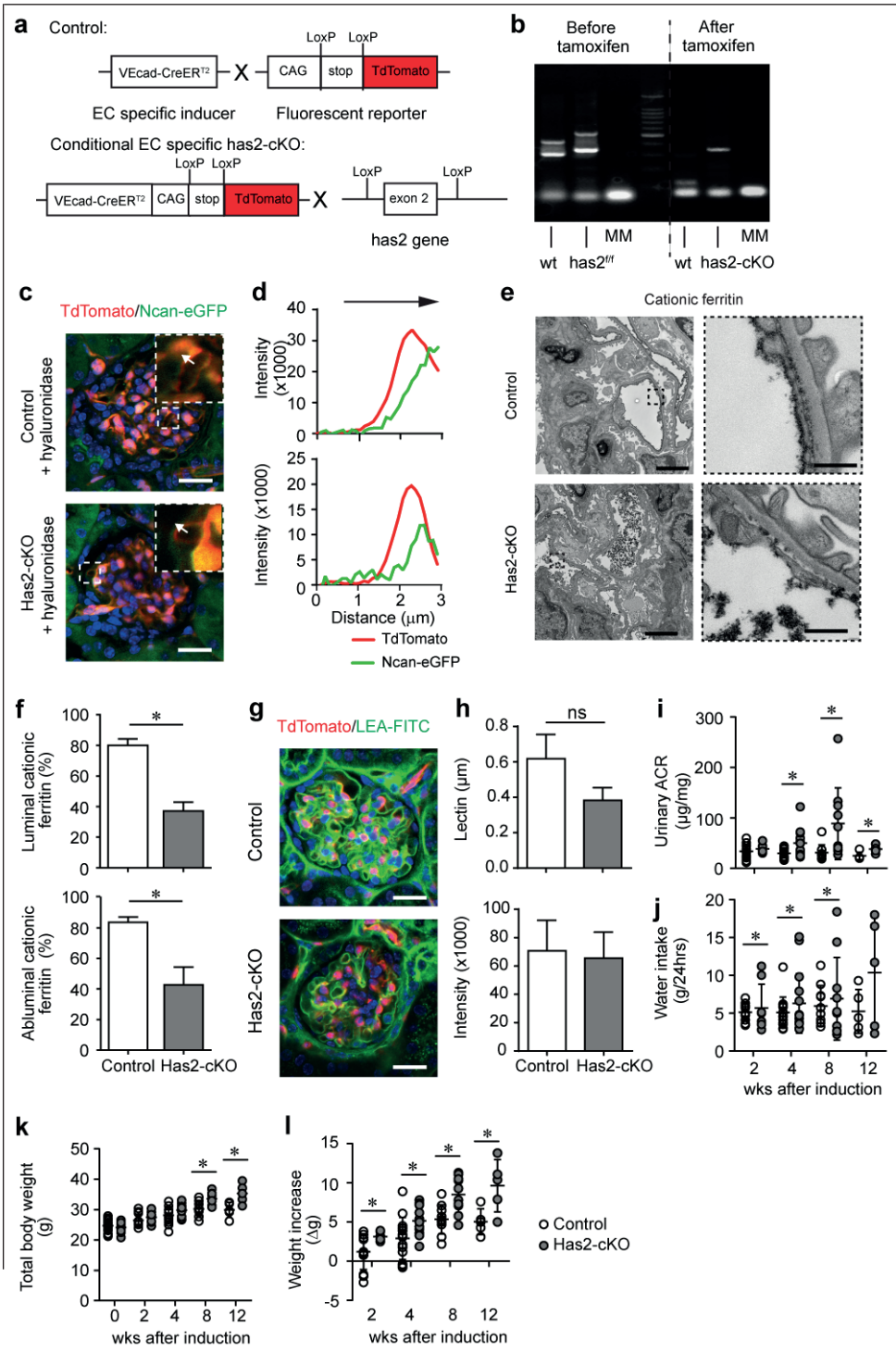
Supplementary Table 1. Detailed glomerular morphology quantification 12 weeks after tamoxifen induction (related to fig. 1).

	Control	Has2-cKO
Endothelial cell layer thickness (nm)	89.8 ± 14.4	136.5 ± 21.8*
% Endothelial fenestration (nm)	38.6 ± 6.5	19.1 ± 4.8*
GBM thickness (nm)	191.7 ± 12.4c	234.7 ± 10.2*
Podocyte foot process base width (nm)	491.0 ± 19.5	621.5 ± 46.9*

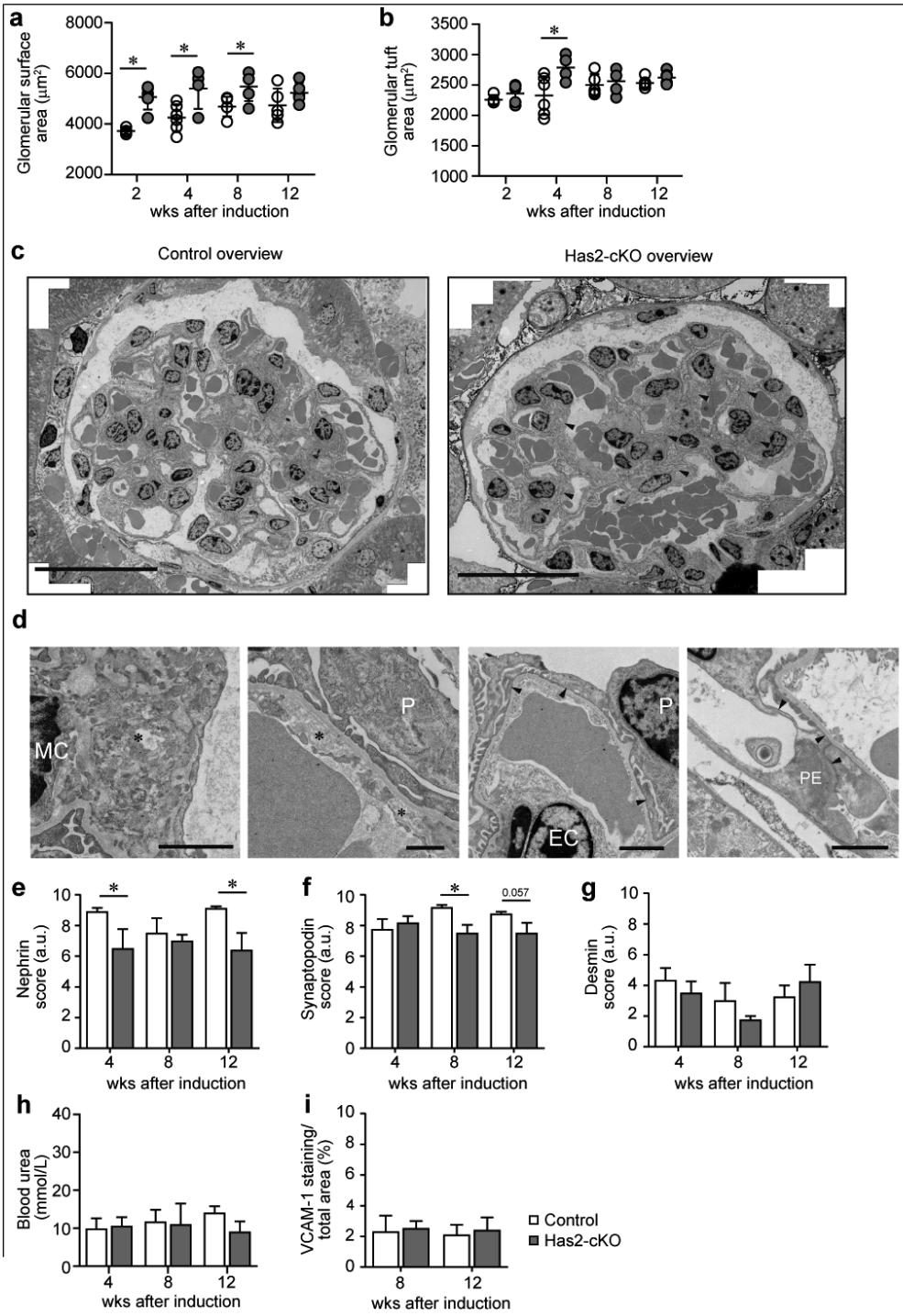
Mean ± s.d.
*$P< 0.05$ versus control

Supplementary Table S2. Primers used for genotyping (Related to Methods).

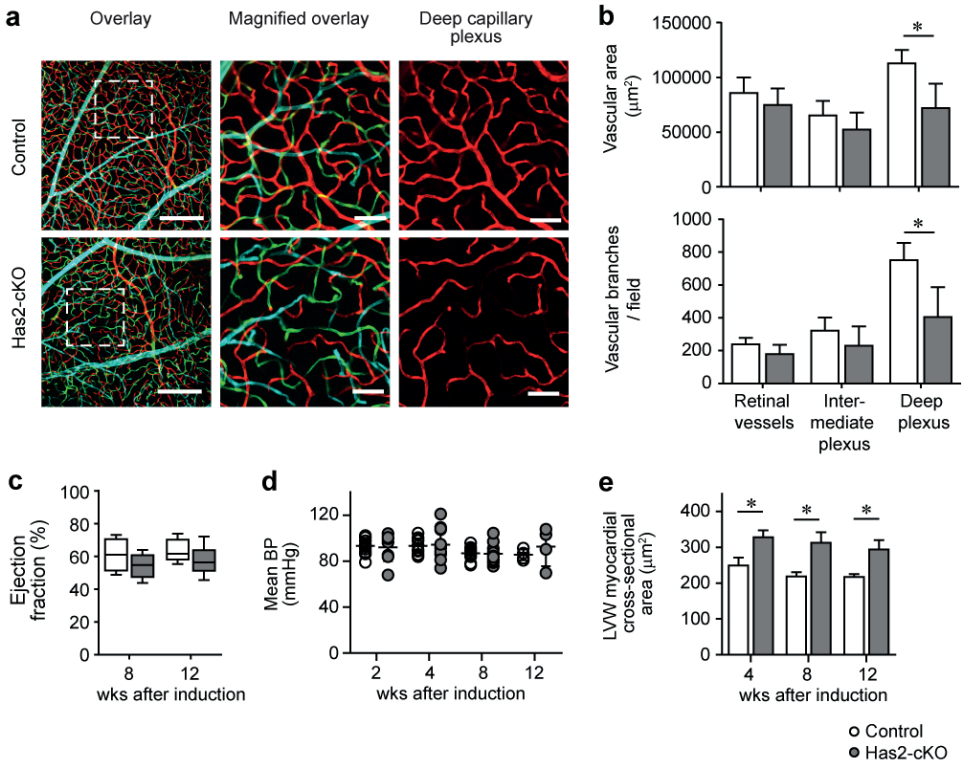
	Forward (5'-3')	Reverse (5'-3')	Product (bp)
VE cadherin	gcaggcagctcacaaaggaacaat	tgtccttgctgagtgacagtggaa	550
VE cad-CreERT2	gcaggcagctcacaaaggaacaat	atcactcgttgcatcgaccggtaa	950
R26R wt	aagggagctgcagtggagta	ccgaaaatctgtgggaagtc	297
R26R-TdTomato	ctgttcctgtacggcatgg	ggcattaaagcagcgtatcc	196
Has2 wt	tgcagaatttaggggcgaattgggagctaa	atgaggttagagattagcaagactgagttc	441
	cttgaaccttgagtgtgccattttgtagtc	cattcttgttttgaagtttgtttccttgac	322
Has2 floxed	tgcagaatttaggggcgaattgggagctaa	atgaggttagagattagcaagactgagttc	550
	cttgaaccttgagtgtgccattttgtagtc	cattcttgttttgaagtttgtttccttgac	355
Has2 mutant	tcacatgcatgcacaatcag	acagatggtcacagccttcc	660

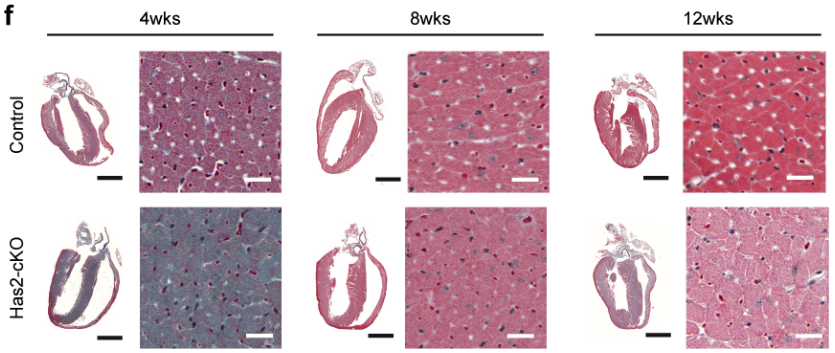

a
Control:
LoxP LoxP
VEcad-CreER^{T2} X CAG stop TdTomato
EC specific inducer
Fluorescent reporter
Conditional EC specific has2-cKO:
LoxP LoxP
VEcad-CreER^{T2} CAG stop TdTomato X
LoxP LoxP
exon 2
has2 gene
b
Before tamoxifen
After tamoxifen
MM
MM
wt has2$^{f/f}$
wt has2-cKO
c
TdTomato/Ncan-eGFP
Control + hyaluronidase
Has2-cKO + hyaluronidase
d
Intensity (x1000)
Intensity (x1000)
Distance (μm)
TdTomato
Ncan-eGFP
e
Cationic ferritin
Control
Has2-cKO
f
Luminal cationic ferritin (%)
Abluminal cationic ferritin (%)
Control Has2-cKO
g
TdTomato/LEA-FITC
Control
Has2-cKO
h
Lectin (μm)
ns
Intensity (x1000)
Control Has2-cKO
i
Urinary ACR (μg/mg)
j
Water intake (g/24hrs)
wks after induction
k
Total body weight (g)
wks after induction
l
Weight increase (Δg)
wks after induction
Control
Has2-cKO

Supplementary Figure 1. Loss of endothelial hyaluronan and glycocalyx results in proteinuria (Related to Fig. 1 and Methods). Generation of conditional endothelial specific hyaluronan synthase 2 knock-out mice. **(a)** Schematic representation of specific genes introduced in control and hyaluronan synthase 2 knock-out (has2-cKO) mice to allow for conditional endothelial changes. CAG = synthetic CAG promoter; stop = stop sequence; LoxP = Cre-Lox specific recombination site. **(b)** Example of genotyping of mice homozygous for the floxed has2 gene ($has2^{f/f}$) before tamoxifen induction (left lanes) and confirmation of mutation of has2 gene (exon 2 deletion) after tamoxifen induction (right panel). MM = PCR master mix only. **(c)** Representative cross-sectional average intensity projections of control (upper panel) and has2-cKO (lower panel) glomerular tissue sections incubated with the HA degrading enzyme hyaluronidase before staining with the hyaluronan binding probe Ncan-eGFP. Endothelial cells are colored red (TdTomato label) upon tamoxifen induction. **(d)** Insets show measurement lines producing the line-graphs on the right demonstrating the absence of luminal hyaluronan. **(e)** Representative TEM images of CF staining in control and has2-cKO glomeruli in mice, 4 weeks after tamoxifen induction. In contrast to the clearly aligned CF bound at the endothelial cell surface in control glomeruli (upper right), there was a clear loss of glycocalyx coverage (lower right) while CF stained material was found in the lumen of glomerular capillaries in has2-cKO mice (lower left). **(f)** Luminal- and subendothelial CF coverage was reduced in has2-cKO mice (*n = 3/group*). **(g)** Representative cross-sectional confocal images of glomerular tissue sections, 4 weeks after tamoxifen induction. Sections are stained with the lectin *Lycopersicon esculentum* (LEA-FITC), endothelial cells are labelled with TdTomato (red) upon induction with tamoxifen. **(h)** Graphs of respective intraluminal lectin localization and fluorescence intensity, revealed that both thickness and luminal expression is not significantly changed in has2-cKO mice, suggesting that without the presence of hyaluronan still an endothelial glycocalyx is present (n = 3/group). **(i)** Albumin to creatinine ratio (ACR) in 24hrs-urine samples significantly increases in has2-cKO from week 4. During the 12-week period after tamoxifen induction has2-cKO mice drunk more water (**j**, no change in food intake) and total body weight significantly raised from week 8 onward **(k)**, whereas bodyweight increase already was significantly higher from week 2 onwards **(l)**. 2- (*n = 8-, 12/group*), 4- (*n = 14/group*), 8- (*n = 10/group*) and 12wks (*n = 5/group*). Scale bars, 30µm (C, G), 5µm (E, right) and 0.5µm (E, left). Values are given in mean ± s.e.m. (f, h) or mean ± s.d. (i-l). Difference was assessed by non-paired 2-tailed Student's *t* test or, when not normally distributed, by two-tailed F-test; *P < 0.05.


a
Glomerular surface area (µm²)
8000
6000
4000
2000
2
4
8
12
wks after induction
b
Glomerular tuft area (µm²)
3500
3000
2500
2000
1500
1000
wks after induction
c
Control overview
Has2-cKO overview
d
MC
P
P
EC
PE
e
Nephrin score (a.u.)
wks after induction
f
Synaptopodin score (a.u.)
0.057
wks after induction
g
Desmin score (a.u.)
wks after induction
h
Blood urea (mmol/L)
wks after induction
i
VCAM-1 staining/ total area (%)
Control
Has2-cKO
wks after induction

Supplementary Figure 2. Loss of endothelial hyaluronan results in renal morphology changes (Related to Fig. 1). Further glomerular morphologic analyses showed that the outer glomerular surface area is already significantly increased from week 2 onwards **(a)**, while the overall the glomerular tuft area did, however, not change during the 12-week period **(b)**. 2- (*n = 4-, 5/group*), 4- (*n = 6-, 4/group*), 8- (*n = 5/group*) and 12wks (*n = 5/group*). **(c)** TEM overview of a glomerular stitch of a control- and has2-cKO mouse for reference with indications of matrix expansion (arrowheads). **(d)** Detailed TEM images from week 8 up to 12 after has2 deletion shows mesangial sclerosis (left panel, asterisk), focal subendothelial matrix accumulation (middle panel left, asterisk), foot process effacement (middle panel right, arrowheads), and occasional parietal epithelial cells bound to the capillary loop basement membranes and podocytes (right panel, arrowhead). Loss of podocyte mass was also reflected by mild reduction in **(e)** nephrin and **(f)** synaptopodin expression. (*n = 4-, 5/*group). **(g)** During the 12-week period glomerular changes were without changes in cytoskeletal protein desmin levels. (*n = 4-, 5/group*). Throughout the entire experimental period **(h)** blood urea levels remained unchanged, and **(i)** glomerular endothelial inflammatory marker VCAM-1 expression did not change after tamoxifen induction. (*n = 4-, 5/group*). Scale bars, 25µm **(c)**, 5µm (left image) and 0.5µm (other images) **(d)**. EC, endothelial cell; MG, mesangial cell; P, podocyte; PE, parietal epithelial cell. Values are given as mean ± s.d. **(a, b, e-i)**. Differences between control (white) and has2-cKO (grey) mice were assessed by non-paired 2-tailed Student's *t* test. *P < 0.05.

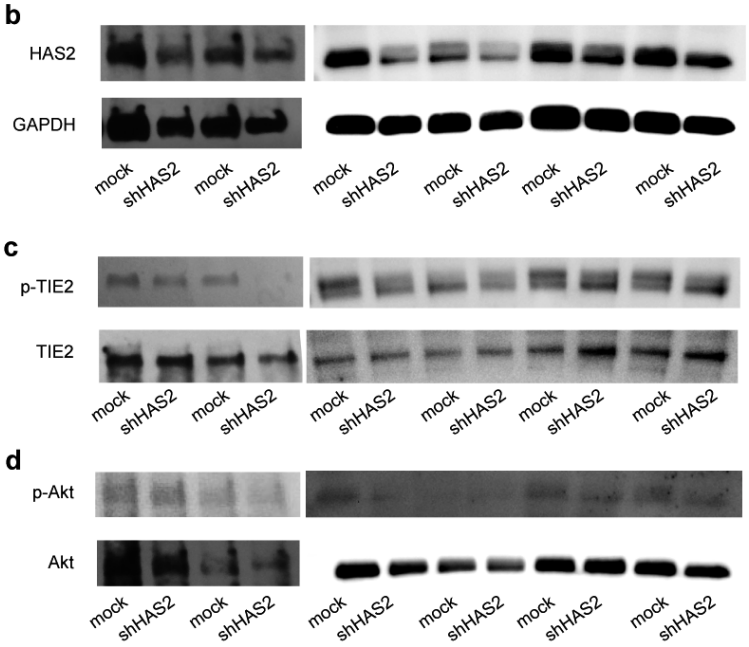

a
Overlay
Magnified overlay
Deep capillary plexus
Control
Has2-cKO
b
Vascular area (μm²)
150000
100000
50000
0
*
Vascular branches / field
1000
800
600
400
200
0
*
Retinal vessels
Inter-mediate plexus
Deep plexus
c
Ejection fraction (%)
100
80
60
40
20
0
8
12
wks after induction
d
Mean BP (mmHg)
120
80
40
0
2
4
8
12
wks after induction
e
LVW myocardial cross-sectional area (μm²)
400
300
200
100
0
*
*
*
4
8
12
wks after induction
Control
Has2-cKO


f
4wks
8wks
12wks
Control
Has2-cKO

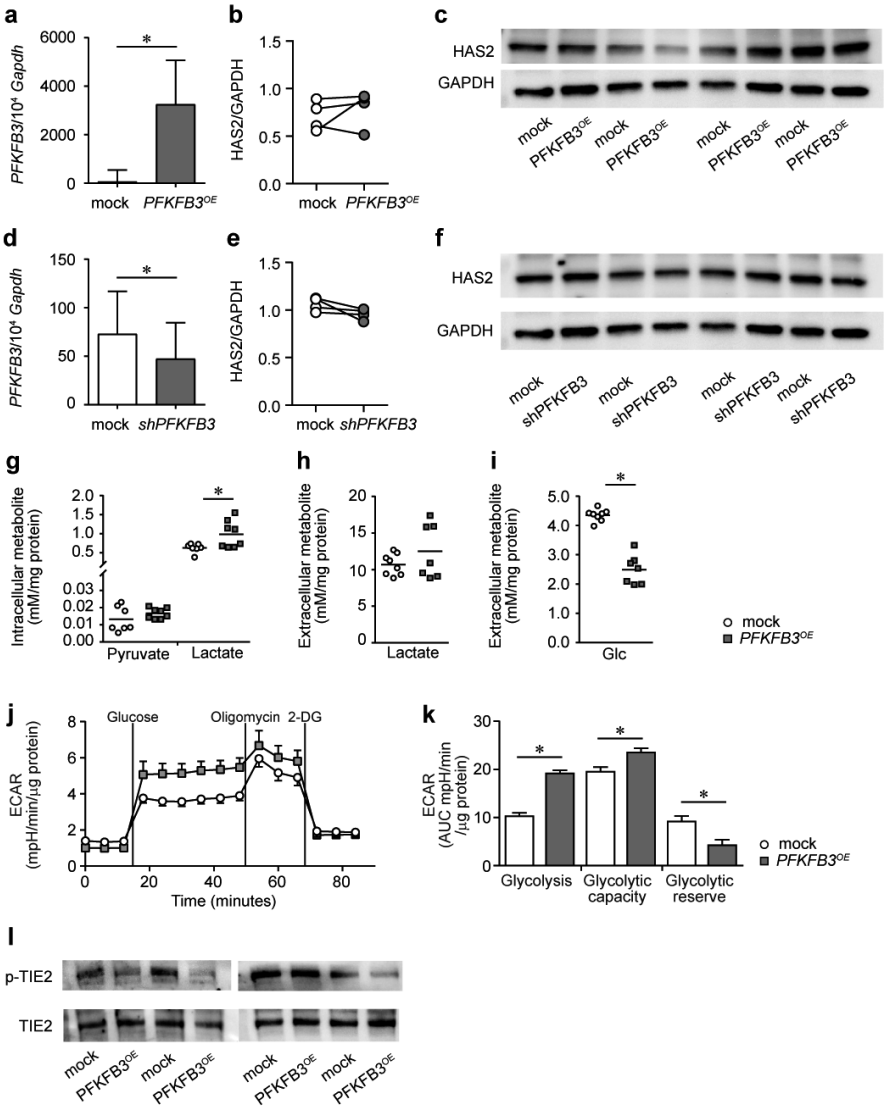
Supplementary Figure 3. Loss of endothelial hyaluronan results in retinal capillary rarefaction and cardiac morphologic- and functional changes (Related to Fig. 2). As endothelial loss of hyaluronan was not confined to kidneys, we also studied the microvasculature in retina and myocardium. **(a)** Representative images depicting endothelial cell-TdTomato reporter fluorescence of isolated retinal vascular plexus of control (upper panels) and has2-cKO (lower panels) mice (*n = 3-5/group*). Left panels show a pseudo-colored overview of the retinal vascular network with central feeding artery and vein plus branches in cyan, the superficial capillary plexus in green and the deep capillary plexus in red. Middle panels show a magnified overlay of left panels, and right panels show the TdTomato stained endothelial cells of the deep capillary plexus. Compared to control plexus loss of endothelial cells in the has2-cKO retina can be observed, which is quantified in **(b)** vascular area and number of vascular branches per field. Addressing the myocardial microcirculation, we tested cardiac function in response to the systemic loss of endothelial hyaluronan. **(c)** Cardiac ejection fraction, calculated from *in vivo* M-mode Doppler echocardiography, in control and has2-cKO mice at 8- (*n = 5- ,6/group*) and 12wks (*n = 5-, 6/group*). **(d)** Mean blood pressure (BP) in conscious animals via tail cuff measurements at 2- (*n = 11-, 8/group*), 4- (*n = 16-, 14/group*), 8- (*n = 10/group*) and 12wks (*n = 4/group*). **(e)** Quantification of LVW cross-sectional area reveals significant larger myocardial cells already at 4 weeks. **(f)** Representative cardiac images in sagittal view (left) and detailed morphology of left ventricle wall (LVW), stained with Goldner's trichrome elastica for collagen, of control (upper panels) and has2-cKO (lower panels) mice at 4- (*n = 6-, 4/group*), 8- (*n = 5/group*) and 12wks (*n = 5/group*) after tamoxifen induction. No evidence was found for sclerotic tissue or interstitial edema during the 12-week period. Scale bars, 200µm (a, overview), 50µm (a, middle and right, detailed views), 2mm (f, sagittal overviews) and 50µm (f, details) Values are given as mean ± s.d. (b-e) and differences between control (white) and has2-cKO (grey) mice were assessed by non-paired 2-tailed Student's *t* test; *P < 0.05.

a

	Free binding energy ΔG (kcal/mol)
Fibrinogen	- 11.99
CD44	- 11.69
Ang1	- 12.49



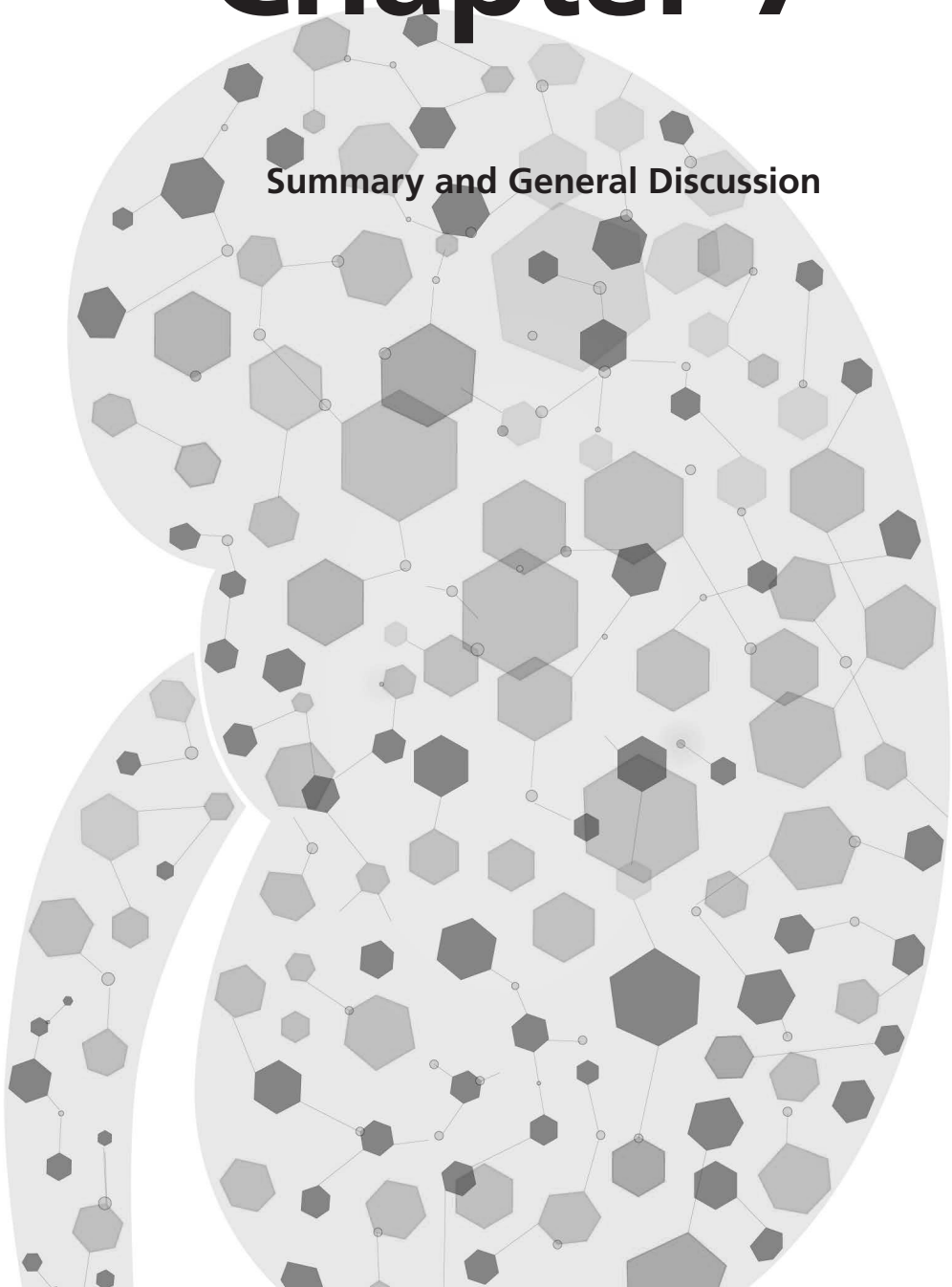
Supplementary Figure 4. Loss of endothelial hyaluronan results in reduced Tie2 activation (Related to Fig. 4). (a) Comparison of free binding energies obtained from binding predictions of hyaluronan to fibrinogen, CD44 and Ang1, respectively. No binding was found for HA to Ang2. Western-blot of protein samples of primary human glomerular-derived microvascular endothelial cells (hgMVEC), transduced with an empty- (mock) or a HAS2-shRNA containing lenti-viral construct (HAS2 shRNA), exposed to a laminar shear stress of 5 dyne/cm^2 for 3 days in the presence of 100ng/mL recombinant human Ang1. Western-blot samples stained for **(b)** HAS2 and GAPDH, **(c)** p-Tie2 and Tie2, and **(d)** p-Akt and Akt, which were used for analysis as shown in fig. 4a,h,i.



Supplementary Figure 5. Endothelial hyaluronan synthesis is dependent on glycolytic PFKFB3 activity (Related to Fig. 5). To test whether changes in endothelial metabolism can affect HA biosynthesis, HUVECs are cultured overexpressing the glycolytic activator PFKFB3 (PFKFB3^{OE}) or genetically silencing PFKFB3 (shPFKFB3) using lentiviral constructs. **(a)** qPCR analysis of PFKFB3^{OE} transduction revealed highly elevated *PFKFB3* mRNA expression without affecting **(b)** HAS2 protein levels, as quantified from Western-Blot (**c**, *n = 4*). **(d)** qPCR analysis of shPFKFB3 transduction revealed reduced *PFKFB3* mRNA expression without affecting **(e)** HAS2 protein levels, as quantified from Western-Blot (**f**, *n = 4*). **(g)** Intracellular glucose metabolite pyruvate and lactate concentrations by NMR measurement upon inducing the glycolytic pathway in HUVECs through PFKFB3^{OE} (*n = 8*). Control **(h)** extracellular lactate and **(i)** glucose (Glc) concentrations by NMR. Confirmation of these results were obtained measuring the extracellular acidification rate (ECAR), an indicator of cellular lactate production. Using a Seahorse XF flux analyzer, 48hrs after transduction PFKFB3^{OE} induced a **(j)** higher glycolytic increase, overall glycolytic capacity and glycolytic reserve, as quantified in (**k**; *n = 4*). **(l)** Western-blot samples stained for p-Tie2 and Tie2, which were used for analysis as shown in fig. 5i. Values are given as mean ± s.d. and differences between mock transduced (white) and PFKFB3^{OE} or shPFKFB3 transduced cells (grey) were assessed by paired 2-tailed Student's *t* test; *P < 0.05.

Chapter 7

Summary and General Discussion



A hallmark of renal diseases is proteinuria. Proteinuria is caused by damage to the glomerular barrier function, in which the endothelial cells with their glycocalyx form the first barrier to retain plasma proteins in the systemic circulation. The luminal location of the glycocalyx provides direct contact with pathogenic factors. Certain heparan sulfate domains have been shown to play a major role in specific protein binding (1). The heparan sulfate degrading enzyme heparanase is increased in diabetic nephropathy and modifies the endothelial glycocalyx. The primary aim of this thesis was to study the role of the endothelial glycocalyx in diabetic nephropathy. The extracellular processing of heparan sulfate by heparanase can be causal for the disease progression; therefore the secondary aim was to study the precise remodeling of heparan sulfate domains by systemic heparanase. Lastly, the effect of ablation of another major endothelial glycocalyx component, hyaluronan, has been studied in multiple vascular processes. This thesis provides evidence that inhibiting glycocalyx-degrading enzymes is a conceivable potent treatment strategy against diabetic nephropathy.

Summary of study findings

As diabetes progresses, different organs are under stress and endothelial damage can be seen as a common denominator. In chapter 2, we examined the renoprotective effects of orally administrated atrasentan, a selective endothelin A receptor blocker, in an experimental diabetic nephropathy mouse model. We show that treatment with atrasentan attenuated albuminuria, without changing gross glomerular morphology and systemic hemodynamics. Nevertheless, atrasentan treatment increased glycocalyx coverage on glomerular endothelium, which was accompanied by increased renal nitric oxide concentrations and, most strikingly, reduced expression of glomerular cathepsin L and heparanase.

In chapter 3, we used the same diabetes model to uncover a mechanistic explanation for the recent finding that inhibition of the pro-inflammatory chemokine monocyte chemotactic protein-1 (MCP-1) with the Spiegelmer® emapticap pegol (NOX-E36) has long-lasting albuminuria reducing effect in patients with diabetic nephropathy. MCP-1 regulates immunocyte recruitment and differentiation of macrophages. The mouse analogue of NOX-E36 (mNOX-E36) attenuated albuminuria without any change in systemic hemodynamics (similar to atrasentan, chapter 2). Also, podocytes were not affected by MCP-1 inhibition. However, glomerular endothelial glycocalyx coverage was restored and both glomerular cathepsin L and heparanase presence were reduced as well.

In both studies above, macrophages were affected. Atrasentan effectively shifts the balance of inflammatory / anti-inflammatory macrophages towards anti-inflammatory macrophages and MCP-1 inhibition shifts macrophage function towards increased anti-inflammatory function as shown by increased IL-10 production and decreased TNFα release. These studies indicate a pivotal role for heparanase activation by immunocytes in the progression of diabetic nephropathy. Macrophages secrete cathepsin L that has been shown to activate heparanase. Both studies show reduced local presence of cathepsin L in glomeruli as well as reduced activation of the

glycocalyx degrading enzyme heparanase, ultimately resulting in restoration of the glomerular endothelial glycocalyx and barrier function.

In chapter 4 we addressed the question of conflicting reports about nitric oxide production during diabetic pathogenesis. In our model, renal nitric oxide availability is induced sixteen weeks after the induction of diabetes, despite the presence of factors that cause endothelial dysfunction, and the presence of the endogenous nitric oxide synthesis (NOS) inhibitor symmetric dimethyl arginine (ADMA). Targeting uncoupled NOS with the tetrahydrobiopterin precursor sepiapterin further increases nitric oxide availability, however, had no beneficial effect on renal glomerular injury nor on albuminuria. Notably, glomerular heparanase activity as a driver for loss of glomerular barrier function was not reduced. From this we conclude that enhancing diabetes-induced nitric oxide levels in an isolated fashion through inhibiting NOS uncoupling with sepiapterin, does not rescue kidney function necessarily. This chapter affirms the potential overruling role for glomerular macrophages in glycocalyx degradation in diabetic nephropathy.

To confirm the above studies, we showed *in vitro* that a diabetic milieu affects endothelial cell function and glycocalyx presence negatively. In our first *in vitro* study, endothelial cells were exposed to prolonged laminar shear stress and co-cultured with pericytes (chapter 2). Such prolonged laminar shear is a prerequisite for endothelial function and to obtain a quiescent phenotype (chapter 5). Important to note is that this is accompanied with qualitative changes in heparan sulfate expression, with emphasis on reducing the amount of the inflammatory heparan sulfate domains. A diabetic milieu decreased the thickness of the luminal glycocalyx, whereas atrasentan could reduce heparanase expression and restore glycocalyx coverage. In succession of these results we continued to specifically address the question how the presence of extracellular active heparanase modifies luminal glycocalyx composition on endothelial cells *in vitro* (chapter 5). Enzymatic cleavage of heparan sulfates with recombinant heparanase reduced the total amount of luminal glycosaminoglycan content, however it increased inflammatory heparan sulfate epitopes, resulting in reduced shear stress-induced quiescent phenotype. This shows that the composition of heparan sulfate on the endothelial surface is indicative for endothelial function as well as functional relevant itself. In chapter 5, these observations were confirmed *in vivo* where we observed that systemic perfusion with recombinant heparanase increased similar inflammatory heparan sulfate epitopes in zebrafish larvae. Therefore, disease induced heparanase could be a druggable target to stabilize the endothelium.

In chapter 6 we demonstrate that endothelial-specific loss of hyaluronan results in loss of endothelial barrier function, as exemplified by the development of glomerular proteinuria and edema, as well as generalized capillary destabilization, associated with reduced binding of the vascular stabilizing protein angiopoietin 1 (ANG1). This newly developed mouse model recapitulates in particular microangiopathy, as can be observed clinically in diabetes: i.e. progressive glomerular nephropathy, characterized by mesangiolysis, capillary destabilization followed by secondary rarefaction, as well as hypoxic retinopathy and ischemic cardiomyopathy. Besides we show that the retinal deep capillary plexus reveals signs of endothelial rarefaction. We showed that loss of endothelial hyaluronan prevents proper receptor tyrosine kinase TIE2 activation

through ANG1 and thus destabilizes VE-cadherin interactions. This provides mechanistic evidence for a direct role of hyaluronan on ANG1/TIE2 activation and VE-cadherin stabilization. The clinical relevance of this study lies in our observation that hyaluronan is also lost in disease conditions characterized by endothelial activation, such as diabetes and tumor angiogenesis.

Heparan sulfates, heparanase and diabetic nephropathy

This thesis provides evidence for the potent role of the heparan sulfates degrading enzyme heparanase in the progression and treatment of diabetes and diabetic nephropathy. The first reason for this potential is the capacity of particular heparan sulfate domains to mediate very specific protein binding, such as the growth factors fibroblast growth factor-2 (FGF-2) and vascular endothelial growth factor (VEGF) (1-3). In these interactions, heparan sulfate assists in protein-receptor interactions, but also creates chemotactic gradients of growth factors and chemokines (4, 5). The vascular complications resulting from diabetes can be initiated by these changes in glycocalyx composition.

Secondly, heparanase facilitates heparan sulfates turnover predominantly intracellular, which is tightly regulated under physiological conditions. Extracellular remodeling of heparan sulfates is restricted to locations with sufficient low pH (6). This is observed in pathological conditions such as atherosclerosis, diabetes and cancer (7). For example, monocytes can release heparanase from intracellular granules to facilitate local low pH (7). Sustained pathological degradation of extracellular heparan sulfates may release and modulate growth factors and chemokines and generate more inflammation related heparan sulfate fragments (8-10). This way selectins and integrins will be more exposed and immunocytes will be able to bind more easily and recruited locally (6, 11, 12). Furthermore, the intracellular upregulation of heparanase enhances the production of the angiogenic growth factor VEGF (13), which induces angiogenesis and vessel destabilization. This will ultimately cause glomerular capillary destabilization and subsequent mesangiolysis and glomerular hypertrophy, all classical symptoms of the glomerular lesions in diabetic nephropathy (14).

Thirdly, increased glomerular heparanase activity is demonstrated in diabetic nephropathy and other glomerular diseases (15, 16). It also has been shown that heparanase is critical to the development of diabetic nephropathy (17-21). Specifically, hyperglycemia and glycated serum proteins stimulate the upregulation of heparanase in endothelial cells (22, 23). Furthermore, heparanase-deficient mice are resistant to diabetes-induced proteinuria and renal damage (24).

A discussion about the role of heparanase in inflammation touches immediately upon the role of cathepsin L, the predominant activator of proheparanase in the extracellular environment, in these processes (25). Macrophages can secrete cathepsin L and thus activate heparanase extracellular. This process is self-accelerating, because active heparanase itself will activate macrophages by enhancing toll-like receptor and/or RAGE signaling (26). In line with the findings in chapter 3, cathepsin L deficient mice were protected against diabetes-induced albuminuria, renal macrophage influx, and renal function decline (27). The above indicates that the role of

heparanase in the development of diabetic nephropathy may lie in its effects on macrophage driven inflammation.

Hyaluronan and diabetic nephropathy

Hyaluronan is the second most prominent endothelial glycocalyx constituent and the only glycosaminoglycan that is not covalently attached to a core protein. Hyaluronan has manifold biological functions dependent on the molecular mass of hyaluronan: high molecular weight (HMW) hyaluronan has immunosuppressive properties, whereas low molecular weight hyaluronan (LMW) induces endothelial stress (28).

Systemic concentrations of hyaluronan are increased in diabetic patients (29, 30). A finding that is supported by the fact that hyaluronan production is strongly regulated by cell metabolism, therefore a diabetic milieu may affect hyaluronan production (31, 32). In rats, hyperglycemia induces hyaluronan production in mesangial cells, which is followed by recruitment of immunocytes (33). This systemic induction of hyaluronan and/or induction in stromal cells have been shown frequently. Our study shows that endothelial ablation of hyaluronan production induces vascular destabilization. This seems to be in contrast with literature focusing on enhanced hyaluronan in diabetic nephropathy. However, one should keep in mind the different activities of LMW and HMW. Increase in LMW will induce endothelial stress, a reduction in HMW hyaluronan reduces protective effects of HMW, thus may induce similar processes as increased LMW. Furthermore, recently hyaluronidase deficiency has been shown to be protective in early experimental diabetes, by preventing increased systemic P-selectin concentrations, vasorelaxation and glycocalyx damage (34). Though little is known about endothelial specific hyaluronan, this study, together with our data, indicates that cellular orientation of hyaluronan denominates its vasculoprotective vs. detrimental effect.

The glycocalyx as a therapeutic target in renal diseases

The role of the endothelial glycocalyx in inflammatory diseases has been studied in this thesis, as well as by other research groups in manifold research domains. In the introduction, we raised the question whether the glycocalyx could also be pharmacologically protected or replenished. In chapter 2 we attempted to do so by stimulating endothelial nitric oxide synthesis (eNOS) with an endothelial A receptor antagonist. These results are promising, however in chapter 4 we showed that isolated nitric oxide increase itself did not protect the endothelial glycocalyx. Therefore the protection of the endothelial glycocalyx via endothelial A receptor blockage is probably multifactorial, with potential for an indirect role for eNOS in stable synthesis of the glycocalyx. The concomitant suppression of heparanase activity (independent of eNOS) indicates a potential more pronounced role for immunocytes. Targeting immunocytes to reduce albuminuria in diabetic nephropathy is further supported by chapter 3, its human analogue (empaticap pegol NOX-E36 (35)), and a clinical study that targeted monocytes by blockade of

their chemokine receptor CCR2 (36). Taken this approach one step further, we can consider cathepsin L itself as a potential therapeutic target, since cathepsin L is essential for the formation of active heparanase. Currently, proteinuria can be reduced by several unspecific cathepsin inhibitors (37, 38), therefore more specific cathepsin L inhibitors offer potentially stronger proteinuria reducing effects without unwanted off-target effects.

Chapter 2 and 3 add substantial evidence that heparanase is a highly promising target in stabilizing de endothelial glycocalyx and demising inflammatory renal diseases with currently available treatment options. Similar animal studies may provide mechanistic evidence for unexpected (prolonged) treatment effects of other treatment options that interfere with renin angiotensin aldosterone system (RAAS) or immunocyte trafficking. Another approach to target heparanase is by the use of glycomimetics (39, 40). Such as non-degradable heparan sulfate-based drugs that bind to the enzyme heparanase, thereby decreasing accessibility to endogenous heparan sulfates. The role of heparanase in cancer is studied comprehensively and several carbohydrate-based heparanase inhibitors have been used in clinical trials (41, 42). However, off-target effects should be taken into account, because of their similarity to heparin and thereby possible binding to heparin-binding proteins, such as the protein C inhibitor that acts on thrombin (43). Moreover, these heparin-like structures may be taken up by cells and affect physiological intracellular processes. The glycomimetics sulodexide has been discussed in the introduction. Promising results were obtained in patients with type 2 diabetes (44-46), however, phase 3 studies could not replicate these effects, probably due to different manufacture protocols and/or sources of the heparin (pig intestinal mucosa) (47, 48).

Lastly, diabetic nephropathy increases urinary heparanase excretion (49). This suggests that heparanase can also be used as a biomarker for glomerular diabetic complications. Not only heparanase, but also specific heparan sulfate fragments can serve as biomarkers in either urine or plasma. This can be applied not only to diabetic nephropathy, but may also be applicable in diseases like systemic lupus erythematosus (SLE), hemolytic uremic syndrome (HUS, chapter 1) and in (renal) transplantation. In the latter, glycocalyx biomarkers may hypothetically be used in addition to HLA matching.

The therapeutic potential of the glycocalyx can also be extended toward other (renal) diseases. If, for example, glycomimetics are applied to the dialyses membrane, these compounds cannot only inhibit heparanase activity in the dialyses filtrate, but also bind growth factors and immunocytes, as well as modulate complement activity. The further exploration of such applications may provide druggable targets to modify treatment of renal diseases.

To conclude, this thesis provides evidence that inhibition of glycocalyx degrading enzymes is a potent treatment option in diabetic nephropathy. Further research towards the mechanism behind therapeutical interventions may reveal the involvement of the endothelial glycocalyx in multiple vascular diseases. Aside from being the target of therapeutic interventions, the plasma or urinary levels of glycocalyx (degrading enzymes) may provide biomarkers for the prediction of treatment efficiency.

References

1. Esko JD, Selleck SB. Order out of chaos: assembly of ligand binding sites in heparan sulfate. Annual review of biochemistry. 2002;71(1):435-71.
2. Taylor KR, Gallo RL. Glycosaminoglycans and their proteoglycans: host-associated molecular patterns for initiation and modulation of inflammation. FASEB journal : official publication of the Federation of American Societies for Experimental Biology. 2006;20(1):9-22.
3. Bartlett CS, Jeansson M, Quaggin SE. Vascular Growth Factors and Glomerular Disease. Annu Rev Physiol. 2016;78:437-61.
4. Sarrazin S, Lamanna WC, Esko JD. Heparan sulfate proteoglycans. Cold Spring Harbor perspectives in biology. 2011;3(7).
5. Bishop JR, Schuksz M, Esko JD. Heparan sulphate proteoglycans fine-tune mammalian physiology. Nature. 2007;446(7139):1030-7.
6. Gilat D, Hershkoviz R, Goldkorn I, Cahalon L, Korner G, Vlodavsky I, et al. Molecular behavior adapts to context: heparanase functions as an extracellular matrix-degrading enzyme or as a T cell adhesion molecule, depending on the local pH. The Journal of experimental medicine. 1995;181(5):1929-34.
7. Sasaki N, Higashi N, Taka T, Nakajima M, Irimura T. Cell surface localization of heparanase on macrophages regulates degradation of extracellular matrix heparan sulfate. Journal of immunology. 2004;172(6):3830-5.
8. Esko JD, Lindahl U. Molecular diversity of heparan sulfate. The Journal of clinical investigation. 2001;108(2):169-73.
9. Quarto N, Amalric F. Heparan sulfate proteoglycans as transducers of FGF-2 signalling. J Cell Sci. 1994;107 (Pt 11):3201-12.
10. Yayon A, Klagsbrun M, Esko JD, Leder P, Ornitz DM. Cell surface, heparin-like molecules are required for binding of basic fibroblast growth factor to its high affinity receptor. Cell. 1991;64(4):841-8.
11. Lever R, Rose MJ, McKenzie EA, Page CP. Heparanase induces inflammatory cell recruitment in vivo by promoting adhesion to vascular endothelium. American journal of physiology Cell physiology. 2014;306(12):C1184-90.
12. Fantin A, Vieira JM, Gestri G, Denti L, Schwarz Q, Prykhozhij S, et al. Tissue macrophages act as cellular chaperones for vascular anastomosis downstream of VEGF-mediated endothelial tip cell induction. Blood. 2010;116(5):829-40.
13. Zetser A, Bashenko Y, Edovitsky E, Levy-Adam F, Vlodavsky I, Ilan N. Heparanase induces vascular endothelial growth factor expression: correlation with p38 phosphorylation levels and Src activation. Cancer Res. 2006;66(3):1455-63.
14. Nakagawa T, Kosugi T, Haneda M, Rivard CJ, Long DA. Abnormal angiogenesis in diabetic nephropathy. Diabetes. 2009;58(7):1471-8.
15. van den Born J, van den Heuvel LP, Bakker MA, Veerkamp JH, Assmann KJ, Weening JJ, et al. Distribution of GBM heparan sulfate proteoglycan core protein and side chains in human glomerular diseases. Kidney international. 1993;43(2):454-63.
16. van den Hoven MJ, Rops AL, Vlodavsky I, Levidiotis V, Berden JH, van der Vlag J. Heparanase in glomerular diseases. Kidney international. 2007;72(5):543-8.
17. Katz A, Van-Dijk DJ, Aingorn H, Erman A, Davies M, Darmon D, et al. Involvement of human heparanase in the pathogenesis of diabetic nephropathy. Isr Med Assoc J. 2002;4(11):996-1002.
18. Maxhimer JB, Somenek M, Rao G, Pesce CE, Baldwin D, Jr., Gattuso P, et al. Heparanase-1 gene expression and regulation by high glucose in renal epithelial cells: a potential role in the pathogenesis of proteinuria in diabetic patients. Diabetes. 2005;54(7):2172-8.
19. Shafat I, Zcharia E, Nisman B, Nadir Y, Nakhoul F, Vlodavsky I, et al. An ELISA method for the detection and quantification of human heparanase. Biochemical and biophysical research communications. 2006;341(4):958-63.
20. van den Hoven MJ, Rops AL, Bakker MA, Aten J, Rutjes N, Roestenberg P, et al. Increased expression of heparanase in overt diabetic nephropathy. Kidney international. 2006;70(12):2100-8.
21. Wijnhoven TJ, van den Hoven MJ, Ding H, van Kuppevelt TH, van der Vlag J, Berden JH, et al. Heparanase induces a differential loss of heparan sulphate domains in overt diabetic nephropathy. Diabetologia. 2008;51(2):372-82.
22. Abu El-Asrar AM, Alam K, Nawaz MI, Mohammad G, Van den Eynde K, Siddiquei MM, et al. Upregu-

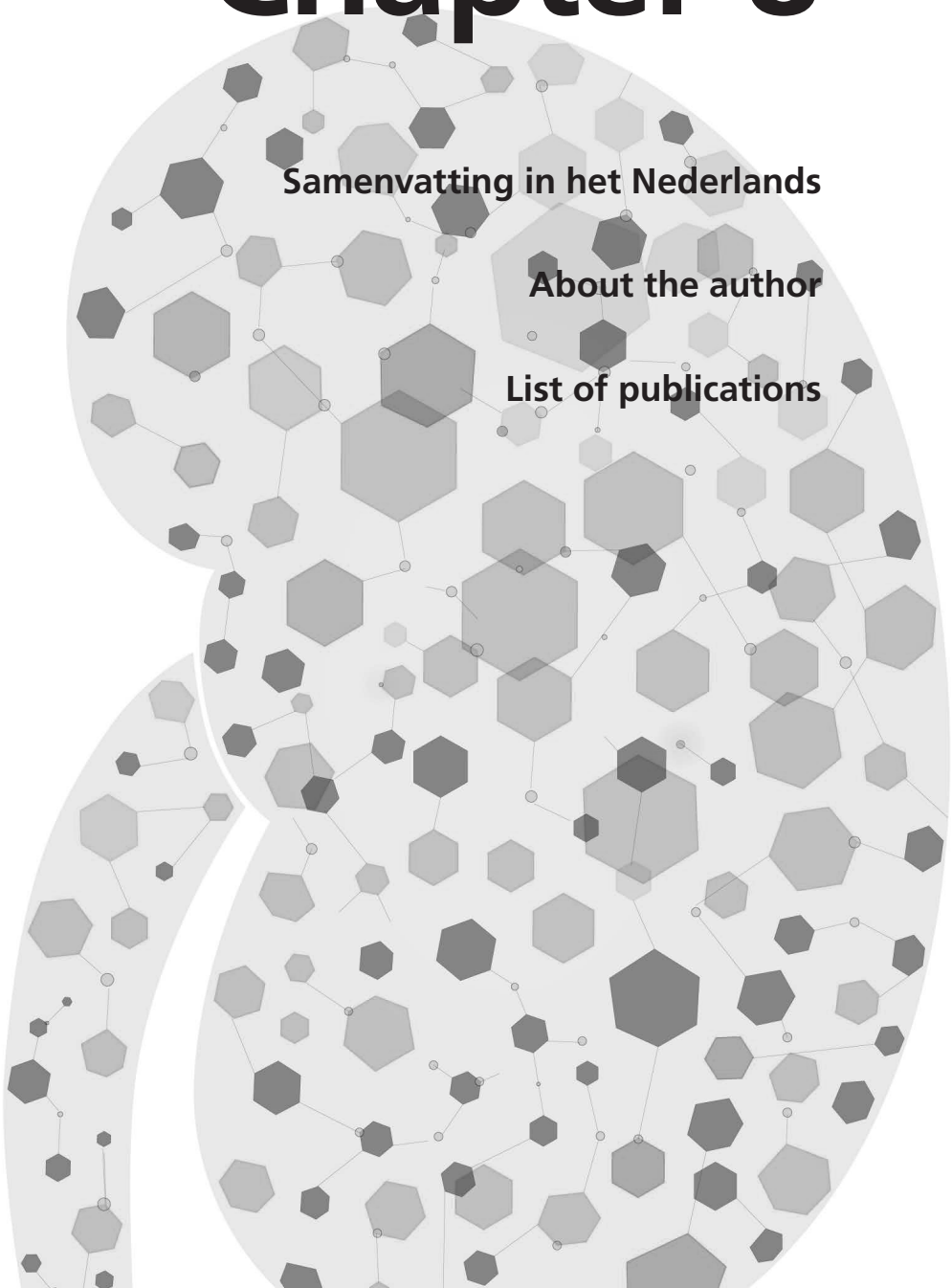
lated Expression of Heparanase in the Vitreous of Patients With Proliferative Diabetic Retinopathy Originates From Activated Endothelial Cells and Leukocytes. Investigative ophthalmology & visual science. 2015;56(13):8239-47.

23. Boels MG, Avramut MC, Koudijs A, Dane MJ, Lee DH, van der Vlag J, et al. Atrasentan Reduces Albuminuria by Restoring the Glomerular Endothelial Glycocalyx Barrier in Diabetic Nephropathy. Diabetes. 2016;65(8):2429-39.
24. Gil N, Goldberg R, Neuman T, Garsen M, Zcharia E, Rubinstein AM, et al. Heparanase is essential for the development of diabetic nephropathy in mice. Diabetes. 2012;61(1):208-16.
25. Simeonovic CJ, Ziolkowski AF, Wu Z, Choong FJ, Freeman C, Parish CR. Heparanase and autoimmune diabetes. Frontiers in immunology. 2013;4:471.
26. Goldberg R, Rubinstein AM, Gil N, Hermano E, Li JP, van der Vlag J, et al. Role of heparanase-driven inflammatory cascade in pathogenesis of diabetic nephropathy. Diabetes. 2014;63(12):4302-13.
27. Garsen M, Rops AL, Dijkman H, Willemsen B, van Kuppevelt TH, Russel FG, et al. Cathepsin L is crucial for the development of early experimental diabetic nephropathy. Kidney international. 2016 Nov;90(5):1012-1022.
28. Becker BF, Jacob M, Leipert S, Salmon AH, Chappell D. Degradation of the endothelial glycocalyx in clinical settings: searching for the sheddases. British journal of clinical pharmacology. 2015 Sep;80(3):389-402.
29. Moretto P, Karousou E, Viola M, Caon I, D'Angelo ML, De Luca G, et al. Regulation of Hyaluronan Synthesis in Vascular Diseases and Diabetes. Journal of diabetes research. 2015;2015:167283.
30. Morita M, Yano S, Ishibashi Y, Nakata N, Kurioka S, Sugimoto T. Close relationship between serum hyaluronan levels and vascular function in patients with type 2 diabetes. Biomarkers : biochemical indicators of exposure, response, and susceptibility to chemicals. 2014:1-5.
31. Buse MG. Hexosamines, insulin resistance, and the complications of diabetes: current status. Am J Physiol Endocrinol Metab. 2006;290(1):E1-E8.
32. Slawson C, Copeland RJ, Hart GW. O-GlcNAc signaling: a metabolic link between diabetes and cancer? Trends Biochem Sci. 2010;35(10):547-55.
33. Wang A, Hascall VC. Hyaluronan structures synthesized by rat mesangial cells in response to hyperglycemia induce monocyte adhesion. The Journal of biological chemistry. 2004;279(11):10279-85.
34. Dogne S, Rath G, Jouret F, Caron N, Dessy C, Flamion B. Hyaluronidase 1 Deficiency Preserves Endothelial Function and Glycocalyx Integrity in Early Streptozotocin-Induced Diabetes. Diabetes. 2016;65(9):2742-53.
35. Menne J, Eulberg D, Beyer D, Baumann M, Saudek F, Valkusz Z, et al. C-C motif-ligand 2 inhibition with emapticap pegol (NOX-E36) in type 2 diabetic patients with albuminuria. Nephrology, dialysis, transplantation : official publication of the European Dialysis and Transplant Association - European Renal Association. 2017 Feb 1;32(2):307-315.
36. de Zeeuw D, Bekker P, Henkel E, Hasslacher C, Gouni-Berthold I, Mehling H, et al. The effect of CCR2 inhibitor CCX140-B on residual albuminuria in patients with type 2 diabetes and nephropathy: a randomised trial. Lancet Diabetes Endocrinol. 2015;3(9):687-96.
37. Baricos WH, Cortez SL, Le QC, Wu LT, Shaw E, Hanada K, et al. Evidence suggesting a role for cathepsin L in an experimental model of glomerulonephritis. Archives of biochemistry and biophysics. 1991;288(2):468-72.
38. Baricos WH, O'Connor SE, Cortez SL, Wu LT, Shah SV. The cysteine proteinase inhibitor, E-64, reduces proteinuria in an experimental model of glomerulonephritis. Biochemical and biophysical research communications. 1988;155(3):1318-23.
39. Niu TT, Zhang DS, Chen HM, Yan XJ. Modulation of the binding of basic fibroblast growth factor and heparanase activity by purified lambda-carrageenan oligosaccharides. Carbohydr Polym. 2015;125:76-84.
40. Gomes CL, Leao CL, Venturotti C, Barreira AL, Guimaraes G, Fonseca RJ, et al. The protective role of fucosylated chondroitin sulfate, a distinct glycosaminoglycan, in a murine model of streptozotocin-induced diabetic nephropathy. PloS one. 2014;9(9):e106929.
41. Ritchie JP, Ramani VC, Ren Y, Naggi A, Torri G, Casu B, et al. SST0001, a chemically modified heparin, inhibits myeloma growth and angiogenesis via disruption of the heparanase/syndecan-1 axis. Clinical cancer research : an official journal

of the American Association for Cancer Research. 2011;17(6):1382-93.

42. Hammond E, Handley P, Dredge K, Bytheway I. Mechanisms of heparanase inhibition by the heparan sulfate mimetic PG545 and three structural analogues. FEBS open bio. 2013;3:346-51.
43. Xu D, Esko JD. Demystifying heparan sulfate-protein interactions. Annual review of biochemistry. 2014;83:129-57.
44. Poplawska A, Szelachowska M, Topolska J, Wysocka-Solowie B, Kinalska I. Effect of glycosaminoglycans on urinary albumin excretion in insulin-dependent diabetic patients with micro- or macroalbuminuria. Diabetes research and clinical practice. 1997;38(2):109-14.
45. Gambaro G, Kinalska I, Oksa A, Pont'uch P, Hertlová M, Olsovsky J, et al. Oral Sulodexide Reduces Albuminuria in Microalbuminuric and Macroalbuminuric Type 1 and Type 2 Diabetic Patients: The Di.N.A.S. Randomized Trial. Journal of the American Society of Nephrology. 2002;13(6):1615-25.
46. Bang K, Chin HJ, Chae DW, Joo KW, Kim YS, Kim S, et al. Anti-proteinuric effect of sulodexide in immunoglobulin a nephropathy. Yonsei medical journal. 2011;52(4):588-94.
47. Lewis EJ, Lewis JB, Greene T, Hunsicker LG, Berl T, Pohl MA, et al. Sulodexide for kidney protection in type 2 diabetes patients with microalbuminuria: a randomized controlled trial. American journal of kidney diseases : the official journal of the National Kidney Foundation. 2011;58(5):729-36.
48. Packham DK, Wolfe R, Reutens AT, Berl T, Heerspink HL, Rohde R, et al. Sulodexide Fails to Demonstrate Renoprotection in Overt Type 2 Diabetic Nephropathy. Journal of the American Society of Nephrology. 2012;23(1):123-30.
49. Shafat I, Ilan N, Zoabi S, Vlodavsky I, Nakhoul F. Heparanase levels are elevated in the urine and plasma of type 2 diabetes patients and associate with blood glucose levels. PloS one. 2011;6(2):e17312.

Chapter 8



Samenvatting in het Nederlands

About the author

List of publications

Samenvatting in het Nederlands

Onze nieren zijn van levensbelang. Ze filteren afvalstoffen uit het bloed, reguleren de vocht- en zouthuishouding en de bloeddruk. Wanneer de nieren niet goed functioneren wordt er vaak gekeken naar het eiwitverlies in de urine. Eiwitverlies kan optreden wanneer er schade is ontstaan in de filterunit van de nier, de glomerulus. Deze filterunit bestaat uit een kluwen van zeer kleine bloedvaatjes en een ruimte waar de eerste urine gevormd wordt. Deze kleine bloedvaatjes zijn opgebouwd uit verschillende cellen, waarvan de endotheelcellen de binnenste laag vormen. Rondom deze cellen zit een suikerlaag, de glycocalyx. Deze suikerlaag vormt de eerste barrière om eiwitverlies via de urine tegen te gaan door ze in de bloedsomloop te houden. Dit is van cruciaal belang omdat deze eiwitten niet alleen in het lichaam gebruikt kunnen worden, maar ook omdat te veel eiwit in de urine schade aanricht in de cellen die de rest van het filter bekleden. De exacte samenstelling van deze suikerlaag is vooralsnog grotendeels onbekend maar het staat ondertussen onomstotelijk vast dat de glycocalyx verandert in uiteenlopende ziektebeelden. **Hoofdstuk 1** verhaalt over de structuur en functie van de glycocalyx, maar beschrijft ook drie karakteristieke vormen van nierfalen waarin de suikerlaag aangetast is: het hemolytisch-uremisch syndroom, acute nierschade en nierfalen als gevolg van diabetes.

Er zijn verschillende processen betrokken bij de afbraak van de glycocalyx. Zo kan je denken aan een verstoorde aanmaak van de verschillende suikerketens hierin, maar momenteel heerst de overtuiging dat de belangrijkste oorzaak juist ligt in eiwitten die de suikerketens afbreken, zogenaamde enzymen. Plasmawaarden van deze enzymen zijn bijvoorbeeld verhoogd bij diabetespatiënten met nierfalen. In hoofdstuk 2 en 3 onderzoeken we het proces van suikerafbraak aan de hand van onderzoek met specifieke muizen, "een muismodel". We bekijken of de glycocalyx een rol speelt in de beschermende werking van verschillende medicijnen op de nier. Atrasentan is zo'n middel dat in patiënten met diabetisch nierfalen de eitwitlekkage van de nier vermindert. In **hoofdstuk 2** laten we zien dat dit middel ook beschermend werkt in muizen met diabetes. In dit muismodel hebben we de glycocalyx onder andere bestudeerd met behulp van elektronenmicroscopie, een techniek die gebruik maakt van een bundel elektronen om de filterunit van de nier in kaart te brengen. Door het gebruik van elektronen is de resolutie van een elektronenmicroscoop veel hoger dan die van een lichtmicroscoop en kijken we op een gedetailleerder niveau naar het weefsel. Terwijl diabetes leidt tot een 40% afname van endotheliale glycocalyx, herstelt atrasentan dit tot bijna gezonde waarden. We onderzochten of ook de glycocalyxafbrekende eiwitten verhoogd aanwezig waren in de filterunits en dit bleek het geval. Het feit dat dit enzym na geproduceerd te zijn nog geactiveerd moet worden deed al vermoeden dat ontstekingscellen hierbij een rol spelen, omdat deze glycocalyxafbrekende enzymen produceren en kunnen activeren. In **hoofdstuk 3** beschrijven we dan ook een ander medicijn, de spiegelmer®, NOX-E36, welke direct ingrijpt op deze ontstekingscellen. Ook dit middel gaat bij patiënten met diabetisch nierfalen eiwitlekkage tegen maar anders dan bij andere middelen blijft dit effect enkele weken na het stoppen van de behandeling te zien. Ontstekingscellen in het lichaam zijn enkele weken actief en worden dan vernieuwd. Indien dit middel ingrijpt op deze ontstekingscellen en deze cellen dus minder glycocalyxafbrekende

activiteiten stimuleren, zou dit kunnen verklaren waarom het effect langer aanhoud. Ook in deze studie zagen we dat de glycocalyxafbrekende stoffen minder aanwezig waren en de glycocalyx herstelde.

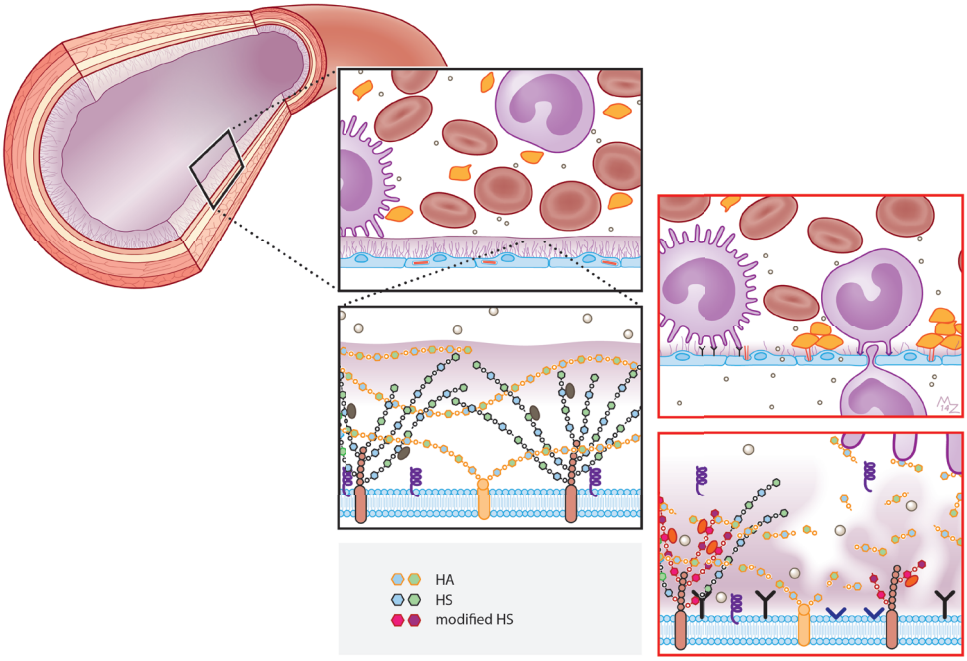


Figure 1. Schematische weergave van de glycocalyx. De glycocalyx wordt geproduceerd door endotheelcellen als een intacte laag (links). Hier biedt de laag bescherming tegen eiwitlekkage en ontsteking. Tijdens ziekte (rechts) raken de endotheelcellen beschadigd en breken enzymen in het bloed de glycocalyx af. Door deze beschadigingen kunnen eiwitten gemakkelijker de endotheel cellen passeren en de zogenaamde sub-endotheliale ruimte bereiken. In gewone bloedvaten kan dit leiden tot oedeem terwijl in het nierfilter dit juist leidt tot verlies van eiwitten in de urine *(Dane et al., AJPRenal 2015)*.

Beide studies wijzen op een belangrijke rol voor het enzym heparanase. Heparanase is doorgaans in ons lichaam aanwezig in een inactieve vorm. Ontstekingscellen kunnen de stof cathepsine L uitscheiden welke het heparanase activeert en daardoor bepaalde suikerketens uit de glycocalyx afbreekt, de heparaan sulfaat ketens. Doordat beide studies aantonen dat de ontstekingscellen zijn veranderd en zowel cathepsine L als heparanase minder aanwezig zijn in de glycocalyx, concluderen we dat beide medicijnen de glycocalyx beschermen door het aanpakken van deze ontstekingscellen.

In **hoofdstuk 4** wordt een ander aspect van de regulatie van het eiwit heparanase besproken: stikstofoxide, een signaal stof, dat gemaakt wordt door de endotheelcellen en tegelijkertijd deze cellen beschermt (waar de glycocalyx door geproduceerd wordt). Deze bescherming zou in principe ook aanleiding kunnen zijn voor verminderde aanwezigheid van heparanase in de nier. In het muismodel dat wij hebben gebruikt, zien we echter dat de hoeveelheid stikstofoxide is toegenomen nadat de muizen diabetes ontwikkelden. Een ding om rekening mee te houden

is dat stikstofoxide ook gemaakt kan worden door andere cellen, juist tijdens ziekteprocessen. Omdat we niet kunnen onderscheiden van welke cellen deze toename in stikstofoxide afkomstig is, hebben we een stof toegediend die alleen de hoeveelheid stikstofoxide gemaakt door de endotheelcellen sterk verhoogd, sepiapterin. Echter bleek deze toegenomen hoeveelheid stikstofoxide geen positieve uitwerking te hebben op de nierfunctie en ook de hoeveelheid heparanase in de filterunits was niet verminderd. Dit bevestigt nogmaals dat de ontstekingscellen een grote rol hebben in de status van de glycocalyx in diabetische nierfalen en de aanmaak van de glycocalyx door endotheelcellen kunnen overrulen door de afbraak te stimuleren.

Bovenstaande bevindingen hebben we geverifieerd in een *in vitro*-systeem waarin we endotheelcellen hebben gekweekt onder een constante vloeistofstroom van kweekmedium (vloeibare voeding) terwijl ze zich bevonden bovenop een laag pericyten. Op deze manier hebben we getracht de omstandigheden in de bloedvaten na te bootsen waarin endotheelcellen omringt worden door pericyten en blootgesteld worden aan een continue bloedstroom. Met deze methode zien we dat toevoegen van diabetische (bloed)factoren in het kweekmedium de endotheelcellen en de glycocalyx negatief beïnvloeden. Het toevoegen van Atrasentan zorgt ook hier voor herstel van de glycocalyxlaag en verlaging van de hoeveelheid heparanase (**hoofdstuk 2**). In **hoofdsuk 5** laten we zien dat wanneer je heparanase toevoegt aan het medium, de dikte van de glycocalyx afneemt. Tegelijkertijd nemen de structuren waarvan bekend is dat ze ontstekingscellen aantrekken, juist toe. Dit wijst op een prominente rol voor de precieze samenstelling van de suikerstructuren voor zowel het functioneren van de glycocalyx als de endotheelcellen. In hoofdstuk 5 werden deze observaties nogmaals bevestigd in een ander diermodel, de zebravis. Wanneer heparanase werd ingebracht in de bloedbaan, zagen we dezelfde ontstekingsbevorderende suikerstructuren toenemen. Deze bevindingen tonen aan dat heparanase een mogelijke target kan zijn van medische interventies om het endotheel te stabiliseren en zo de bloedvaten beter te beschermen.

In **hoofdstuk 6** zoomen we in op een ander onderdeel van de glycocalyx. We switchen van heparanase dat de heparan sulfate in de glycocalyx afbreekt, naar hyaluronan. Hiervoor gebruiken we een nieuw muismodel waarin alleen de endotheelcellen geen hyaluronan aanmaken, maar de overige cellen nog wel. Hiermee kunnen we specifiek de rol van de aanmaak van de glycocalyx in de endotheelcellen onderzoeken. We tonen met dit muismodel aan dat de barrièrefunctie van de nierfilters afneemt (er ontstaat proteïnurie), maar ook in de overige bloedvaten is lekkage zichtbaar, door het ontstaan van oedeem. We zien dat de endotheelcellen slechter aan elkaar hechten, wat zorgt voor nog meer lekkage en verstoring van specifieke bloedvaten. Dit hebben we onderzocht in de ogen van de muizen (waar de kleinste vaten goed zichtbaar zijn, maar ook hebben we wederom een *in vitro*-systeem gebruikt om deze vaatjes na te bootsen. We vonden dat bepaalde receptoren minder werden gestimuleerd, waardoor de hechting tussen endotheelcellen (via VE-cadherin) verzwakte. In verschillende ziektebeelden waarin het endotheel geactiveerd wordt, zoals diabetes en bloedvatvorming bij kanker, zien we een soortgelijke afname van hyaluronan. Dit maakt deze observaties klinisch relevant.

Ten slotte geeft **hoofdstuk 7** een beschouwing van alle studies die in dit proefschrift zijn beschreven en bediscussieert het onderzoek.

Al het bovenstaande in ogenschouw nemend is stabilisatie van de glycocalyx een klinisch relevante target bij de behandeling van nierziekten en andere vasculaire ziektebeelden. Vooruitkijkend naar de toekomst zijn er verscheidene mogelijkheden om de glycocalyx in te zetten in de behandeling. Zo kunnen glycocalyx mimetica ingezet worden om glycocalyxafbrekende enzymen en ontstekingscellen te binden en zo weg te houden van het endotheel. Evenzo kunnen in nader onderzoek de glycocalyxafbrekende enzymen dienen als rechtstreeks target van medicijnen. Biomarkers om na te gaan of een ziektebeeld verslechterd en/of een behandeling aanslaat zijn er nog niet voldoende. Ook hierin kan de glycocalyx een rol spelen: de aanwezigheid van glycocalyxcomponenten of -afbraakenzymen in plasma of urine kunnen mogelijk dienen als biomarkers.

About the author

Margien (Martha Geesje Sientje) Boels was born on 02 June 1987 in Groningen, the Netherlands. She grew up in Ten Boer and Aduard and gained her athenaeum diploma from Gomarus College in Groningen in 2005. She commenced studying nutrition and dietetics at Hanzehogeschool Groningen that same year. During this study she performed a bachelors research internship to study the role of pre- and probiotics in infant formula. In 2009 she continued her studies in Nitrition and Health at Wageningen University where her interest for laboratory based scientific research was risen by studying the anti-inflammatory effects of fish oil derived fatty acids. From this point onwards, all her work was related to human health, disease and/or nutrition, one way or another. She continued her research at the Rowett Institute in Aberdeen, UK by investigating the effect of fatty acid on platelet function under the supervision of Baukje de Roos.

At the end of 2009 Margien received her M.Sc. in Nutrition and Health and became a PhD candidate in 2010 at the Department of Nephrology within the division of Internal Medicine, Leiden University Medical Centre. During the following years she set up and coordinated studies in mice, zebrafish and cells under the supervision of prof. T.J. Rabelink and dr. B.M. van den Berg. This PhD project was part of the Glycoren consortium, thus funded by the Dutch kidney foundation. The results of her research are published in peer-reviewed international scientific journals and presented in this thesis. Besides, she has presented her research at several (inter) national conferences, as well as non-scientific meetings for children (Boerhaave Institute, 2013 Leiden) and patients (Patientendag Nierpatiënten Vereniging Nederland, 2016 Lunteren). She won prices with her presentations at the Kidney Week of the American Society of Nephrology (2014), the Rembrandt Symposium of Cardiovascular Science (2015) and the "Nederlandse federatie voor nefrologie" (2016).

It is her wish and ambition to contribute to the improvement of quality of life. Margien is currently working as Medical Liaison Manager at Nutricia Advanced Medical Nutrition in Zoetermeer.

List of publications

M.G.S. Boels, A. Koudijs, M.C. Avramut, W.M.P.J. Sol, G. Wang, A.M. van Oeveren-Rietdijk, A.J. van Zonneveld, H.C. de Boer, J. van der Vlag, C. van Kooten, D. Eulberg, B.M. van den Berg, D.H.T. IJpelaar, T.J. Rabelink
Systemic Monocyte Chemotactic Protein-1 Inhibition Modifies Renal Macrophages and Restores Glomerular Endothelial Glycocalyx and Barrier Function in Diabetic Nephropathy.
American Journal of Pathology 187(11):2430-2440 (2017)

M.G.S. Boels, E.E. van Faassen, M.C. Avramut, J. van der Vlag, B.M. van den Berg, T.J. Rabelink
Direct Observation of Enhanced Nitric Oxide in a Murine Model of Diabetic Nephropathy.
PLOS ONE 12(1):e0170065 (2017)

M.G.S. Boels, M.C. Avramut, A. Koudijs, M.J. Dane, D.H. Lee, J. van der Vlag, A.J. Koster, A.J. van Zonneveld, E.F.F. van Faassen, H.J. Grone, B.M. van den Berg and T.J. Rabelink
Atrasentan Reduces Albuminuria by Restoring the Glomerular Endothelial Glycocalyx Barrier in Diabetic Nephropathy.
Diabetes 65(8):2429-2439 (2016)

M.J. Dane, B.M. van den Berg, D.H. Lee, **M.G.S. Boels**, G.L. Tiemeier, M.C. Avramut, A.J. van Zonneveld, J. van der Vlag, H. Vink and T.J. Rabelink
A microscopic view on the renal endothelial glycocalyx.
American Journal of Physiology - Renal Physiology 308(9): F956-966 (2015)

D.H. Lee, M.J. Dane, B.M. van den Berg, **M.G.S. Boels**, J.W. van Teeffelen, R. de Mutsert, M. den Heijer, F.R. Rosendaal, J. van der Vlag, A.J. van Zonneveld, H. Vink, T.J. Rabelink and NEOstudy group
Deeper penetration of erythrocytes into the endothelial glycocalyx is associated with impaired microvascular perfusion.
PLOS ONE 9(5): e96477 (2014)

M.J. Dane, M. Khairoun, D.H. Lee, B.M. van den Berg, B.J. Eskens, **M.G.S. Boels**, J.W. van Teeffelen, A.L. Rops, J. van der Vlag, A.J. van Zonneveld, M.E. Reinders, H. Vink and T.J. Rabelink
Association of kidney function with changes in the endothelial surface layer.
Clinical Journal of the American Society of Nephroly 9(4): 698-704 (2014)

M.G.S. Boels, D.H. Lee, B.M. van den Berg, M.J. Dane, J. van der Vlag and T.J. Rabelink
The endothelial glycocalyx as a potential modifier of the hemolytic uremic syndrome.
European Journal of Internal Medicine 24(6): 503-509 (2013)